Author:
Eapen, Alen

Title:
Development of GluK2 selective kainate receptor antagonists and investigations into the roles of the NMDA receptor subunit GluN2D in hippocampal synaptic plasticity

Development of GluK2 selective kainate receptor antagonists and investigations into the roles of the NMDA receptor subunit GluN2D in hippocampal synaptic plasticity

Alen Varghese Eapen

A dissertation submitted to the University of Bristol in accordance with the requirements of the degree of Doctor of Philosophy in the Faculty of Biomedical Sciences

School of Physiology, Pharmacology and Neuroscience

September 2018

Abstract

Novel compounds related to kynurenic acid were synthesised in-house and were pharmacologically characterised with the aim of developing novel GluK2 subunit-selective antagonists. Compounds with relative selectivity on GluN2A, GluN2B and GluN2D subunits of NMDA receptors and GluN2D genetic knockout mice were used to characterise the physiological roles of GluN2D-containing NMDA receptors.

Derivatives of kynurenic acid were tested on GluK1, GluK2 and GluA1 homomeric receptors expressed on HEK293 cells using a calcium fluorescence assay, and on f-EPSP recordings from the CA1 subregion of the hippocampus with the aim to develop novel GluK2 antagonists with GluK2 over AMPAR and GluK2 over GluK1 selectivity. Substitutions were made on the 6-position to develop 6-ethylkynurenic acid (UBP2054), which has a GluK2 K_i of 54.0 ± 10.9 μM and estimated IC_{50} values of > 1 mM and > 2 mM on GluK1 and GluA1, respectively.

UBP2054 has an IC_{50} of > 300 μM for inhibiting AMPAR-mediated f-EPSPs from the CA1 subregion of the hippocampus. Molecular modelling was used to rationalise the pharmacological profile observed in the functional assays.

Physiological investigations of GluN2D receptors revealed that the GluN2D NMDAR subunit mediates the induction of LTP in hippocampal Schaffer collateral to CA1 pyramidal cell synapses.

Acknowledgments

I thank and dedicate this work to my mentors

David Jane, Robert Thatcher, Arturas Volianskis,
Diego Fernandez-Fernandez and Stafford Lightman

And to my family

Amma, Appa and Akil

Author’s Declaration

I declare that the work in this dissertation was carried out in accordance with the requirements of the University's Regulations and Code of Practice for Research Degree Programmes and that it has not been submitted for any other academic award. Except where indicated by specific reference in the text, the work is the candidate's own work. Work done in collaboration with, or with the assistance of, others, is indicated as such. Any views expressed in the dissertation are those of the author.

SIGNED: .....

DATE: .....

Table of contents

List of Figures

List of Tables

Abbreviations

ACET or UBP316	GluK1 antagonist; (2-amino-2-carboxyethyl)-3-(2-carboxy-5-phenylthiophene-3-yl-methyl)-5-methylpyrimidine-2,4-dione
ADP	Adenosine diphosphate
AMPA(R)	(*S*)-α-amino-3-hydroxy-5-methylisoxazole-4-propionic acid (receptor)
ANOVA	Analysis of variance
ATD	Amino terminal domain
ATP	Adenosine triphosphate
ATPA	GluK1 agonist; (*S*)-2-amino-3-(5-tert-butyl-3-hydroxy-4-isoxazolyl)propionic acid
ATPase pump	A pump that uses energy from the hydrolysis of ATP to ADP in order to transport ions across a membrane
CA (1-3)	Cornu ammonis (1-3) - three sub-regions of the hippocampus
CamKII	Type II Ca^{2+}/calmodulin-dependent protein kinase
CNQX	AMPAR and KAR antagonist; 6-cyano-7-nitroquinoxaline-2,3-dione
CNS	Central nervous system
Con A	KAR positive allosteric modulator; Concanavalin A
CPP	NMDAR antagonist; 3-((*R*)-2-carboxypiperazin-4-yl)-propyl-1-phosphonic acid
CTD	Carboxy terminal domain
D1 and D2	The two lobes of the ligand binding domain of iGluRs
D-AP5	NMDAR antagonist; D-(-)-2-Amino-5-phosphonopentanoic acid
DCKA	GluN1 antagonist; 5-,7-dichlorokynurenic acid
DG	Dentate gyrus
DRG	Dorsal root ganglion
DT	Dunnett's multiple comparison test

EAATs	Excitatory amino acid transporters
E-LTP	Early long-term potentiation
EPSC	Excitatory postsynaptic current
EPSP	Excitatory postsynaptic potential
f-EPSP	Field excitatory postsynaptic potential
GABA(R)	γ-aminobutyric acid (receptor)
GAMS	γ-D-glutamylaminomethylsulfonate
GRIP	Glutamate receptor interacting protein
GYKI53655	AMPAR antagonist (GluK3 antagonist activity has also been reported); 1-(4-Aminophenyl)-3-methylcarbamyl-4-methyl-3,4-dihydro-7,8-methylenedioxy-5*H*-2,3-benzodiazepine hydrochloride
HEK293 cell line	Human embryonic kidney 293 cell line
HFS	High-frequency stimulation
I_{AHP}	Afterhyperpolarisation current
IFD	Induced fit docking; a docking routine used to calculate best-fit poses for a ligand-receptor interaction
iGluR	Ionotropic glutamate receptor
IHC	Immunohistochemistry
IPSC	Inhibitory post synaptic current
ISH	In situ hybridisation
KAR	Kainate receptor
KO	Genetic knockout
Kynurenic acid	4-oxo-1,4-dihydro-quinoline-2-carboxylic acid
L689,560	Antagonist of the GluN1 subunit of NMDARs; 4-*trans*-2-carboxy-5,7-dichloro-4-phenylaminocarbonylamino-1,2,3,4-tetrahydroquinoline
LBD	Ligand binding domain

LFS	Low frequency stimulation
L-LTP	Late long-term potentiation
LTD	Long-term depression
LTP	Long-term potentiation
LY293558	GluK1 and AMPAR antagonist; (3*S*,4a*R*,6*R*,8a*R*)-6-[2-(1(2)*H*-tetrazole-5-yl)ethyl]decahydroisoquinoline-3-carboxylic acid
LY294486	GluK1 antagonist; (3*SR*,4*aRS*,6*SR*,8*aRS*)-6-((((1*H*-tetrazol-5-yl)methyl)oxy)methyl)-1,2,3,4,4a,5,6,7,8,8a-decahydroisoquinoline-3-carboxylic acid
LY339434	GluK1 antagonist; (2*S*,4*R*)-4-[3-(2-naphthyl)-2-(*E*)-propenyl]glutamic acid
LY382884	GluK1 antagonist; (3*S*,4*aR*,6*S*,8*aR*)-6-((4-carboxyphenyl)methyl)-1,2,3,4,4a,5,6,7,8,8a-decahydroisoquinoline-3-carboxylic acid
LY466195	GluK1 antagonist; (3*S*,4*aR*,6*S*,8*aR*)-6-[[(2*S*)-2-carboxy-4,4-difluoro-1-pyrro-lidinyl]methyl]decahydro-3-isoquinolinecarboxylicacid
M1, M3 and M4 helices	Transmembrane α-helices, which together with the re-entrant loop M2 forms the transmembrane domain of ionotropic glutamate receptors
M2	Re-entrant loop, which is part of the transmembrane domain of ionotropic glutamate receptors
mEPSC	Miniature excitatory postsynaptic current
MF	Mossy fibre axons of the dentate gyrus granule cells
MF-CA3 synapse	Synapse between the mossy fibre axons of the dentate gyrus granule cells and CA3 pyramidal cells
MF-GC synapse	Recurrent synapse between the mossy fibre axons and granule cells of the dentate gyrus
mGluR	Metabotropic glutamate receptor
MK-801	NMDAR channel blocker
MW test	Mann-Whitney test
NAM	Negative allosteric modulator
NBQX	AMPAR and KAR antagonist; 2,3-dihydroxy-6-nitro-7-sulfamoyl-benzo[*f*]quinoxaline
neoDH	Neodysiherbaine

Neto (1 and 2)	Neuropilin and tolloid-like protein (1 and 2)
NGX426	Prodrug of LY293558
NMDA(R)	*N*-methyl-D-aspartate (receptor)
NS-102	KAR and AMPAR antagonist; 5-nitro-6,7,8,9-tetrahydrobenzo[*g*]indole-2,3-dione-3-oxime
NSF	*N*-ethylmaleimide-sensitive factor
NVP-AAM007 (NVP)	GluN2A-preferring antagonist; (*R*)-[(*S*)-1-(4-bromo-phenyl)-ethylamino]-(2,3-dioxo-1,2,3,4-tetrahydroquinoxalin-5-yl)-methyl-phosphonic acid
PAM	Positive allosteric modulator
p-BB-PzDA	1-(4-Bromobenzoyl)piperazine-2,3-dicarboxylic acid
p-CB-PzDA	1-(4-Chlorobenzoyl)piperazine-2,3-dicarboxylic acid
PDB	Protein data bank
PICK1	Protein interacting with C kinase 1
PKA	Protein kinase A
PKC	Protein kinase C
PP fibres	Perforant path fibres
PPDA	NMDAR antagonist; (2*S*,3*R*)-1-(phenanthren-2-carbonyl)piperazine-2,3-dicarboxylic acid
PPF	Paired-pulse facilitation
PSD95	Postsynaptic density protein 95
PTP	Post-tetanic potentiation
Q/R site	RNA editing site in the M2 region of the transmembrane domain of ionotropic glutamate receptors
Ro 25-6981 (Ro)	GluN2B negative allosteric modulator; α-(4-hydroxyphenyl)-β-methyl-4-(phenylmethyl)-1-piperidine propanol
S1 and S2 (LBD)	Segment 1 and 2 of polypeptides which form the LBD
SAR	Structure-activity relationship
SC-CA1 pyramidal cell synapse	Schaffer collateral-CA1 pyramidal cell synapse

SM proteins	Sec1/Munc18-like proteins
SNAREs	Soluble NSF attachment receptor proteins (includes vesicular- and target-SNAREs)
STDP	Spike timing-dependent potentiation
STP	Short-term potentiation
SYM2081	KAR and AMPAR agonist; (2*S*,4*R*)-4-Methylglutamate
TARP	Transmembrane AMPAR regulatory proteins
TBOA	Blocker of excitatory amino acid transporters; DL-*threo*-β-benzyloxyaspartic acid
TBS	Theta burst stimulation; 10 bursts of 4 shocks at 100 Hz delivered at an interval of 200 ms
TLE	Temporal lobe epilepsy
TMD	Transmembrane domain
UBP145	GluN2D-preferring antagonist; (2*R**,3*S**)-1-(9-bromophenanthrene-3-carbonyl)piperazine-2,3-dicarboxylic acid
UBP302	GluK1 antagonist; (*S*)-1-(2-amino-2-carboxyethyl)-3-(2-carboxybenzyl)pyrimidine-2,4-dione
UBP310	GluK1 antagonist; (*S*)-1-(2-amino-2-carboxyethyl)-3-(2-carboxythiophene-3-yl-methyl)-5-methylpyrimidine-2,4-dione
UBP316	GluK1 antagonist; another name for ACET
VGLUT	Vesicular glutamate transporters
WMPSR test	Wilcoxon matched pairs signed rank test
X. laevis	Xenopus laevis
α-SNAP	α-Soluble NSF attachment protein

Chapter 1

Introduction

A central question in neuroscience is: what are the cellular processes that lead to the storage and processing of information in the human brain? Cells of the nervous system (neurons) communicate with each other at specialised junctions known as synapses. While different types of synapses have been discovered, majority of the communication between neurons is believed to occur at chemical synapses, which use molecules known as neurotransmitters to transmit signals from one neuron to another (see Glickstein, 2006 for a review). Early studies that investigated the neuronal responses of exogenously applied molecules provided evidence for the role of L-glutamate (or (*S*)-glutamate), a naturally occurring metabolite of cellular respiration, as a neurotransmitter in the mammalian brain (Hayashi, 1954).

The abundance of amino acids in the brain and their requirement in metabolic pathways, including for protein synthesis, raised doubts regarding their identity as neurotransmitters (see Watkins and Jane, 2006 for a review). These suspicions were supported by early reports suggesting that negatively charged amino acids such as L-glutamate and L-aspartate activated, whereas neutral amino acids such as γ-aminobutyric acid (GABA), β-alanine and taurine inhibited neurons in a non-specific manner (Curtis and Watkins, 1960, 1963; Takeuchi and Takeuchi, 1963). However, further pharmacological investigations revealed that the inhibitory effects of GABA and glycine were selectively blocked by bicuculline and strychnine, respectively (Curtis and Johnston, 1974). These results suggested that excitatory signalling may also be mediated by amino acids. Furthermore, the differential distribution of L-glutamate and L-aspartate in the central nervous system (CNS) also suggested that these excitatory amino acids mediated different roles in neurotransmission (Graham et al., 1967; Johnston, 1968; Duggan and Johnston, 1970). While L-glutamate and L-aspartate activated excitatory synapses in neuronal populations across the CNS, studies on thalamic and spinal neurons revealed that excitatory neurons have different sensitivities to L-glutamate and L-aspartate which suggested that they may have acted on different targets to produce the excitatory responses (Mclennan et al., 1968; Duggan, 1974).

Pharmacological studies of the neurotransmission mediated by L-glutamate (and L-aspartate) have spanned over six decades and have led to the discovery of glutamate receptors, which are responsible for binding L-glutamate (and L-aspartate) and eliciting excitatory responses in neurons (Nakanishi, 1992; Hollmann and Heinemann, 1994). These glutamate receptors are classified according to their mechanism of signal transduction, their

pharmacology and amino acid sequence homology (reviewed in Niswender and Conn, 2010 and Traynelis et al., 2010).

1.1. Glutamate receptors and neurotransmission

1.1.1. Classification of glutamate receptors

Glutamate receptors are broadly classed according to their mechanism of signal transduction once L-glutamate (herein referred to as glutamate unless specified) binds to and activates the receptor (Figure 1.1). Ionotropic glutamate receptors (iGluRs) have an integral ion channel, which opens upon receptor activation to allow conductance of cations such as sodium (Na^+), potassium (K^+) and calcium (Ca^{2+}) between the extracellular space and the neuron (MacDermott et al., 1986; Mayer and Westbrook, 1987). Another class of glutamate receptors, namely metabotropic glutamate receptors (mGluRs), mediates neurotransmission by binding to intracellular guanine nucleotide-binding proteins (or G proteins) once activated by glutamate or other agonists (Monaghan et al., 1989; Niswender and Conn, 2010).

Diversity in the types of depolarising responses mediated by iGluRs led to the classification of iGluRs based on selective agonists (Figure 1.2), which elicited distinct responses, and selective antagonists, which inhibited the distinct responses mediated by those selective agonists (Davies and Watkins, 1979; Honoré et al., 1988). Hence, these iGluRs were named according to the agonists that most potently and selectively activated them, i.e. (*S*)-α-amino-3-hydroxy-5-methylisoxazole-4-propionic acid (AMPA) activated receptors (AMPARs), *N*-methyl-D-aspartate activated receptors (NMDARs), and kainic acid activated receptors (KARs) (Davies and Watkins, 1981, 1985; Lodge, 2009). Analysis of the gene sequences that code for glutamate receptors initially suggested, and X-ray crystal structures of glutamate receptors later confirmed that functional glutamate receptors are assembled from modular proteins known as subunits (Hollmann et al., 1989; Armstrong et al., 1998; Sobolevsky et al., 2009). While there are amino acid sequence similarities between subunits that compose each family of iGluRs (AMPAR, NMDAR, and KAR), the differences between subunits are responsible for the variability in their regional- and developmental-specific functions (e.g. Lerma and Marques, 2013 and Paoletti et al., 2013).

Advances in molecular biology techniques led to the cloning of functional iGluRs based on DNA sequence homology to each other and led to the identification of genes that encode the four AMPAR subunits (GluA1-4), five KAR subunits (GluK1-5) and the seven genes that encode the NMDAR subunits (GluN1, GluN2A-D, GluN3A-B) (Hollmann et al., 1989; Bettler et al., 1990; Boulter et al., 1990; Nakanishi et al., 1990; Egebjerg et al., 1991; Moriyoshi et al., 1991; Hollmann and Heinemann, 1994). Subunits for another class of iGluR – known as delta (δ) receptors – were also cloned based on DNA sequence homology: GluD1 and GluD2 (Lomeli et al., 1993) (Figure 1.1). Over the years, different names have been used to refer to iGluR subunits, which was a cause for confusion when comparing studies of iGluRs from different research groups; therefore, the naming of the iGluR subunits was unified in 2010 to match the names of the subunit with the genes that encode them (Collingridge et al., 2009). Similarly, eight genes which code for mGluR subunits (mGluR1-8) were also discovered and classified into three groups (I, II and III) based on amino acid sequence homology, agonist pharmacology and second messenger systems that are activated following glutamate binding to mGluRs (reviewed in Niswender and Conn, 2010).

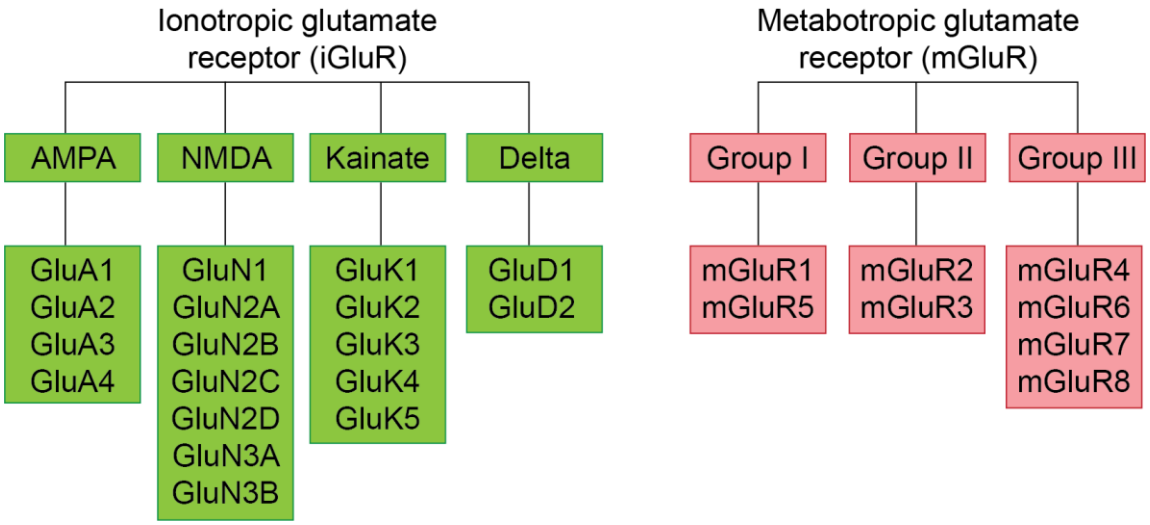

Figure 1.1. Classification of glutamate receptor subunits. Subunits for ionotropic glutamate receptors are divided into groups based on agonist pharmacology (AMPA, NMDA and kainate) and sequence homology (delta). Metabotropic glutamate receptor subunits are grouped (Group I-III) according to agonist pharmacology, second messenger systems and amino acid sequence homology.

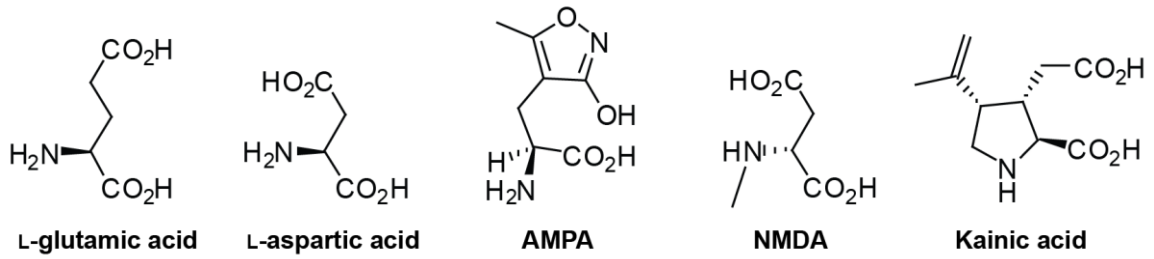

Figure 1.2. Agonists of ionotropic glutamate receptors. L-glutamate and L-aspartate were prototypic agonists of glutamate receptors before subtype selective agonists (AMPA, NMDA and kainic acid) were identified.

1.1.2. Structure of ionotropic glutamate receptors

The iGluR protein complex is formed by four subunits assembled in a dimer of dimer arrangement (e.g. Sobolevsky et al., 2009) (Figure 1.3). Each subunit in the protein contains an extracellular amino-terminal domain (ATD), an extracellular ligand binding domain (LBD), a transmembrane domain (TMD) which contains 3 membrane-spanning helices (M1, M3, M4) and a re-entrant loop (M2), and an intracellular carboxyl-terminal domain (CTD) (Sobolevsky et al., 2009). The semi-autonomous nature of the subunit domains was demonstrated by the fact that the LBD can be isolated and still formed dimers that are structurally similar to the LBD found in functional iGluRs (Kuusinen et al., 1995; Deming et al., 2003).

X-ray crystallography studies have revealed the structure of the full length iGluR complex at high resolutions (e.g. 3.6 Å, Sobolevsky et al., 2009) (Figure 1.4). The ATD of iGluR subunits contains a signal peptide (14–33 residues) that is responsible for trafficking the receptor to the plasma membrane but is cleaved upon successful assembly of the receptor (von Heijne, 1986; Hollmann et al., 1989; Traynelis et al., 2010). The numbering of amino acid sequences of AMPARs and KARs has traditionally omitted the signalling peptide whereas NMDAR amino acid numbering begins at the initiating methionine (Armstrong et al., 1998; Furukawa and Gouaux, 2003). This convention of amino acid numbering is followed in this thesis to aid comparisons with previous studies.

The subunit arrangement in the ATD layer of the GluA2 homomeric receptor structure is such that there are two local dimers – one dimer formed by subunits A and B, and the other

dimer formed by subunits C and D (Sobolevsky et al., 2009). From the ATD to the LBD, there is a crossover of the subunits that make up the two dimers – subunits A and D form one dimer, and subunits B and C form the other dimer in the LBD (Sobolevsky et al., 2009). In both the ATD and LBD, there is a two-fold axis of rotational symmetry whereas in the TMD, a four-fold rotational symmetry is observed (Sobolevsky et al., 2009; Karakas and Furukawa, 2014; Meyerson et al., 2014).

The X-ray crystal structure of the GluA2 homomeric tetramer revealed that the ATD of each iGluR subunit assumes a clamshell-like shape (Figure 1.3), which contains two lobes (R1 and R2) (Sobolevsky et al., 2009). In the dimer of dimer arrangement of the ATD layer of the GluA2 homomeric receptor, an inter-dimer interface is created by subunits B and D (Sobolevsky et al., 2009). In the case of the GluN1- and GluN2A-containing diheteromeric receptor, the subunit arrangement in the ATD is: GluN1-GluN2-GluN1-GluN2, with inter-dimer interactions occurring between the upper (R1) lobes of GluN1 and GluN2 whereas there is a weak interface between the R2 lobes (Karakas and Furukawa, 2014). The ATD contains binding sites for extracellular ligands such as Zn^{2+} (in the case of NMDARs) and allosteric modulators (Karakas et al., 2009; Perin-Dureau et al., 2002). The ATD also controls the kinetics of the ion channel, desensitisation of the receptor, trafficking of the receptor to the plasma membrane, assembly of the tetrameric receptor complex, and affects agonist and antagonist pharmacology (Kuusinen et al., 1999; Leuschner and Hoch, 1999; Ayalon et al., 2005; Yuan et al., 2009a). A significant difference between AMPAR and NMDAR structures is the greater interactions between the ATD and the upper lobe of the LBD in NMDARs, which gives NMDARs a more compact structure compared to AMPARs (Karakas and Furukawa, 2014). The ATD-LBD interface in NMDARs contains the binding site for allosteric modulators (Khatri et al., 2014).

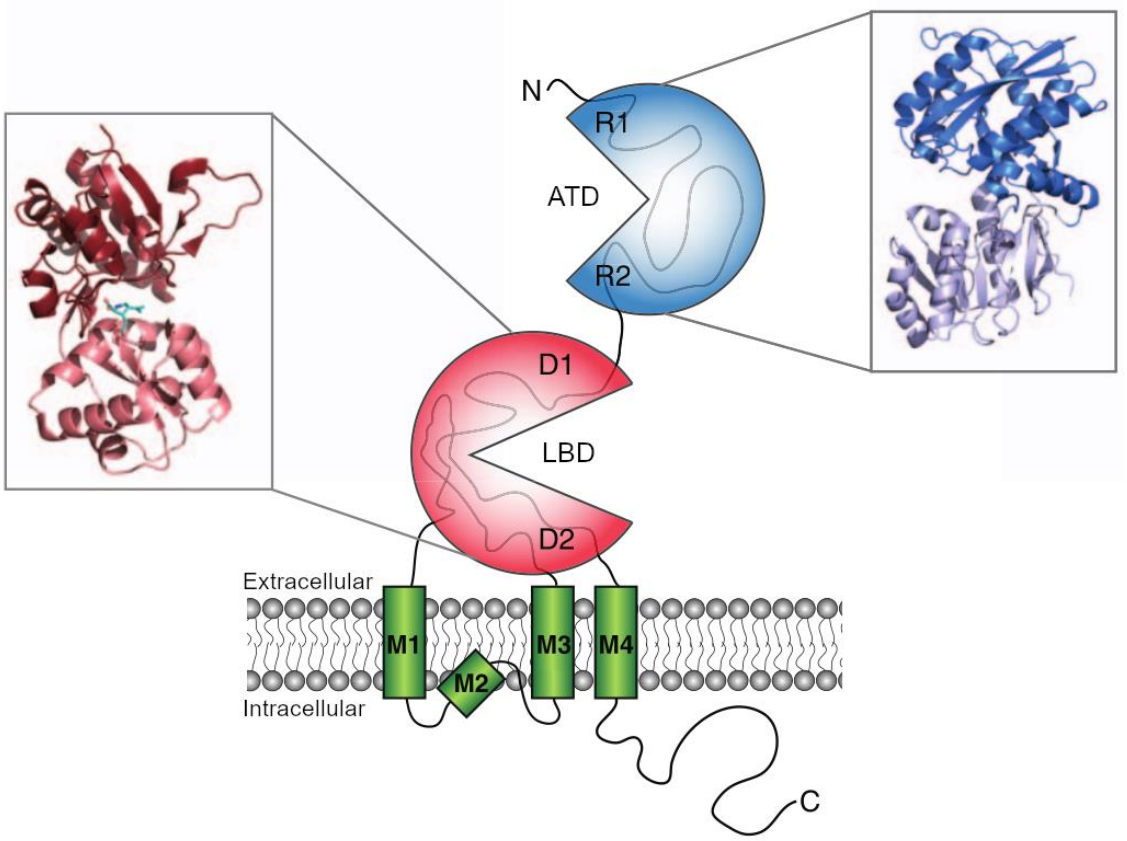

Figure 1.3. The topology of an ionotropic glutamate receptor subunit showing the X-ray crystal structure of the amino terminal domain and ligand binding domain. Topology of a KAR subunit depicting the amino terminal domain (ATD), ligand binding domain (LBD) and transmembrane domain (TMD). D1 and D2 are the lobes of the LBD whereas R1 and R2 corresponds to the lobes of the ATD. The TMD is composed of helices M1, M3 and M4 and the re-entrant loop (M2). Adapted from Contractor et al., (2011). Images of ATD and LBD structures in inset are from Kumar et al., (2009) and Mayer, (2005), respectively.

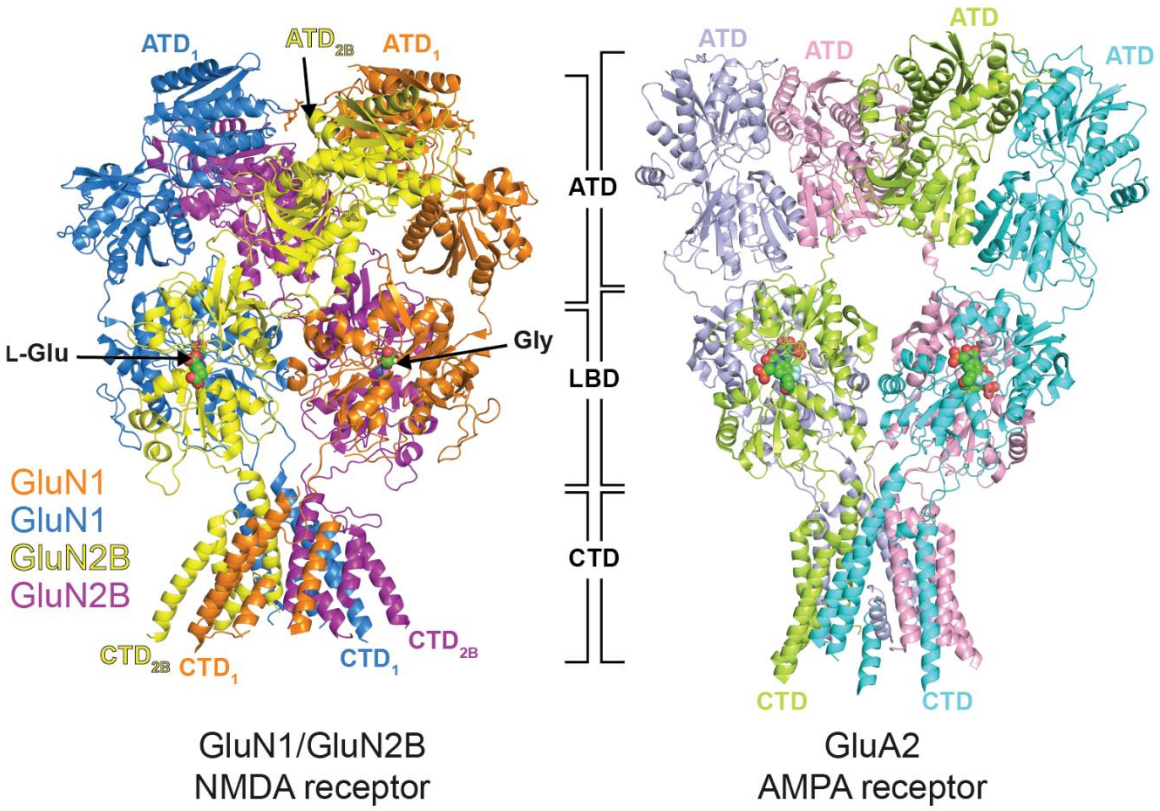

Figure 1.4. X-ray structure of NMDAR and AMPAR. Full length X-ray structure of the GluN1/GluN2 diheteromeric NMDAR (left) and the GluA2 homomeric AMPAR (right). The amino terminal (ATD) and carboxy terminal (CTD) domains of some subunits are labelled for clarity. L-glutamate (L-Glu) and glycine (Gly) bound to the NMDAR GluN2B and GluN1 subunits, respectively are shown as spheres. The NMDAR structure was taken from Karakas and Furukawa (2014) and the AMPAR structure was taken from Sobolevsky et al. (2009).

The LBD contains the glutamate binding site and has high sequence homology between subunits of the same iGluR family (Traynelis et al., 2010). The LBD of each subunit is formed from two peptide sequences, one of the sequences (S1) is formed by the polypeptide chain linking the ATD to the M1 helix of TMD whereas the other peptide sequence (S2) is formed from the polypeptide chain between M3 and M4 (Hollmann and Heinemann, 1994). The S1 and S2 polypeptide chains have been isolated and when artificially linked, form a water-soluble LBD (Hollmann and Heinemann, 1994; Armstrong et al., 1998). The LBD assumes a clamshell-like conformation which contains two lobes, D1 and D2, separated by a cleft in which glutamate and other orthosteric ligands bind (Figure 1.3 and Figure 1.4). The AMPAR crystal structure has revealed that the LBD layer of the iGluR has a dimer of dimer arrangement similar to the ATD (see above), but there is a crossover of subunits

compared to the ATD such that one LBD dimer is composed of subunits A and D, and the other dimer is composed of subunits B and C (Sobolevsky et al., 2009). This arrangement results in an inter-dimer interface between subunits A and C (Sobolevsky et al., 2009). The inter-dimer interface of AMPAR (GluA2 homomer) LBDs contains the binding sites for positive allosteric modulators (such as cyclothiazide and aniracetam), which block desensitisation of the receptor and causes slowing of deactivation (Sun et al., 2002; Jin et al., 2005). Studies in GluK2 homomeric receptors have also shown that stability of the LBD dimer interface affects the rate of desensitisation (Nayeem et al., 2011, 2013). In NMDARs (specifically the GluN1/GluN2A heterotetramer), the LBD dimer interface has an aromatic ring of a tyrosine residue (Tyr-535) from GluN1, which overlaps with the positive allosteric modulator aniracetam in AMPAR, acts as a naturally tethered ligand in the primary sequence (Furukawa et al., 2005). In summary, the inter-dimer interactions in the LBD layer determines the desensitisation and deactivation rates in iGluRs and the presence of Tyr-535 in NMDARs may explain the slower currents (less desensitisation and deactivation) produced by NMDARs compared to AMPARs.

Upon agonist binding to the LBD cleft, the LBD undergoes conformational changes leading to the closing of the D1–D2 cleft which pulls the S2 polypeptide chain linking the LBD to the TMD and leads to opening of the ion channel (Armstrong et al., 1998; Armstrong and Gouaux, 2000; Mayer, 2005). The movements of the receptor TMD caused by the LBD domain closure induces strain on the receptor complex, which is relieved by the opening of the LBD clamshell and the subsequent closing of the ion channel (Armstrong and Gouaux, 2000; Hansen et al., 2007). A significant feature of the AMPAR LBD is that alternative splicing creates two isoforms of the LBD termed flip and flop (Sommer et al., 1990) which affects receptor desensitisation and sensitivity to positive allosteric modulators (Mosbacher et al., 1994; Partin et al., 1994, 1995). For example, the AMPAR positive allosteric modulator cyclothiazide significantly inhibits the desensitisation of flip splice variants but only slows the rate of onset of desensitisation for the flop variant (Johansen et al., 1995; Partin et al., 1996).

The TMD contributes to the ion channel of the iGluR and contains amino acid sequences responsible for channel properties such as ion selectivity and gating (Hume et al., 1991; Watanabe et al., 2002). The core of an iGluR ion channel is composed of the

transmembrane helices M1, M3 and M4 from each of the four subunits in the tetrameric receptor complex (Wo and Oswald, 1995; Kuner et al., 2003). The inner cavity of the ion channel pore is formed by the M2 re-entrant loop from each subunit in the tetramer (Sobolevsky et al., 2009). At the apex of the re-entrant M2 loop of GluA2-containing AMPARs and GluK1 and GluK2 KARs is a glutamine/arginine RNA editing site (also known as Q/R site) which is subject to post-transcriptional modification by the enzyme adenosine deaminase (Sommer et al., 1991). Upon editing of the AMPAR or KAR Q/R site from glutamine (Q) to arginine (R), the Ca^{2+} permeability of the ion channel is significantly lowered (Burnashev et al., 1996). Editing at the Q/R site also renders AMPARs and KARs insensitive to block by intracellular and extracellular polyamines such as spermine and spermidine, which block the unedited (Q) receptor's ion channel (Bowie and Mayer, 1995; Donevan and Rogawski, 1995; Kamboj et al., 1995). In the brain, the Q/R site of the GluA2 subunit RNA is found almost exclusively in the edited form (containing arginine) (Seeburg et al., 1998). In GluN1 and GluN2 NMDAR subunits, the Q/R site equivalent always contains an asparagine (N) residue, which confers NMDARs with Ca^{2+} permeability and Mg^{2+} block of the ion channel pore (Burnashev et al., 1992a; Mori et al., 1992).

Amongst all domains of iGluRs, the CTD has the least amino acid sequence homology between each iGluR family and encodes docking motifs for intracellular binding proteins (Traynelis et al., 2010). The deletion of the CTD does not abolish the receptor's function but alters its regulation in some subunits (e.g. GluN1, GluN2A) (Köhr and Seeburg, 1996; Ehlers et al., 1998). Indeed, the regulation of iGluR activity by intracellular kinases depends on phosphorylation sites in the CTD (Tingley et al., 1997; Barria et al., 1997; Rivera et al., 2007). In addition, many iGluR subunits directly associate with signalling proteins; e.g. NMDAR subunits and type II Ca^{2+}/calmodulin-dependent protein kinase (CamKII) (Gardoni et al., 1998; Strack and Colbran, 1998). In summary, the CTD interacts with intracellular proteins that are involved in second messenger signalling, localisation of the receptor to specific cellular regions, stabilisation of the receptor within synapses, posttranslational modifications and targeting for degradation (Derkach et al., 1999; Boehm et al., 2006).

1.1.3. Accessory proteins of ionotropic glutamate receptors

In addition to the four subunits that form an iGluR complex, many accessory proteins that interact with iGluRs in the CNS have been described (Tomita, 2010; Lerma and Marques, 2013). Accessory proteins (also known as auxiliary subunits) have been shown to control the pharmacology and channel current kinetics of the receptor (Menuz et al., 2007; Kato et al., 2008) and affect trafficking and localisation of the receptor to the plasma membrane (Hashimoto et al., 1999; Tomita et al., 2003).

The importance of accessory proteins to iGluR function became apparent with the lack of agreement between studies using recombinant AMPARs expressed in heterologous systems and those using native AMPARs. Particularly, efficacy of agonists (measured as the currents mediated by AMPARs upon activation by glutamate) in recombinant AMPARs without accessory proteins is lower compared to the presence of accessory proteins (Tomita et al., 2003; Cho et al., 2007; Kott et al., 2007). These discrepancies were partly attributed to transmembrane AMPAR regulatory proteins (TARPs), which are accessory proteins of AMPAR found in native tissue (Chen et al., 2000; Tomita et al., 2003). TARPs are integral membrane proteins, which include four members; γ-2, γ-3, γ-4 and γ-8 (Chen et al., 2000; Tomita et al., 2003). TARPs can associate with AMPARs early during protein translation and trafficking (Vandenberghe et al., 2005). Additionally, TARPs may interact with AMPARs at the plasma membrane to increase single channel conductance, increase the channel open probability, increase the activation rate, slow the deactivation rate, and reduce desensitisation (Chen et al., 2003; Tomita et al., 2004, 2005; Carbone and Plested, 2016).

The majority of AMPARs in the brain are associated with TARPs (Fukata et al., 2005; Nakagawa et al., 2005). Association of TARPs with AMPAR subunits also seems to be subunit dependent (Soto et al., 2007, 2009; Kato et al., 2008). Indeed, the γ-2 TARP reduced AMPAR affinity for polyamine block but only in GluA2-lacking receptors (Soto et al., 2007). The γ-8 TARP is preferentially expressed in the hippocampus (Tomita et al., 2003) whereas in the cerebellum, most AMPARs are associated with the γ-2 TARP (Letts et al., 1998; Chen et al., 2000). Knockout mice lacking the γ-8 TARP produced AMPARs with reduced current amplitudes and impaired AMPAR neurotransmission in the hippocampus (Rouach et al., 2005). Therefore, the expression of γ-8 TARP is not necessary for AMPAR expression but does alter AMPAR function in the hippocampus.

In the case of KARs, the accessory proteins Neuropilin and tolloid-like protein-1 and -2 (Neto1 and Neto2), have been demonstrated to alter the onset and recovery from desensitisation of the ion channel (Zhang et al., 2009; Wyeth et al., 2014). Other accessory proteins including postsynaptic density protein 95 (PSD95) (Garcia et al., 1998), protein interacting with C kinase 1 (PICK1) and glutamate receptor interacting protein (GRIP) (Hirbec et al., 2003) have been shown to interact with KARs (see Lerma and Marques, 2013). The heterogeneity of the accessory proteins is believed to confer the KAR complex with the ability to mediate its multiphasic regulatory functions in the CNS (as discussed later).

In similarity with AMPARs, accessory proteins modulate KAR ion channel function and affects expression of KARs (Laezza et al., 2007; Copits et al., 2011; Tomita and Castillo, 2012). Native KARs have higher current amplitudes compared to recombinant KARs (Zhang et al., 2009). Subsequently, co-expression of KARs with Neto2 in cultured cerebellar granule cells resulted in currents with larger amplitudes in response to glutamate compared to KARs expressed without Neto2 (Zhang et al., 2009). Neto also slows the decay of the current following removal of glutamate (Zhang et al., 2009). This slowing of the KAR deactivation current by Neto suggests that steady state glutamate affinity of KARs may be higher in the presence of Neto and reconcile the difference in affinities between native and recombinant KARs.

Another critical effect of Neto on KAR-mediated EPSCs is the slowing of the KAR EPSC decay (Zhang et al., 2009; Straub et al., 2011). EPSCs mediated by KARs without Neto and EPSCs mediated by AMPARs have similar decay kinetics (Straub et al., 2011). However, in native conditions, KARs mediate slower decaying EPSCs compared to AMPARs (Castillo et al., 1997). The slower current of KARs may allow them to act as synaptic integrators of activity (Straub et al., 2011), whereby the slower decay of KAR EPSCs allows persistent AMPAR activity (which has faster decay) to depolarise the membrane potential and subsequently activate NMDARs and other intracellular mechanisms (discussed later).

Neto may not be necessary for trafficking of KARs to the plasma membrane because Neto knockout mice have KAR expression at synapses (Straub et al., 2011; Tang et al., 2011)

and expression of Neto in Xenopus laevis (X. laevis) oocytes increases glutamate-evoked KAR currents without increasing surface expression (Zhang et al., 2009). Moreover, Neto can also associate with other receptors (Ng et al., 2009; Ivakine et al., 2013) and may therefore act as general modulatory proteins at the plasma membrane. This has led to the theory that there may be two populations of KARs – those with and without Neto association (Lerma and Marques, 2013).

Neto1 was first suggested to act as an NMDAR-interacting protein as mice lacking Neto had impaired NMDAR-mediated synaptic plasticity and reduced GluN2A expression in the hippocampus (Ng et al., 2009). However, a subsequent study showed that Neto1 knockout did not affect expression of GluN1, GluN2A or GluN2B, and Neto1 knockout did not affect NMDAR current kinetics (Straub et al., 2011). Another study suggested that Neto1 may interact with the CTD of GluN2A subunits but not with the extracellular ATD or the TMD and therefore, may not be auxiliary subunits (Cousins et al., 2013). Another study has suggested that Neto protein may also regulate the expression of GluN2B-containing NMDARs in the cornu ammonis 3 (CA3) subregion of the hippocampus (Wyeth et al., 2014). More recently, genetic screening in C. elegans discovered a presynaptically released accessory protein known as NMDAR auxiliary protein 1 (NRAP-1) that may be critical for activation of NMDARs (Lei et al., 2017).

In summary, any investigation of iGluRs requires the consideration of the contribution of its accessory proteins. The effects of accessory proteins are particularly important in studies that employ glutamate (and possibly other orthosteric ligands) binding to the iGluR because accessory proteins affect the kinetics of glutamate induced currents. The possible influence of accessory proteins on the current study will be discussed in later chapters.

1.1.4. The roles of ionotropic glutamate receptors in neuronal signalling

What are the processes by which billions of neurons in the brain coordinate their activity? An important step in answering that question is to understand neurotransmission, the process by which activity in one neuron (presynaptic neuron) is transmitted to another (postsynaptic neuron). A brief introduction to neurotransmission, and the roles that iGluRs play in neurotransmission and activity dependent modulation in efficacy of neurotransmission is presented in this section. The specific roles of iGluRs studied in this

thesis, namely KARs and NMDARs, are discussed in subsequent sections. In this thesis, the study of glutamatergic neurotransmission was conducted in the hippocampus; therefore, the discussion of neurotransmission will be based on findings from the hippocampus but results from other brain regions will be discussed when relevant.

Prior to beginning the discussion on neurotransmission mediated by glutamate, it is necessary to briefly describe the molecular events underlying electrical activity in neurons. The membrane potential, or potential difference across the plasma membrane of a cell, is dependent on the concentrations of physiologically permeable ions (mainly Na^+, K^+ and Cl^-) across the membrane and the permeability of the membrane to those ions (Hodgkin and Huxley, 1952). Each ion separated by the plasma membrane is acted on by an electromotive force, which depends on the charge of the ion, and the ion's concentration gradient across the membrane; the force acting on the ion can be determined from the ion's equilibrium potential (the membrane potential at equilibrium, i.e. when there is no net flow of the ion across the membrane) and the membrane potential (which depends on the concentration gradients and membrane permeabilities of all permeable ions) (Hodgkin and Huxley, 1952). At rest, the ionic concentration gradients across the neuronal plasma membrane for the most permeable ions, namely Na^+, K^+, Cl^-, and Ca^{2+}, are maintained by (1) pumps that require the hydrolysis of adenosine triphosphate (ATP) to adenosine diphosphate (ADP) for energy, collectively known as ATPase pumps (e.g. Na^+/K^+-ATPase), and (2) ion exchangers, which use the concentration gradient of one ion species to transport another ion species across the membrane (e.g. Na^+/Ca^{2+} exchanger) (e.g. Rang and Ritchie, 1968; Philipson et al., 2002). The typical resting membrane potential in neurons (in the range of –85 mV to –60 mV in hippocampal pyramidal neurons) is due to (1) the Na^+/K^+-ATPase pump, which carries three Na^+ ions out of the cell for every two K^+ ions that are carried into the cell (Rang and Ritchie, 1968), and (2) the higher permeability of the plasma membrane to K^+ ions than Cl^- and Na^+ ions at rest (Hodgkin and Huxley, 1952). The membrane permeabilities of Ca^{2+} and Cl^- may also change during neurotransmission, leading to the disruption of resting concentration gradients for both Ca^{2+} and Cl^-; the resting concentration gradients for these ions are then restored (discussed later).

An action potential is a regenerative, all-or-none, electrical event caused by a voltage-dependent change in the plasma membrane's permeabilities to Na^+ and K^+ ions; and is

responsible for neurotransmission (discussed in 1.1.4.1). The neuron's membrane potential waveform during an action potential is determined mainly by the movement of Na^+ and K^+ ions across the plasma membrane (Hodgkin and Huxley, 1952). The initial rising phase of the action potential (depolarisation) is mediated by the influx of Na^+ into the neuron through voltage-gated sodium channels (VGSCs) due to the higher concentration of Na^+ outside the neuron compared to inside (Hodgkin et al., 1952; see Hille, 1992 for VGSCs). The influx of Na^+ ions drives the membrane potential towards the equilibrium potential of Na^+ (~60 mV); however, the VGSCs inactivate (see Hille, 1992). Inactivation of VGSCs coincides with the opening of voltage-gated potassium channels (VGKCs), which causes the efflux of K^+ down its concentration gradient (higher inside the cell than outside). The efflux of K^+ repolarises the membrane potential towards the K^+ equilibrium potential (approximately – 100 mV), which causes the membrane potential to become hyperpolarised (Hodgkin et al., 1952; see Hille, 1992). During hyperpolarisation, VGKCs inactivate and the membrane potential is restored to the resting membrane potential by the combined actions of (1) the Na^+/K^+-ATPase pump, and (2) potassium leak channels, which render the plasma membrane more permeable to K^+ than other ions at resting membrane potentials (Rang and Ritchie, 1968; Gustafsson et al., 1982; Storm, 1990).

1.1.4.1. Synthesis and release of the neurotransmitter glutamate

Neurotransmission takes place at the synapse, a specialised junction between the pre- and postsynaptic neurons (the term synapse was coined by Charles Sherrington; see Foster and Sherrington, 1897, p. 60, for an early description). Two types of synapses, which differ in their mechanism of transmission are known – electrical and chemical synapses. At electrical synapses, signalling occurs by passive flow of electrical current between neurons via specialisations known as gap junctions (reviewed in Bennett and Zukin, 2004, and Connors and Long, 2004). The more common type of synapses in the mammalian brain is the chemical synapse, which involves the release of a neurotransmitter from the presynaptic neuron (reviewed in Zucker et al., 2014). Glutamatergic synapses are chemical synapses that use glutamate as the neurotransmitter. The presynaptic portion of chemical synapses contains the active zone, which is an electron-dense entity containing the molecular machinery that participate in the release of the neurotransmitter (reviewed in Südhof, 2012). The postsynaptic side of excitatory synapses such as glutamatergic synapses contains a pronounced post-synaptic density (PSD) that contains receptor and effector

proteins, which sense the neurotransmitter and transduce the signal in the postsynaptic neuron (see Boeckers, 2006 for a review). At glutamatergic synapses, glutamate is packaged into synaptic vesicles in the terminals of the presynaptic neuron (Palay and Palade, 1955). Cytoplasmic glutamate in the presynaptic neuron is synthesised from α-ketoglutarate, which is an intermediate in the Kreb's cycle, by transaminases (e.g. Cho et al., 2001). Glutamate can also be synthesised from glutamine by the enzyme glutaminase (Hu et al., 2010). Glutamate in the presynaptic neuron is loaded into presynaptic vesicles via vesicular glutamate transporters (VGLUTs; VGLUT1-3) of which VGLUT1 is the predominantly expressed form in the hippocampus (van der Hel et al., 2009). VGLUTs use the H^+ ion concentration gradient (higher H^+ concentration inside the vesicle compared to the cytoplasm) created by the H^+-ATPase pump, to transport glutamate into the vesicle and counter-transport H^+ (reviewed in Ozkan and Ueda, 1998). The H^+-ATPase pump requires hydrolysis of cytosolic adenosine triphosphate (ATP) to adenosine diphosphate (ADP) to direct H^+ flow into the synaptic vesicle (Naito and Ueda, 1983). Vesicles in the presynaptic bouton are reversibly tethered by synapsin molecules to the presynaptic actin scaffold (Huttner et al., 1983). A subset of presynaptic vesicles is in close proximity to the presynaptic active zone (known as "docked"), possibly in readiness for exocytosis (Harris and Sultan, 1995). This set of vesicles may form a physiologically defined readily releasable pool of vesicles, which are available for release at a rapid time scale (Stevens and Tsujimoto, 1995).

An action potential reaching the presynaptic terminal results in the opening of P/Q- and N-type voltage-gated calcium channels (VGCCs), which are located near the docked vesicles in the presynaptic terminal, leading to a transient increase of Ca^{2+} ions in the presynaptic active zone (Koester and Sakmann, 2000). The transient Ca^{2+} increase is sensed by synaptotagmin I, which leads to the fusion of vesicular membrane with the presynaptic neuron plasma membrane and release of glutamate into the synaptic cleft (Fernández-Chacón et al., 2001). The fusion of vesicles with the presynaptic membrane is mediated by (1) SNAREs (for soluble NSF attachment receptor proteins; NSF: *N*-ethylmaleimide-sensitive factor) on the vesicular and target (the presynaptic neuron) membranes, and (2) SM proteins (for Sec1/Munc18-like proteins) (see Südhof, 2013 for a review). Vesicular SNAREs (v-SNAREs) include vesicle-associated membrane protein (VAMP), also known as synaptobrevin; and target SNAREs (t-SNAREs) include SNAP-25 and syntaxin

(Südhof, 2013). A complex between synaptobrevin, and SNAP-25 and syntaxin mediated by the SM proteins forces the vesicular and presynaptic membrane together in preparation for the fusion of two membranes (Söllner et al., 1993a). Fusion of the membranes causes release of the intravesicular glutamate into the synaptic cleft so that glutamate can passively diffuse to its targets.

The Ca^{2+} increase caused by the opening of VGCCs disrupts the resting electrochemical gradient for Ca^{2+}. The electrochemical gradient for Ca^{2+} is re-established by (1) buffering of intracellular Ca^{2+} by calcium binding proteins such as parvalbumin and calbindin, (2) uptake of Ca^{2+} into mitochondria and smooth endoplasmic reticulum, and (3) removal of Ca^{2+} ions from the neuron by ATP-dependent Ca^{2+} pumps and by Ca^{2+} exchangers (see Blaustein, 1988 for a review). Under prolonged influx of Ca^{2+}, the restoration of Ca^{2+} concentration gradient could take several minutes (e.g. Müller and Connor, 1991) and this clearance of Ca^{2+} could lead to successive action potentials to become increasingly effective in triggering neurotransmitter release (further discussed in 1.1.4.3). The SNARE proteins are made available for another round of exocytosis by the soluble ATPase NSF and α-SNAP (soluble NSF attachment protein) (Söllner et al., 1993b; Mayer et al., 1996). The process of recovering fused synaptic vesicles proceeds by the formation of a coat of clathrin molecules on the cytoplasmic face of the plasma membrane (Wickelgren et al., 1985). The clathrin coating increases the membrane curvature and initiates budding of the vesicular membrane (Heuser and Reese, 1973). The coated vesicles are “pinched off” the plasma membrane partly by the enzyme dynamin, following which the recycled vesicle enters the presynaptic pool (Heuser and Reese, 1973).

Glutamate in the synaptic cleft binds to glutamate receptors (both iGluRs and mGluRs) expressed on either the presynaptic (e.g. Berretta and Jones, 1996; Rodríguez-Moreno et al., 2000; Rusakov et al., 2005; McGuinness et al., 2010) or postsynaptic terminal (e.g. Collingridge et al., 1983; Malinow and Malenka, 2002). The glutamate concentration in the synaptic cleft is controlled by passive diffusion of glutamate (down its electrochemical gradient) away from the synaptic cleft and reuptake of glutamate via excitatory amino acid transporters (EAATs) located on astrocytes or neurons (Clark and Barbour, 1997; Bergles and Jahr, 1997). In hippocampal astrocytes, EAAT2 has the highest expression whereas EAAT3 is expressed in neurons at low levels (see Danbolt, 2001). Glutamate concentration

in astrocytes is kept low by the action of glutamine synthetase, which converts glutamate to glutamine (Martinez-Hernandez et al., 1977; Ottersen et al., 1992; Laake et al., 1995). The lower intracellular glutamate in astrocytes creates the concentration gradient by which EAATs can transport glutamate into astrocytes (reviewed in Marcaggi and Attwell, 2004). In addition to the glutamate concentration gradient, EAATs also use the electrochemical gradient of Na^+ and K^+ such that three Na^+ ions are co-transported with each glutamate (into the cell) and one K^+ ion is counter-transported (out of the cell) (Zerangue and Kavanaugh, 1996). Astrocytic glutamine, which is formed from glutamate, diffuses down its concentration gradient into the extracellular space and into the presynaptic neuron where it can be recycled to glutamate and packaged into vesicles for further release (reviewed in Danbolt, 2001). High levels of extracellular glutamate leads to the death of neurons due to activation of glutamate receptors, a phenomenon known as excitotoxicity (Lucas and Newhouse, 1957; Olney, 1969). Glutamate clearance from the extracellular space depends on the concentration gradients of Na^+ and K^+, which is maintained by the Na^+/K^+-ATPase pump (Rang and Ritchie, 1968). Neuronal death in animal models of ischaemia has been attributed to excitotoxicity caused by increased extracellular glutamate (Hirose and Chan, 1993; Fujisawa et al., 1993). The energy-dependent removal of glutamate from the synaptic cleft may be disrupted due to low ATP levels in ischaemia (e.g. Olney, 1971; Rothman, 1983) and exacerbate neuronal cell death.

1.1.4.2. Ionotropic glutamate receptors mediate neurotransmission

Ionotropic glutamate receptors contain an ion channel that opens when the receptor is activated following agonist binding (Sobolevsky et al., 2009). Through the open iGluR ion channel, cations such as Na^+, K^+ and Ca^{2+} may flow according to their electrochemical gradients across the plasma membrane. The permeabilities of AMPARs, KARs and NMDARs to Na^+ and K^+ ions (P_{Na} and P_K, respectively) are roughly equal – P_K/P_{Na} ~1.25 for AMPARs and KARs and P_K/P_{Na} ~1.14 for NMDARs (Jatzke et al., 2002). As described earlier, RNA editing of the Q/R site glutamine residue to arginine in AMPARs and KARs renders them Ca^{2+} impermeable (see section 1.1.2). However, NMDARs (GluN2A- or GluN2B-containing) have ~3-fold greater Ca^{2+} permeability compared to Q/R un-edited AMPARs and KARs (e.g. Burnashev et al., 1995).

The flow of ions through iGluRs produce synaptic currents, which can be recorded from groups of synapses using field potential recordings or from individual cells using intracellular recordings or whole-cell patch-clamp recordings (Figure 1.5) (Neher and Sakmann, 1976; MacDermott et al., 1986; Mayer and Westbrook, 1987). The iGluR channel gating properties (such as rates of activation, desensitisation and deactivation) define the time course of synaptic currents at glutamate synapses (Lester et al., 1990). The AMPA-preferring iGluRs (AMPARs) have fast activation and deactivation rates and show strong desensitisation, which limits AMPAR-mediated neuronal transmission to the millisecond time scale (Mosbacher et al., 1994; Edmonds et al., 1995; Erreger et al., 2004). However, currents mediated by KARs and NMDARs have slower activation and decay time courses compared to AMPAR currents (Figure 1.5B) (Monyer et al., 1992; Castillo et al., 1997; Kidd and Isaac, 1999, 2001). NMDAR activation has two important differences when compared to AMPARs. Firstly, NMDAR activation also requires binding of the co-agonist glycine in addition to glutamate (Johnson and Ascher, 1987; Kleckner and Dingledine, 1988). The second important difference is that at resting membrane potential (approximately –70 mV for hippocampal neurons), NMDARs are blocked by magnesium ions (Mg^{2+}) (Mayer et al., 1984; Nowak et al., 1984). The sensitivity of Mg^{2+} block of NMDARs is dependent on the subunit composition of NMDARs such that GluN2A- or GluN2B-containing NMDARs have higher sensitivity to Mg^{2+} block compared to GluN2C- or GluN2D-containing NMDARs (Mayer et al., 1984; Nowak et al., 1984; Monyer et al., 1992). NMDARs also have higher Ca^{2+} permeability but slower activating and desensitising currents than AMPARs and KARs; therefore, NMDAR currents activate in milliseconds and deactivate between tens and thousands of milliseconds with minimal desensitisation (Monyer et al., 1992; Vicini et al., 1998; Wyllie et al., 1998).

Movement of cations across AMPARs and KARs has multiple effects on the cell: firstly, the influx of Na^{+} along its concentration gradient leads to depolarisation of the membrane potential from the resting potential towards the threshold voltage required for generation of an action potential (Geiger et al., 1997). When the sum of membrane voltage caused by synaptic currents exceeds the threshold required for an action potential, voltage-dependent sodium channels in the axon initial segment are activated, which leads to the formation of an action potential within the postsynaptic neuron (e.g. Colbert and Johnston, 1996). The second consequence of activation of AMPARs and KARs is that the resultant

depolarisation also facilitates the removal of Mg^{2+} from the NMDAR channel pore, allowing Ca^{2+} ions to enter the cell through the open NMDARs (Mayer et al., 1984; Ascher and Nowak, 1988; Monyer et al., 1992). The increased intracellular Ca^{2+} acts as a second messenger and leads to (1) modulation of AMPAR trafficking to the plasma membrane, (2) modulation of AMPAR channel conductance due to phosphorylation (or dephosphorylation) by intracellular kinases (or phosphatases), and (3) synthesis of AMPAR proteins (Kang and Schuman, 1996; Huber et al., 2000; Scheetz et al., 2000; Lee et al., 2000; Huang et al., 2002). In summary, glutamate mediates fast excitatory synaptic transmission in synapses of the CNS by activating iGluRs, which have varied channel properties owing to its subunit heterogeneity.

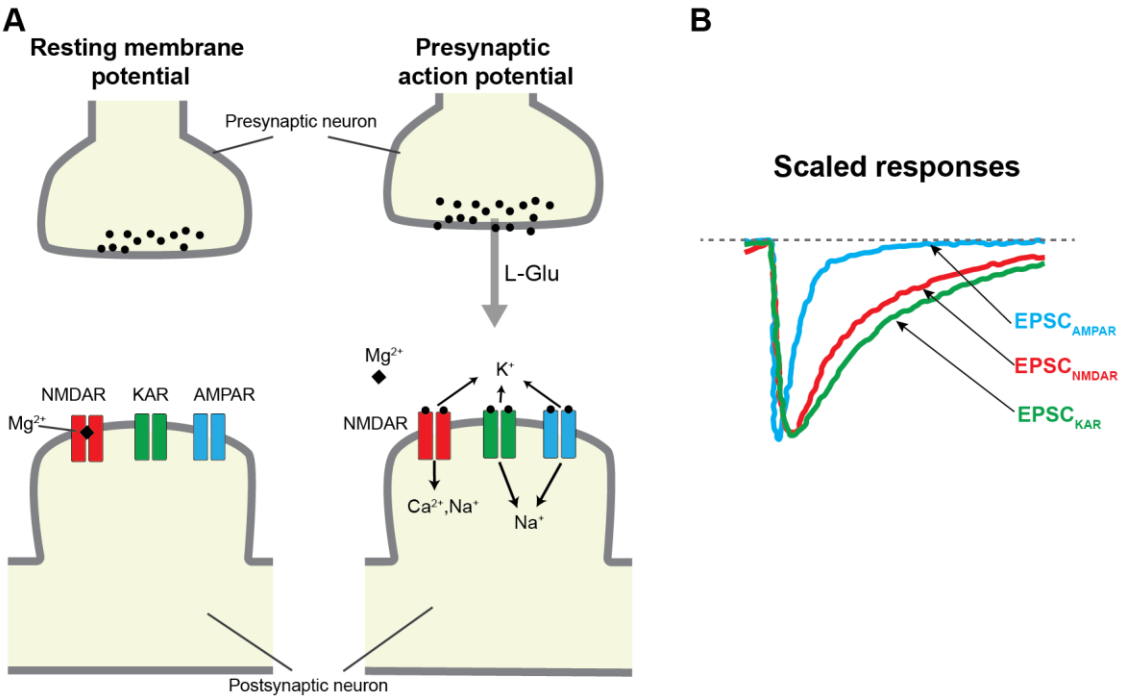

Figure 1.5. Ionotropic glutamate receptors mediate neurotransmission. A, Glutamate (L-Glu) release by a presynaptic action potential leads to activation and ion flux into the cell through AMPARs, KARs and NMDARs. The Mg^{2+} block of NMDARs at resting membrane potential is relieved by depolarisation of the postsynaptic neuron caused by activation of AMPARs and KARs and the subsequent influx of ions Na^{+}. **B,** Schematic showing scaled responses (excitatory postsynaptic current or EPSC) from postsynaptic neurons highlight the slower rate of decay of KAR- and NMDAR-mediated EPSCs compared to the AMPAR mediated EPSC (based on (Lerma and Marques, 2013)).

1.1.4.3. Ionotropic glutamate receptors mediate induction of synaptic plasticity

Even before the discovery of the mechanisms underlying neurotransmission at the neuromuscular junction, the possibility of neuronal changes that might explain the basis of learning and memory were suggested. The Polish psychologist Jerzy Konorski coined the term "plasticity" in reference to the nervous system to describe the ability of neurons in the cortex to undergo "*certain permanent functional transformations*" that might explain the mechanisms underlying learning in the brain (Konorski, 1948). The Canadian psychologist Donald Hebb formulated a theory of how learning might occur in the brain (Hebb, 1949). Hebb's postulate was that "*when an axon of cell A is near enough to excite a cell B and repeatedly or persistently takes part in firing it, some growth process or metabolic change takes place in one or both cells such that A's efficiency, as one of the cells firing B, is increased*" (Hebb, 1949). Given that synapses are the regions that allow transmission of activity between neurons, synapses which encode information must be those that support the activity-dependent change in efficacy of synaptic transmission (synaptic plasticity) and if the plasticity at the synapse follows Hebb's rules, it is often referred to as a Hebbian synapse. Hebb also theorised that in the brain, memories are represented by an ensemble of neurons connected together in order to build a memory structure (he referred to this ensemble as a cell assembly), and that a series of cell assemblies fire consecutively to form a phase sequence, which represents a more complete mental model or a "train of thought" (Hebb, 1949).

In the 1970s, the first detailed description of long-lasting potentiation in the CNS was published (Bliss and Lømo, 1973; Bliss and Gardner-Medwin, 1973). Bliss and colleagues demonstrated that tetanisation (trains of high frequency stimulation) of perforant path fibres (presynaptic axons) from the entorhinal cortex, which projects to granule cells (postsynaptic cell) in the hippocampus, produced a long-term potentiation (LTP) of extracellularly recorded postsynaptic responses (Bliss and Lømo, 1973). The study of this phenomenon was greatly aided by the development of the in vitro hippocampal slice preparation, which allows (1) stable extracellular and intracellular recordings, (2) application of pharmacological agents to the extracellular environment and (3) access to dentate gyrus and all cornu ammonis (CA) regions of the hippocampus and the pathways between the cells of these regions (Andersen et al., 1971; Skrede and Westgaard, 1971). Hippocampus-targeted lesion studies in animals, and results from surgical excision of parts

of temporal cortex, including the hippocampus in humans, have suggested that the hippocampus is responsible for processing of at least some forms of memory; including processes involved in spatial and declarative memory (e.g. O'Keefe and Dostrovsky, 1971; O'Keefe and Nadel, 1978; Morris et al., 1990; Squire, 1992; VanElzakker et al., 2008). Therefore, the study of hippocampal LTP has become an established model for the study of synaptic plasticity in the mammalian brain and the quest to understand the physiological basis of learning and memory. In this section, the features of LTP and the early links between LTP and iGluRs (AMPARs, KARs and NMDARs) in the hippocampus will be described. In the subsequent sections (1.2.5 and 1.3.7), more specific roles that KARs and NMDARs fulfil in synaptic plasticity will be discussed.

While LTP was first observed using in vivo extracellular recordings from a population of neurons (Bliss and Lømo, 1970, 1973), the potentiation of synaptic signalling during LTP can also be recorded from individual postsynaptic neurons using intracellular recording techniques such as the whole-cell configuration of the patch clamp technique (e.g. Cormier and Kelly, 1996; Stricker et al., 1999). LTP can be induced by delivering a train of pulses (typically between 50-100) at a frequency of 100 Hz or more to the afferent pathway of interest (a protocol known as high frequency stimulation or HFS) (Dunwiddie and Lynch, 1978). LTP can also be induced by the theta burst stimulation (TBS) protocol which involves 10 bursts of 4 shocks at 100 Hz delivered at an interval of 200 ms (Larson et al., 1986). The interval of 200 ms between the bursts represents frequency in the theta range (4-5 Hz), which is a neuronal firing rate observed for the hippocampus cornu ammonis (CA) 1 pyramidal cells and dentate granule cells from in vivo electroencephalograph (EEG) recordings (Bland et al., 1980; Larson et al., 1986). When recording from individual neurons, two additional protocols can be used for induction of LTP, namely pairing and spike timing. In the pairing protocol, single afferent stimuli repeated at low frequency (e.g. 0.1 Hz) are paired with depolarising pulses (lasting 200 – 400 ms) that induce firing of the postsynaptic neuron (Abraham et al., 1986). In the case of spike timing, potentiation (spike timing-dependent potentiation, or STDP) is induced when a single afferent stimulus is paired with a brief depolarisation of the postsynaptic neuron that fires the postsynaptic neuron only once (Kelso et al., 1986; Bi and Poo, 1998). The timing between pre- and postsynaptic firing in STDP is critical – presynaptic stimulus must precede the firing of the postsynaptic neuron for induction of LTP (Bi and Poo, 1998).

Not all changes in synaptic efficacy represent long-term potentiation. Two transient forms of synaptic plasticity are observed when a pair of stimuli is delivered to the target pathway of interest – facilitation and depression. Initially discovered in the neuromuscular junction, transient facilitation and depression during paired-pulse stimulation, was also observed at hippocampal synapses (McNaughton, 1980). When the interstimulus interval between the paired pulses is less than ~100-150 ms, the response to the second pulse is larger in its magnitude when compared to the first, i.e. paired-pulse facilitation (PPF) (Eccles et al., 1941; McNaughton, 1980). PPF is caused by an increase in Ca^{2+} levels in the presynaptic terminal following the first stimulus, which causes an increase in the probability of neurotransmitter release for a subsequent stimulus (Wu and Saggau, 1994). In contrast to PPF, depression of the second response compared to the first during paired pulse stimulation at short interstimulus intervals can be observed in synapses with high probability of neurotransmitter release (Zucker and Regehr, 2002). The primary reason for transient depression is believed to be a decrease in presynaptic probability of neurotransmitter release following the first stimulus through depletion of readily releasable vesicles; this was suggested by experiments in which extracellular Ca^{2+} was artificially reduced thus leading to decrease in probability of neurotransmitter release, which led to attenuation of depression compared to normal extracellular Ca^{2+} (e.g. Betz, 1970 and Dittman and Regehr, 1998). However, release from presynaptic terminals can also be affected by autoreceptors on the presynaptic terminal's plasma membrane, which are activated by neurotransmitter released by the first stimulus and lead to a negative feedback loop in order to reduce neurotransmitter release from subsequent stimuli (Davies et al., 1991). Therefore, paired-pulse facilitation and depression are generally considered as presynaptic phenomena and paired-pulse stimulation has been used to investigate the locus of expression of synaptic potentiation (McNaughton, 1980, 1982). However, some postsynaptic forms of PPF and PPD have also been discussed in the literature (e.g. Rozov and Burnashev, 1999; Brenowitz and Trussell, 2001).

LTP is defined by three hallmark features that highlight its suitability as a physiological model for information storage: input specificity, cooperativity and associativity. Input specificity is a feature of Hebb's postulate such that firing in the postsynaptic neuron ("cell B") is mediated by persistent activity in the presynaptic neuron ("cell A") (Hebb, 1949). The input specificity of LTP was first described by studies using the transverse

hippocampal slice preparation in which two sets of fibres converging onto the CA1 pyramidal cell dendrites were activated independently of each other (Andersen et al., 1977; Lynch et al., 1977). Tetanisation of either pathway caused selective potentiation in that pathway and not the other pathway (Andersen et al., 1977). However, input specificity recorded by two-pathway experiments does not necessarily guarantee that there is specificity of potentiation at the synapse level. Synapse specificity was investigated intracellularly using spatially restricted induction of LTP at specific synapses (using the pairing protocol), which suggested that synapse specificity breaks down at distances < 70 µm but specificity is maintained at distances > 100 µm (Engert and Bonhoeffer, 1997).

The cooperativity feature of LTP induction means that a threshold number of inputs needs to be co-activated for LTP to be induced, meaning that "weak" tetani activating relatively few afferent fibres do not trigger LTP (McNaughton et al., 1978). An extension of the cooperativity idea is that LTP is associative, meaning that a weak tetanus otherwise insufficient to induce LTP would induce LTP if paired with a strong tetanus in an independent input onto the same postsynaptic neuron (McNaughton et al., 1978; Levy and Steward, 1979). The threshold requirement for induction of LTP was highlighted by studies in which a "sub-threshold" tetanus led to a transient form of potentiation of synaptic responses, post-tetanic potentiation (PTP), which decayed to baseline levels within minutes but did not produce a long-term increase in synaptic efficacy (McNaughton, 1982). PTP is caused by an increase in Ca^{2+} in the presynaptic terminal which gradually decayed to pre-tetanic levels as the increased Ca^{2+} was cleared (Wu and Saggau, 1994).

In addition to the perforant path to granule cell synapses, LTP was also demonstrated at many other synapses in the CNS; including the neurons of layers II-IV of visual cortex (Artola and Singer, 1987), and in the motor cortex after stimulation of sensory cortex fibres (Sakamoto et al., 1987), and neurons in the lateral and basolateral nuclei of the amygdala after stimulation of the external capsule (Chapman et al., 1990), to mention a few. Perhaps the most extensively characterised synapse in relation to synaptic plasticity is the Schaffer collateral to CA1 pyramidal cell (SC-CA1) synapse of the hippocampus (Figure 1.6) (Andersen et al., 1977; Collingridge et al., 1983; Bortolotto et al., 1999; Volianskis and Jensen, 2003; Christie and Jahr, 2006).

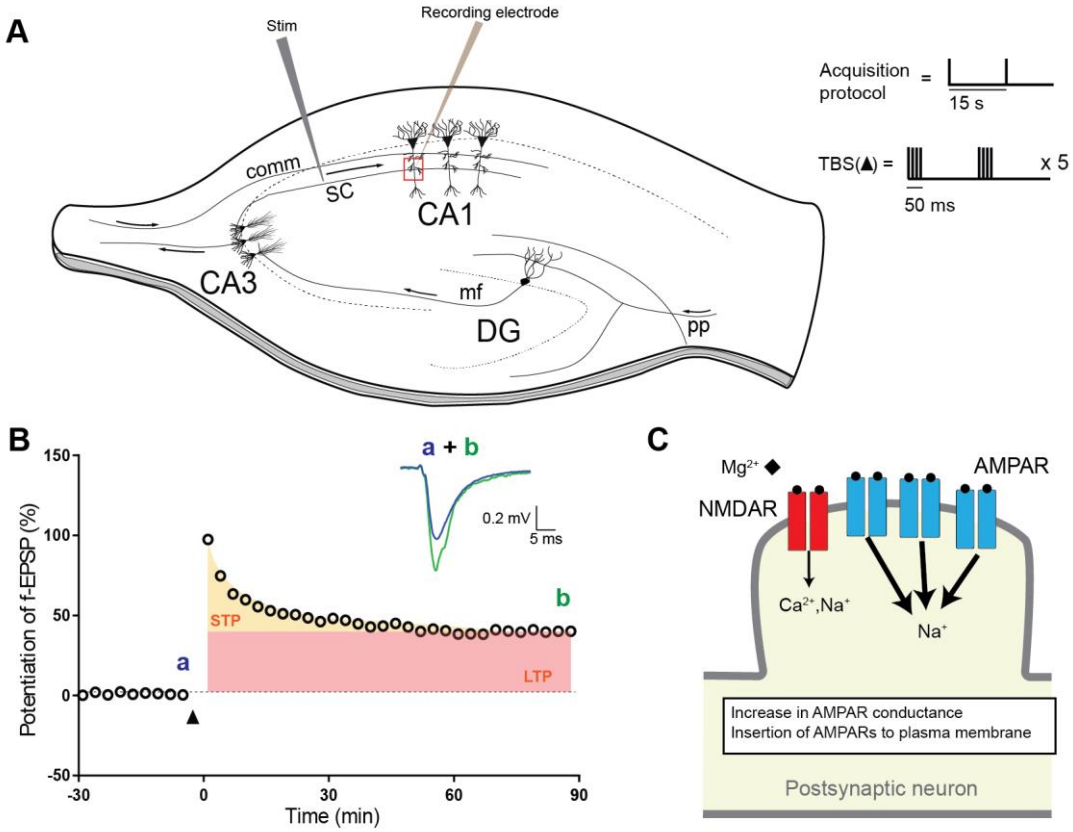

Figure 1.6. Potentiation of synaptic responses in the hippocampus. A, the hippocampal slice preparation has been used extensively to study synaptic plasticity (Skrede and Westgaard, 1971). The perforant path (pp) fibres originate from the entorhinal cortex and form synapses with dentate gyrus principle cells. The mossy fibre (mf) axons originate from the dentate gyrus (DG) principle cells and synapse with CA3 principle cells. The Schaffer collateral (SC) axons and commissural (comm) axons originate from the principle cells of the cornu ammonis (CA) 3 region of the hippocampus of the same and opposite brain hemispheres, respectively. Sch and comm fibres form synapses with pyramidal cells of the CA1 region (SC-CA1). Pulses are delivered to the Sch and comm axons using a stimulation electrode (Stim) and extracellular field excitatory postsynaptic potential (f-EPSP) responses are recorded from the SC-CA1 synapses (red box). Responses are acquired at a frequency of $\frac{1}{15}$ Hz whereas potentiation can be induced using a theta burst stimulation (TBS) protocol. **B,** tetanisation of SC-CA1 axons using TBS (arrowhead) leads to a sudden increase in synaptic responses short-term potentiation (STP), which decays to a stable long-term potentiation of synaptic responses (LTP). Recording of post-tetanic potentiation (PTP) was avoided by pausing stimulation for 3 min after tetanus. **C,** potentiation in the SC-CA1 synapses is induced by Ca^{2+} entry through NMDARs and activation of Ca^{2+}-dependent kinases; in the postsynaptic neuron, this leads to an increase in AMPAR conductance and increased AMPAR trafficking to the membrane.

The identity of the neurotransmitter that mediated signalling at the excitatory synapses that displayed LTP in hippocampus was resolved about a decade after the discovery of LTP (Dolphin et al., 1982). Dolphin and colleagues used the push-pull cannula technique to demonstrate that glutamate concentration is increased during LTP at the perforant path to dentate gyrus granule cell synapse, suggesting that glutamate was the neurotransmitter that was responsible for LTP (Dolphin et al., 1982). This finding complemented previous investigations (Biscoe and Straughan, 1966; Storm-Mathisen and Iversen, 1979) and was corroborated by later studies using the dialysis electrode technique (Walker et al., 1995) and antibody staining of glutamate (Ottersen et al., 1990), together showing that glutamate is indeed the excitatory neurotransmitter at hippocampal synapses. Investigations of the molecular mechanisms underlying LTP were aided by the development of subtype-selective glutamate receptor antagonists (Davies et al., 1981a; Watkins and Jane, 2006).

Collingridge and colleagues demonstrated first that the NMDAR-selective antagonist D-2-amino-5-phosphonopentanoic acid (D-AP5) blocked the induction of LTP at the SC-CA1 synapse, suggesting that NMDAR activation was critical for the induction of LTP (Collingridge et al., 1983). Application of D-AP5 during baseline neurotransmission or after induction of LTP did not affect the synaptic responses (specifically, the f-EPSPs); therefore, D-AP5 blocked the induction of LTP and not baseline transmission nor the maintenance of LTP (Collingridge et al., 1983). In another study, Lynch and colleagues demonstrated that injection of the calcium chelator ethyleneglycol-bis-(β-aminoethylether)-*N*,*N*,*N′*,*N′*,-tetraacetic acid (EGTA) into the postsynaptic CA1 neuron blocked the induction of LTP at SC-CA1 synapses, suggesting that a rise in postsynaptic Ca^{2+} was also critical for induction of LTP (Lynch et al., 1983). Following the two observations described above, it was found that NMDAR activation is voltage-dependent and that at the resting membrane potential, NMDARs are blocked by extracellular Mg^{2+}; the Mg^{2+} block was relieved by depolarisation of the plasma membrane during depolarisation (Mayer et al., 1984; Nowak et al., 1984). At synapses, dependence of the induction of LTP on postsynaptic depolarisation was observed in intracellular studies in which the postsynaptic depolarisation could be paired to presynaptic stimuli (Kelso et al., 1986; Malinow and Miller, 1986; Gustafsson et al., 1987). Further investigations examining the equilibrium potential created by NDMAR opening, and the use of Ca^{2+} sensitive dyes revealed that NMDARs were permeable to Ca^{2+} (Ascher and Nowak, 1988; MacDermott

et al., 1986). Taken together, these findings provided an explanation for the synaptic changes that underlie induction of synaptic plasticity at the SC-CA1 synapse; i.e. glutamate release from presynaptic cell and subsequent binding to NMDARs leads to Ca^{2+} influx provided that the postsynaptic neuron is sufficiently depolarised to remove the Mg^{2+} block (Figure 1.6B and C) (Collingridge, 1985). Indeed, these observations explain the Hebbian features of LTP, the requirement of concurrent activity in pre- and postsynaptic neurons, synapse specificity, cooperativity and associativity.

As mentioned earlier, D-AP5 application does not affect the baseline neurotransmission in LTP experiments (Collingridge et al., 1983). Pharmacological studies using AMPAR-selective antagonists found that synaptic population responses to low frequency stimulation (e.g. $\frac{1}{15}$ Hz) of afferent fibres at the SC-CA1 synapse are mediated by AMPARs on the postsynaptic neuron (Davies and Collingridge, 1989). While the role of NMDARs in inducing LTP was established, it was becoming clear that NMDAR activation is not the only mechanism by which LTP can be induced at synapses, including the SC-CA1 synapse. The rise in intracellular Ca^{2+} during LTP can come from a variety of sources, such as opening of calcium channels or through release of Ca^{2+} from intracellular sources (e.g. smooth endoplasmic reticulum); LTP can even be induced by activation of Ca^{2+}-permeable AMPARs, and L-type voltage-gated calcium channels using different protocols from that required for the NMDAR-dependent form of LTP (Jia et al., 1996; Plant et al., 2006; Grover and Teyler, 1990). Furthermore, blockade of KARs inhibits induction of LTP at the mossy-fibre to CA3 pyramidal cell (MF-CA3) synapse (Bortolotto et al., 1999). Therefore, AMPARs, KARs and NMDARs all can play a role in inducing long-term synaptic plasticity in the hippocampus and a role for mGluRs in the induction of LTP has also been described (Bashir et al., 1993; Bortolotto and Collingridge, 1993).

Long-term depression (LTD) of synaptic responses has also been observed (Lynch et al., 1977). Induction of LTD requires a different set of protocols compared to LTP and, at some synapses, requires NMDARs and/or mGluRs for its induction (e.g. NMDAR-dependent LTD at the SC-CA1 synapse can be induced in slices from juvenile rats by delivering 900 pulses at 1 Hz pulse) (e.g. Kemp et al., 2000). LTP has been further characterised based on its temporal features and sensitivity to kinase inhibitors (McNaughton, 1982; Kauer et al., 1988). Particularly, the initial decaying phase of potentiation following PTP, which lasts

for 30-60 min and precedes the long-lasting non-decremental component of stable LTP, is referred to as short-term potentiation (STP) (Figure 1.6B). STP, like the stable phase of LTP, is absent when NMDARs are pharmacologically blocked during induction (Collingridge et al., 1983; Malenka, 1991). Induction of STP depends also on the transient rise in postsynaptic Ca^{2+} (Malenka et al., 1988; Anwyl et al., 1988; Malenka et al., 1992).

Although the discussion above has focused on the induction mechanisms that trigger potentiation, the expression mechanisms that underlie STP and LTP have also been studied. An early indication that STP and LTP may be expressed by different mechanisms was that STP cannot but LTP can be blocked when protein kinase C (PKC) is pharmacologically inhibited (Kauer et al., 1988). The non-decremental phase of potentiation (LTP) is further classified as early-LTP (E-LTP) and late-LTP (L-LTP) based on its onset of expression and sensitivity to protein synthesis inhibitors (Krug et al., 1984; Frey et al., 1988). Application of protein synthesis inhibitors, inhibitors of mRNA transcription, or inhibitors of PKMζ, which is the autonomously active catalytic domain of the PKC isoform PKCζ, during the induction of potentiation prevents the expression of L-LTP, which begins ~2 hours after LTP induction, but does not prevent expression of E-LTP (Krug et al., 1984; Frey et al., 1988; Ling et al., 2002; Serrano et al., 2005). Moreover, many kinases (including PKA and CaMKII) are believed to play a role in the expression of E-LTP (Malenka et al., 1986; Malinow et al., 1989; Ito et al., 1991; Silva et al., 1992; Huang and Kandel, 1994). In addition to kinases, many secondary messengers and retrograde messengers (such as nitric oxide and arachidonic acid), which communicate between the pre- and postsynaptic compartments have been demonstrated to be involved in the induction and expression of LTP (Dumuis et al., 1988; Williams and Bliss, 1988; Böhme et al., 1991; Son et al., 1996). Pre- and postsynaptic forms of LTP have been described, whereas the precise understanding of the mechanisms that regulate their induction and expression are still under discussion (reviewed in MacDougall and Fine, 2013, and Padamsey and Emptage, 2013).

1.2. Kainate receptors

Much of the knowledge regarding the physiological significance of iGluRs comes from studies employing subtype-selective pharmacological tools. However, the identity of the subunit within the iGluR complex affects the pharmacological and physiological features of the receptor (Chittajallu et al., 1999). The KAR subtype family of iGluRs contains five

subunits, GluK1-5, which have structural and amino acid sequence similarities to AMPAR and NMDAR subunits (Bettler and Mulle, 1995; Traynelis et al., 2010). The principle subunits GluK1, GluK2 and GluK3 can form homomeric glutamate-gated ion channels in heterologous expression systems (Herb et al., 1992). However, native KARs exist in the heteromeric form containing GluK4 and/or GluK5 subunits in addition to the principle subunits (Werner et al., 1991; Herb et al., 1992). The structural diversity of KARs is increased by the presence of splice variants of GluK1-3 with a different cytoplasmic carboxy-terminal domain (CTD) amino-acid sequence, which may affect the modes of cellular trafficking and associations with intracellular proteins of the KAR (Contractor et al., 2011; Lerma and Marques, 2013).

Development of subunit-selective antagonists is a significant avenue to aid future studies of KARs. An aim of this thesis is to develop novel GluK2-selective competitive antagonists. In this section, the rationale for development of novel subunit-selective antagonists is made by firstly discussing currently available pharmacological tools such as agonists, antagonists and allosteric modulators of KARs. Secondly, studies investigating the roles of KARs in synaptic signalling are discussed, which highlight the need for better competitive antagonists with selectivity for GluK2 over other iGluR subunits. Thirdly, studies investigating the therapeutic potential of KAR antagonists are described to show that GluK2-selective antagonists may help to better understand the roles of KAR subunits in pathophysiology and may lead to the development of more selective therapeutic agents.

1.2.1. Agonists of kainate receptors

Kainic acid (Figure 1.7), a glutamate analogue isolated from the seaweed Diegenea simplex (Nitta et al., 1958; Shinozaki and Konishi, 1970) is a potent agonist for KARs. The structurally related domoic acid is a higher potency KAR agonist than kainate on GluK1 and GluK2 but not GluK3 (Biscoe et al., 1975; Schiffer et al., 1997). Domoic acid acts as a selective agonist of KARs over AMPARs at low concentrations (Bureau et al., 1999) and produces non-desensitising currents from KARs (Christensen et al., 2004a). Other agonists of KARs include (2*S*,4*R*)-4-methylglutamate (SYM2081, Figure 1.7), quisqualate and the synthetic glutamate derivative, AMPA which activates recombinant GluK2/GluK5 heteromeric KARs (Alt et al., 2004; Mayer, 2005).

While the KAR agonists described above also activate AMPARs, SYM2081 was reported to have weaker effects on AMPARs compared to KARs (Jones et al., 1997; Zhou et al., 1997; Donevan et al., 1998; Alt et al., 2004). An analogue of SYM2081, (2*S*,4*R*)-4-[3-(2-naphthyl)-2-(*E*)-propenyl]glutamic acid (LY339434, Figure 1.7), was reported to have high affinity on GluK1 with much lower affinity on GluK2, GluA1, GluA2 and GluA4 (Small et al., 1998; Baker et al., 2000). Another class of agonists showing KAR over AMPAR selectivity was based on neodysiherbaine (neoDH, Figure 1.7), a naturally occurring analogue of the 4-substituted glutamate analogue, dysiherbaine, isolated from the marine sponge Dysidea herbacea (Sakai et al., 1997). Particularly, analogues such as 8-deoxy-neoDH, 9-F-8-epi-neoDH and 9-deoxy-neoDH had high affinity on GluK1 compared to GluK2, GluK3, GluK5, GluA1 and GluA2 (Lash et al., 2008). Selectivity for KAR over AMPAR was also reported with derivatives of the natural product willardiine, which can be isolated from the seeds of Acacia willardiiana. Notably, (*S*)-5-iodowillardiine (Figure 1.7) has high affinity for GluK1 and selectivity for KAR vs. AMPARs and NMDARs (Jane et al., 1997). Another KAR selective agonist is the AMPA analogue, (*S*)-2-amino-3-(5-tert-butyl-3-hydroxy-4-isoxazolyl)propionic acid (ATPA, Figure 1.7), which activated recombinant GluK1 receptors with > 1000-fold greater affinity compared to AMPARs (Alt et al., 2004).

Despite the development of GluK1 over AMPAR selective agonists such as ATPA and 5-iodowillardiine, GluK2-selective agonists are still unavailable. An important consideration when comparing activity of most KAR agonists mentioned above (with the notable exception of domoic acid) is that they produce fast desensitisation of KARs which must be overcome using a desensitisation blocker such as the plant lectin, concanavalin A (con A) (Wong et al., 1994).

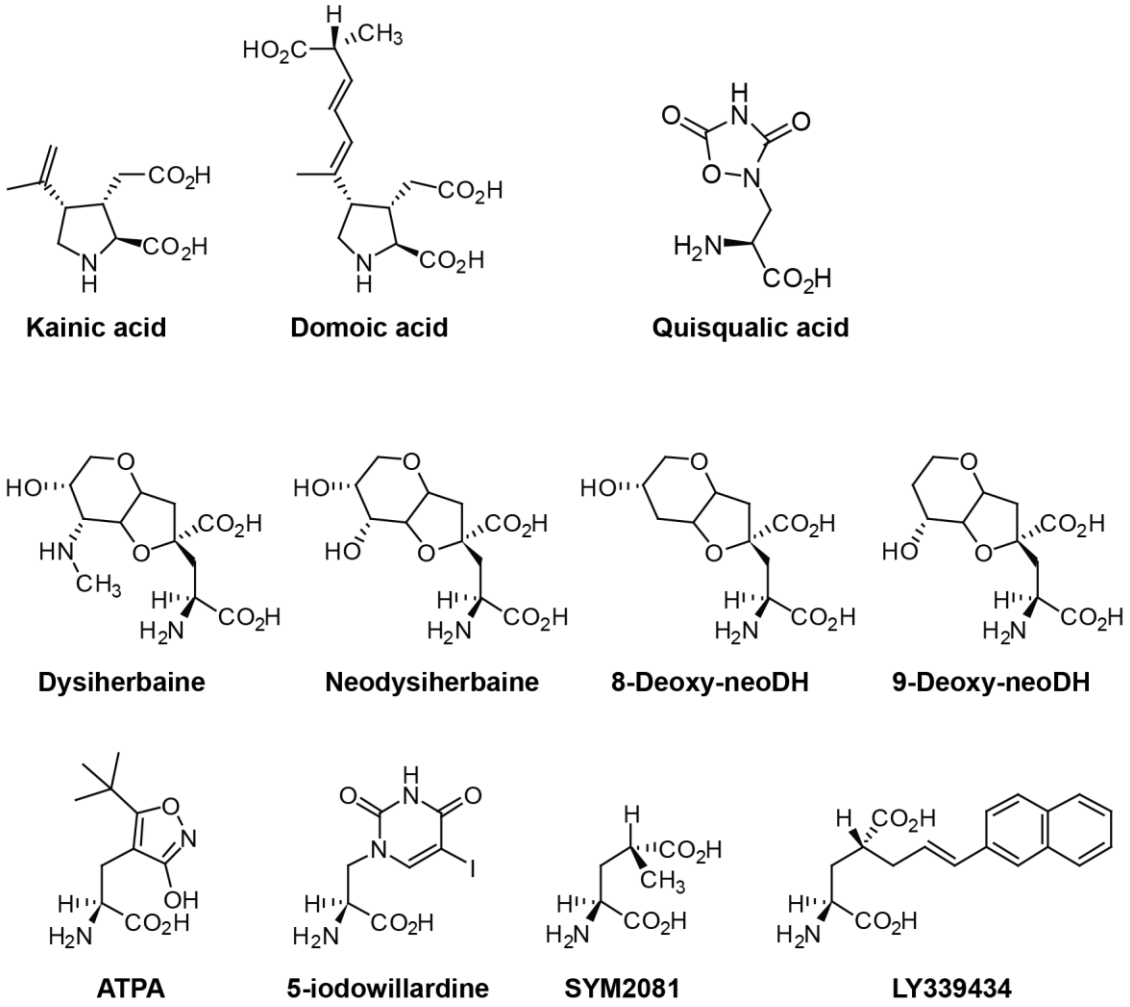

Figure 1.7. Structures of kainate receptor agonists.

1.2.2. Antagonists of kainate receptors

Development of KAR-selective antagonists has lagged behind that of AMPAR- and NMDAR-selective antagonists partly due to a lack of KAR-selective agonists for use in functional assays that investigated native KARs (Jane et al., 2009). Native tissue preparations in which GluK1-containing KARs were expressed without the presence of AMPARs, e.g. the dorsal root ganglion (DRG) cells and the isolated dorsal root preparation (Bettler et al., 1990; Partin et al., 1993) aided the development of GluK1-selective antagonists.

Early studies used quisqualate and kainate as agonists to evoke KAR responses from native tissue, but these agonists are not specific to KARs. Particularly, quisqualate also activates AMPARs and group I metabotropic glutamate receptors (mGluRs), which made it difficult

to determine the antagonist activity of compounds on KARs (Abe et al., 1992; Aramori and Nakanishi, 1992; Mayer, 2005). Moreover, preparations such as cortical slices were shown to express both AMPARs and KARs (Wisden and Seeburg, 1993). Kainate produced non-desensitising currents at AMPARs which further complicated the interpretation of results from early studies (Kiskin et al., 1986). More recently, cloning of KAR subunits and their expression in heterologous systems such as human embryonic kidney 293 (HEK293) cells have helped to characterise the activity of compounds selectively on KARs (Hollmann and Heinemann, 1994; Alt et al., 2004).

Early studies of iGluR antagonists in dorsal horn neurons led to the AMPAR and KAR antagonist γ-D-glutamylaminomethylsulfonate (GAMS, Figure 1.9) (Davies and Watkins, 1985). While these studies used quisqualate as the agonist to evoke KAR responses, later studies using the more selective agonists kainate and AMPA reported that GAMS may be a KAR antagonist (Zhou et al., 1993). Studies using recombinant KARs reported that GAMS was a weak KAR antagonist with no effect on GluK2 homomeric receptors up to 30 mM (Alt et al., 2004). Other early AMPAR/KAR antagonists include 1-(4-bromo-benzoyl)piperazine-2,3-dicarboxylic acid (p-BB-PzDA) and 1-(4-chlorobenzoyl)piperazine-2,3-dicarboxylic acid (p-CB-PzDA) (Figure 1.8) (Davies et al., 1984). However, both p-BB-PzDA and p-CB-PzDA were reported to inhibit NMDA-evoked receptors with greater potency than kainate-induced responses (Ganong et al., 1986). Despite the weak antagonist effect of p-BB-PzDA and p-CB-PzDA on KARs expressed in the dorsal root preparation (Evans et al., 1987), their effects on recombinant KARs and AMPARs remain undetermined. Another early KAR antagonist with greater selectivity for KARs over AMPARs was the oxime derivative, 5-nitro-6,7,8,9-tetrahydrobenzo[*g*]indole-2,3-dione-3-oxime (NS-102, Figure 1.9) which had GluK2 and GluK1 antagonist activity with weaker effects on recombinant GluA2/GluA4-containing AMPARs and native AMPARs in cortical slices (Verdoorn et al., 1994; Wilding and Huettner, 1996). However, NS-102 has limited use as a pharmacological tool due to its poor water solubility (see Verdoorn et al., 1994).

Work at Eli Lilly led to the development of KAR selective antagonists based on the decahydroisoquinoline structure, which led to the development of (3*S*,4a*R*,6*S*,8a*R*)-6-((4-carboxyphenyl)methyl)-1,2,3,4,4a,5,6,7,8,8a-decahydroisoquinoline-3-carboxylic acid

(LY382884, Figure 1.9), which had an IC_{50} value of 2 μM on GluK1 with no activity on GluK2 at concentrations up to 100 μM (Bleisch et al., 1997). Subsequently, the more potent antagonist (3*S*,4a*R*,6*S*,8a*R*)-6-[[(2*S*)-2-carboxy-4,4-difluoro-1-pyrrolidinyl]methyl]decahydro-3-isoquinolinecarboxylicacid (LY466195, Figure 1.9) was developed, and was demonstrated to have a GluK1 K_b value of 13 nM with little or no activity on AMPARs and NMDARs (Jones et al., 2006; Weiss et al., 2006).

Another class of KAR-selective antagonists with greater activity on GluK1 compared to AMPAR subunits is derived from willardiine with substitutions on the N^3 position of the uracil ring (More et al., 2004; Dolman et al., 2005, 2006, 2007; Mayer et al., 2006). These include (*S*)-1-(2-amino-2-carboxyethyl)-3-(2-carboxybenzyl)pyrimidine-2,4-dione (UBP302, Figure 1.9) (More et al., 2004). A thiophene ring at the N^3 position and a methyl group on the 5-position of the uracil ring of willardiine resulted in (*S*)-1-(2-amino-2-carboxyethyl)-3-(2-carboxythiophene-3-yl-methyl)-5-methylpyrimidine-2,4-dione (UBP310, Figure 1.9), with nanomolar potency for GluK1 homomers and GluK1/GluK5 heteromers, and > 100 μM potency at GluK2 homomers and GluA2-containing AMPARs (Dolman et al., 2007). X-ray crystal structures of UBP310 in complex with the GluK1 ligand binding domain (LBD) revealed that UBP310 stabilises an even greater degree of clamshell opening of the LBD than observed in structures of antagonists in complex with the GluA2 and GluN1 LBD (Mayer et al., 2006; Alushin et al., 2011).

Based on the X-ray structure and modelling studies of the GluK1, GluK2, GluK3 and AMPARs, a compound with greater GluK1 affinity and improved GluK1 over native AMPAR selectivity was developed, namely ((*S*)-2-amino-2-carboxyethyl)-3-(2-carboxy-5-phenylthiophene-3-yl-methyl)-5-methylpyrimidine-2,4-dione (UBP316, also known as ACET, Figure 1.9) (Dolman et al., 2007; Dargan et al., 2009). ACET was shown to have greater GluK1 affinity and selectivity for GluK1 over AMPAR in functional assays using recombinant GluK1 receptors and native KARs expressed on dorsal root ganglion (DRG) C-fibres (Dolman et al., 2007). Further characterisation of ACET has revealed that recombinant GluK3 homomeric receptors are blocked by ACET with an IC_{50} value for inhibition of GluK3-mediated currents of approximately 92 nM (Perrais et al., 2009). The GluK3 activity of ACET is surprising because earlier derivatives of willardiine structurally similar to ACET has K_i > 100 μM on recombinant human GluK3 homomeric receptors

(Dolman et al., 2005, 2006). Moreover, UBP310 has 30-fold lower GluK3 affinity compared to GluK1 in a radioligand saturation binding assay (Atlason et al., 2010). The lack of NMDAR activity and high KAR over AMPAR selectivity of ACET and similar willardiine derivatives have made these compounds useful tools to elucidate the roles of the GluK1 subunit for induction of LTP in the CNS (Barker et al., 2006; Huxter et al., 2007).

An endogenous metabolite of tryptophan, 4-oxo-1,4-dihydro-quinoline-2-carboxylic acid (kynurenic acid, Figure 1.8), is an antagonist of AMPAR, KAR and NMDARs (Ganong et al., 1983; Leeson et al., 1991). Derivatives of kynurenic acid have been developed to produce potent NMDAR antagonists that bind to the glycine site of the NMDAR (discussed in more detail in Chapter 2). An example of a widely used NMDAR antagonist based on kynurenic acid is 5-,7-dichlorokynurenic acid (DCKA) which binds to NMDARs with a K_b value of 3.0 μM (Leeson et al., 1991). DCKA was used to obtain an X-ray crystal structure of the GluN1 LBD in complex with the NMDAR co-agonist glycine (further discussed in Chapter 3) (Furukawa and Gouaux, 2003).

In assays that use native tissue containing a mixture of AMPARs and KARs, an important strategy to better understand KARs is to isolate the KAR-mediated responses by inhibiting AMPAR responses selectively. In such cases, AMPAR-selective antagonists are required for the study of KARs. Attempts to improve AMPAR over KAR selectivity of iGluR antagonists resulted in quinoxalinedione derivates such as 6-cyano-7-nitroquinoxaline-2,3-dione (CNQX) and 2,3-dihydroxy-6-nitro-7-sulfamoyl-benzo[*f*]quinoxaline (NBQX) (Figure 1.8) (Fletcher et al., 1988; Sheardown et al., 1990). AMPAR over KAR selectivity of CNQX is poor (approximately similar affinity on AMPARs and KARs) but NBQX has approximately 3-fold selectivity for AMPARs over KARs (Wilding and Huettner, 1996); however, NBQX alone cannot be used to completely isolate KAR-mediated responses from native tissue due to its overlapping activity on AMPARs and KARs.

An important advancement in the quest to isolate KAR-mediated responses was the development of 1-(4-aminophenyl)-3-methylcarbamyl-4-methyl-3,4-dihydro-7,8-methylenedioxy-5*H*-2,3-benzodiazepine hydrochloride (GYKI53655), a 2,3-benzodiazepine derivative (Paternain et al., 1995). GYKI53655 is a negative allosteric

modulator (NAM) at AMPARs and has been used to selectively inhibit AMPARs to study KAR function (Chittajallu et al., 1996; Frerking et al., 2001). However, there has been a report of GYKI53655 inhibiting GluK3 homomeric and GluK2/GluK3 heteromeric KARs at concentrations used to block AMPARs (50 μM) (Perrais et al., 2009).

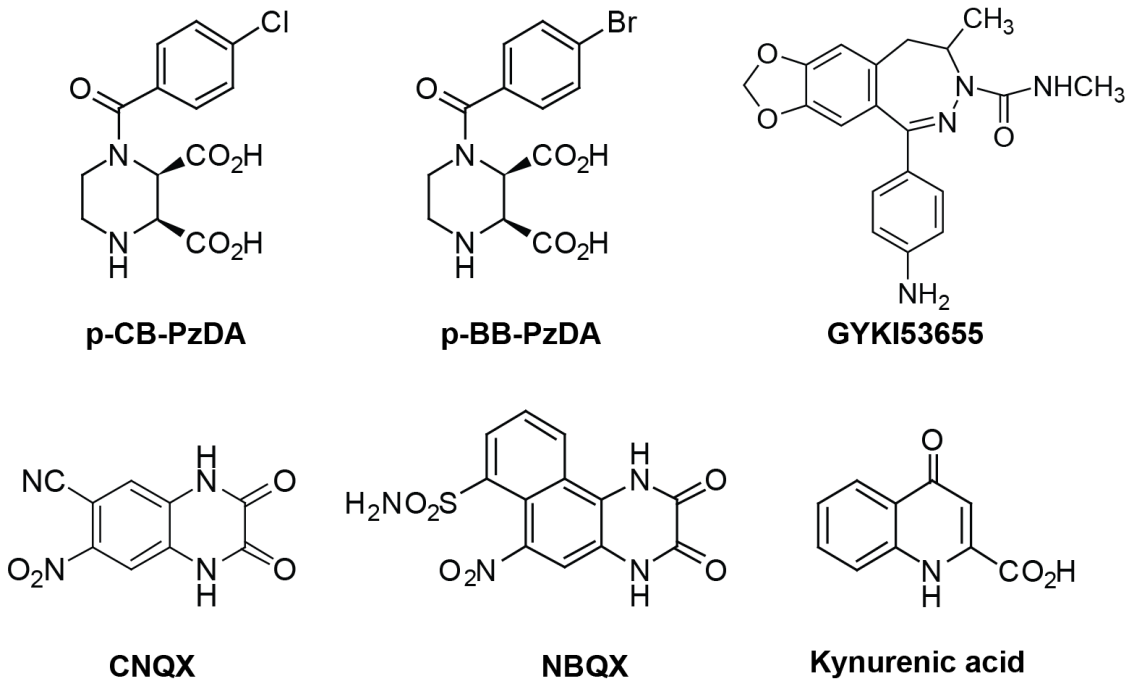

Figure 1.8. Structures of antagonists that block AMPARs and KARs.

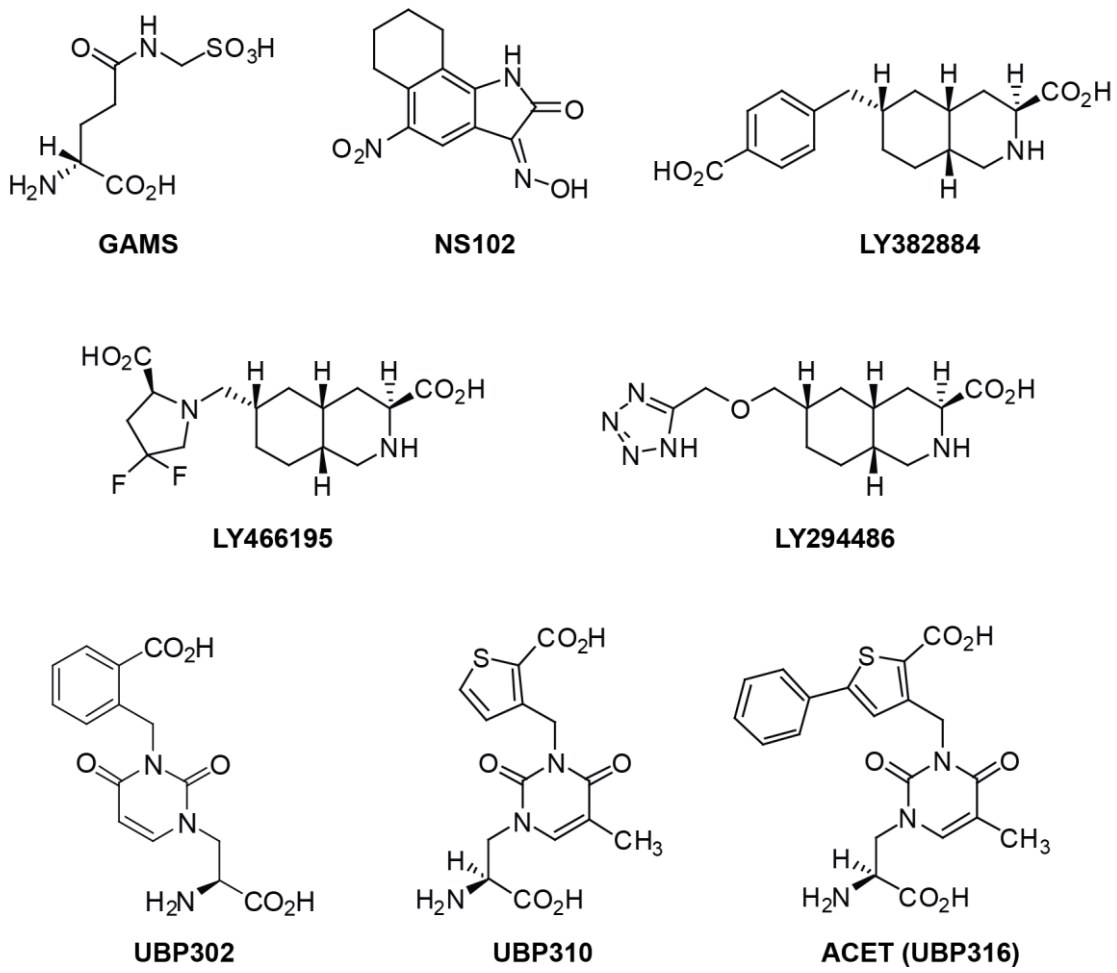

Figure 1.9. Structures of KAR-selective orthosteric antagonists.

1.2.3. Allosteric modulators of kainate receptors

Allosteric modulators are molecules that bind to a site remote to the glutamate binding site (see Yelshanskaya et al., 2016 and Yi et al., 2016). Development of allosteric modulators may provide an avenue to obtain greater selectivity between AMPARs and KARs compared to orthosteric agonists and antagonists because allosteric binding sites usually have lower amino acid sequence homology between iGluR subtypes than the glutamate binding site, which is highly conserved between all iGluRs (Traynelis et al., 2010). Because negative allosteric modulators (NAMs) do not compete with glutamate to bind to the receptor, they are also non-competitive antagonists.

NAMs of KARs based on 2-arylureidobenzoic acids (AUBAs) were assayed on recombinant homomeric and heteromeric KARs (Valgeirsson et al., 2003). These

compounds did not displace binding of [^{3}H]ATPA to GluK1 and therefore are believed to be non-competitive antagonists (Valgeirsson et al., 2003). Of these compounds, compound I (Figure 1.10), displayed 50-fold selectivity for GluK1 over GluK2 while compound II (Figure 1.10) antagonised GluK1 and GluK2 with similar potency (Valgeirsson et al., 2003, 2004). Neither of these compounds displayed activity on GluA1-4 AMPAR subunits at 100 μM (Valgeirsson et al., 2003, 2004).

Another NAM of KAR subunits is the GluK1-selective 5-carboxy-2,4-dibenzamido-benzoic acid (NS3763, Figure 1.10), which has no activity on heteromeric GluK1/GluK5 or GluK1/GluK2 receptors, AMPARs and NMDARs (Christensen et al., 2004a, 2004b). NS3763 and LY382884 (an antagonist of GluK1-containing KARs) has been used to determine that GluK1 heteromeric KARs are expressed presynaptically in the hippocampal CA1 inhibitory interneurons (Christensen et al., 2004b). The GluK1 NAM NS3763 has also been used to inhibit the ATPA-induced activation of KARs to suggest that GluK1 activation may lead to neuroprotection against ischaemic neuronal injury (Lv et al., 2012). The activity of NS3763 on GluK3-containing KARs remains to be determined.

Another class of allosteric modulators that have been useful in studies of KARs are positive allosteric modulators (PAMs), which bind to an allosteric site on the receptor and subsequently potentiate KAR currents in the presence of orthosteric agonists such as glutamate and kainate. In native and recombinant KARs, glutamate induces a rapid desensitisation and the recovery from the desensitisation is slow (Wong et al., 1994; Wilding and Huettner, 1997). The plant lectin concanavalin A (con A) blocks the desensitisation of KAR-mediated currents in DRG neurons and in recombinant GluK1- and GluK2-containing KARs (Huettner, 1990; Partin et al., 1993; Paternain et al., 1998). Therefore, con A has been used to characterise novel antagonists in assays, which use recombinant GluK1- and GluK2-containing KARs (Bleakman et al., 1996; Alt et al., 2004). Desensitisation of recombinant GluK3-containing KARs is less susceptible to inhibition by con A; therefore, recombinant GluK3-containing KARs have been more difficult to use in pharmacological characterisation assays (Schiffer et al., 1997).

More recently, a class of KAR PAMs based on benzothiadiazine was characterised (Larsen et al., 2017). Of these benzothiadiazine-based PAMs, 4-cyclopropyl-7-fluoro-3,4-dihydro-

2H-1,2,4-benzothiadiazine-1,1-dioxide (BPAM344) potentiated glutamate-evoked currents in GluK1-3 and GluA1 subunits (Larsen et al., 2017). Other PAMs of KARs include volatile anaesthetics such as halothane and isofluorane, which potentiate GluK2 channel currents (Dildy-Mayfield et al., 1996) and the triarylmethane dye, brilliant green (Bufler et al., 2001). The activity of brilliant green on different KAR subunits remains to be determined. Due to the fast desensitisation of KARs caused by agonists, development of novel subunit-selective KAR PAMs can be of great utility in studies investigating the functional roles of specific KAR subunits.

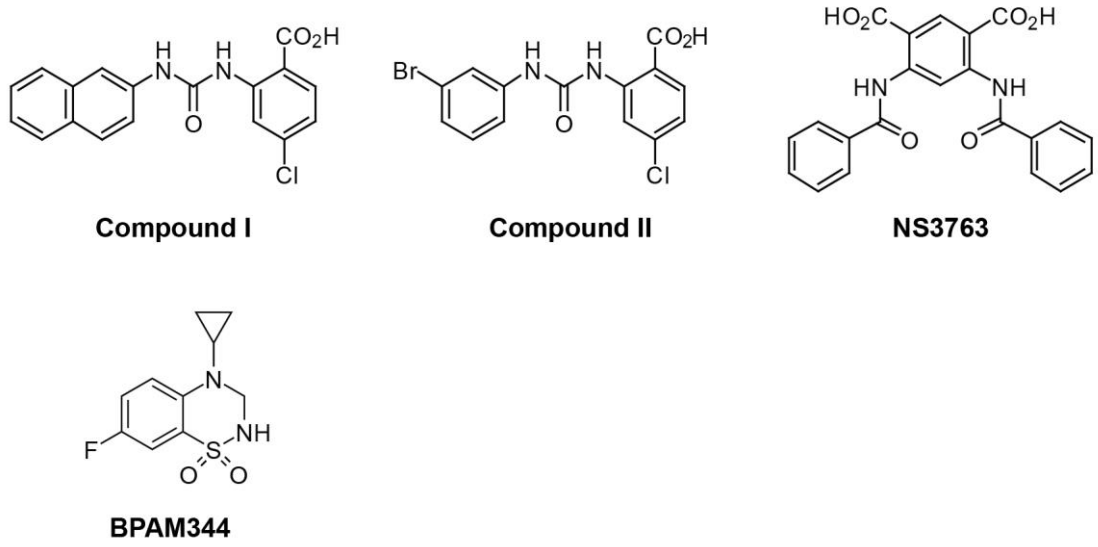

Figure 1.10. Structures of KAR-selective negative allosteric modulators (NAMs).

1.2.4. Kainate receptor expression in the hippocampus

Early studies employed radioligand binding using [^{3}H]kainate to find kainate binding sites in the brain (Monaghan and Cotman, 1982). Using in situ hybridisation (ISH), KAR subunit mRNA was detected in many regions of the brain including the hippocampus, amygdala, dorsal root ganglia (DRG), cerebellum and cerebral cortex (Wisden and Seeburg, 1993). A lack of specific antibodies for KAR subunits has made detection of KAR protein levels using immunohistochemistry (IHC) difficult, however, genetic knockout mice lacking specific KAR subunits have been used to assess the degree of antibody specificity in the case of antibodies targeting GluK2, GluK4 or GluK5 (Darstein et al., 2003; Ruiz et al., 2005). While the neuronal localisation of the KAR subunit proteins in many regions of the CNS is yet to be determined, a large body of work describes the distribution and functional

roles of KARs in the hippocampus (Wisden and Seeburg, 1993; Bureau et al., 1999; Paternain et al., 2000; Breustedt and Schmitz, 2004; Wondolowski and Frerking, 2009). Radioligand binding studies, ISH and IHC have helped to detect the presence of KARs in the hippocampus, however investigations of the neuronal localisation (presynaptic or postsynaptic) and the functional roles of each subunit requires selective pharmacological tools (agonists, antagonists and allosteric modulators). In fact, studies that have used one or more of the techniques mentioned above have revealed that KAR subunit expression in the hippocampus depends on the cell type, developmental stage and sub-cellular localisation (Bahn et al., 1994; Castillo et al., 1997; Pinheiro and Mulle, 2006).

Radioligand binding studies revealed that the hippocampus contains a high density of kainate binding sites, particularly in the cornu ammonis 3 (CA3) subregion of hippocampus (Monaghan and Cotman, 1982). Studies probing mRNA levels using ISH revealed that GluK1 mRNA is expressed in interneurons in all subregions of rat and mouse hippocampus (Bureau et al., 1999; Paternain et al., 2000). The GluK2 subunit mRNA is expressed in the principle cells and interneurons of CA1-CA3 subregions in the hippocampus (Paternain et al., 2000; Fisahn et al., 2004). GluK3 is expressed in granule cells of the dentate gyrus subregion of the hippocampus and in interneurons of stratum oriens and stratum radiatum layers of the hippocampus (Wisden and Seeburg, 1993; Contractor et al., 2001). GluK4 is expressed in CA3 pyramidal cells and in the CA1 and dentate gyrus subregions (Wisden and Seeburg, 1993; Fernandes et al., 2009; Lowry et al., 2013). GluK5 mRNA shows the highest expression levels amongst KAR subunits in the hippocampus, with presence in all subregions and mainly in the principle cell layer of the hippocampus (Wisden and Seeburg, 1993). The expression patterns suggested by ISH and knockout mice were later confirmed using pharmacological tools (as discussed below).

1.2.5. Kainate receptors in synaptic signalling

Determining the functional roles that KARs play in neuronal signalling was initially difficult due to lack of KAR-selective agonists and antagonists. The functions of natively expressed KARs remained a mystery until the AMPAR-selective non-competitive antagonist based on 2,3-benzodiazepines, GYKI53655, was used to block AMPARs selectively (although GYKI53655 was later found to have antagonist activity on GluK3 and GluK2/GluK3-containng KARs at high concentrations) (Paternain et al., 1995; Perrais et

al., 2009). In the presence of AMPAR blockage using GYKI53655, kainate can be used as KAR agonists without activating AMPARs (e.g. Wilding and Huettner, 1997). Chittajallu and colleagues used whole-cell patch-clamp recordings to show that application of low concentration (300 nM) of kainate after AMPAR blockage using GYKI52466 (an earlier analogue of GYKI53655) causes facilitation of synaptic responses (NMDAR-mediated EPSCs) in CA1 pyramidal cells, whereas a high concentration (1 μM) of kainate causes depression of synaptic responses (Chittajallu et al., 1996). In the same study, both the facilitation and depression of synaptic responses mediated by kainate (and domoate) were partially blocked by the KAR antagonists NS-102 and CNQX (Chittajallu et al., 1996). These findings were taken as evidence for the presence of KARs on presynaptic terminals in the Schaffer-collateral to CA1 pyramidal cell (SC-CA1) synapse and further studies have corroborated this hypothesis (Figure 1.11) (Kamiya and Ozawa, 1998; Frerking et al., 2001).

In addition to modulating glutamate release from presynaptic terminals (i.e. as autoreceptors), presynaptic KARs in the CA1 function as autoreceptors that can modulate the release of γ-aminobutyric acid (GABA) from presynaptic terminals of GABAergic interneurons (Figure 1.11) (Clarke et al., 1997; Rodríguez-Moreno et al., 1997). Clarke and colleagues used GYKI53655 to block AMPARs and D-2-amino-5-phosphonopentanoate (D-AP5) to block NMDARs while performing intracellular recordings from the hippocampal CA1 cell body layer to record inhibitory postsynaptic currents (IPSCs), which are mediated by GABA receptors (Clarke et al., 1997). Application of kainate and the GluK1-selective agonist ATPA after blocking AMPARs and NMDARs revealed that activation of KARs depresses monosynaptic inhibition mediated by GABA (Clarke et al., 1997). Moreover, the inhibition of IPSCs by kainate and ATPA can be blocked by the GluK1 antagonist (3*SR*,4a*RS*,6*SR*,8a*RS*)-6-((((1H-tetrazol-5-yl)methyl)oxy)methyl)-1,2,3,4, 4a,5,6,7,8,8a-decahydroisoquinoline-3-carboxylic acid (LY294486 – an analogue of LY382884, which was discussed earlier). The use of the GluK1-selective agonist (ATPA) and antagonist (LY294486) in the study by Clarke and colleagues further suggested that the KARs that mediate the presynaptic modulation may contain GluK1 subunits (Clarke et al., 1997). The presynaptic locus of the KARs that inhibit GABA release by the CA1 interneurons were also reported by Rodríguez-Moreno and colleagues who showed that in the CA1 pyramidal cells, the frequency of miniature IPSCs (mIPSCs) is

decreased by kainate (Rodríguez-Moreno et al., 1997). This result suggests that activation of KAR autoreceptors at the GABAergic interneurons depresses GABA release onto CA1 pyramidal cells. In similarity with SC-CA1 pyramidal cell synapses, application of low concentrations of kainate facilitates, whereas high concentrations of kainate depresses, GABA release at the interneuron-pyramidal cell synapses in the CA1 (Jiang et al., 2001).

An intriguing facet of KAR function is that KARs exert their effects partly through a metabotropic mechanism (by association with G-proteins) and subsequent activation of protein kinase C (PKC) (Rodríguez-Moreno and Lerma, 1998; Rodríguez-Moreno et al., 2000). The metabotropic signalling was observed in the case of presynaptic KARs that inhibit GABA release (Rodríguez-Moreno et al., 2000). The metabotropic mode of KAR signalling has also been established in dorsal root ganglion neurons and occurrs independent of the KAR ion channel function (Rozas et al., 2003). A significant effect of the metabotropic signalling of KARs in the CA1 pyramidal cells of the hippocampus is its inhibition of the slow afterhyperpolarisation current (I_{AHP}) mediated by Ca^{2+}-dependent K^+ channels, which is observed during trains of action potentials (the activation of the I_{AHP} being dependent on the number and frequency of action potentials in the train) (Melyan et al., 2002). Importantly, the slow I_{AHP} regulates spike frequency adaptation in neurons (reviewed in Ha and Cheong, 2017). Spike frequency adaptation ensures that following an extended period of excitation, the frequency of discharge of action potentials (or spikes) from a neuron progressively slows after an initial high frequency of firing. Spike frequency adaptation therefore controls the ability of neurons to generate action potentials in response to sustained stimulus and disruption of spike frequency adaptation due to the inhibition of I_{AHP} highlights a regulatory role for KARs in generation of action potentials in the CA1 pyramidal cells (Melyan et al., 2002). Inhibition of I_{AHP} mediated by KARs has also been found in mossy fibre to CA3 pyramidal cell synapses and studies at these synapses demonstrated that KARs containing the GluK2 and GluK5 subunits are necessary for the metabotropic signalling (Ruiz et al., 2005). However, another study has shown that double knockout of GluK4 and GluK5 did not affect inhibition of I_{AHP} (Fernandes et al., 2009). More recently, GluK2-containing KARs employing metabotropic signalling were shown to contribute to an NMDAR-independent form of LTP in the SC-CA1 synapse (Petrovic et al., 2017). Therefore, the studies investigating metabotropic mode of signalling by KARs could also be aided by the development of GluK2 selective antagonists.

In addition to the presynaptic KARs in the SC-CA1 synapse, postsynaptic currents in many CA1 GABAergic interneurons (including the stratum oriens–lacunosum moleculare cells) are believed to contain a KAR-mediated component (Figure 1.11) (Cossart et al., 1998; Frerking et al., 1998). While GluK1-containing KARs have been suggested to mediate EPSCs in CA1 interneurons (using GluK1-selective antagonists, e.g. Cossart et al., 1998), it is known that GluK2 subunits are also present in interneurons, therefore whether the GluK2 subunit is part of the KAR complex, which contributes to synaptic currents in interneurons, remains to be determined (Bureau et al., 1999; Mulle et al., 2000). Hippocampal interneuron activity is involved in the generation and maintenance of behaviourally relevant neural oscillations (Klausberger and Somogyi, 2008). Moreover, the GluK1 antagonist UBP304 (willardiine derivative analogue of UBP302, which was discussed earlier) reduces the frequency of neural oscillations in the theta frequency range in all layers of the hippocampus (Huxter et al., 2007). However, analogues of UBP304 such as UBP310 and UBP316 also inhibit native (Pinheiro et al., 2013) but not recombinant (Dolman et al., 2007) GluK2/GluK5 heteromers at high concentrations. Therefore, UBP304 may also inhibit KARs in the hippocampus where GluK2 and GluK5 are abundantly expressed (Wisden and Seeburg, 1993). In addition to the postsynaptic KARs on many GABAergic interneurons, presynaptic KARs were found to be autoreceptors on Schaffer collaterals making synaptic contacts onto a subset of stratum radiatum interneurons (Sun and Dobrunz, 2006). These autoreceptors are believed to control short-term facilitation of glutamate release onto interneurons which was attenuated by the KAR antagonist NS-102 (Sylwestrak and Ghosh, 2012). In summary, the resolution of uncertainties regarding the identity of KAR subunits that contribute to the synaptic signalling in interneurons will be aided by GluK2-selective antagonists.

Other studies also pointed to a role for KARs (containing the GluK1 subunit) in postsynaptic neurotransmission in the hippocampal mossy fibre-CA3 pyramidal cell (MF-CA3) synapses (Figure 1.11) (Castillo et al., 1997; Vignes et al., 1997). Vignes and colleagues blocked AMPARs and NMDARs and recorded from CA3 pyramidal cells to show that KARs mediate currents in the CA3 which were inhibited by the KAR antagonist CNQX and the GluK1-selective antagonist LY294486 (Vignes and Collingridge, 1997; Vignes et al., 1997). Therefore, KARs (containing the GluK1 subunit) mediate postsynaptic currents in response to activation by glutamate. The currents mediated by KARs had slower

activation and decay than AMPAR-mediated currents (Castillo et al., 1997; Kidd and Isaac, 2001). The slower current kinetics of KARs compared to AMPARs means that instead of mediating fast neuronal signalling, KARs could function as integrators of persistent presynaptic activity by summation of subsequent EPSCs – thereby increasing the probability for formation of action potentials in the postsynaptic neuron especially during prolonged stimulation or trains of stimuli (e.g. Frerking and Ohliger-Frerking, 2002; Sachidhanandam et al., 2009). In contrast with the suggestions that GluK1-containing KARs mediate EPSCs in MF-CA3 synapse, reports have suggested that GluK2 but not GluK1 or GluK3 knockout mice lack KAR-mediated EPSCs (Mulle et al., 1998; Sachidhanandam et al., 2009).

Further studies using either the GluK1-selective antagonist LY382884 or genetic GluK1 or GluK2 knockout mice have revealed that KARs mediate synaptic plasticity at the MF-CA3 synapse in a subunit-specific manner (Bortolotto et al., 1999; Paternain et al., 2000; Contractor et al., 2001; Breustedt and Schmitz, 2004). The MF-CA3 synapse exhibits long-term potentiation (LTP) that is not dependent on NMDARs (Harris and Cotman, 1986). Bortolotto and colleagues showed that LY382884 inhibited LTP of field excitatory postsynaptic potentials (f-EPSPs) at the MF-CA3 synapse whereas LTP mediated by NMDARs as a result of tetanisation of associational/commissural fibres was resistant to LY382884 (Bortolotto et al., 1999). Therefore, MF-CA3 synaptic plasticity was suggested to be mediated by GluK1-containing KARs. A later study by Breustedt and Schmitz using both LY382884 and GluK1 or GluK2 knockout mice showed that MF-CA3 LTP was present in GluK1 knockout mice but absent in GluK2 knockout mice (Breustedt and Schmitz, 2004). Moreover, the same study found that MF-CA3 LTP was not blocked by LY382884 (10 μM, same concentration as in the study by Bortolotto and colleagues). The contradicting results from these studies have been attributed to the differences in slice preparations (parasagittal slices by Bortolotto et al. compared to transverse by Breustedt et al.) used in these two studies, which ultimately changes the neuronal population which contributes to the synaptic potentials recorded (Sherwood et al., 2012). Another explanation for the discrepancies is that knockout of the GluK1 subunit may lead to compensatory mechanisms such as increased contribution from another KAR subunit type (e.g. Christensen et al., 2004). A comprehensive investigation of the involvement of KAR

subunits in synaptic plasticity will therefore be facilitated by development of selective GluK2 antagonists.

Another set of studies has shown that KARs act as presynaptic facilitatory receptors at the MF-CA3 synapse (Figure 1.11) (Contractor et al., 2001; Lauri et al., 2001). Lauri and colleagues showed that the GluK1 antagonist LY382884 blocked facilitation of mossy fibre EPSCs evoked at a frequency of 50 Hz (Lauri et al., 2001). Lauri and colleagues suggested that the KAR-mediated facilitation of EPSCs was due to presynaptic KARs and blockage of the KAR-mediated facilitation with LY382884 prevents MF-CA3 LTP (Lauri et al., 2001). Interestingly, during MF-CA3 LTP, the frequency facilitation was occluded, suggesting that both MF-CA3 LTP and frequency facilitation may involve the presynaptic GluK1-containing KARs (Lauri et al., 2001). However, studies by Contractor and colleagues using GluK1 and GluK2 knockout mice have suggested that GluK2 but not GluK1 is the subunit in the KAR presynaptic autoreceptors at MF-CA3 synapses (Contractor et al., 2000, 2001). These discrepancies have further highlighted the need for better genetic and pharmacological tools. Particularly, a long-term knockout of GluK1 can lead to compensatory mechanisms from other KAR subunits as mentioned earlier. Moreover, while LY382884 is thought to be inactive at GluK2 and GluK3 homomers and the GluK2/GluK5 heteromers (Bortolotto et al., 1999), the activity of LY382884 on other GluK1-lacking heteromeric KARs remains to be determined.

In the MF-CA3 synapse, measuring Ca^{2+} movement into the presynaptic bouton revealed that activation of presynaptic KARs could induce Ca^{2+} transients (a transient increase in intracellular Ca^{2+} levels) following a single action potential (Lauri et al., 2003; Nisticò et al., 2011). But not all synapses show the Ca^{2+} signal – only giant boutons of mossy fibre axons (from the dentate gyrus) which form synapses with pyramidal cells have the Ca^{2+} movement (Scott and Rusakov, 2006). The GluK1 antagonist ACET blocks the Ca^{2+} influx at MF-CA3 synapses (Dargan et al., 2009) whereas studies using GluK2 and GluK3 knockout mice suggests a role for these subunits in presynaptic KARs in MF-CA3 synapses (Contractor et al., 2001; Pinheiro et al., 2007). These discrepancies further highlight the need for better pharmacological agents with selectivity for specific KAR subunits (including the GluK2 subunit) to determine the identity of the subunits that are responsible for presynaptic facilitation at the MF-CA3 synapse.

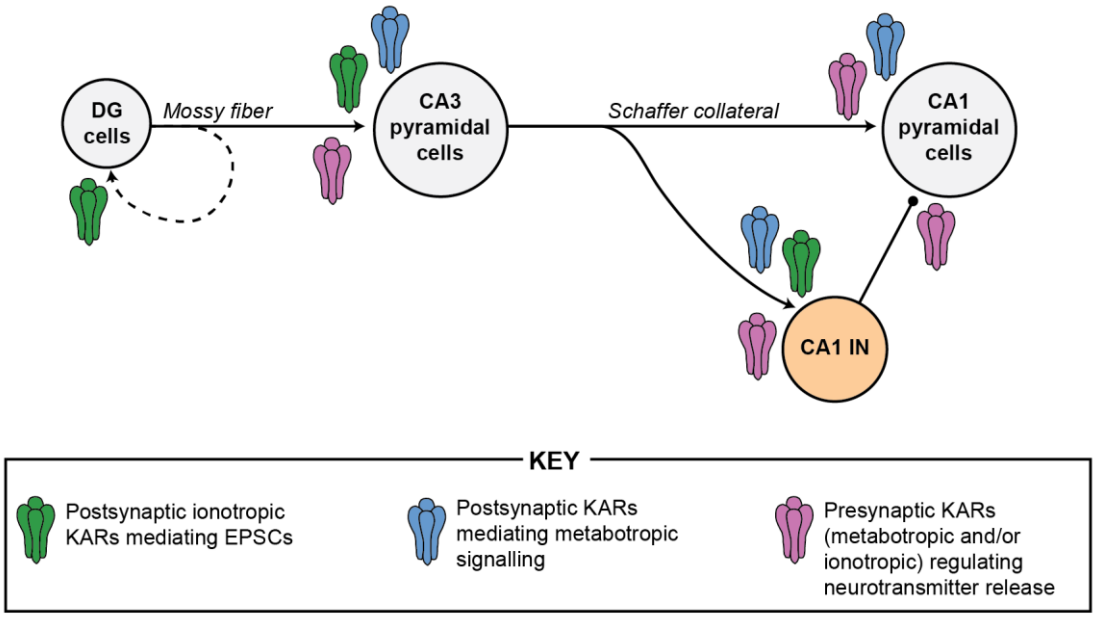

Figure 1.11. Neuronal signalling mediated by kainate receptors in the hippocampus. Schematic showing the localisation of KARs within hippocampal synapses (arrowheads for glutamatergic synapses and arrows terminating with black circles for GABAergic synapses) based on the current evidence (discussed in text). KARs on pre- and postsynaptic terminals can signal using ionotropic and metabotropic mechanisms. Recurrent excitatory synapses (dashed line) at dentate gyrus granule cells (DG cells) are observed in preclinical models of temporal lobe epilepsy (more details in section 1.2.6.1). Physiological studies have demonstrated KAR-mediated synaptic processes in the pyramidal cells of CA1 and CA3 subregions, and in CA1 interneurons (CA1 IN). The subunit identity in KARs at pre- and postsynaptic sites is not fully understood due to a lack of subunit-selective pharmacological tools and limitations of long-term genetic knockout mice.

1.2.6. Clinical relevance of kainate receptors

There is overwhelming evidence that KARs are regulatory receptors in addition to postsynaptic targets for glutamate during neurotransmission (see above). Moreover, the direction of modulation by KARs may depend on the type of subunit that make up the receptor (Chittajallu et al., 1996; Bortolotto et al., 1999). Therefore, KAR subunits may be suitable therapeutic targets for pathophysiological conditions in which the balance of excitatory-inhibitory neurotransmission is impaired. Early observations that systemic injection of kainic acid led to convulsions and neurotoxicity pointed to a role for KARs in these pathological conditions (e.g. Ben-Ari, 1985). Moreover, kainic acid causes depolarisation of sensory neurons in the dorsal root, which are responsible for conveying pain information to the spinal cord (Davies and Watkins, 1979; Agrawal and Evans, 1986).

Subsequent studies found KAR-mediated currents in the dorsal root ganglia (DRG) cells (Huettner, 1990). The rationale for targeting of KARs in epilepsy and pain are described below to highlight the need for more GluK2-selective pharmacological agents, which may be therapeutically beneficial and help to understand the role of KARs in these pathophysiological states.

1.2.6.1. Epilepsy

Epilepsy is a neurological disorder characterised by the occurrence of prolonged and synchronised neuronal discharges (also known as spontaneous neuronal seizures) (reviewed in Stafstrom and Carmant, 2015). The recurrent seizures arise from multiple brain structures – including the hippocampus and may propagate to the amygdala and the entorhinal cortex (Lothman et al., 1991). Many current antiepileptic drugs work by inhibiting voltage-gated sodium (Na^+) and calcium (Ca^{2+}) channels, which results in the reduction of neuronal excitability, or by an enhancement in GABAergic inhibition (see Stafstrom and Carmant, 2015). Given the pervasive nature of the voltage-gated Na^+ and Ca^{2+} channels, current anticonvulsant drugs have many unwanted side effects including cognitive impairments, tremor and depression (Perucca and Meador, 2005; Goldenberg, 2010). Moreover, the treatment window for severe cases of epilepsy is narrow and in a significant proportion of cases, drug treatments are ineffective (Goldenberg, 2010). Given the modulatory roles that KARs play in maintaining the excitatory-inhibitory balance in the hippocampus and other structures in the CNS, using subunit-selective antagonists to target KARs for therapy of epilepsy is an exciting prospect (Rogawski et al., 2003).

Intraventricular injections and intra-amygdaloid application of kainate in rats induced cell degeneration in the hippocampus and seizures originating in the CA3 region of the hippocampus (Nadler et al., 1978; Ben-Ari et al., 1979; Nadler, 1981), and variants of this protocol has been used as animal models of acute and chronic seizures and it resembles aspects of temporal lobe epilepsy (a common form of epilepsy in humans) (Rodríguez-Moreno et al., 1997; Mulle et al., 1998; Fritsch et al., 2014). However, whether the kainate-induced forms of epilepsy is caused by direct activation of KARs or through indirect mechanisms involving other receptors (such as AMPARs at which kainate is a non-desensitising agonist (Swanson et al., 1997)) is unknown. Chronic epilepsy develops in a large proportion of animals that receive systemic administration of kainate or pilocarpine

(an agonist of muscarinic cholinergic receptors) for 1-3 days (Ben-Ari, 1985; Leite et al., 1990). A long-lasting phase of spontaneous recurrent limbic seizures with increasing frequency develops after a period of days or weeks (Hellier et al., 1998; Williams et al., 2009). Kainate-induced seizures in animals leads to activity-dependent neuronal and cell loss, and cell death of astrocytes and hippocampal CA1 and CA3 pyramidal cells, characteristics which resemble human temporal lobe epilepsy (TLE) (Nadler et al., 1978; Ben-Ari, 1985).

The acute seizures induced by kainate have been the subject of many studies and the epileptogenesis is believed to be caused by KAR-mediated inhibition of GABA release and activation of postsynaptic KARs on glutamatergic neurons (Rodríguez-Moreno et al., 1997; Mulle et al., 1998). GluK1-containing KARs are present in the axons and dendrites of hippocampal interneurons in the CA1 region (Paternain et al., 2000; Rodríguez-Moreno et al., 2000). As described earlier for the hippocampus, kainate facilitates GABA release and therefore is responsible for controlling the inhibitory drive of the neuronal network (Cossart et al., 1998). KARs expressed at the interneuron-pyramidal cell synapses display concentration-dependent effects wherein GABA release is suppressed at high concentrations of kainate (Clarke et al., 1997; Rodríguez-Moreno et al., 1997) but GABA release is facilitated at low kainate concentrations (300 nM) (Jiang et al., 2001; Khalilov et al., 2002). Contrary to the conclusions from the physiological studies, which predicted that application of low doses of a KAR agonist would increase inhibition through GABA, systemic application of the GluK1 agonist ATPA in vivo led to hippocampal and amygdala seizures, an effect that was missing from GluK1 knockout mice (Fritsch et al., 2014). Consistently, antagonism of GluK1-containing KARs in vivo blocked seizures induced by pilocarpine (Smolders et al., 2002). Additionally, the excitatory glutamatergic neurons also contain KARs on presynaptic and postsynaptic terminals (see section 1.2.5). At presynaptic terminals, low concentrations of kainate facilitate whereas high concentrations of kainate depress synaptic responses of CA1 pyramidal cells (Chittajallu et al., 1996). The postsynaptic KARs are thought to contain at least one GluK2 subunit and their activation leads to modulation of neuronal excitability through ionotropic and metabotropic KAR signalling (see section 1.2.5) (Melyan et al., 2002, 2004). In summary, KAR activation decreases GABA release and increases excitability in the postsynaptic glutamatergic neurons, which promotes epileptic activity by creating an imbalance between excitation

and inhibition in the neuronal networks involved. In agreement with the studies in animals, a clinical study of members of a family affected by idiopathic juvenile absence epilepsy reported increased levels of polymorphisms of the Grik1 gene which codes for the GluK1 subunit (Sander et al., 1997). Moreover, reorganisation of KAR subunits may occur in patients of TLE who have upregulation of GluK1 (Li et al., 2010). The AMPAR and KAR antagonist NS1209 alleviated refractory status epilepticus (prolonged or sequential seizures lasting for more than 30 minutes with resistance to current antiepileptic drugs) in phase II clinical trials and may have partly mediated its effects by blocking KARs (Swanson, 2009).

In contrast to the evidence in preclinical and clinical studies of acute seizures described above, the roles that KARs play in producing chronic seizures that last for many months after repetitive treatment with kainate (e.g. Hellier et al., 1998) or pilocarpine (an agonist of muscarinic acetylcholine receptor) (e.g. Leite et al., 1990) remain a mystery. However, based on similarities in recordable symptoms and changes in neuronal morphology between clinical and animal studies of chronic epilepsy, a role for KARs has been proposed. The CA3 region of the hippocampus has been long-proposed to be a key area for origin of seizures (reviewed in Ben-Ari and Cossart, 2000). In the CA3 region, KARs that contain GluK2 are abundantly expressed and modulate synaptic signalling (see sections 1.2.4 and 1.2.5); therefore, GluK2 has been proposed to be important in limbic epilepsies (Werner et al., 1991). In agreement with this theory, deletion of GluK2 in mice led to lower sensitivities to seizures after kainate injection (Mulle et al., 1998). A major characteristic of TLE patients and animal models of kainate-induced epilepsy is mossy fibre sprouting in the dentate gyrus of the hippocampus (Epsztein et al., 2005; Artinian et al., 2011, 2015). Mossy fibre sprouting occurs as a result of the neuronal reorganisation in the dentate gyrus during chronic epilepsy (Ben-Ari et al., 2008). The mossy fibre axons of the dentate gyrus granule cells undergo sprouting and form novel synapses with the dentate granule cells to create a recurrent mossy fibre network (Tauck and Nadler, 1985; Represa et al., 1987; Sutula and Dudek, 2007). The formation of these new aberrant synapses results in an upregulation of KARs, which are expressed abundantly in the dentate gyrus (Represa et al., 1987, 1989). In the dentate gyrus, postsynaptic KARs mediates glutamatergic transmission at the mossy fibre to granule cell (MF-GC) synapses (Epsztein et al., 2005). Therefore, the novel synapses and the upregulation of postsynaptic KARs affects the synaptic signalling at MF-GC synapses by causing overexcitability in granule cells (Epsztein et al., 2005; Peret

et al., 2014). This overexcitability is believed to result in epileptiform activity in the dentate gyrus, a pathophysiological trait that may be aggravated by the suppression of GABAergic inhibitory transmission in the network (Epsztein et al., 2005).

In a study by Pinheiro and colleagues, UBP310 (a compound developed as GluK1-selective antagonist, see section on KAR agonists) was shown to be an antagonist of recombinant GluK2/GluK5-containing heteromeric KARs with fast glutamate application mimicking synaptic conditions (IC_{50} ~1 μM) (Pinheiro et al., 2013). Pinheiro and colleagues reported that the postsynaptic KARs inserted in the novel aberrant MF-GC synapses in pilocarpine-induced TLE animal model are likely heteromeric KARs containing GluK2/GluK5 subunits (Pinheiro et al., 2013). Indeed, studies using genetic knockout mice have suggested that KARs containing one of more of GluK2, GluK4 and GluK5 subunits may mediate postsynaptic neurotransmission and may be involved in generation of recurrent seizures during chronic epilepsy (Mulle et al., 1998; Contractor et al., 2003; Fernandes et al., 2009). At the dentate granule cells, addition of novel KARs has been proposed to induce seizures by altering the firing rate of dentate granule cells which have basally sparse firing rates (Artinian et al., 2011, 2015). In addition to KARs in the dentate gyrus, mossy fibre presynaptic KARs containing GluK2, GluK5 and possibly GluK1 have also been reported to mediate synaptic plasticity (see section 1.2.5). Further evidence for the involvement of KARs in epilepsy comes from Yu and colleagues who used genetically modified mice (see Nakashiba et al., 2008), which had inducible CA3 synaptic silencing wherein the protein tetanus toxin (inhibitor of neurotransmitter release) was inducible in CA3 pyramidal cells, to show that kainate-induced seizures and network oscillations were reduced during CA3 synaptic silencing (Yu et al., 2016).

Explorations of the therapeutic potential of KAR targeting in chronic seizures have been rare. In a study using a TLE animal model (where TLE was induced by pilocarpine), interictal (between seizures) and ictal (during seizure) discharges were reduced in mice lacking the GluK2 subunit but not in mice lacking GluK1 or when postsynaptic GluK2/GluK5-containing heteromeric KARs were blocked with UBP310 (Peret et al., 2014). However, the ATD of GluK2 is critical in forming the GluK2/GluK5 heteromer and subsequently affects surface expression of GluK5-containing KARs (Gallyas et al., 2003; Kumar et al., 2011), whether GluK1 subunit also forms part of this receptor complex is

unknown. Therefore, investigations into the role of specific subunits in chronic epilepsy (and subsequently more specific therapeutic targeting) warrants the development of subunit selective KAR antagonists.

1.2.6.2. Pain

While sensation of acute pain is a beneficial process involving multiple levels of peripheral and central nervous systems (Basbaum et al., 2009), which prevents tissue damage, chronic pain has unknown causes and arises from overactivation (or sensitisation) of (one or more of) the peripheral or central components of pain transduction pathways (Costigan et al., 2009; Woolf, 2011). Overactivation of the peripheral nociceptors is initially due to overexposure to neurogenic inflammatory factors such as substance P, adenosine triphosphate (ATP), serotonin, or noxious chemicals (Basbaum et al., 2009). Overactivation (or sensitisation) of central pain transduction pathways may be a result of the nociceptive sensory neurons of the spinal cord dorsal horn becoming hyperexcitable, which is manifested as an increase in responses from the dorsal horn neurons caused by repetitive activation (a phenomenon known as wind-up), or LTP of excitatory synapses of these neurons (Seal et al., 2009; Pfau et al., 2011). The overexcitability in pain sensing neurons may be expressed as loss of presynaptic inhibition in transmitter release or increase in postsynaptic membrane excitability (Fang et al., 2002; Lee et al., 2002; Witschi et al., 2011). KARs are present on both presynaptic and postsynaptic terminals of synapses involved in processing pain information, including neurons in the dorsal horn of spinal cord (Lu et al., 2005) and dorsal root ganglion (DRG) neurons (Huettner, 1990; Partin et al., 1993; Lucifora et al., 2006).

The DRG KAR currents had similar activation and decay kinetics as those gated by recombinant GluK1-containing receptors expressed in HEK293 cells (Huettner, 1990; Herb et al., 1992; Swanson and Heinemann, 1998). Consistently, GluK1 mRNA is prominently expressed by DRG neurons however smaller amounts of mRNAs of other KAR subunits have also been reported (Partin et al., 1993). Moreover, mice lacking the GluK1 subunit lack KAR currents in DRG neurons (Mulle et al., 2000) and genetic deletion of GluK2 subunit increased the rate and extent of desensitisation of the current from DRG neurons but in dorsal horn neurons, GluK2 deletion abolished KAR currents (Kerchner et al., 2002). The use of the GluK1-selective antagonist LY382884 and genetic knockout of GluK1 or

GluK2 revealed that GluK1-containing KARs are required for expression of KAR currents in the DRG neurons (Kerchner et al., 2002). GluK1-selective agonists such as ATPA and 5-iodowillardiine (see section 1.2.1) activate GluK1-containing KARs in DRG neurons with similar potencies and gating properties compared to recombinant GluK1-containing receptors (Wong et al., 1994; Clarke et al., 1997; Kerchner et al., 2001; Wilding and Huettner, 2001). Moreover, GluK1-selective antagonists with a wide range of GluK1-selectivity, including LY382884 (and analogues) and the antagonists based on willardiine (see section 1.2.2), inhibited KAR currents in DRG neurons (Bleakman et al., 1996; Dolman et al., 2005; Weiss et al., 2006). Therefore, there is strong evidence for KAR expression in nociceptive neurons of DRG and dorsal horn.

Peripheral application of KAR agonists leads to nociceptive signalling and pain behaviours (Ault and Hildebrand, 1993; Du et al., 2006). Experimental induction of inflammation in rodent paw increased KAR immunoreactivity (Carlton and Coggeshall, 1999; Du et al., 2006). An upregulation of KAR expression in some sensory neurons was proposed to also occur when inflammation was induced experimentally (using complete Freund's adjuvant injection) (Du et al., 2006). In DRG neurons, a major function of KARs appears to be as presynaptic autoreceptors that inhibit glutamate release at the synapses of DRG neurons at the dorsal horn (Kerchner et al., 2001). However, the modulation of neurotransmission by KARs at the dorsal horn seems to be biphasic (both inhibitory and facilitatory) because low concentrations (30 nM) of kainate facilitated but higher concentrations (3 μM) depressed glutamate release (Youn and Randic, 2004). Presynaptically mediated inhibition of dorsal horn EPSCs by KARs is absent in GluK1 knockout mice (Kerchner et al., 2002) however the involvement of GluK2 in presynaptic KARs remains to determined and will require GluK2-selective pharmacological agents.

Early studies demonstrated that non-selectively blocking AMPARs and KARs reduces inflammatory signalling and behaviours linked to pain in rats (Hunter and Singh, 1994; Jackson et al., 1995; Simmons et al., 1998; Stanfa and Dickenson, 1999). Subsequently, targeting GluK1 with selective antagonists or genetic deletion produced analgesic effects following induction of chronic pain (Wu et al., 2007). While these results agreed with the inhibitory roles of presynaptic KARs that contain the GluK1 subunit (Kerchner et al., 2002; Youn and Randic, 2004), investigations of the roles of other KAR subunits requires

subunit-selective pharmacological agents that target specific subunits. A preclinical model of pain, namely assessment of pain behaviour after formalin injection into rat paw, also demonstrated the analgesic effects of the GluK1 antagonist LY382884, without the side-effect of ataxia that followed inhibition of AMPARs (Simmons et al., 1998). Esterified prodrugs of LY382884 (see section 1.2.2) and the less GluK1-selective analogue, LY293558, also produced analgesic effects when delivered orally in the formalin model and in inflammation models of carrageenan-induced thermal hyperalgesia and capsaicin-induced mechanical hyperalgesia (Dominguez et al., 2005; Jones et al., 2006). LY293558 also produced analgesia in rats in the paw incision model of postoperative pain (which resulted in mechanical hyperalgesia) (Lee et al., 2006). Central infusion of decahydroisoquinoline class of compounds (such as LY382884) into the cisterna magna produced antinociceptive effects which correlated well with their activity on GluK1-containing receptors (Jones et al., 2006), suggesting that supraspinal KARs may be a target for analgesic KAR antagonists.

As discussed earlier, KAR agonists such as glutamate (and kainate) produces fast and persistent desensitisation in KARs following the initial activation (Wilding and Huettner, 1997); this might allow KAR agonists to act as functional antagonists and analgesics. The high affinity agonist (2*S*,4*R*)-4-methylglutamate (SYM2081) produces fast desensitisation of both GluK1- and GluK2-containing KARs (Alt et al., 2004). SYM2081 has produced analgesic effects when administered intrathecally and intraperitoneally in thermal and mechanical hyperalgesia in preclinical models of pain, including chronic nerve constriction, capsaicin and carrageenan injections (Sutton et al., 1999; Ta et al., 2000; Turner et al., 2003). Another agonist of KARs MSVIII-19 also acts as a functional high-affinity inhibitor of GluK1-containing KARs and produced analgesia for thermal and mechanical hyperalgesia in inflammatory and chronic constriction models (Qiu et al., 2011).

Genetic ablation of the GluK1 subunit reduced pain behaviours such as paw licking caused by capsaicin or formalin injections in mice, which was not seen in genetic knockout of the GluK2 subunit (Ko et al., 2005). However, knockout mice did not show a change in mechanical allodynia (in which an otherwise innocuous stimuli such as light touch causes pain) induced by injection of complete Freund's adjuvant or in acute thermal and

mechanical sensitivity (Ko et al., 2005). The effects of long-term genetic deletion of KAR subunits on contribution from other KAR subunits or neurotransmitter systems, remains to be determined. Therefore, using developmental stage-specific or inducible knockout mice may help to better understand the role that KAR subunits play in neuronal signalling pathways of pain.

In addition to preclinical validation, KAR antagonists have entered clinical trials for the treatment of pain with varied success. The decahydroisoquinoline LY293558 was effective in alleviation of migraine pain and pain induced by capsaicin injections (Sang et al., 1998). LY293558 was also efficacious in alleviating postoperative pain with minimal side-effects and acceptable tolerance (Gilron et al., 2000). LY293558 was tested in phase II clinical trials for treatment of migraine pain and the study reported alleviation of pain (Murphy et al., 2008). A prodrug of LY293558, known as NGX426, has been reported to significantly reduce pain and hyperalgesia induced by capsaicin injection (Wallace et al., 2012). A phase I clinical trial for use of NGX426 in hyperalgesia was conducted in 2008 but the results have not been published to-date (ClinicalTrials.gov reference: NCT00832546).

In summary, a combination of pharmacological and genetic studies suggests that KARs are a viable target for treatment of pain. Both preclinical and clinical studies have also confirmed results from physiological investigations that compounds targeting KARs hold potential as therapeutic agents for treatment of pain. While the availability of GluK1-selective pharmacological agents has helped to formalise the targeting of GluK1 in hyperalgesia, investigations of other KAR subunits require more subunit-selective agonists, antagonists and allosteric modulators. Therefore, development of novel KAR subunit-selective compounds is an important step in establishing novel therapies for pain.

1.3. NMDA receptors

So far, the discussion about iGluRs has highlighted that postsynaptic neurotransmission in the CNS is mediated mainly by AMPARs and NMDARs whereas KARs act primarily as regulators of synaptic transmission. The multiplicity of KAR subunits and the lack of knowledge regarding the contribution of different KAR subunits to the KAR-mediated plasticity were previously highlighted. In contrast to KARs, the study of NMDARs has been more successful partly due to the availability of NMDAR-selective pharmacological

agents owing to lower amino acid sequence similarity between NMDARs and other iGluR subtypes (Traynelis et al., 2010).

There is significant diversity in the composition of the tetrameric NMDAR due to the existence of seven NMDAR subunits, namely GluN1, GluN2A-D, GluN3A-B. Functional NMDARs require assembly of two GluN1 subunits along with either two GluN2 or GluN3 subunits, or a combination of GluN2 and GluN3 subunits (Monyer et al., 1992; Chatterton et al., 2002; Schorge and Colquhoun, 2003; Ulbrich and Isacoff, 2007, 2008). The different NMDAR subtypes that result through the combination of these subunits have unique structural features, which accounts for their distinct pharmacological (Erreger et al., 2007) and functional (Monyer et al., 1992; Volianskis et al., 2013a) properties, which allows tuning of the receptor complex for a particular function (Cull-Candy et al., 2001).

The involvement of NMDARs in LTP was briefly discussed previously (see section 1.1.4.3). While NMDARs are expressed at synapses throughout the CNS, the wealth of information regarding NMDAR components in the cells of the hippocampus (discussed in sections 1.1.4.2, 1.1.4.3 and 1.3.7) has made it an ideal brain region to study novel functions of NMDARs. Therefore, the following review and our investigations will focus on the expression and synaptic functions of NMDAR subunits in the hippocampus.

1.3.1. Glycine and its analogues are co-agonists of NMDA receptors

An interesting characteristic of NMDAR activation is that a co-agonist, typically glycine (or D-serine), in addition to glutamate, is required for the activation of the receptor (Kleckner and Dingledine, 1988). X-ray crystal structures have revealed that glycine binds to the ligand binding domain (LBD) of GluN1 and GluN3 subunits (Furukawa and Gouaux, 2003; Yao and Mayer, 2006; Yao et al., 2008). Glycine binding to the GluN1- and GluN3-LBD involves some residues that are conserved between the two subunits although the amino acid sequence homology of GluN1 and GluN3 subunits is only ~30% (Traynelis et al., 2010). This difference in residues lining the LBD cleft contributes to larger number of possible interdomain interactions in GluN3 which could explain the 600-fold greater affinity of glycine for the GluN3 subunit compared to GluN1 (Yao and Mayer, 2006; Yao et al., 2008).

In diheteromeric GluN1/GluN2 NMDARs, the identity of the GluN2 subunit affects the potency of glycine through intra-receptor interactions (Sheinin et al., 2001; Chen et al., 2008; Dravid et al., 2010; Jessen et al., 2017). Indeed, the potency of glycine at GluN1/GluN2A is ~10-fold lower than at GluN1/GluN2D (Chen et al., 2008). D-cycloserine is a cyclic analogue of glycine that acts as a partial agonist at the GluN1 subunit (Hood et al., 1989; Dravid et al., 2010). While D-cyloserine (Figure 1.12) acts as a partial agonist at GluN2A-, GluN2B- and GluN2D-containing NMDARs, it produces much higher responses from GluN2C-containing NMDARs compared to glycine (Sheinin et al., 2001; Dravid et al., 2010). Therefore, the identity of the GluN2 subunit within the NMDAR also determines the potencies of D-cycloserine.

In addition to glycine, D- and L-isomers of serine and alanine are also agonists at the GluN1 subunit (Figure 1.12) (Pullan et al., 1987; McBain et al., 1989). D-Serine is more potent than L-serine and whether D-serine or glycine is the co-agonist may depend on the brain region and subcellular localisation of the NMDAR (Panatier et al., 2006; Papouin et al., 2012; Mothet et al., 2015). For example, D-serine may be the primary co-agonist for NMDARs in the supraoptic nucleus (Panatier et al., 2006). Indeed, a study has suggested that at the hippocampal SC-CA1 pyramidal cell synapses, D-serine is the primary co-agonist whereas glycine is more important at extrasynaptic sites (Papouin et al., 2012). While extracellular glycine (or D-serine) concentrations are fairly constant, it is unlikely to be at a saturating concentration for NMDAR co-agonist binding (Berger et al., 1998; Bergeron et al., 1998; Billups and Attwell, 2003). Therefore, the requirement of a co-agonist provides an additional mechanism by which synaptic activation can be modulated by targeting the co-agonist binding site of NDMARs (Ahmadi et al., 2003; Meunier et al., 2017).

While GluN1/GluN2 diheteromeric NMDARs binds glycine as a co-agonist, GluN1 and GluN3 subunits are capable of forming diheteromeric GluN1/GluN3 receptors that produce excitatory currents after binding glycine in X. laevis oocytes and cerebrocortical neurons (Chatterton et al., 2002). It is also possible to have a GluN1/GluN2/GluN3 triheteromeric receptor in the X. laevis oocyte expression system (Das et al., 1998; Perez-Otano et al., 2001). Diheteromeric (GluN1/GluN3A) and triheteromeric (GluN1/GluN3A/GluN3B) NMDARs have lower Ca^{2+} permeability and lower sensitivity to blockage by Mg^{2+}

compared to NMDARs containing only GluN1 and GluN2 (Das et al., 1998; Perez-Otano et al., 2001; Sasaki et al., 2002).

1.3.2. Glutamate site agonists of NMDA receptors

GluN2 subunits can be activated by glutamate, D- and L-aspartate (Benveniste, 1989; Nicholls, 1989; Fleck et al., 1993), homocysteate, and cysteinesulfinate (Do et al., 1986, 1988; Olney et al., 1987). Cyclic analogues of glutamate such as (*R*,*S*)-(tetrazol-5-yl)glycine (compound III) and (2*S*,3*R*,4*S*)-2-(carboxycyclopropyl) glycine (L-CCG-IV) are potent agonists of GluN2 subunits with EC_{50} values up to 10 times lower than glutamate (Figure 1.12) (Shinozaki et al., 1989; Schoepp et al., 1991; Erreger et al., 2007). Amongst most orthosteric agonists, there is a gradation of potency from GluN2A to GluN2D such that the agonist is least potent at GluN2A (highest EC_{50} value) and most potent at GluN2D (lowest EC_{50} value) (Kutsuwada et al., 1992; Monyer et al., 1992; Erreger et al., 2007). Subunit-selective agonists are unavailable but some agonists such as *N*-hydroxypyrazol-5-ylglycine derivatives and SYM2081 (also a KAR agonist, see section 1.2.1) have promising subunit selectivity (Erreger et al., 2007; Clausen et al., 2008). For example, SYM2081 has 46-fold greater potency on GluN2D over GluN2A containing NMDARs as represented by the EC_{50} for activation of diheteromers expressed on X. laevis oocytes (Erreger et al., 2007). A significant physiological feature of the GluN2 subunits in the function of NMDAR complex is the decay of the currents mediated by diheteromeric NMDARs containing the four GluN2 subunits (Figure 1.13). GluN2A shows the fastest current decay (decay time constant, τ_{decay} ~22-230 ms) whereas GluN2D shows significantly slower decay ($\tau_{decay} > 2$ s) following receptor activation by glutamate (and the co-agonist glycine) (Figure 1.13) (Monyer et al., 1992; Vicini et al., 1998). Given that NMDARs have a significant Ca^{2+} permeability (Mayer et al., 1984; Nowak et al., 1984), the nature of the intracellular signal transduction mechanism, which is dependent on Ca^{2+} influx through NMDARs, may be affected by the identity of subunits in the NMDAR complex (e.g. Erreger et al., 2005; Sobczyk et al., 2005; also reviewed in Shipton and Paulsen, 2014).

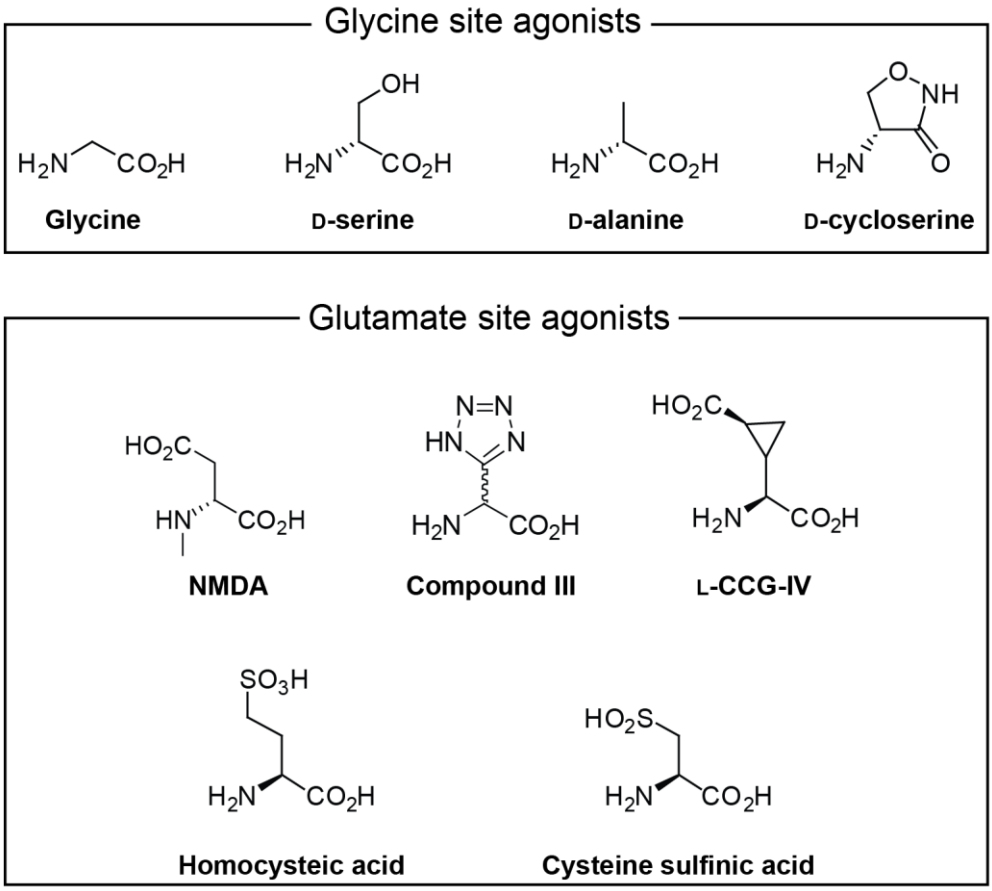

Figure 1.12. Structures of NMDA receptor agonists.

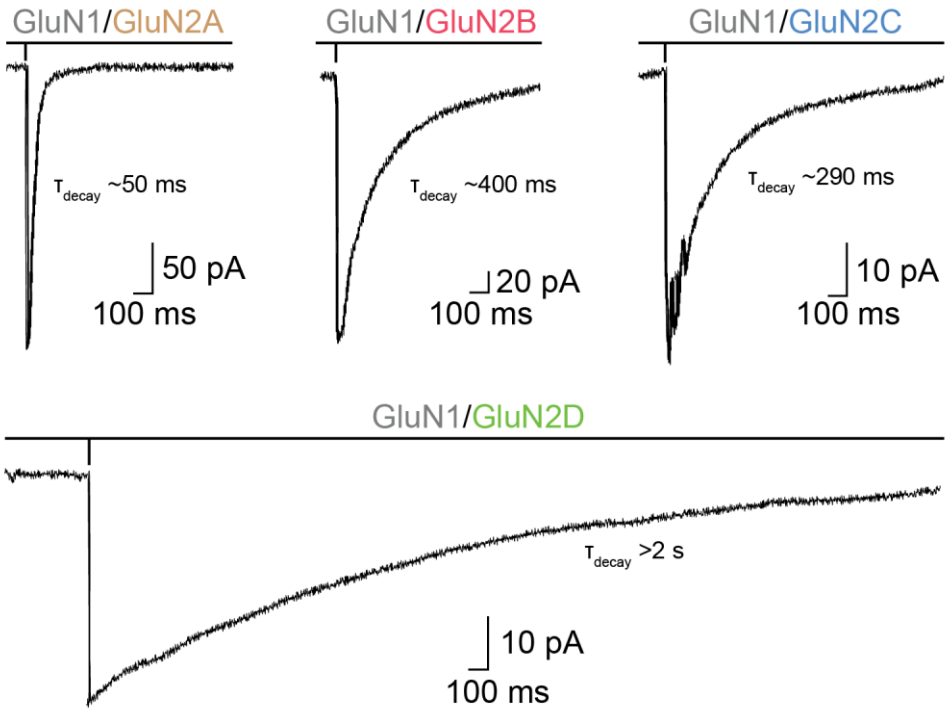

Figure 1.13. Current kinetics of GluN2-containing diheteromeric *N*-methyl-D-aspartate receptors. Schematic showing the decay (decay time constant, τ_{decay}) of whole-cell patch-clamp currents (voltage clamped at –50 mV) mediated by diheteromeric glutamate-gated NMDARs expressed on HEK293 cells. The extracellular media was free of Mg^{2+} and contained 10 µM glycine. The receptors were activated by a 1 ms pulse of 1 mM glutamate indicated by open tip current (vertical deflection) above each current trace (decay traces based on Vicini et al., 1998).

1.3.3. Competitive antagonists of NMDA receptors

Competitive antagonists that act on the GluN1 subunit include the kynurenic acid derivative 7-chlorokynurenic acid and its analogue 5,7-dichlorokynurenic acid (DCKA) (Figure 1.14) (Birch et al., 1988; Kemp et al., 1988; Mayer et al., 1988). In similarity with GluN1 agonists, the identity of the GluN2 subunit in the NMDAR complex affects the potency of DCKA (Hess et al., 1998). Other antagonists that bind to the LBD of the GluN1 subunit include 4-*trans*-2-carboxy-5,7-dichloro-4-phenylaminocarbonylamino-1,2,3,4-tetrahydroquinoline (L689,560) (Figure 1.14), which inhibits currents from GluN1/GluN2A and GluN1/GluN2B recombinant diheteromers expressed on X. laevis oocytes with K_i values of 4 nM and 20 nM, respectively (Hess et al., 1996).

The competitive antagonist of GluN2 subunits, (*R*)-2-amino-5-phosphonopentanoate (D-AP5) (Figure 1.14), and its analogues have been used to selectively block NMDAR

mediated responses without antagonist activity on AMPARs and KARs (Davies et al., 1981a, 1986; Evans et al., 1982; Lester et al., 1990). The antagonist D-AP5 inhibited NMDARs expressed in X. laevis oocytes with K_i values between 0.28 and 3.7 μM such that the potency was highest at GluN2A- and lowest at GluN2D-containing diheteromers (Feng et al., 2005). Subunit-selective competitive antagonists of GluN2 have been difficult to develop due to the high sequence similarity between the binding clefts of GluN2A through to GluN2D (Traynelis et al., 2010). One example of a modestly GluN2A-selective competitive antagonist is (*R*)-[(*S*)-1-(4-bromo-phenyl)-ethylamino]-(2,3-dioxo-1,2,3,4-tetrahydroquinoxalin-5-yl)-methyl-phosphonic acid (NVP-AAM077) which has 5- to 10-fold selectivity for GluN2A over GluN2B containing receptors (GluN2A K_i = 5.4 nM) (Frizelle et al., 2006; Neyton and Paoletti, 2006; Volianskis et al., 2013a). Another example is the antagonist 3-((*R*)-2-carboxypiperazin-4-yl)-propyl-1-phosphonic acid (CPP) (Figure 1.14) which has ~50-fold preference for GluN2A over GluN2D (GluN2A K_i = 41 nM) but intermediate affinities for GluN2B (K_i = 270 nM) and GluN2C (K_i = 630 nM) (Kutsuwada et al., 1992; Feng et al., 2005).

Some competitive antagonists such as (2*S*,3*R*)-1-(phenanthren-2-carbonyl)piperazine-2,3-dicarboxylic acid (PPDA) (Figure 1.14) and some of its derivatives have increased potency for GluN2C and GluN2D subunits compared to GluN2A and GluN2B subunits (Feng et al., 2005). Attachment of the carbonyl linker in PPDA to the 3-position rather than the 2-postion of the phenanthrene ring led to the development of a series of competitive antagonists with greater selectivity for GluN2D over GluN2A and GluN2B (Feng et al., 2004, 2005; Morley et al., 2005; Costa et al., 2009; Irvine et al., 2012). The most selective in this class were (2*R**,3*S**)-1-(phenanthrene-3-carbonyl)piperazine-2,3-dicarboxylic acid (UBP141) and (2*R**,3*S**)-1-(9-bromophenanthrene-3-carbonyl)piperazine-2,3-dicarboxylic acid (UBP145) both of which had ~10-fold selectivity for GluN2D (K_i ~1 μM, on recombinant diheteromers on X. laevis oocytes) over GluN2A or GluN2B (Costa et al., 2009). Recent attempts to improve the GluN2D selectivity of PPDA analogues led to the development of (2*R**,3*S**)-1-(7-(2-carboxyethyl)phenanthrene-2-carbonyl)piperazine-2,3-dicarboxylic acid (UBP791) in which a 2-carboxyethyl substituent was added to the 7-position of the phenanthrene moiety of PPDA (Sapkota, 2016). UBP791 was shown to have much greater selectivity for GluN2D over GluN2A (> 130-fold; GluN2D K_i = 140 nM) and

GluN2B (~20-fold) subunits but similar potency on GluN2C and GluN2D subunits (Sapkota, 2016).

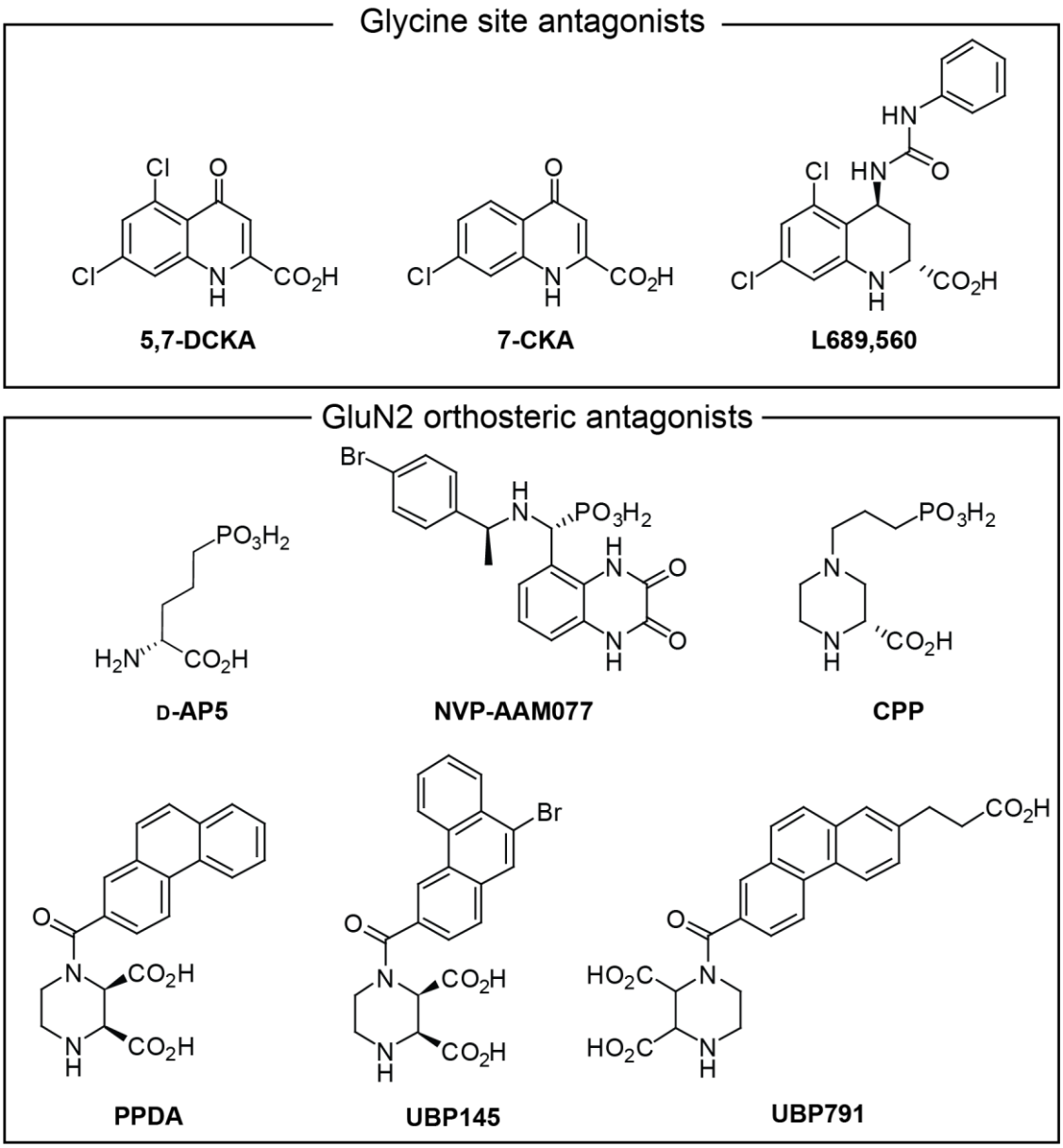

Figure 1.14. Structures of antagonists of GluN1 glycine binding site and GluN2 glutamate binding site.

1.3.4. Negative allosteric modulators of NMDA receptors

Developing subunit-selective competitive antagonists are difficult due to the high sequence similarity in the LBD of subunit families (see section 1.3.3). However, negative allosteric modulators (NAMs), which bind to a site remote from the ligand binding site where the sequence similarity between subunits is lower compared to LBD, may be better candidates

for obtaining greater subunit selectivity. Indeed, the first subunit-selective inhibitor of NMDARs was the phenylethanolamine ifenprodil, a voltage-independent negative allosteric modulator of GluN2B-containing NMDARs (Williams, 1993; Hess et al., 1998). Ifenprodil (Figure 1.15) inhibits GluN2B-containing NMDARs with high affinity and is 200-400-fold potent for GluN2B (IC_{50} ~150 nM) over GluN2A-, GluN2C- and GluN2D-containing NMDARs (Williams, 1993; Hess et al., 1998). More potent analogues of ifenprodil include α-(4-hydroxyphenyl)-β-methyl-4-(phenylmethyl)-1-piperidine propanol (Ro 25-6981) and traxoprodil mesylate (CP-101,606) (Figure 1.15) (Chenard et al., 1995; Fischer et al., 1997; Mott et al., 1998). Ro 25-6981 inhibits GluN2B diheteromeric receptors in X. laevis oocytes with IC_{50} value of 9 nM and is > 5000-fold selective for GluN2B over other GluN2 subunits (Fischer et al., 1997). Crystal structures of ifenprodil and Ro 25-6981 suggests that they bind to a known modulatory domain in the GluN2B amino terminal domain (ATD) and may stabilise an agonist-bound state of the receptor which has low open probability (Karakas et al., 2009). While ifenprodil has high affinity for diheteromeric GluN1/GluN2B NMDARs, its affinity for triheteromeric GluN1/GluN2A/GluN2B receptors is intermediate between its affinity for GluN1/GluN2A and GluN1/GluN2B diheteromers (Hatton and Paoletti, 2005; Hansen et al., 2014). Moreover, the effects of ifenprodil on current kinetics is different in GluN1/GluN2A/GluN2B triheteromeric receptors compared to GluN1/GluN2B diheteromers such that in the presence of ifenprodil, the rate of onset of the current was slower and the rate of decay of the current was faster in GluN1/GluN2A/GluN2B triheteromers compared to diheteromeric GluN1/GluN2B receptors (Hatton and Paoletti, 2005).

Another class of non-competitive NMDAR antagonists is based on the non-competitive antagonist of AMPARs, (*S*)-3-(2-chlorophenyl)-2-[2-(6-diethylaminomethyl-pyridin-2-yl)-vinyl]-6-fluoro-3*H*-quinazolin-4-one (CP-465,022) (Mosley et al., 2010). Modification of the CP-465,022 ring structure led to quinazolin-4-ones with > 100-fold NMDAR selectivity over AMPAR and KAR (Mosley et al., 2010). Furthermore, some analogues were 50-fold more selective for GluN2C and GluN2D than for GluN2A and GluN2B (Mosley et al., 2010). These compounds do not interfere with glutamate binding and their action is voltage-independent, suggesting that they are not ion channel blockers (Mosley et al., 2010; Hansen and Traynelis, 2011).

More recently, a NAM of the glycine site of NMDARs, 3-chloro-4-fluoro-*N*-[(4-[(2-(phenylcarbonyl)hydrazino)carbonyl]phenyl)methyl]-benzenesulfonamide (TCN-201), has been developed as a GluN2A-selective antagonist (Edman et al., 2012; Hansen et al., 2012). TCN-201 (Figure 1.15) inhibits the binding of glycine (and D-serine) by binding to the GluN1/GluN2A LBD dimer interface (Hansen et al., 2012). TCN-201 inhibited GluN1/GluN2A diheteromers expressed in X. laevis oocytes with an IC_{50} of 320 nM and had no effect on GluN2B-D subunits at concentrations < 10 μM (Hansen et al., 2012).

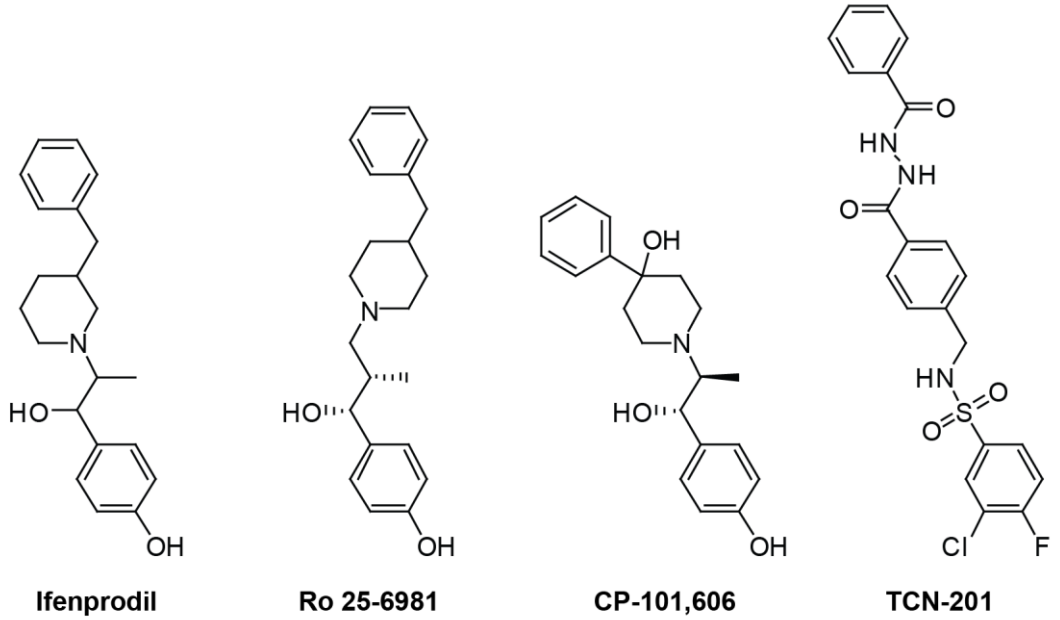

Figure 1.15. Structures of negative allosteric modulators of NMDA receptors

1.3.5. Channel blockers of NMDA receptors

As discussed earlier, NMDAR ion channel is blocked at resting membrane potential by Mg^{2+} (see section 1.1.4.3). Other molecules that block the ion channel include open channel blockers, which require the channels to be open for the blockers to bind to the ion channel pore in the transmembrane domain (TMD) (thus they are also known as uncompetitive antagonists) (Neely and Lingle, 1986; Huettner and Bean, 1988). Due to the requirement of the channel opening, the effect of channel blockers is use-dependent and increases with increase in channel open probability. Some channel blockers can become trapped in the ion channel after channel closure and their dissociation from the channel requires reopening of the channel and the dissociation is slow to reverse (Brackley et al., 1993; Parsons et al., 1995; Blanpied et al., 1997). These blockers (known as trapping blockers) include the

dissociative anaesthetics dizocilpine maleate (MK-801), ketamine and phencyclidine (PCP) (Figure 1.16) (Anis et al., 1983; Martin and Lodge, 1985; Wong et al., 1986; Huettner and Bean, 1988). Some trapping blockers such as amantadine and memantine (Figure 1.16) have faster reversal of channel block (due to faster unbinding) and are known as partially trapping blockers (Blanpied et al., 1997). The faster unbinding of partial trapping blockers may be therapeutically beneficial because they block the overactivation of NMDARs while leaving the normal synaptic transmission unaffected (Chen and Lipton, 2005).

Most NMDAR channel blockers display some selectivity between GluN2 subunits, which contain the obligatory glutamate binding site in an NMDAR (Yamakura et al., 1993). For example, MK-801 is ~10-fold more selective for GluN2A- and GluN2B-containing receptors than GluN2C- and GluN2D-containing receptors (Bresink et al., 1996; Dravid et al., 2007). The amino acid sequence homology in the pore-forming regions of GluN2 subunits means that targeting the pore region (i.e. using channel blockers) for subunit selectivity with small molecules may be difficult. An important consideration when determining the activity of channel blockers is to consider the pH and Mg^{2+} concentration in the pharmacological characterisation assay. For example, the association rate of the trapping blocker MK-801 is increased at lower pH (Dravid et al., 2007). Moreover, ketamine and memantine have 5- to 10-fold selectivity for GluN2C- and GluN2D-containing receptors over GluN2A- and GluN2B-containing receptors in the presence of 1 mM extracellular Mg^{2+}, which is a physiological concentration of Mg^{2+} in rats; whereas no such selectivity is observed in the absence of extracellular Mg^{2+} (Jeong et al., 2006; Kotermanski and Johnson, 2009). In summary, channel blockers of NMDARs may be used to target specific NMDAR subunits and may help to elucidate the role of specific NMDAR subunits in both physiological and pathophysiological conditions.

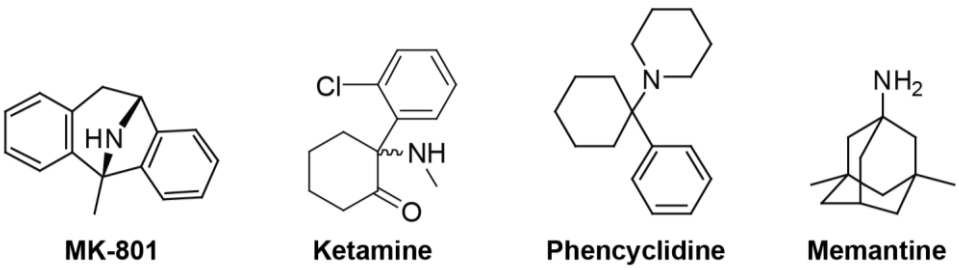

Figure 1.16. Structures of NMDA receptor channel blockers.

1.3.6. Zinc ions and protons inhibit NMDA receptors

The zinc ion (Zn^{2+}) is a potent inhibitor of native and recombinant NMDARs (Peters et al., 1987; Westbrook and Mayer, 1987; Williams, 1996). At mammalian presynaptic neurons Zn^{2+} is co-packaged into vesicles with glutamate in the terminals of many synapses including synapses in the hippocampus where Zn^{2+} may be co-released with glutamate during neuronal activity (Pérez-Clausell and Danscher, 1985; Frederickson, 1989; Paoletti et al., 2009). GluN1/GluN2A diheteromeric receptors are inhibited by Zn^{2+} in a biphasic manner; the inhibition of GluN2A by Zn^{2+} involves a voltage-independent high-affinity (K_i = 80 nM) phase and a voltage-dependent low-affinity component (K_i = 45 µM) (Christine and Choi, 1990; Chen et al., 1997). GluN1/GluN2B diheteromeric receptors are inhibited by Zn^{2+} in a voltage-dependent and voltage-independent manner (K_i = 1.6 µM) (Williams, 1996; Traynelis et al., 1998; Rachline et al., 2005). The high-affinity inhibition of GluN2A by Zn^{2+} is mediated through Zn^{2+} binding to the amino terminal domain (ATD) of the GluN2A (Gielen et al., 2009; Yuan et al., 2009a, 2009b). The low-affinity Zn^{2+} inhibition of GluN2A depends on residues inside the M2 re-entrant loop, which contributes to the channel pore (Legendre and Westbrook, 1990; Paoletti et al., 2000). Crystallographic studies suggest that Zn^{2+} inhibits GluN2B by binding to the cleft in the ATD bi-lobed domain and stabilises a closed cleft conformation within the ATD (Karakas et al., 2009). The structural changes that translate Zn^{2+} binding to ion channel closing is not fully understood; however, studies from ifenprodil binding to ATD demonstrated that the conformational changes in the ATD is translated to the LBD such that LBD dimer interaction is disrupted in a manner analogous to receptor desensitisation (Tajima et al., 2016; see section 1.1.2), which is believed to lead to ion channel closure (reviewed in Hansen et al., 2018).

In addition to the inhibition by Zn^{2+}, NMDARs are also inhibited by protons in a voltage- and agonist-independent manner (Christensen and Hida, 1990; Giffard et al., 1990; Traynelis and Cull-Candy, 1990). Alternative RNA splicing of the GluN1 subunit in the ATD affects the potency of proton inhibition (Traynelis et al., 1995). Additionally, mutagenesis studies suggest that residues near the ion channel pore, which contribute to the channel gate and residues in the ligand binding domain (LBD) dimer interface mediate pH sensitivity (Low et al., 2003; Sobolevsky et al., 2009). Therefore, pH may have tight

coupling to the gating properties of the channel as suggested by the sensitivity of MK-801 to pH (see section 1.3.5).

1.3.7. NMDA receptors and induction of potentiation of synaptic responses

Previously, the role that NMDAR plays in induction of LTP at the SC-CA1 synapses was briefly discussed (see section 1.1.4.3). The first evidence for the involvement of NMDAR in synaptic plasticity came from a study by Collingridge and colleagues, which demonstrated that inhibition of NMDARs using the NMDAR-specific antagonist D-AP5 blocked the induction of long-term potentiation (LTP) at the SC-CA1 synapses in the hippocampus (Collingridge et al., 1983). In this study, LTP was induced by high frequency stimulation (HFS, pulses at 100 Hz given for 1 sec) of the afferent Schaffer collateral fibres to CA1 (Collingridge et al., 1983). In live animals, bursts of discharges at an interval that is aligned with the theta rhythm (neural oscillations with frequencies in the range 4-7 Hz) is observed (Bland et al., 1980). In line with this observation, a physiologically relevant stimulation paradigm, the theta burst stimulation (TBS, 10 bursts of 4 pulses at 100 Hz given at an interval of 200 ms) (Larson et al., 1986), has also been employed to induce NMDAR-mediated LTP blocked by the NMDAR antagonist D-AP5 (e.g. Volianskis and Jensen, 2003). The finding that NMDARs mediate induction of LTP has been confirmed by studies that used competitive NMDAR antagonists related to D-AP5 (Harris et al., 1984), the use-dependent antagonist MK-801 (Coan et al., 1987) and the glycine site antagonist 7-chlorokynurenic acid (Bashir et al., 1990). Further evidence came from studies using genetically engineered mice, the obligatory GluN1 subunit was selectively knocked out in the CA1 region but not the dentate gyrus. In such studies, LTP could not be induced in the CA1 region but was induced in the dentate gyrus (Tsien et al., 1996).

How does the NMDAR contribute to the induction of LTP? Hebbian plasticity requires that the presynaptic neuron engages in firing postsynaptic neuron for the synaptic weight to change (see section 1.1.4.3). However, there is evidence to suggest that firing of the postsynaptic cell is not necessary in all cases for the induction of LTP; this is the case in some investigations of pairing-induced LTP where a compound that inhibits postsynaptic cell firing (by blocking voltage-gated sodium channels) still produced LTP (Kelso et al., 1986; Gustafsson et al., 1987). Whether depolarisation of the postsynaptic neuron occurs independently of the neuron firing in vivo is unresolved whereas experimentally, it is

possible to depolarise the postsynaptic membrane sufficiently without causing firing of the postsynaptic neuron (e.g. using caged glutamate that can be activated, or uncaged, specifically at dendritic spines by two-photon excitation; see Matsuzaki et al., 2004). The Hebbian rule described in section 1.1.4.3 can therefore be modified such that the coupling of presynaptic activity with the postsynaptic depolarisation can induce LTP.

1.3.7.1. NMDA receptors mediate induction of long-term potentiation

As discussed earlier, three important features of LTP are (1) cooperativity, (2) input-specificity and (3) associativity (see section 1.1.4.3). NMDARs have been shown to be central in all three of these features.

Input specificity is a property of LTP, which states that only the tetanised inputs are potentiated (see section 1.1.4.3); the voltage dependence and the high calcium (Ca^{2+}) permeability of NMDAR ion channel confers NMDAR-dependent LTP with input specificity (MacDermott et al., 1986; Burnashev et al., 1995; Schneggenburger, 1996). The voltage-dependence of NMDARs means that the membrane potential must be sufficiently depolarised to allow opening of the NMDAR ion channel and induce LTP caused by increased influx of Ca^{2+} ions (Mayer et al., 1984; Nowak et al., 1984). During HFS or TBS, such a depolarisation is possible due to the prolonged activation of AMPAR (by glutamate) which depolarises the membrane and leads to removal of the NMDARs block Mg^{2+} (Dale and Roberts, 1985). Therefore, the voltage-dependent activation of NMDARs allows Ca^{2+} entry through the NMDAR ion channel, and lead to induction of LTP at inputs that have been tetanised but not at untetanised inputs (e.g. Müller and Connor, 1991).

The rise in intracellular Ca^{2+} during LTP is important as LTP induction is prevented by chelation of Ca^{2+} in the postsynaptic neuron (Lynch et al., 1983). A combination of confocal calcium imaging (using Ca^{2+} sensitive dye) and whole-cell patch-clamping of CA1 pyramidal neurons have shown that HFS leads to an increase in Ca^{2+} signal (observed as transient Ca^{2+} signal) mediated by NMDARs in the dendritic spine of postsynaptic neurons (in these experiments, voltage-gated Ca^{2+} channels were eliminated by clamping membrane at -35mV and intracellular Ca^{2+} stores were depleted using thapsigargin) (Regehr and Tank, 1990; Müller and Connor, 1991). In dendritic spines activated by the HFS, the transient Ca^{2+} signal peaks at 200 ms and decays to pre-tetanic levels with a half-

time of approximately 5 s (Alford et al., 1993). The Ca^{2+} transients were abolished by the NMDAR-selective antagonist D-AP5 but not CNQX (an AMPAR/KAR antagonist) (Alford et al., 1993). Moreover, the Ca^{2+} transients in spines that are potentiated lasts for > 7 min, whereas the Ca^{2+} signal in the dendritic tree decayed to pre-tetanic levels before 7 min (Müller and Connor, 1991). Therefore, the spine-specific long-lasting Ca^{2+} transients mediated by NMDARs provide further evidence for the input-specific nature of NMDAR-mediated LTP.

Cooperativity and associativity are features of LTP that assumes the requirement for a threshold for the induction of LTP (see section 1.1.4.3). A consequence of the voltage dependent Mg^{2+} block of NMDARs is that it allows NMDARs to act as co-incidence detectors of neuronal activity, which means that during persistent firing of the presynaptic neuron and the release of glutamate that follows, the depolarisation of postsynaptic neuron (caused by activation of AMPARs) is detected by NMDARs (Wigström and Gustafsson, 1985). The co-incidence detection by NMDARs also explains the cooperative and associative nature of NMDAR-mediated LTP, such that a weak input stimulus onto a dendrite could lower the threshold for subsequent input stimuli (McNaughton et al., 1978; Levy and Steward, 1979; Wigström and Gustafsson, 1985). The intracellular increase in calcium caused by NDMAR activation is augmented by Ca^{2+} release from the endoplasmic reticulum (ER) (Alford et al., 1993). The NMDAR-mediated Ca^{2+} transients are significantly reduced by compounds that inhibit Ca^{2+}-induced Ca^{2+} release from the ER and those that deplete intracellular Ca^{2+} stores – ryanodine and thapsigargin, respectively (Harvey and Collingridge, 1992; Alford et al., 1993). Blocking intracellular Ca^{2+} release from the ER using dantrolene (which inhibits ryanodine receptors to block intracellular Ca^{2+} release from the ER) and thapsigargin (which prevents refilling of intracellular Ca^{2+} stores by inhibiting Ca^{2+}-ATPase pumps on the ER), result in inhibition of LTP (Obenaus et al., 1989; Harvey and Collingridge, 1992; Bortolotto and Collingridge, 1993). Studies have shown that activation of metabotropic glutamate receptors (mGluRs) is also involved in release of Ca^{2+} from the ER and can induce LTP by a thapsigargin-sensitive mechanism, even if NMDARs are blocked (Bortolotto and Collingridge, 1993). Indeed, NMDAR-independent forms of LTP induction at the SC-CA1 synapse have been reported – such as LTP induced by L-type voltage-gated calcium channels (Grover and Teyler, 1990;

reviewed in Blundon and Zakharenko, 2008) and calcium permeable AMPARs (Jia et al., 1996; Park et al., 2016).

The EPSP in the CA1 pyramidal cell, which is evoked by the stimulation of Schaffer collateral axons using low-frequency stimulation (e.g. $\frac{1}{15}$ Hz) is mediated by AMPARs as revealed by application of AMPAR-selective antagonist GYKI53655 (Seifert et al., 2000). Stimulation of Schaffer collateral also activates feedforward GABAergic interneurons through glutamatergic synapses (Davies and Collingridge, 1989). Activation of GABAergic interneurons by Schaffer collateral causes GABA release at GABAergic synapses from the interneurons onto CA1 pyramidal cells and leads to an inhibitory postsynaptic potential (IPSP) in the CA1 pyramidal cell (Andersen et al., 1964a, 1964b). The IPSP comprises a rapid $GABA_A$ receptor-mediated component and a slower $GABA_B$ receptor-mediated component (Alger and Nicoll, 1982). The IPSP is created by (1) the influx of Cl^- ions via the integral ion channel of activated $GABA_A$ receptors (Biscoe and Duchen, 1985), and (2) the opening of K^+ channels and modulation of voltage-gated Ca^{2+} channels caused by the activation of metabotropic $GABA_B$ receptors (Newberry and Nicoll, 1985; Kavalali et al., 1997). The IPSPs act to hyperpolarise the cell, which intensifies the Mg^{2+} block of NMDAR and prevents NMDAR activation during low-frequency stimulation (Alger and Nicoll, 1982; Nowak et al., 1984). Application of $GABA_A$ receptor inhibitors during low-frequency stimulation revealed an NMDAR-mediated synaptic response (Herron et al., 1985; Dingledine et al., 1986). Moreover, blockade of GABA receptors (and therefore the GABA receptor mediated hyperpolarisation) can greatly facilitate the induction of NMDAR-dependent LTP (Wigström and Gustafsson, 1983).

During high-frequency stimulation, the CA1 pyramidal cell is maintained in a depolarised state, which may be due to the temporal summation of AMPAR-mediated currents (e.g. Stuart and Sakmann, 1995) and shifting of the Cl^- and K^+ reversal potentials to more depolarised potentials due to the build-up of intracellular Cl^- and extracellular K^+ (Biscoe and Duchen, 1985; K^+ currents are reviewed in Storm, 1990). In addition to postsynaptic GABA receptors, which mediate the biphasic IPSP, presynaptic $GABA_B$ autoreceptors on GABAergic interneurons also play a significant role in the induction of TBS-induced LTP such that activation of presynaptic $GABA_B$ autoreceptors leads to suppression of subsequent GABA release from the interneuron (Davies et al., 1991). The $GABA_B$

autoreceptor mechanism takes ~20 ms to develop, peaks around 200 ms and has a duration of ~1 s (Davies et al., 1990). Therefore, theta patterns of activity (such as TBS, which has an interval of 200 ms between each train in the stimulus) are likely to most effectively suppress GABA release through the $GABA_B$ autoreceptor mechanism.

1.3.7.2. NMDA receptors mediate short term potentiation

Potentiation of excitatory field potentials, which is induced by HFS and TBS at the SC-CA1 synapse has several components with distinct underlying mechanisms (see Bliss and Collingridge, 2013 for a review). The initial decaying phase of potentiation following tetanus, called post-tetanic potentiation (PTP), is followed by a decaying phase known as short-term potentiation (STP), and a stable phase of potentiation generally referred to as LTP (see section 1.1.4.3). Induction of STP is blocked by application of D-AP5 during tetanus whereas the presynaptically expressed Ca^{2+}-dependent PTP was induced even in the presence of D-AP5 (e.g. Malenka, 1991). In vivo studies in which extracellular field potentials were recorded before, during and after exploratory learning in rats have reported a process resembling STP (potentiation that decayed to pre-learning levels in ~30 min) at perforant path to dentate gyrus granule cell synapses in the hippocampus (Moser et al., 1993, 1994).

Early evidence that STP could be induced and expressed independently of LTP was provided by experiments where a lower intensity tetanus than that required for induction of LTP could lead to STP (McNaughton, 1982). Experiments where potentiation was induced by application of NMDA instead of HFS (where NMDA was applied iontophoretically) also suggested that STP could be induced independently of LTP (Kauer et al., 1988). In the same study by Kauer and colleagues, induction of STP by NMDA application was not affected by the PKC inhibitor sphingosine, which blocked the induction of LTP (Kauer et al., 1988). The postsynaptic intracellular rise in Ca^{2+} following tetanus, which is required for LTP, is also necessary for STP induction (Anwyl et al., 1988; Malenka et al., 1988). Studies from single cells also suggest that induction of STP differs from that of LTP in that lower levels of postsynaptic depolarisation than that required for the induction of LTP can induce STP (through activation of the voltage-dependent NMDARs) (Malenka, 1991). Another difference in induction of STP and LTP is that the amplitude of STP depends on

the frequency of stimuli in the tetanus whereas amplitude of LTP depends on the number stimuli in the tetanus (Volianskis and Jensen, 2003).

In addition to the differences in induction protocols that augment or decrease STP independently from LTP, there is substantial evidence that expression of STP may be separate from that of LTP (e.g. Schulz and Fitzgibbons, 1997; Volianskis and Jensen, 2003). The first experiment to use paired-pulse stimulation during LTP expression also found that in the perforant path-dentate granule cell synapse, the early phase of LTP is associated with a decrease in paired-pulse facilitation (PPF) (McNaughton, 1982). Volianskis and Jensen conducted a detailed paired-pulse study to demonstrate that PPF was decreased during the STP phase of potentiation but PPF increased towards pre-tetanic levels as STP decayed (Volianskis and Jensen, 2003). As noted earlier, PPF is believed to be due to an increase in neurotransmitter release (i.e. it is a presynaptic phenomenon) (Wu and Saggau, 1994). However, changes in PPF during LTP may not be observed when recruitment of silent synapses are involved (Isaac et al., 1995; Liao et al., 1995). Postsynaptically silent synapses that lack AMPARs but contain only NMDARs are recruited during induction of LTP with the pairing protocol (Isaac et al., 1995; Liao et al., 1995). Another postsynaptic explanation for a change in PPF after tetanus is that GluA2-containing AMPARs may be inserted into the synapse after tetanus (Bagal et al., 2005). The increase in GluA2 subunit means that AMPARs have lower sensitivity to polyamine block since the GluA2 subunit is predominantly found in the Q/R edited form, which reduces the receptor's sensitivity to block by polyamines (see section 1.1.2) (Bagal et al., 2005). The lower sensitivity to blockage by polyamines of GluA2-containing AMPARs may explain the decrease in PPF after the tetanus due to the first pulse producing a larger response (than the second pulse) when compared to the pretetanic response to the first pulse (Bagal et al., 2005). In summary, while a change in PPF could arise due to postsynaptic mechanisms, the simplest explanation for these results is that STP involves a presynaptic component whereas LTP involves postsynaptic changes, at least in the SC-CA1 synapse.

In addition to possible differences in expression mechanisms underlying STP and LTP, STP was found to have some remarkable properties. Firstly, decay of the STP depends on the number on the number of stimuli in the low-frequency stimulation following induction of potentiation (the lower the frequency the slower the decay) (Volianskis and Jensen,

2003). Taken to an extreme, if stimulation is stopped for a duration following the induction of potentiation, STP does not decay until the stimulation recommences. Indeed, STP can be stored for at least 6 hours during discontinued stimulation (Volianskis and Jensen, 2003). Moreover, the duration of STP (i.e. its decay time constant) depends on the number of stimuli in the HFS used for inducing potentiation (larger number of stimuli leads to slower decay of STP) whereas higher frequency stimuli in the HFS train increases the amplitude of STP (Volianskis and Jensen, 2003).

An intriguing question concerning the different phases of potentiation is: do STP and LTP have different functional properties? Recordings from a population of neurons suggests that repetitive induction of STP using weak stimuli (30 Hz for 0.1 to 0.2s) and NMDA application transiently (lasting 50 to 80 min) increases the threshold for induction of LTP using a strong tetanus (100 Hz, 0.5 s) (Huang et al., 1992). A similar phenomenon is also observed in single CA1 pyramidal cells using the pairing protocol, where repetitive pairing of pre- and postsynaptic activity that produces STP led to smaller amplitude LTP after 10 min (Huang et al., 1992). However, another study found that the induction of STP using a single HFS tetanus 20 min before the tetanisation with two HFS tetani leads to induction of LTP (Schulz and Fitzgibbons, 1997). The reason(s) for the difference between the induction of LTP after induction of STP in these studies may be due to the differences in tetanus protocols (five repetitive HFS in the study by Huang and colleagues whereas a single HFS tetanus by Schulz and Fitzgibbons) (Huang et al., 1992; Schulz and Fitzgibbons, 1997). Nevertheless, these studies suggest that prior activity that leads to STP induction affects the induction of LTP. Another study investigating the effects of STP and LTP on neurotransmission found that during STP, synaptic responses to short bursts of pulses are potentiated in a non-linear manner (Volianskis et al., 2013b). However, the same burst of pulses during LTP results in linear amplification of synaptic responses (Volianskis et al., 2013b; also see Pananceau et al., 1998; Selig et al., 1999). This suggests that STP confers on synapses the ability to dynamically control short-term facilitation (and potentiation) of synaptic responses compared to during control (pre-tetanic) periods and during LTP (Pananceau et al., 1998; Volianskis et al., 2013b).

Pharmacological studies have shown that STP is less sensitive than LTP to the NMDAR antagonist D-AP5 (Malenka, 1991; Volianskis et al., 2013a). A study by Volianskis and

colleagues showed that induction of STP is inhibited by D-AP5 in a biphasic manner, comprising two distinct phases of roughly equal contribution to total STP (Volianskis et al., 2013a); however, sensitivity of LTP to D-AP5 contains a single component (Volianskis et al., 2013a). The components of STP were termed STP1 and STP2, where the sensitivity of D-AP5 is as follows: STP1 > LTP > STP2 (Volianskis et al., 2013a). STP1 and STP2 appears to be distinct in that STP1 contributes to the peak of the total STP response, whereas STP2 contributes by slowing the decay of STP (Volianskis et al., 2013a). However, decay of both STP1 and STP2 is activity-dependent and both types of STP can be stored if stimulation is stopped following induction of potentiation (as described earlier).

1.3.7.3. Different NMDA receptor subtypes mediate induction of short- and long-term potentiation

Much of the information regarding the roles that distinct NMDAR subunits play in induction of STP and LTP has come from pharmacological studies that used NMDAR antagonists with relative selectivity for one subunit over another. The NMDAR antagonists that are typically used are: D-AP5 (GluN2A- and GluN2B-selective at ≤1 μM) (Davies et al., 1981b), NVP-AAM007 (NVP: GluN2A-preferring) (Auberson et al., 2002; Neyton and Paoletti, 2006), Ro 25–6981 (Ro: GluN2B-selective) (Fischer et al., 1997) and UBP145 (GluN2D-preferring) (Costa et al., 2009); see sections 1.3.3 (D-AP5, NVP, UBP145) and 1.3.4 (Ro) for more details about activities of the compounds. A pharmacological study using the GluN2A- and GluN2B-selective antagonist D-CPPene (~13-fold selectivity for GluN2A and GluN2B over GluN2C and GluN2D) suggested that GluN2A and/or GluN2B may be responsible for LTP whereas GluN2C and/or GluN2D may contribute to induction of LTD (Hrabetova et al., 2000). In the study by Hrabetova and colleagues, 1 μM D-CPPene (a concentration expected to block GluN2A and GluN2B but not GluN2C and GluN2D) blocked the induction of LTP with HFS (100 Hz train for 1 sec) but did not block the induction of LTD (Hrabetova et al., 2000). Another study, which used the NMDAR antagonists NVP, Ro, ifenprodil and GluN2A- and GluN2B-selective concentrations of D-AP5, demonstrated that LTP induction (using HFS) is blocked by GluN2A-blocking concentration of NVP (0.4 μM) and D-AP5 (0.5 μM) but not the GluN2B diheteromer-selective concentrations of ifenprodil (3 μM) and Ro (0.5 μM) (Liu et al., 2004). Other studies at the SC-CA1 synapse have corroborated the finding that blockage of GluN2A (using NVP at 0.1–0.4 μM) inhibits the induction of LTP, and concentrations of Ro capable

of blocking GluN2A/GluN2B triheteromeric receptors (using Ro at 5 and 10 μM) blocks induction of LTP at the SC-CA1 synapse especially of juvenile mice (postnatal day 14 or P14) (e.g. Bartlett et al., 2007; France et al., 2017).

The discovery of dual components of STP (see section 1.3.7.2) was accompanied by a characterisation of the sensitivity of STP and LTP to various NMDAR antagonists with varying selectivity for the GluN2A, GluN2B or GluN2D NMDAR subunits, namely D-AP5, Ro, NVP and UBP145 (Volianskis et al., 2013a). Concentration-response relationships describing the ability of these antagonists to inhibit STP and LTP revealed that inhibition of STP1 and LTP had the same rank order of potency amongst the antagonists – NVP > AP5 > Ro > UBP145 (Volianskis et al., 2013a). However, STP2, which contributes to the slow decay of STP, had a different rank order of potency, namely: Ro > NVP > UBP145 > AP5. Therefore, STP2 was suggested to represent a pharmacologically distinct component when compared to STP1 and LTP. At a test frequency of $\frac{1}{15}$ Hz, STP1 decayed at a faster rate with a single exponential decay time constant (τ) of around 7 min when compared to STP2, which decayed with a τ value of around 16 min (Figure 1.17). In conclusion, it was found that STP2 contributes more to the decay of global STP whereas STP1 contributes more to the peak of potentiation (Figure 1.17) (Volianskis et al., 2013a).

The compounds mentioned above (D-AP5, NVP, Ro, UBP145) were also tested on pharmacologically isolated NMDAR-mediated postsynaptic currents (NMDAR-EPSCs) from CA1 pyramidal cells using the same slice preparations as was used for the LTP experiments (Volianskis et al., 2013a). The rank order of potency for inhibition of NMDAR-EPSCs, STP1 and LTP were highly correlated – i.e. the rank order was NVP > AP5 > Ro > UBP145 (Volianskis et al., 2013a). In contrast, STP2 did not correlate well to the rank order for inhibition of NMDAR-EPSCs, STP1 or LTP (Volianskis et al., 2013a). These results agree with the view that NMDARs that are responsible for mediating the postsynaptic response are also responsible for induction of LTP and STP1 whereas STP2 is induced by a different population of receptors that do not (at least directly) contribute to the postsynaptic response. The NMDAR population that mediates the induction of STP2 may be located at another cellular location such as on the presynaptic neuron (Berretta and

Jones, 1996; McGuinness et al., 2010) or at an extrasynaptic site on the postsynaptic neuron (e.g. Brickley et al., 2003; Lozovaya et al., 2004; Harney et al., 2008).

Despite the overlapping subunit inhibitory activities of NMDAR antagonists used in the study by Volianskis and colleagues, constructing concentration-response relationships for these antagonists, allowed differences between LTP, STP1 and STP2 to be identified (Volianskis et al., 2013a). The results from Volianskis and colleagues (2013a) suggest that TBS-induced LTP requires the activation of both GluN2A- and GluN2B-containing receptors for induction. This was partly established by the high sensitivity of LTP to D-AP5 (LTP IC_{50} = 0.95 µM) and NVP (LTP IC_{50} = 20 nM), in contrast to the other antagonists (Volianskis et al., 2013a). Induction of LTP was also sensitive to high concentrations (> 3 µM) of Ro (GluN2B-selective antagonist; LTP IC_{50} = 3.8 µM) however, Ro inhibits GluN2A- and GluN2B-containing recombinant triheteromeric NMDARs at these concentrations (Lü et al., 2017).

In contrast to LTP, induction of STP2 was highly sensitive to Ro at low concentrations (Ro's STP2 IC_{50} = 20 nM), suggesting that GluN2B-containing NMDARs mediate induction of STP2 (Volianskis et al., 2013a). The GluN2D-preferring antagonist UBP145 also inhibited induction of STP2 at concentrations that were selective for GluN2D-containing NMDARs (UBP145's STP2 IC_{50} = 2.18 µM), whereas LTP (IC_{50} = 31.6 µM) and STP1 (IC_{50} = 30.3 µM) inhibition needed higher concentrations of UBP145 (Volianskis et al., 2013a). It can be suggested therefore that induction of STP2 is dependent on GluN2B and GluN2D diheteromers or GluN2B/GluN2D triheteromeric receptors. The activity of Ro on native GluN2B/GluN2D triheteromeric receptors remains to be determined and it is not known whether the inhibition of STP2 induction by Ro is due to its inhibitory action on GluN2B/GluN2D triheteromers. Notably, Ro did not block GluN2D diheteromeric receptors (at concentrations up to 100 µM) whereas Ro had an IC_{50} value of ~100 µM on GluN2A diheteromeric receptors expressed on HEK293 cells (Volianskis et al., 2013a). The exact pharmacological basis of the early phase of STP, which contributes to its amplitude, namely STP1 was difficult to ascertain based on the NMDAR antagonists used in the study by Volianskis and colleagues because of the overlap in GluN2A and GluN2B activities of D-AP5 and NVP (Feng et al., 2005; Frizelle et al., 2006), which prevented selective block of GluN2A (and therefore STP1). Whether STP1 and LTP are mediated by

the identical population of receptors or those with similar pharmacology requires further study.

In summary, current evidence points to at least two pharmacologically and mechanistically distinct forms of STP, namely STP1 and STP2. Moreover, the induction of STP2 may be mediated by GluN2B- and GluN2D-containing NMDARs whereas induction of LTP (and possibly STP1) is mediated by GluN2A- and GluN2B-containing NMDARs. With regards to STP1, the results from the study by Volianskis and colleagues (2013a) supports the suggestion that the early phase of LTP (traditionally referred to as STP, but specifically STP1) is mediated by similar mechanisms as LTP (Gustafsson and Wigström, 1990).

In addition to the pharmacological studies mentioned above, genetic knockout animals have also provided evidence for subunit-selective roles of NMDARs. Knockout of GluN2A in mice led to reduced LTP compared to controls (Sakimura et al., 1995) and an increase in the threshold for induction of LTP compared to controls (Kiyama et al., 1998), at the SC-CA1 synapse. Another study using a genetic mutant mice lacking the C-terminal of GluN2A subunit suggests that in the hippocampus of younger animals (P14), GluN2A- and GluN2B-mediated components are required for inducing LTP whereas in adult (> P42) mice, the GluN2A component of LTP induction dominates even though LTP can be induced in genetically GluN2A CTD-truncated mice with multiple tetanisation (Köhr et al., 2003). In contrast to GluN2A knockout mice, mice lacking the GluN2B subunit globally (Kutsuwada et al., 1996) or expressing a CTD-truncated form of the GluN2B subunit globally (Sprengel et al., 1998), die at birth. However, conditional knockout of GluN2B in hippocampal pyramidal cells leads to mice with reduced (although not statistically significant) capability to induce LTP (with single tetanus and four tetani of HFS) at the SC-CA1 synapse, and deficits in short-term spatial working memory (Engelhardt et al., 2008). Conditional knockout of GluN2B in the pyramidal cells of the cortex and hippocampus CA1 led to impairment of LTP induction (at the SC-CA1 synapse) using two tetani of HFS but the LTP could be restored by repeated tetanisation (Brigman et al., 2010). In the CA3 region of the hippocampus, conditional knockout of GluN2B in pyramidal cells could not induce LTP (using HFS) in the commissural/associational-CA3 pyramidal cell synapses but did not affect KAR-mediated LTP induction in the MF-CA3 synapse (Akashi et al., 2009; see 1.2.5 for a discussion on KAR-mediated LTP in CA3).

Knockout of the GluN2D subunit leads to mice with deficits in spontaneous locomoter activity (reduced walking distance in an open field compared to wildtype littermates) (Ikeda et al., 1995) and lower sensitivity to stress (Miyamoto et al., 2002). Another study used a combination of GluN2D knockout mice and the GluN2B antagonist ifenprodil to demonstrate that NMDAR currents in CA1 pyramidal cells and parvalbumin positive interneurons of young (P3-5) mice but not older (P20-25) mice may be mediated by GluN2D-containing NMDARs (Engelhardt et al., 2015). Although GluN2D knockout mice have been used to study the role of GluN2D subunits in schizophrenia (e.g. Sapkota et al., 2016), these mice have not been used to study STP and LTP in the hippocampus.

In summary, both pharmacological and genetic studies have pointed to a role for GluN2A and GluN2B in the induction of NMDAR-mediated LTP in the SC-CA1 synapse (e.g. Kiyama et al., 1998; Hrabetova et al., 2000; Köhr et al., 2003; Liu et al., 2004; Bartlett et al., 2007; Volianskis et al., 2013a). A pharmacological investigation of the NMDAR subunit-specific roles in the induction of the early decremental phase of LTP (known as STP) has suggested that STP contains two pharmacologically distinct components (STP1 and STP2) (Volianskis et al., 2013a). The induction of STP1, which is the faster decaying component of STP that contributes mainly to STP amplitude, was selectively inhibited by GluN2A-selective antagonists whereas the induction of STP2 was inhibited by GluN2B- and GluN2D-selective antagonists (Volianskis et al., 2013a; France et al., 2017).

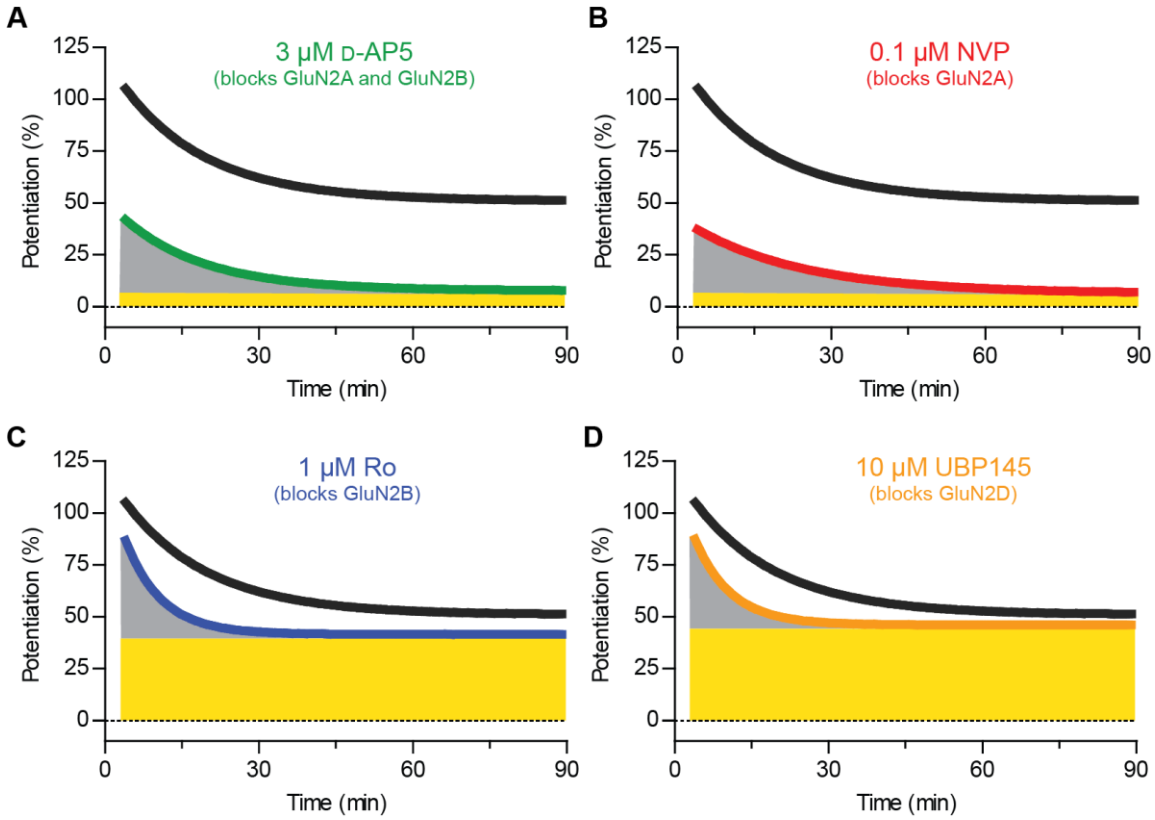

Figure 1.17. Different NMDAR subunits mediate induction of STP and LTP. Schematic diagrams in **A**-**D** are based on Volianskis et al., 2013a. **A**, Schematic showing the potentiation of field-excitatory postsynaptic potentials (f-EPSPs), which was induced in the presence of 3 μM D-AP5 (green line) compared to the control potentiation (black line). Residual STP (shaded grey) had a decay time constant (τ) of ~16.0 min whereas τ of control STP was ~16.4 min. Residual LTP (shaded yellow) was significantly inhibited compared to control LTP (D-AP5's IC_{50} of LTP = 0.95 μM). **B,** Similar to **A** but potentiation was induced in the presence of 0.1 μM NVP (red line). Residual STP and LTP are similar to that in the presence of 3 μM D-AP5. **C,** Similar to **A** but potentiation was induced in the presence of 1 μM Ro (blue line). Residual STP had a τ of ~7 min, which was different from τ of control potentiation (16.4 min); whereas residual LTP was not significantly reduced compared to control LTP (Ro's IC_{50} of LTP = 3.8 μM). **D,** Similar to **A** but potentiation was induced in the presence of 10 μM UBP145 (orange line). Residual STP and LTP were similar to that in presence of 1 μM Ro. The component of STP with fast decay (the residual STP in **C** and **D**), which is inhibited by concentrations of D-AP5 and NVP that block GluN2A, has been termed STP1; whereas the slowly decaying component of STP (the residual STP in **A** and **B**), which depends on GluN2B and GluN2D, has been termed STP2. Amplitude of LTP primarily depends on GluN2A- and GluN2B-containing receptors.

1.4. Aims of the thesis

So far, the introduction has focused mainly on two aspects of investigations involving iGluRs. Firstly, a need for subunit selective antagonists (namely GluK2-selective) that may help to better understand the physiological role of GluK2-containing KARs in physiology (see section 1.2.5) and disease (see section 1.2.6). Secondly, while pharmacological studies have suggested that GluN2D-containing receptors mediate induction of a component of STP (Volianskis et al., 2013a; France et al., 2017; Ingram et al., 2018), confirmation of this finding using a combination of GluN2D knockout animals and GluN2D-selective antagonists may help to further understand the roles of this subunit for potentiation.

The Bristol glutamate research group focus on investigating the role of NMDARs and KARs in hippocampal synaptic plasticity. We have developed a range of GluK1-selective antagonists, but GluK2-selective antagonists are not available, which is hampering research into the role of KAR subtypes in synaptic plasticity in the CA3 region of the hippocampus. In this study, a series of kynurenate derivatives, developed as potential GluK2-selective antagonists, were characterised on recombinant KAR and AMPAR subtypes and NMDARs and AMPARs expressed in the hippocampus.

With regards to NMDARs, we have recently published a study on the role of GluN2A, GluN2B and GluN2D in hippocampal synaptic plasticity (Volianskis et al., 2013a). UBP145 has only approximately 10-fold selectivity for GluN2D versus GluN2A and GluN2B (Costa et al., 2009; Volianskis et al., 2013a), so in this study the GluN2D selectivity of UBP145 was validated in GluN2D knockout mice. GluN2D knockout mice were also used alongside selective antagonists to investigate the role of GluN2D in STP and LTP. It was not possible to be involved in the pharmacological characterisation of antagonists on NMDAR subunits as the cloned receptor cell lines were not available in Bristol and the testing of compounds on NMDAR subunits expressed in X. laevis oocytes is carried out by a collaborator in Nebraska.

Despite the apparent disparity between the KAR and NMDAR sections of this thesis, the pharmacological principles used in the KAR section (which focuses on the development of GluK2-selective antagonists) are relevant for the NMDAR section (which focuses on

investigation of GluN2D subunits) in that development of novel GluN2D-selective antagonists would follow the same principles.

In summary, the aims of the thesis are:

1. to pharmacologically characterise novel compounds in order to develop novel GluK2-selective competitive antagonists (described in Chapter 2)
2. to use computational modelling to explain the GluK2-selectivity and potency of competitive KAR antagonists (described in Chapter 3)
3. to investigate the roles that GluN2D play in synaptic potentiation at the SC-CA1 synapse (described in Chapter 4)

Chapter 2

Pharmacological characterisation of GluK2-selective antagonists based on kynurenic acid

Physiological studies of GluK2 subunits have suffered from a lack of GluK2-selective antagonists (Jane et al., 2009; Møllerud et al., 2017). Previous work has led to the development of GluK1-selective antagonists using structure-activity relationship (SAR) studies and computer-aided drug design, notably based on the willardiine and decahydroisoquinoline series of compounds (Jones et al., 2006; Weiss et al., 2006; Dolman et al., 2007; Jane et al., 2009). In the study discussed in this chapter, the activities of kynurenic acid derivatives on various KAR and AMPAR subunits were determined and this SAR was used to develop more selective GluK2 antagonists. Biological characterisation of compounds was carried out using human GluK2, GluK1 and GluA1 homomeric receptors expressed in HEK293 cells using a calcium fluorescence assay. Compounds were further characterised on native iGluRs expressed in rat hippocampal slices using f-EPSP recordings.

2.1. Introduction

2.1.1. Rationale for developing GluK2-selective antagonists

It has become clear that KARs facilitate or depress both excitatory and inhibitory synaptic transmission in a cell type-, region-, and age-specific manner (Lerma and Marques, 2013; Carta et al., 2014). The functional differences of KARs is partly due to the combination of different subunits that form the KAR complex (Mulle et al., 1998; Contractor et al., 2003). The low-affinity KAR subunit, GluK2, is thought to be expressed in many synapses in the brain, including in the hippocampus CA3 region (Wisden and Seeburg, 1993; Watanabe-Iida et al., 2016).

In the hippocampal MF-CA3 synapse, studies using genetic knockout and antagonists of the GluK1 subunit have found that GluK2 may play an important role in potentiation of synaptic responses (Contractor et al., 2003), although studies using GluK1-selective antagonists have suggested that GluK1, but not GluK2 subunits, are important for the MF-CA3 synaptic potentiation (Bortolotto et al., 1999; Wallis et al., 2015). This disparity in results has been rationalised by the cell type-specific nature of expression of GluK2 subunits in the CA3 region and the possibility of heteromeric KARs containing both GluK1 and GluK2 subunits in addition to the high affinity GluK4 or GluK5 subunits (Jane et al., 2009). Uncertainty regarding the contributions of different KAR subunits to physiological

processes in other brain regions is likely to arise in the absence of pharmacological agents that allow the selective inhibition of GluK2 subunits.

From the currently available antagonists of KAR subunits, NS-102 (see section 1.2.2) has only ~6-fold selectivity for GluK2 over other KAR subunits and has poor water solubility (Verdoorn et al., 1994; Wilding and Huettner, 1996), limiting its use in physiological studies where GluK2-containing receptors also contain other KAR subunits and/or high concentrations of the compound may need to be used. Another avenue (in addition to NS-102) for GluK2 antagonists were the anaesthetic barbiturates, pentobarbital and phenobarbital, which were shown to inhibit GluK2 responses more potently than GluA3 responses (based on %-inhibition of kainate-mediated responses in X. laevis oocytes expressing GluK2 or GluA3 homomeric receptors) but their selectivity for GluK2 over other KAR subunits was not characterised (Dildy-Mayfield et al., 1996). More recent attempts at development of GluK2 antagonists have yielded the GluK2 negative allosteric modulator, ethyl-2-amino-4-methyl-5-phenylthiophene-3-carboxylate, which has ~16-fold selectivity for the GluK2 subunit (IC_{50} = 0.75 μM, determined from GluK2 homomeric receptors expressed in HEK293 cells) over GluK1 but its GluK2 selectivity over AMPARs or NMDARs has not been determined (Briel et al., 2010). Therefore, novel GluK2-selective antagonists are needed for future studies which investigate functions of the GluK2 subunit.

2.1.2. Kynurenic acid derivatives as GluK2 antagonists

Derivatives of kynurenic acid (Figure 2.1A) were previously investigated as potential competitive glycine site antagonists of NMDARs (Leeson et al., 1991). The 1991 SAR study by Leeson and colleagues found that 5,7-dichloro substituted kynurenic acid was a potent antagonist binding to the NMDAR glycine site. Moreover, the same study also found that simple substitutions at the 6-position on the phenyl ring of kynurenic acid decreased the NMDAR antagonist activity of kynurenic acid derivates but preserved the non-NMDAR antagonist activity. In the study by Leeson et al. (1991), activity of compounds on AMPARs and KARs were mainly characterised in rat cortical slices using the cortical wedge preparation in which quisqualic acid (QUIS) and kainic acid (KA) were used to induce responses from AMPARs and KARs, respectively, to test for inhibition by compounds. However, both QUIS and KA are agonists for AMPARs and KARs (Holm et al., 2005; Mayer, 2005), meaning that the compounds that caused inhibition of QUIS-

induced responses also caused inhibition of KA-induced responses. QUIS is also an agonist of group I metabotropic glutamate receptors (mGluRs) (see section 1.1.1) (Abe et al., 1992), further confounding the interpretation of results when using this agonist to induce responses from cortical slices where functional group I mGluRs are known to be expressed (Shigemoto et al., 1992; Wallis et al., 2015). Compounds that inhibited KA-induced responses in the cortical wedge preparation did not inhibit [^{3}H]KA binding to rat cortical membranes, but did correlate with [^{3}H]AMPA binding in radioligand binding studies, suggesting that the KA-induced responses in the cortical wedge preparation were mediated through AMPARs (Leeson et al., 1991). As such, the structure activity relationship of 6-substituted kynurenic acid derivatives in KARs remained unclear.

Since these initial experiments, specific subunits of KARs and AMPARs have been isolated and expressed in heterologous systems, which has greatly facilitated compound screening assays, (Bleakman et al., 1996; Alt et al., 2004). Research by Jane and co-workers has led to the refinement of assays for testing of compounds using HEK293 cells specifically expressing homomeric receptors containing GluK2, GluK1 or GluA1 subunits (Dargan et al., 2009). These protocols have been further adapted in the current study, allowing compound-library screening and a thorough characterisation of the activity of novel kynurenic acid derivatives on GluK2, GluK1 and GluA1 subunits. Suitable kynurenates exhibiting high activity on GluK2 in transfected HEK cells could then be further characterised on native AMPARs and NMDARs expressed in the Schaffer collateral-CA1 synapses of the rat hippocampus.

The kynurenic acid derivatives used in the current study could be classified into those with substitutions on the benzene/phenyl ring and those with modifications to the heterocyclic ring. Kynurenates with substitutions on the phenyl ring were further classified based on the nature of the 6-substitution, which was previously shown to reduce NMDAR activity (Leeson et al., 1991). Namely, the 6-substituted compounds were classed as those with halogen, polar or non-polar 6-substituents (Figure 2.1B-E). This classification ignored the electronegativity of halogens (rank order of electronegativity: F > Cl > Br > I) but provided a simple classification that allowed comparison of antagonist activity with functional groups at the 6-position with similar properties. Qualitative comparison of GluK2 and AMPAR antagonist activity with the hydrophobicity, size and electronic effects of the 6-

substituent was also carried out to investigate the effect of chemical parameters of the 6-substituent on the antagonist activity of kynurenates.

The compounds with substitutions on the heterocyclic ring (Figure 2.1F) were characterised due to a finding from a study by Rowley et al., (1993) that substitutions on the heterocyclic ring produced 3-acyl-4-hydroxyquinolin-2(1H)-ones which were higher affinity NMDAR glycine site antagonists than kynurenates (Rowley et al., 1993). Therefore, the KAR affinities of these compounds were also characterised.

2.1.3. Objectives

1. To screen kynurenic acid derivatives on human GluK2, GluK1 and GluA1 homomeric receptors individually expressed in HEK293 cells using a Ca^{2+} fluorescence assay in the FlexStation.
2. To further characterise the activities of active kynurenic acid derivatives on GluK2, GluK1 and GluA1 recombinant receptors individually expressed in HEK293 cells.
3. To characterise kynurenates with interesting GluK2 antagonist activity on native AMPARs and NMDARs in the rat hippocampus using an electrophysiological assay

A

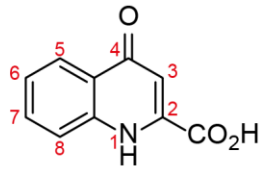

Kynurenic acid

B 5,7-diF substituted

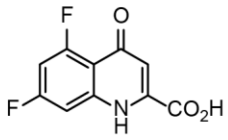

UBP2040

C 6-halogen substituted

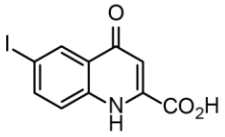

UBP2002

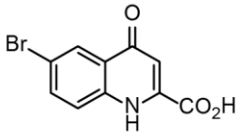

UBP2020

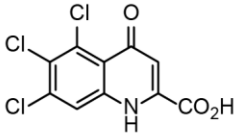

UBP2025

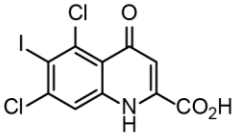

UBP2037

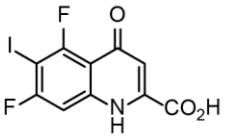

UBP2038

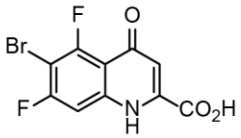

UBP2039

D Polar 6-substituted

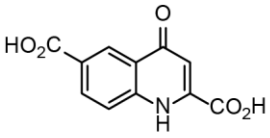

UBP2007

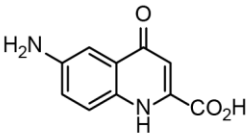

UBP2022

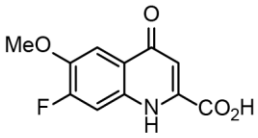

UBP2043

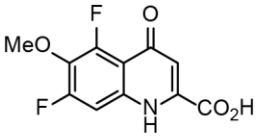

UBP2047

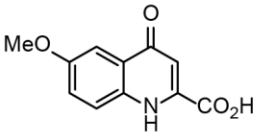

UBP2049

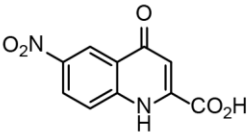

UBP2051

(continued)

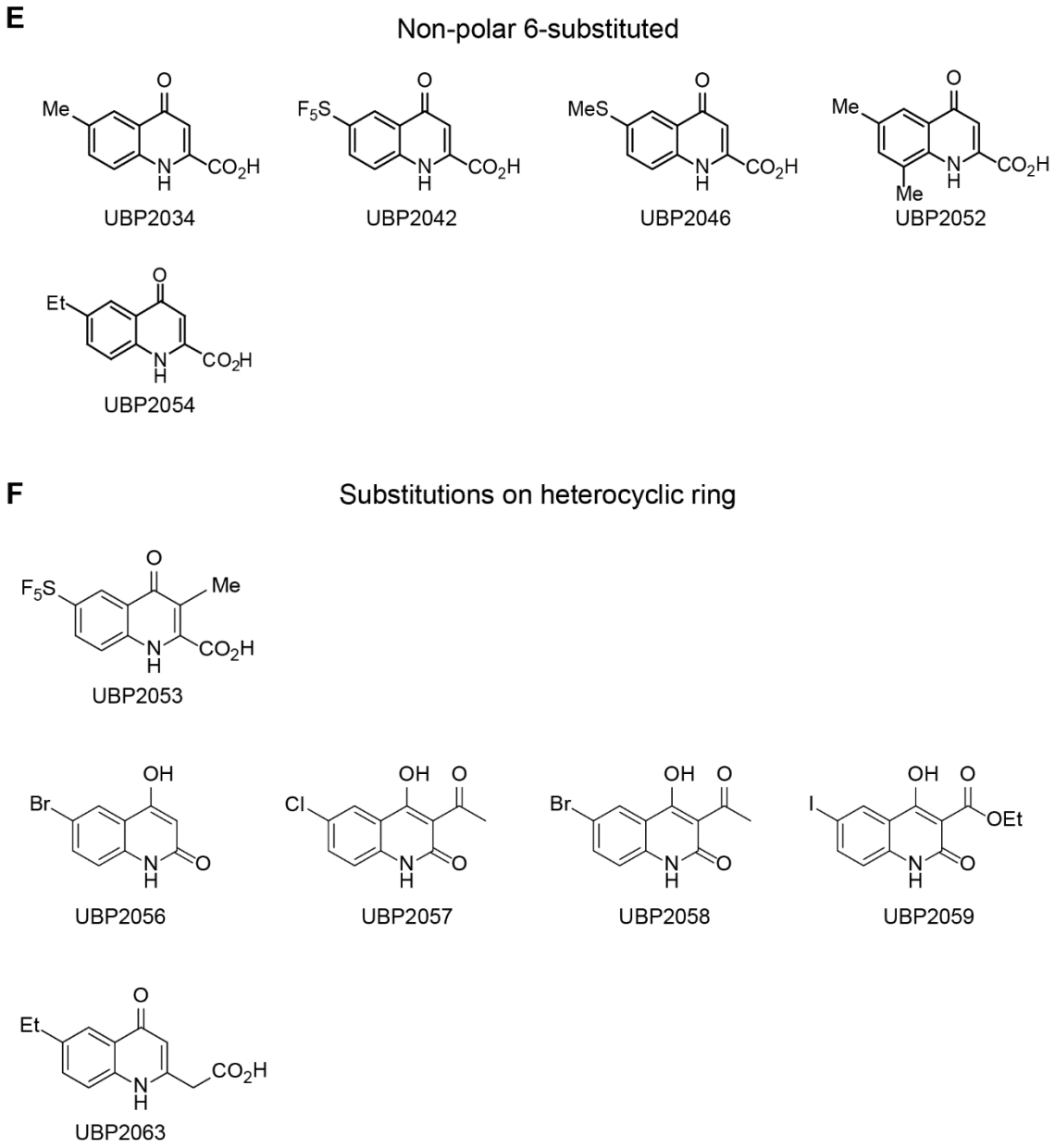

Figure 2.1. Structures of kynurenic acid and derivatives used in the current study. Kynurenates with substitutions on the phenyl ring of kynurenic acid **(A)** could be classed broadly based on the nature of the 6-substitutent: **(B)** 5,7-diF substitutuents, **(C)** halogen 6-substituents, **(D)** polar 6-substitutuents, **(E)** non-polar 6-substituents, and **(F)** derivatives with substitutions on the heterocyclic ring.

2.2. Methods

2.2.1. Cell lines

Human embryonic kidney 293 (HEK293) cells stably transfected with human recombinant GluK1, GluK2 and GluA1 subunits were originally developed at and supplied by Eli Lilly (Hoo et al., 1994; Korczak et al., 1995; Bleakman et al., 1996). All subunits were Q/R unedited (Q) at the ion channel pore and therefore were permeable to Ca^{2+} ions, and the cells were transfected so that each cell line only contained homomeric receptors. Within successfully transfected cells, the plasmid containing the gene for the receptor subunit also contained an antibiotic resistance gene which allowed the selection of cells which contained the gene for the receptor from the total cell population.

2.2.2. Cell culture and preparation of assay plates

Compounds were characterised by quantifying changes in calcium fluorescence in cells expressing the homomeric receptor of choice. Calcium fluorescence in response to glutamate addition in the presence of various concentrations of antagonists were measured. Preparation of cells in assay plates for the fluorescence recordings is detailed below.

Cells were grown in Dulbecco's Modified Eagle's Medium (DMEM) that was supplemented with 2 mM GlutaMAX, 10% v/v foetal bovine serum (FBS), 50 U/ml penicillin and 50 μg/ml streptomycin (herein referred to as modified DMEM). Cells were incubated at 37 °C with 5% CO_2. Cells were passaged when they reached 70-80% confluence and treated periodically with a selection antibiotic. In the case of KAR expressing cell lines, hygromycin B (200 μg/ml) was the selection antibiotic, whereas for AMPAR expressing cells, Geneticin™ (200 μg/ml) was used.

Prior to preparation of cells for experiments, cells were counted using a Tali image-based cytometer (ThermoFischer, UK) and 50-100k cells suspended in 100 μL of modified DMEM was dispensed into each well of a poly-L-lysine coated 96-well plate (Costar 3603) then incubated for ~24 hours. Prior to the experiments, the supernatant was removed, and wells were rinsed twice with supplemented Hank's Balanced Salt solution (sHBSS) containing 5 mM $CaCl_2$ and 20 mM HEPES. The cells were then incubated with a working solution (100 μL/well) of sHBSS supplemented with calcium fluorescence indicator

(Calcium 6 dye, Molecular Devices, UK), and a desensitisation blocker (0.25 mg/mL of concanavalin A (or con A) for KARs, and 100 µM cyclothiazide for GluA1). Plates were incubated for 2-4 hours to allow the fluorescence dye to internalise with the cells.

2.2.3. Agonist and antagonist concentration-response curves

A FlexStation 3 instrument (Figure 2.2; Molecular devices, UK) was used to record the time-resolved fluorescence during the antagonist and agonist addition. The FlexStation allows sampling of fluorescence (in relative fluorescence units, RFU) from individual wells of the assay plate at a frequency of 1.52 Hz, and the FlexStation also allows dispensation of pre-set volumes of solutions from a source plate into the assay plate (prepared as described above) using the SoftMax Pro software (Molecular devices, UK). At the start of all experiments, a one-off absorbance reading was taken to verify that the dye had loaded equally across all wells in the assay plate. For fluorescence recordings, the excitation wavelength was set at 485 nm, and emission was detected at 525 nm, based on the specifications of the Calcium 6 dye. Data from timed measurements of fluorescence (sampling frequency = 1.52 Hz) was smoothed using a 9-point moving average to compensate for noise during data collection.

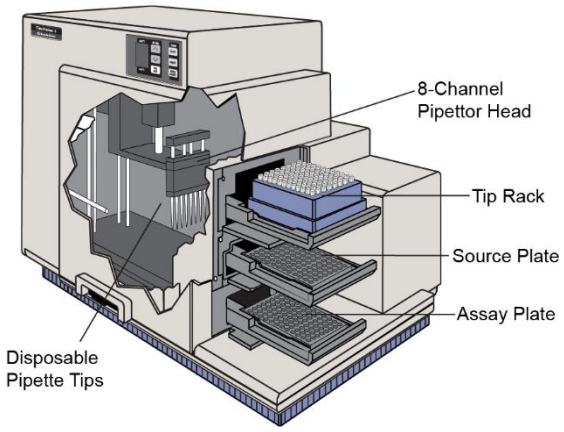

Figure 2.2. Anatomy of the FlexStation 3 plate reader. FlexStation plate reader was used to measure of calcium fluorescence from the assay plate. Dispensation of solution from a source plate to the assay plate was performed with pre-programmed routines in SoftMax Pro software. Image adapted from www.moleculardevices.com.

Concentration-response curves for glutamate were obtained by testing 7 concentrations of glutamate in triplicates (see Figure 2.3A for details). Briefly, glutamate was added to the wells after 20 s of baseline fluorescence measurement. The baseline fluorescence was subtracted from the maximum fluorescence in the presence of glutamate to obtain the change in fluorescence induced by agonist addition in a well (ΔF). The ΔF for each concentration of glutamate was then normalised to ΔF for the highest glutamate concentration (2 mM) and the normalised ΔF was used for further analyses (see Figure 2.4 for fluorescence recordings).

The normalised ΔF in response to different glutamate concentrations was fitted to a four-parameter logistic curve with the following equation in real-time using the SoftMax Pro software:

$$Y = \frac{B - T}{\left(1 + \left(\frac{X}{EC_{50}}\right)^{H}\right) + T} \tag{2.1}$$

where Y is the response (normalised ΔF), T is the maximum response (constrained to 100% for the fit), B is the minimum response (constrained to 0%), X is the glutamate concentration, EC_{50} is the concentration of glutamate that produced half-maximal response, and H is the slope-factor (also known as the Hill slope).

To obtain antagonist concentration-response curves, 8 concentrations of antagonist (including a zero concentration; see Figure 2.3A for details) were applied to wells for 70 s after a baseline of 20 s. A concentration of glutamate that produced 80% of the maximal response (EC_{80}) was extrapolated from the curve generated with eq. (2.1) for the glutamate concentration-response curve in each plate. The EC_{80} agonist concentration was added to the wells 70 s after the addition of antagonists and the ΔF was measured. The ΔF of each antagonist concentration point was then normalised to the ΔF produced with no antagonist (0 μM antagonist). The normalised ΔF was then fitted to eq. (2.2) in real time using SoftMax Pro.

$$Y = \frac{T - B}{\left(1 + \left(\frac{X}{IC_{50}}\right)^{H}\right) + B} \quad (2.2)$$

where Y is the response, T is the maximum response (constrained to 100%), B is the minimum response (constrained to 0%), X is the antagonist concentration, IC_{50} is the concentration of antagonist that inhibited 50% of the response, and H was the slope-factor.

Due to the dependence of IC_{50} on variables such as receptor expression levels, the agonist concentration and agonist EC_{50}, it is not a suitable metric to compare the activity of compounds between cell lines. Therefore, the inhibition constant, K_i, which is an agonist concentration-corrected estimate of affinity, was used to compare affinities of compounds. The K_i was estimated using the Cheng-Prusoff correction (eq. (2.3); Cheng and Prusoff, 1973);

$$K_i = \frac{IC_{50}}{1 + \frac{S}{EC_{50}}} \quad (2.3)$$

where K_i, IC_{50} and EC_{50} are as described above and S is the concentration of agonist used to elicit responses.

All ΔF data points were performed in triplicate on the same assay plate and the median of the 3 replicates were used for further analysis. In all experiments, a known (standard) antagonist was used as a positive control for each assay plate and when the standard antagonist K_i deviated by a factor of > 2 from the cell line-pooled mean K_i, the data from the assay plate was discarded. Standard antagonists were chosen based on their solubility in the experimental media (sHBSS as mentioned before) and their ability to obtain a concentration-response relationship which was well-defined over the concentrations of antagonist tested (see Figure 2.5C for example). Therefore, UBP2038 and UBP2039 were chosen from the kynurenates as standard antagonists. shows the layout of assay plates for concentration-response experiments.

2.2.4. Single concentration library screening using the FlexStation

All compounds were tested at 100 μM on GluK2, GluK1 and GluA1 cell lines to provide a general overview of the antagonist activities of test compounds. In single concentration screening experiments, glutamate and standard antagonist concentration-response curves were obtained as described above. For single concentration screening, wells from columns 7-12 of the assay plate (Figure 2.3B) were used to screen up to 14 compounds at 100 μM in triplicates. The positions of test compounds and vehicle in each column were randomised between assay plates.

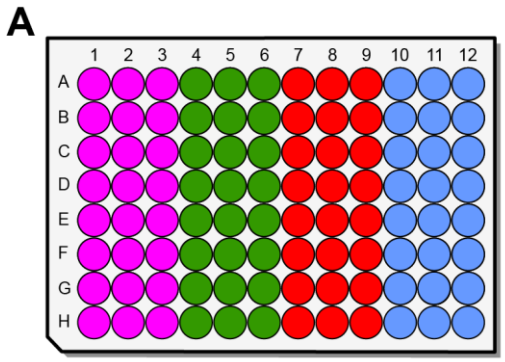

	[Glut] (μM) GluK2 GluA1	[Glut] (μM) GluK1	[Antagonist] (μM) 1	[Antagonist] (μM) 2	[Antagonist] (μM) 3
	Cols 1 – 3		Cols 4 - 12		
A	2000	2000	2000		
B	100	300	300		
C	30	100	100		
D	10	30	30		
E	3	10	10		
F	1	3	3		
G	0.3	1	1		
H	0	0	0		

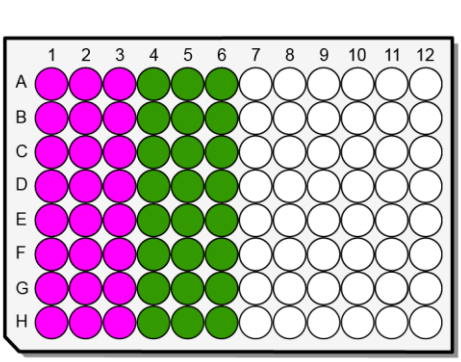

	[Glut] (μM) GluK2 GluA1	[Glut] (μM) GluK1	[Antagonist] (μM)	Test Compounds (100 μM) a – g	Test Compounds (100 μM) i – n
	Cols 1 – 3		Cols 4 - 6	Cols 7 – 9	Cols 10 - 12
A	2000	2000	2000	a	h
B	100	300	300	b	Veh
C	30	100	100	c	i
D	10	30	30	d	j
E	3	10	10	Veh	k
F	1	3	3	e	l
G	0.3	1	1	f	m
H	0	0	0	g	n

Figure 2.3. Layout of assay plate used for FlexStation experiments. A, Layout of the 96-well assay plate (top) showing the arrangement of concentration-response experiment for glutamate (pink) and 3 different antagonists (green, red and blue). Median fluorescence from a triplicate recording was used for further analysis. The concentrations of glutamate and antagonists used in each row (A-H) are shown in the table (bottom). The concentrations of glutamate used in GluK2 and GluA1 cell lines were different from that used for the GluK1 cell line due to higher EC_{50} of glutamate for GluK1 compared to GluK2 or GluA1 subunit containing receptors. **B,** Assay plate layout for single concentration screening (top) used similar layout as **A** for columns 1-6 and a different layout for columns 7-12 (bottom). Three replicates of 14 compounds (represented by letters a – n) could be tested on one plate. Each screening column also contained a vehicle (sHBSS, see Methods) well which was used to normalise data from all other wells in the column.

2.2.5. Analysis and presentation of screening data

Compounds which had > 10% inhibition in single concentration screening were considered for full concentration-response characterisation. The 10% cut-off was chosen based on an estimation of the IC_{50} of antagonists using eq. (2.2) with the slope, T and B constrained to 1, 100 and 0, respectively. Therefore, > 10% inhibition at 100 μM of test compound provided an indicator of a compound with IC_{50} < 900 μM.

2.2.6. Off-line analysis and presentation of concentration-response data

Statistical comparisons and tabulation of activities of compounds on GluK2, GluK1 and GluA1 were carried out using the mean K_i for each compound on the respective cell line. Pooled concentration-response curves for glutamate and antagonists as shown in Results were prepared using GraphPad Prism 7 (GraphPad, USA). For visualisation purposes, the pooled data for glutamate and antagonists were fitted using non-linear regression to 4-parameter logistic curves based on eq. (2.1) and eq. (2.2), respectively. However, the IC_{50} values derived from individual assay plate concentration-response curves, and not from the curve-fit of pooled data, were used to calculate K_i values.

2.2.7. Analysis of physicochemical properties

The antagonist activity of kynurenates on the GluK2 HEK293 cell line (GluK2 K_i value) was qualitatively compared to three physicochemical properties of the substituent at the 6-position of the kynurenate. This comparison was performed in order to understand the properties of the 6-substituent which would provide the highest affinity on GluK2-containing KARs. First, molar refractivity (MR) was used as a measure of the volume occupied by the 6-substituent (larger MR values indicated larger 6-substituents). Secondly, the hydrophobicity constant (π) of a substituent was used as a measure of the hydrophobic nature of the substituent where positive values indicate compounds that were more hydrophobic than hydrogen. The constant π was calculated by subtracting the octanol/water partition coefficient of the substituent (bonded to benzene) from the coefficient of unsubstituted benzene. Thirdly, electronic effects of the 6-substituent were represented by the Hammett substituent constant (σ) of the 6-substituents where positive values indicated more electron withdrawing substituents. The electronic effect of substituents is also dependant on whether the substituent position is para or meta. Therefore, σ_p and σ_m was used to indicate the electronic effects of para and meta substitutions, respectively. Values for MR, π, σ_p and σ_m were taken from Hansch et al., 1973.

2.2.8. Statistical analysis of FlexStation data

Non-parametric tests were used to statistically compare data for single concentration screening data because the number of observations were too few to test for normality of inhibition values. UBP2038 had K_i values that did not follow a normal distribution ($p < 0.05$, D'Agostino & Pearson normality test), therefore, non-parametric tests were used to

compare K_i values. Inhibition from single concentration screening experiments were compared using two-tailed Mann-Whitney (MW) test. Significant differences in K_i values between compounds in each cell line was determined using two-tailed MW test by comparing the K_i values for compounds of interest. Significant differences in K_i values of one compound between different cell lines were determined using Kruskal-Wallis (KW) test followed by Dunn's multiple comparison test (DT). Statistical significance levels were set at $p < 0.05$.

2.2.9. Slice preparation for electrophysiology

All experiments involving rats were performed in accordance with Bristol University regulations and the UK Scientific Procedures Act, 1986 and European Union guidelines for animal care. Wistar rats (Charles River, UK) aged 2-3 months were anaesthetised using isofluorane and euthanised by decapitation (Schedule 1 method). The hippocampi from each hemisphere were extracted and cooled (0-4°C) in artificial cerebrospinal fluid (aCSF) solution consisting of (mM): 124 NaCl, 3.5 KCl, 1.25 NaH_2PO_4, 26 $NaHCO_3$, 2 $CaCl_2$, 2 $MgSO_4$ and 10 glucose, saturated with 95% O_2 and 5% CO_2. Transverse slices (400 µm thick) were cut from dorsal end of each hippocampi using a McIllwain tissue chopper. The slices were incubated in aCSF (pH ~7.4) for at least 2 hours at ~20 ˚C before being transferred to the recording chamber at the beginning of experiments. Extracellular field potentials were recorded from the submerged slices in the recording chamber maintained at 30 °C and continuously perfused with aCSF at a rate of ~3 mL/min.

2.2.10. f-EPSP recordings from hippocampal slices

f-EPSPs mediated by AMPARs and NMDARs were obtained by stimulating the Schaffer collateral axons of CA3 pyramidal cells with a bipolar concentric (stimulating) electrode placed in the stratum radiatum layer on the border between the CA1 and CA2 subregions of the hippocampus. The stimuli were generated using a constant voltage stimulus generator (DS2A Mk2; Digitimer). AMPAR-mediated f-EPSPs from the stratum radiatum of the CA1 subregion were recorded using a maximum stimulation intensity of 3 times that required to elicit a f-EPSP. f-EPSPs were recorded with a glass electrode filled with aCSF solution (electrode resistance: 1.5-2 MΩ). f-EPSP signals were amplified and hardware filtered at 5 kHz (AxoPatch 1D; Axon Instruments, USA). Responses evoked using the stimuli were sampled at 40 kHz and recorded using the WinLTP software (Anderson and Collingridge,

2007). f-EPSPs were evoked at a frequency of 0.067 Hz and average of 4 such f-EPSPs (corresponding to average f-EPSPs for 1 min) were used for all further visualisation and analyses shown in Results.

Inhibition of AMPAR-mediated f-EPSPs by all compounds were measured by application of the test compound after 30 min of stable baseline AMPAR f-EPSP recording. Subsequently, compounds were added (cumulatively) to achieve the concentrations shown in the figures and tables in Results. Compounds were applied for 30 min and compounds that produced any effects were washed out of the recording chamber by perfusing aCSF to show that the effects of compounds were reversible (indicated as washout in figures).

NMDAR-mediated f-EPSPs were isolated by first obtaining a stable AMPAR f-EPSP baseline for at least 20 mins and changing the bath Ca^{2+} and Mg^{2+} concentrations to 3 mM and 1 mM, respectively, and blocking the AMPAR f-EPSPs with 3 μM NBQX. The stimulation intensity was then increased to 3 times that required to obtain AMPAR f-EPSPs to obtain NMDAR mediated f-EPSPs (amplitudes of the baseline NMDAR f-EPSPs were > 0.1 mV) which were free of population spikes and epileptic activity. At the end of NMDAR f-EPSP experiments, 30 μM D-AP5 was added to the bath for 10 min to verify NMDAR-mediated responses.

2.2.11. Data analysis of f-EPSP recordings

Filtered traces obtained from WinLTP were analysed using Platin (developed by Prof. Morten Jensen; University of Aarhus, Denmark). The initial slope of f-EPSPs (measured for a time interval of 0.5 ms) was used as a measure of the AMPAR f-EPSPs. The f-EPSP slope measurement for the whole experiment was normalised to the mean baseline slope such that baseline f-EPSP was 100%.

In experiments using NMDAR mediated f-EPSPs, the f-EPSP peak amplitude was used to calculate inhibition by compounds. In cases where peak amplitude was observed to be contaminated by the fibre volley, the fibre volley in the presence of 30 μM D-AP5 was subtracted from all f-EPSP recordings in the experiment and the resulting f-EPSPs were used for further analyses. Peak amplitudes for the whole experiment were normalised to the baseline period as with the AMPAR mediated f-EPSPs and expressed as baseline-

normalised f-EPSP (such that baseline f-EPSP was 100%). Effect of test compounds on AMPAR- and NMDAR-mediated responses were expressed as %-inhibition of baseline recordings.

2.2.12. Statistical comparisons of electrophysiological data

For statistical comparison of effect sizes for different test compounds, Student's t-test or ANOVA followed by Tukey's multiple comparison test was used as necessary. Some compounds were tested at multiple concentrations to allow estimation of half-maximal inhibitory concentration (IC_{50}) of the compound. For such experiments, a concentration-inhibition curve was constructed using non-linear regression curve fitting (GraphPad, Prism). The concentration-pooled normalised f-EPSPs in the presence of multiple concentrations of the test compound were fitted using a four-parameter logistic curve with eq. (2.2). Top and bottom was constrained to 100% and 0%, respectively. The IC_{50} values of test compounds were estimated from the fitted curve. Statistical comparisons of IC_{50} between compounds were conducted using F-test in GraphPad Prism. All data were presented as mean ± SEM. Statistically significant differences in bar plots are indicated by asterisks (* $P < 0.05$, ** $P < 0.01$, *** $P < 0.001$, **** $P < 0.0001$).

2.2.13. Chemicals and reagents

Kynurenic acid derivatives were synthesised by Jane and co-workers at the University of Bristol and had ^{1}H nuclear magnetic resonance (NMR) spectra, mass spectra and microanalytical data that was consistent with their structure (Thatcher, R, Irvine, M, Jane DE, unpublished). D-AP5 and NBQX were acquired from HelloBio Ltd (Bristol, UK). All kynurenic acid derivatives were prepared as stock solutions in deionised water (Millipore, UK) using 2 equivalents of aqueous NaOH. Compounds with an extra acid group were dissolved using 3 equivalents of aqueous NaOH. Stock solutions were stored as frozen and added to the perfusion medium for durations as indicated in the figures in Results (for electrophysiological field recordings). GlutaMAX was purchased from ThermoFischer, UK. FBS was purchased from Biosera. Penicillin, streptomycin, and selection antibiotics Hygromycin B and Geneticin™ were purchased from Invitrogen and Gibco, respectively. The Calcium 6 dye was purchased from Molecular Devices. All other reagents were obtained from Sigma-Aldrich.

Given name	Chemical name
Kynurenic acid	4-oxo-1,4-dihydroquinoline-2-carboxylic acid
UBP2002	6-iodo-4-oxo-1,4-dihydroquinoline-2-carboxylic acid
UBP2007	6-carboxy-4-oxo-1,4-dihydroquinoline-2-carboxylic acid
UBP2020	6-bromo-4-oxo-1,4-dihydroquinoline-2-carboxylic acid
UBP2022	6-amino-4-oxo-1,4-dihydroquinoline-2-carboxylic acid
UBP2025	5,6,7-trichloro-4-oxo-1,4-dihydroquinoline-2-carboxylic acid
UBP2034	6-methyl-4-oxo-1,4-dihydroquinoline-2-carboxylic acid
UBP2037	5,7-dichloro-6-iodo-4-oxo-1,4-dihydroquinoline-2-carboxylic acid
UBP2038	5,7-difluoro-6-iodo-4-oxo-1,4-dihydroquinoline-2-carboxylic acid
UBP2039	5,7-difluoro-6-bromo-4-oxo-1,4-dihydroquinoline-2-carboxylic acid
UBP2040	5,7-difluoro-4-oxo-1,4-dihydroquinoline-2-carboxylic acid
UBP2042	4-oxo-6-(pentafluoro-λ^6-sulfaneyl)-1,4-dihydroquinoline-2-carboxylic acid
UBP2043	7-fluoro-6-methoxy-4-oxo-1,4-dihydro-quinoline-2-carboxylic acid
UBP2046	6-methylsulfide-4-oxo-1,4-dihydro-quinoline-2-carboxylic acid
UBP2047	5,7-difluoro-6-methoxy-4-oxo-1,4-dihydro-quinoline-2-carboxylic acid
UBP2049	6-methoxy-4-oxo-1,4-dihydro-quinoline-2-carboxylic acid
UBP2051	6-nitro-4-oxo-1,4-dihydro-quinoline-2-carboxylic acid
UBP2053	6-pentafluorosulfanyl-3-methyl-4-oxo-1,4-dihydro-quinoline-2-carboxylic acid
UBP2054	6-ethyl-4-oxo-1,4-dihydroquinoline-2-carboxylic acid
UBP2056	6-bromo-4-hydroxyquinolin-2(1*H*)-one
UBP2057	3-acetyl-6-chloro-4-hydroxyquinolin-2(1*H*)-one
UBP2058	3-acetyl-6-bromo-4-hydroxyquinolin-2(1*H*)-one
UBP2059	ethyl 4-hydroxy-6-iodo-2-oxo-1,2-dihydroquinoline-3-carboxylate
UBP2063	2-(6-ethyl-4-oxo-1,4-dihydroquinolin-2-yl)acetic acid

Table 2.1. Given names and chemical names of compounds used in the study.

2.3. Results

2.3.1. Validation of the calcium fluorescence assay

The calcium fluorescence assay using GluK2, GluK1 and GluA1 cell lines in the current study has previously been used to pharmacologically characterise compounds (Alt et al., 2004; Dargan et al., 2009). The assay developed for the current study is similar in principle and therefore, the results from the current study may be translatable to other studies that use the same cell lines. An example experiment showing the concentration-response relationship for glutamate and the standard antagonist UBP2038 is shown in Figure 2.4. Figure 2.5 shows the concentration-response relationships of glutamate (Figure 2.5A), kynurenic acid (Figure 2.5B) and the standard antagonist UBP2038 (Figure 2.5C), on GluK2, GluK1 and GluA1 homomeric receptors. The EC_{50} values and slope-factors for glutamate were similar to previously published results on the cell lines containing GluK1 and GluK2 homomeric receptors expressed in HEK293 cells (Alt et al., 2004) and GluA1 homomeric receptors expressed in Xenopus oocytes (Donevan et al., 1998). IC_{50} values and slope-factors for kynurenic acid on GluK1 and GluK2 from the current study were broadly similar to previously published results (Alt et al., 2004).

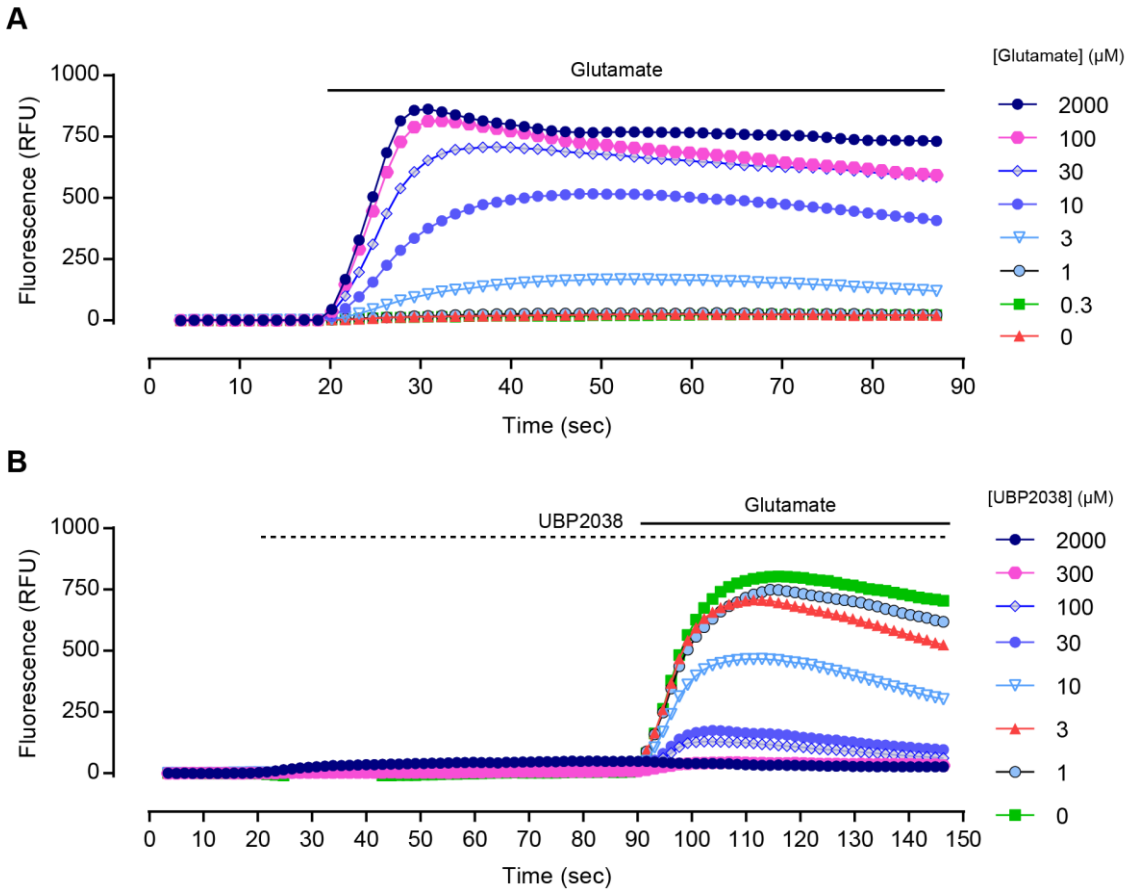

Figure 2.4. Representative experiments showing fluorescence response to glutamate and the standard antagonist UBP2038. A, Data from a representative glutamate concentration-response evaluation showing the fluorescence in response to various concentrations of the agonist, glutamate on GluK2 homomeric receptors. Each data-point represents median fluorescence from 3 replicate wells. Application of various concentrations of glutamate began at 20 s after baseline recording (solid line). **B,** Data from a representative antagonist concentration-response experiment on GluK2 homomeric receptors. The standard antagonist, UBP2038, was applied at various concentrations 20 s after baseline recording (dashed line). A concentration of glutamate producing 80% of the maximal response (EC_{80}) (calculated from the agonist concentration-response curve generated from data in A) was added at 90 s (solid line).

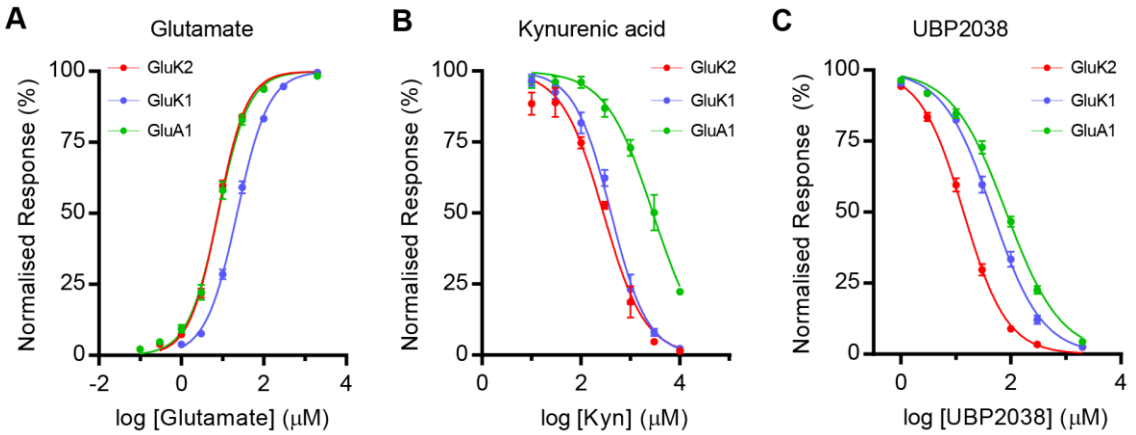

Figure 2.5. Concentration-response curves for glutamate, kynurenic acid and UBP2038 on HEK293 cells expressing GluK2, GluK1 and GluA1 homomeric receptors. A, Pooled glutamate concentration-response curves on homomeric receptors containing GluK2 (red, n = 35), GluK1 (blue, n = 29), and GluA1 (green, n = 21) subunits. Glutamate EC_{50} for GluK2 = 7.7 ± 0.4 μM, GluK1 = 23.1 ± 1.7 μM, and GluA1 = 8.4 ± 0.8 μM. Slope-factor for GluK2 = 1.2 ± 0.03, GluK1 = 1.2 ± 0.03, GluA1 = 1.2 ± 0.05. Data are shown as mean, error bars represent SEM. **B,** Pooled concentration-response curves showing the effect of kynurenic acid on homomeric receptors containing GluK2 (red, n = 3), GluK1 (blue, n = 3), and GluA1 (green, n = 3) subunits. IC_{50} for GluK2 = 282.5 ± 25.5 μM, GluK1 = 402.3 ± 27.9 μM, and GluA1 = 2836.0 ± 253.6 μM. Slope-factor for GluK2 = -1.00 ± 0.09, GluK1 = -1.20 ± 0.08, and GluA1 = -0.90 ± 0.07. **C,** Pooled UBP2038 concentration-response curves for homomeric receptors containing GluK2 (red, n = 28), GluK1 (blue, n = 27), and GluA1 (green, n = 22) subunits. IC_{50} for GluK2 = 15.7 ± 1.1 μM, GluK1 = 52 ± 6.1 μM, and GluA1 = 90.5 ± 8.0 μM. Slope-factor for GluK2 = -1.10 ± 0.04, GluK1 = -0.90 ± 0.04, and GluA1 = -0.90 ± 0.03.

2.3.2. Compound screening at a single concentration

Results from the single concentration screening are shown in Table 2.1. Generally, the compounds which exhibited > 10% inhibitory activity have substituents at the 6-position of the phenyl ring. Therefore, the compounds were loosely grouped based on the nature of the functional group at the 6-position, namely halogen, polar, and non-polar. One exception to this grouping was UBP2040 (6-H-5,7-diF, see Figure 2.1B for structure). Some 6-substituted kynurenates such as UBP2042 (6-SF_5) and UBP2007 (6-CO_2H) had < 10% inhibition of GluK2 homomeric receptors at 100 μM. Kynurenates which had modifications on the heterocyclic ring (see Figure 2.1F for structures) had < 10% inhibition of GluK2 homomeric receptors. Therefore, the compounds with modifications on the heterocyclic ring were not considered for studying concentration-response relationship.

Compound	GluK2 inhibition at 100 µM (%)	GluK1 inhibition at 100 µM (%)	GluA1 inhibition at 100 µM (%)
UBP2038	94.6 ± 0.9 (4)	76.7 ± 5.1 (3)	70.1 ± 7.1 (3)
UBP2039	86.7 ± 0.9 (3)	77.4 ± 2.7 (3)	41.2 ± 4.9 (3)
UBP2043	82.1 ± 2.5 (3)	56.6 ± 1.7 (3)	20.0 ± 0.3 (3)
UBP2046	64.3 ± 9.8 (3)	31.9 ± 2.7 (3)	9.1 ± 4.2 (3)
UBP2002	63.0 ± 5.3 (3)	43.5 ± 5.2 (3)	9.8 ± 4.0 (3)
UBP2020	60.0 ± 6.6 (3)	58.5 ± 5.4 (3)	12.6 ± 1.3 (3)
UBP2049	58.0 ± 9.9 (3)	39.3 ± 3.9 (3)	8.1 ± 4.0 (3)
UBP2025	56.6 ± 12.0 (3)	37.0 ± 1.5 (4)	1.4 ± 5.3 (3)
UBP2051	56.6 ± 6.7 (4)	42.5 ± 3.1 (4)	7.2 ± 1.4 (3)
UBP2037	52.8 ± 9.3 (3)	41.3 ± 5.5 (3)	10.3 ± 3.9 (3)
UBP2047	47.8 ± 11.1 (3)	32.9 ± 2.0 (3)	7.6 ± 8.0 (3)
UBP2040	43.3 ± 4.8 (3)	31.4 ± 1.9 (4)	3.9 ± 3.5 (3)
UBP2034	26.8 ± 4.9 (3)	25.1 ± 2.0 (4)	2.2 ± 1.9 (3)
UBP2054	18.2 ± 2.0 (3)	5.7 ± 1.0 (3)	-3.8 ± 1.2 (3)
UBP2022	16.3 ± 3.1 (3)	11.6 ± 3.6 (3)	-3.0 ± 1.5 (3)
UBP2059	4.8 ± 2.2 (5)	0 ± 1.7 (4)	-1.1 ± 3.7 (3)
UBP2057	4.4 ± 2.4 (5)	2.3 ± 2.2 (4)	-3.5 ± 2.8 (3)
UBP2058	4.2 ± 1.3 (4)	0.8 ± 1.7 (4)	0 ± 1.7 (3)
UBP2053	3.6 ± 2.8 (3)	-0.3 ± 1.9 (4)	-3.5 ± 3.4 (3)
UBP2042	1.9 ± 2.0 (3)	9.0 ± 2.3 (3)	-1.8 ± 2.2 (3)
UBP2056	0.3 ± 3.9 (4)	2.6 ± 0.8 (4)	-3.3 ± 3.3 (3)
UBP2063	-0.9 ± 1.8 (4)	-1.4 ± 1.7 (3)	-0.5 ± 4.8 (3)
UBP2007	-4.4 ± 3.4 (3)	4.8 ± 1.1 (4)	-2.9 ± 5.9 (3)

Table 2.2. Screening of compound library at 100 µM on homomeric GluK2, GluK1 and GluA1 receptors (ordered by GluK2 activity). Values shown are mean ± SEM percentage-inhibition of EC_{80} glutamate response on the respective receptor. Number of independent recordings (n) is shown in parenthesis. Compounds chosen for further characterisation are highlighted based on the type of substituent at the 6-position of the benzene ring of the compound (grey: halogen, green: polar, yellow: non-polar, red: no substitution). Compounds which were eliminated from further characterisation are shown below the red line (indicating an inhibition of < 10% on GluK2 homomeric receptors).

2.3.3. Characterisation of 6-halogen substituted kynurenic acid derivatives on recombinant receptors

Six compounds which were selected for further characterisation from the screening had a halogen at the 6-position of the phenyl ring. Concentration-response curves for these compounds were obtained on GluK2, GluK1 and GluA1 homomeric receptors (Figure 2.6). UBP2038 (5,7-diF-6-I) was the most potent antagonist on GluK2 amongst all 6-halogen substituted compounds (K_i = 4.6 ± 0.3 µM, Figure 2.6A). The rank order of affinity of the compounds on GluK2 was UBP2038 > UBP2039 (5,7-diF-6-Br) > UBP2020 (6-Br) > UBP2002 (6-I) > UBP2037 (5,7-diCl-6-I) > UBP2025 (5,6,7-triCl). This rank order of affinity of these compounds was broadly in agreement with that observed in GluK1 and GluK2 cell lines. In the GluK1 cell line, UBP2039 was slightly more potent than UBP2038 but the difference in GluK1 K_i between UBP2038 and UBP2039 was not statistically significant ($p > 0.05$, MW test). UBP2037 and UBP2025 had poor solubility in the sHBSS media used in the assay at concentrations above 100 µM which may have contributed to the increased variability of the data for UBP2037 and UBP2035 at higher concentrations. The affinities of all compounds were highest in the GluK2 cell line, followed by GluK1 and then GluA1 cell lines. In cases where IC_{50} was greater than 300 µM, K_i was not calculated as the concentration-response curve would be poorly defined because only one concentration above 300 µM (2 mM) was tested due to the poor solubility of the compounds at high concentrations. Of the 6-halogen substituted compounds that also had substitutions at the 5- and 7- positions of the phenyl ring, UBP2038 showed higher inhibition in GluK2 expressing cells than UBP2002, UBP2020, and UBP2025 ($p < 0.05$ for all, MW test).

A

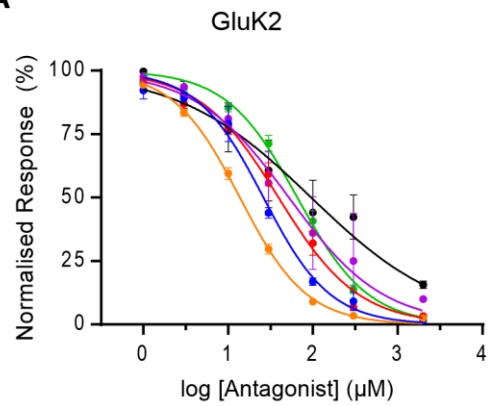

Compound	IC_{50} (μM)	K_i (μM)	n
UBP2038	15.7 ± 1.1	4.6 ± 0.3	28
UBP2039	27.6 ± 2.9	7.9 ± 1.1	5
UBP2020	43.8 ± 6.7	12.0 ± 1.5	11
UBP2002	68.7 ± 8.3	18.4 ± 1.5	10
UBP2037	78.6 ± 50.8	22.8 ± 14.5	3
UBP2025	231 ± 106.2	58.3 ± 26.4	4

B

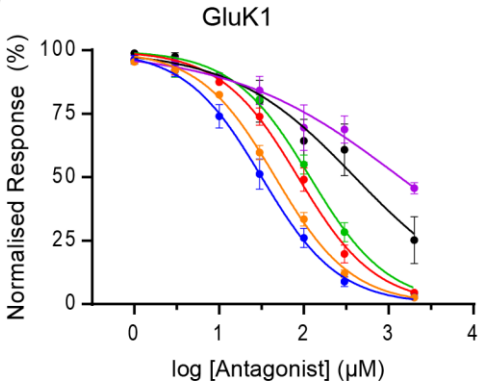

Compound	IC_{50} (μM)	K_i (μM)	n
UBP2038	52.0 ± 6.1	11.1 ± 1.1	27
UBP2039	35.3 ± 9.8	7.7 ± 1.8	6
UBP2020	83.7 ± 16.9	18.7 ± 3.2	9
UBP2002	130.2 ± 17.5	30.6 ± 4.0	11
UBP2037	> 300		4
UBP2025	> 300		3

C

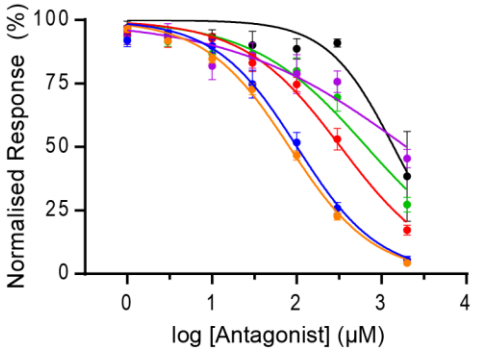

Compound	IC_{50} (μM)	K_i (μM)	n
UBP2038	90.5 ± 8	22.6 ± 2.2	22
UBP2039	104.0 ± 18.5	30.7 ± 7.9	5
UBP2020	> 300		6
UBP2002	> 300		6
UBP2037	> 1000		3
UBP2025	> 2000		3

Figure 2.6. Characterisation of 6-halogen substituted kynurenates on GluK2, GluK1 and GluA1 homomeric receptors. A, Concentration-response curves (left) and summary of IC_{50} and K_i values (right) for 6-halogen substituted compounds on GluK2 homomeric receptors. The key for the figure on left is provided in the table. The table is sorted according to activity on GluK2 homomeric receptors. IC_{50} and K_i values in the table are shown as mean ± SEM. **B**, Similar to **A** but for GluK1 homomeric receptors. In cases where IC_{50} was larger than 300 μM, K_is were not calculated because the curve would not be well defined since only one concentration of antagonist above 300 μM (2000 μM) was tested. **C**, Similar to **A** but for GluA1 homomeric receptors.

2.3.4. Characterisation of polar 6-substituted kynurenic acid derivatives on recombinant receptors

From the initial screening (Table 2.2), the polar 6-substituted compounds were further characterised on GluK2, GluK1, and GluA1 homomeric receptors (Figure 2.7). The rank order of affinity (based on K_i) on GluK2 was UBP2043 (6-OMe-7-F) > UBP2049 (6-OMe) > UBP2051 (6-NO_2) > UBP2047 (5,7-diF-6-OMe) > UBP2022 (6-NH_2) > UBP2007 (6-CO_2H). UBP2007 was excluded from characterisation on GluK1 and GluA1 cell lines due to inactivity on GluK2 (Figure 2.7A). A similar rank order of affinity to that in GluK2 cell lines was seen in GluK1 and GluA1 cell lines. The affinity of polar 6-substituents was highest in GluK2 followed by GluK1 and GluA1.

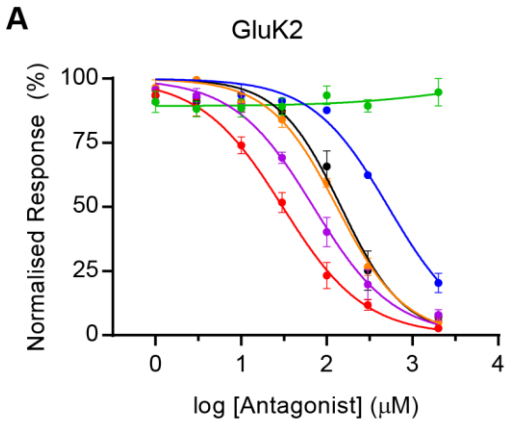

Compound	IC_{50} (μM)	K_i (μM)	n
UBP2043	26.2 ± 3.0	9.8 ± 1.5	6
UBP2049	76.0 ± 11.6	22.0 ± 4.0	5
UBP2051	131.0 ± 8.9	37.7 ± 3.6	3
UBP2047	146.9 ± 35.5	40.5 ± 7.9	3
UBP2022	> 300		3
UBP2007	> 2000		3

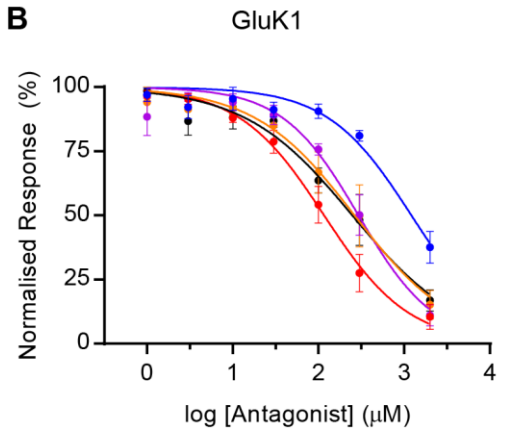

Compound	IC_{50} (μM)	K_i (μM)	n
UBP2043	176.2 ± 56.0	34.3 ± 6.9	8
UBP2049	> 300		5
UBP2051	> 300		3
UBP2047	> 300		4
UBP2022	> 1000		3

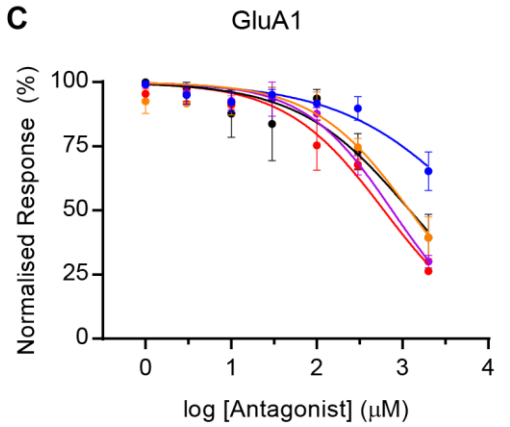

Compound	IC_{50} (μM)	K_i (μM)	n
UBP2043	> 300		3
UBP2049	> 300		3
UBP2051	> 300		3
UBP2047	> 1000		3
UBP2022	> 2000		3

Figure 2.7. Characterisation of polar 6-substituted kynurenates on GluK2, GluK1 and GluA1 homomeric receptors. Concentration-response curves (left) on GluK2 (**A**), GluK1(**B**) and GluA1(**C**) homomeric receptors and the respective mean ± SEM IC_{50} and K_i values generated from the individual experiments (right). The figure key for concentration-response curves are shown next to the compound names in the table. Number of independent observations (n) is also shown in the table. All tables were sorted according to their affinity for GluK2 homomeric receptors.

2.3.5. Characterisation of non-polar 6-substituted kynurenic acid derivatives on recombinant receptors

Compounds with non-polar 6-substitutions on the phenyl ring were further characterised in GluK2, GluK1 and GluA1 homomeric receptors (Figure 2.8). Rank order of affinity in GluK2 is UBP2046 (6-SMe) > UBP2034 (6-Me) > UBP2054 (6-Et) > UBP2042 (6-SF_5) > UBP2052 (6,8-diMe), and a similar rank order of affinity was observed for GluK1 and GluA1 homomeric receptors.

UBP2046 had the highest estimated affinity on GluK2 (K_i = 15.2 ± 3.1 µM) which had a significantly lower K_i value compared to the estimated K_i of UBP2054 (54 ± 10.9 µM; $p < 0.05$, MW test) but not UBP2034 (46 ± 9.3 µM; $p > 0.05$, MW test). Surprisingly, UBP2054 had significantly lower inhibitory activity on GluK1 (IC_{50} > 1000 µM) and GluA1 (IC_{50} > 2000 µM) compared to GluK2 subunits.

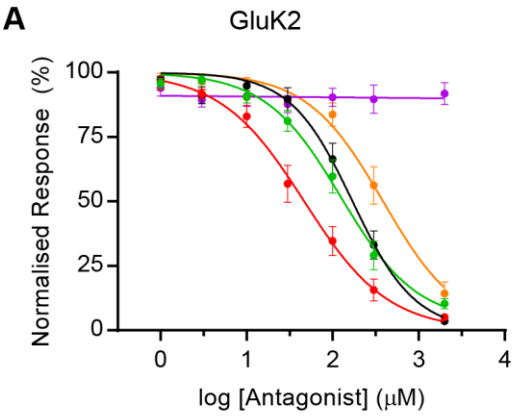

Compound	IC_{50} (μM)	K_i (μM)	n
UBP2046	54.8 ± 10.8	15.2 ± 3.1	6
UBP2034	155.8 ± 35.7	46.5 ± 9.3	6
UBP2054	188.3 ± 39.6	54.0 ± 10.9	7
UBP2042	> 300		3
UBP2052	> 2000		3

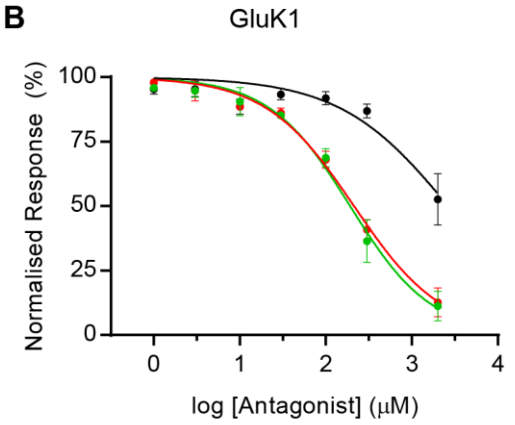

Compound	IC_{50} (μM)	K_i (μM)	n
UBP2046	254.2 ± 73.4	58.8 ± 14.3	5
UBP2034	246.8 ± 82.0	47.8 ± 7.2	5
UBP2054	> 1000		6

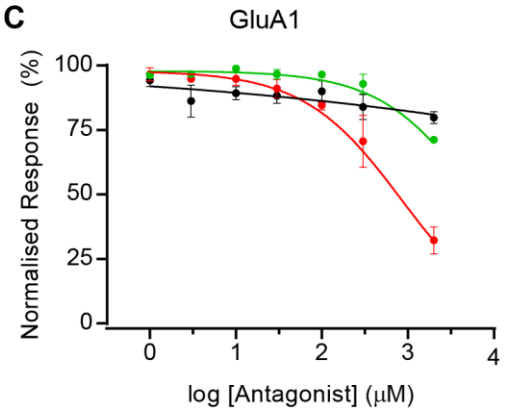

Compound	IC_{50} (μM)	K_i (μM)	n
UBP2046	> 300		5
UBP2034	> 2000		3
UBP2054	> 2000		6

Figure 2.8. Characterisation of non-polar 6-substituted kynurenic acid derivatives on recombinant GluK2, GluK1 and GluA1 homomeric receptors. Pooled concentration-response curves (left) and the IC_{50} and K_i values (mean ± SEM) generated from the individual experiments (right) on GluK2 (**A**), GluK1 (**B**) and GluA1 (**C**) homomeric receptors. The figure key for concentration-response curves is shown next to the compound names in the table. Number of independent observations (n) is also shown in the table. Table is sorted according to affinity for GluK2 homomeric receptors.

2.3.6. Subunit selectivity of kynurenic acid derivatives

To select the kynurenate with highest GluK2 over GluK1 or GluA1 selectivity, the agonist-corrected affinities of antagonists (K_i) on all three cell lines were compared (Table 2.3). Ratios of GluK1/GluK2 K_i values provided a measure of selectivity of the test compound for GluK2 over GluK1 homomers based on affinity. Similarly, GluA1/GluK2 K_i ratios were also calculated. Some kynurenates had IC_{50} greater than the highest concentration tested (2 mM), therefore, their K_i values and selectivity ratios based on K_i values could not be calculated. In cases where the K_i values could not be calculated, an estimated selectivity ratio for GluK2 over GluK1 or GluA1 was calculated by dividing the IC_{50} for GluK1 or GluA1, respectively by the estimated IC_{50} value of GluK2 (Table 2.3).

Compound	GluK2 K_i (μM)	GluK1 K_i (μM)	GluA1 K_i (μM)	GluK1/GluK2	GluA1/GluK2
UBP2038	4.6 ± 0.3 (28)	11.2 ± 1.0 (27)	22.6 ± 2.2 (22)	2.4	4.9
UBP2039	7.9 ± 1.1 (5)	7.7 ± 1.8 (6)	30.7 ± 7.9 (5)	1.0	3.9
UBP2043	9.8 ± 1.5 (6)	34.3 ± 6.9 (8)	IC_{50} >300 (3)	3.5	>11.5#
UBP2020	12.0 ± 1.5 (11)	18.7 ± 3.2 (9)	IC_{50} >300 (6)	1.6	>6.9#
UBP2046	15.2 ± 3.1 (6)	58.8 ± 14.3 (5)	IC_{50} >300 (5)	3.9	>5.5#
UBP2002	18.4 ± 1.5 (10)	30.6 ± 4 (11)	IC_{50} >1000 (6)	1.7	>14.6#
UBP2049	22.0 ± 4.0 (5)	IC_{50} >300 (5)	IC_{50} >300 (3)	>3.9#	>3.9#
UBP2037	22.8 ± 14.5 (3)	IC_{50} >1000 (4)	IC_{50} >1000 (3)	>12.7#	>12.7#
UBP2040	33.8 ± 7.8 (6)	45.4 ± 6.2 (3)	334 ± 26 (3)	1.3	9.9
UBP2051	37.7 ± 3.6 (3)	IC_{50} >300 (3)	IC_{50} >300 (3)	>2.3#	>2.3#
UBP2047	40.5 ± 7.9 (3)	IC_{50} >300 (4)	IC_{50} >1000 (3)	>2.0#	>6.8#
UBP2034	46.5 ± 9.3 (6)	47.8 ± 7.2 (5)	IC_{50} >2000 (3)	1.0	>12.8#
UBP2054	54.0 ± 10.9 (7)	IC_{50} >1000 (6)	IC_{50} >2000 (6)	>5.3#	>10.6#
UBP2025	58.3 ± 26.4 (4)	IC_{50} >300 (3)	IC_{50} >1000 (3)	>1.3#	>8.7#
UBP2022	IC_{50} >300 (3)	IC_{50} >1000 (3)	IC_{50} >2000 (3)	>3.3#	>6.7#

Table 2.3. K_i or IC_{50} values of kynurenates on GluK2, GluK1 and GluA1 homomeric receptors and estimated selectivity of kynurenates between subunits. Compound codes are coloured according to the nature of the 6-substituent: grey: halogen, green: polar, yellow: non-polar, and red: no substitution. Selectivity ratios (GluK1/GluK2 and GluA1/GluK2) is an estimate of the GluK2 over GluK1 or GluA1 selectivity obtained by dividing respectively the GluK1 or GluA1 K_i by the GluK2 K_i of each compound. In cases where K_i values could not be determined, an estimate GluK2 over GluK1 or GluA1 selectivity ratio was calculated by dividing an estimate of the GluK1 or GluA1 IC_{50} value by the GluK2 IC_{50} (such values are suffixed with #).

2.3.7. Substitutions at the 6-position on the benzene ring reduced NMDAR activity of kynurenic acid derivatives

Leeson and colleagues (1991) have shown that simple 6-substitution on the benzene ring decreased the affinity of kynurenic acid derivatives on NMDARs but inhibited non-NMDAR responses (Leeson et al., 1991). To verify this, experiments were carried out on native iGluRs in the rat hippocampus (Figure 2.9). f-EPSP recordings were made from the

SC-CA1 synapses in the hippocampus where AMPARs and NMDARs mediate synaptic transmission (Figure 2.10).

Characterisation of UBP2040 (5,7-diF), UBP2038 (5,7-diF-6-I), and UBP2002 (6-I) at 100 μM in native tissue confirmed that 6-substituted compounds have reduced activity on NMDARs but significant inhibitory activity on AMPARs (Figure 2.11). These results verified previous observations that 6-substituents on the benzene ring decreased NMDAR activity of kynurenic acid and provided validity to the technique used in this study to characterise compounds on native AMPARs.

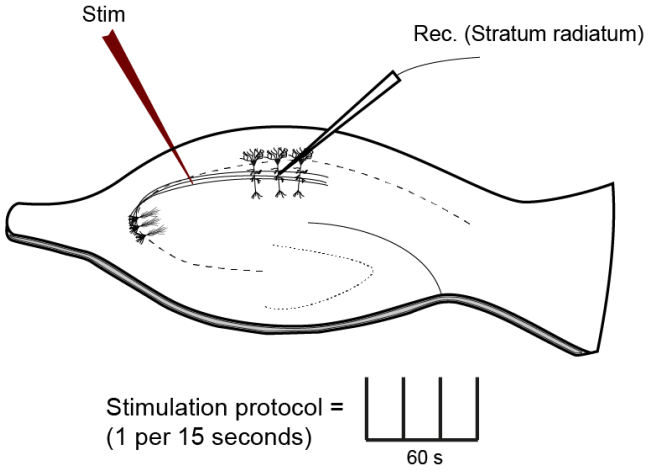

Figure 2.9. Setup of recording field potentials from hippocampal neurons. Experimental set-up for recording responses mediated by native iGluRs in SC-CA1 synapses. Using a stimulating electrode (Stim), pulses were delivered to the Schaffer collaterals at a frequency of 1 per 15 s. Recordings were made from the stratum radiatum of the CA1 region (see section 2.2.10 for more details).

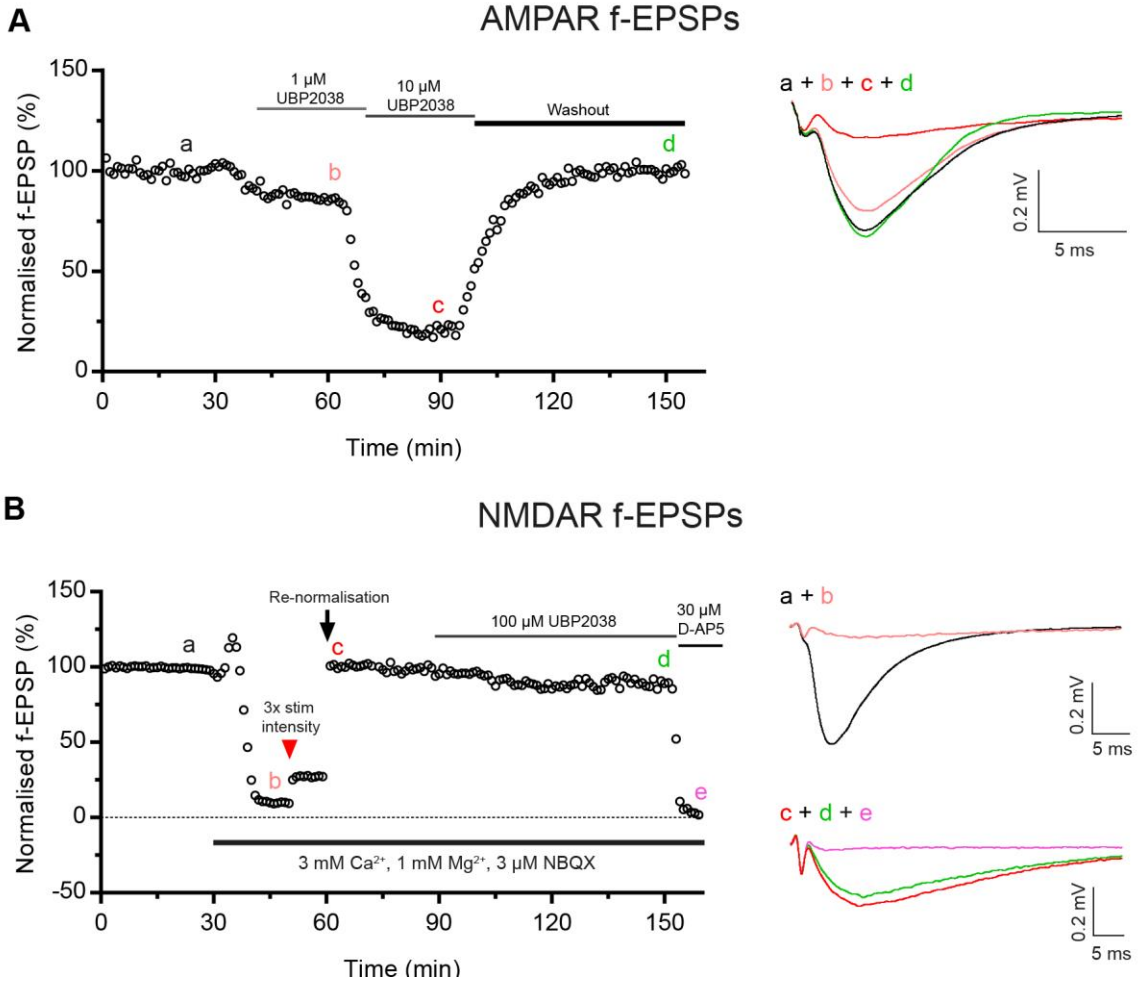

Figure 2.10. Example f-EPSP experiments from the hippocampus. A, Example experiment showing the characterisation of UBP2038 at 1 µM and 10 µM on native AMPARs. Stable baseline recordings were made for 30 min, and UBP2038 was added as indicated in the figure (thin solid lines). At the end of the experiment, UBP2038 was washed out of the recording chamber for 60 min (thick solid line) to verify the reversibility of the compound's inhibition. Representative AMPAR-mediated f-EPSP responses from the time-points indicated on the experiment are shown on the right. **B**, Example experiment showing the characterisation of UBP2038 at 100 µM on native NMDARs. A stable baseline of AMPAR-mediated f-EPSPs for 30 min was initially recorded. Subsequently, the perfusion solution was altered to block AMPARs (3 µM NBQX) and facilitate NMDAR-mediated f-EPSPs (3 mM Ca^{2+}, 1 mM Mg^{2+}). The NMDAR-mediated response amplitude was increased by increasing the stimulation intensity by 3-fold (red arrowhead). The resulting NMDAR-mediated f-EPSPs were re-normalised to a stable baseline containing NMDAR-mediated f-EPSPs recorded for 30 min (starting at black arrow). 100 µM UBP2038 was added as indicated in the figure and at the end of experiments, NMDAR responses were verified using 30 µM D-AP5. Representative f-EPSP responses from the time-points indicated on the experiment are shown on the right.

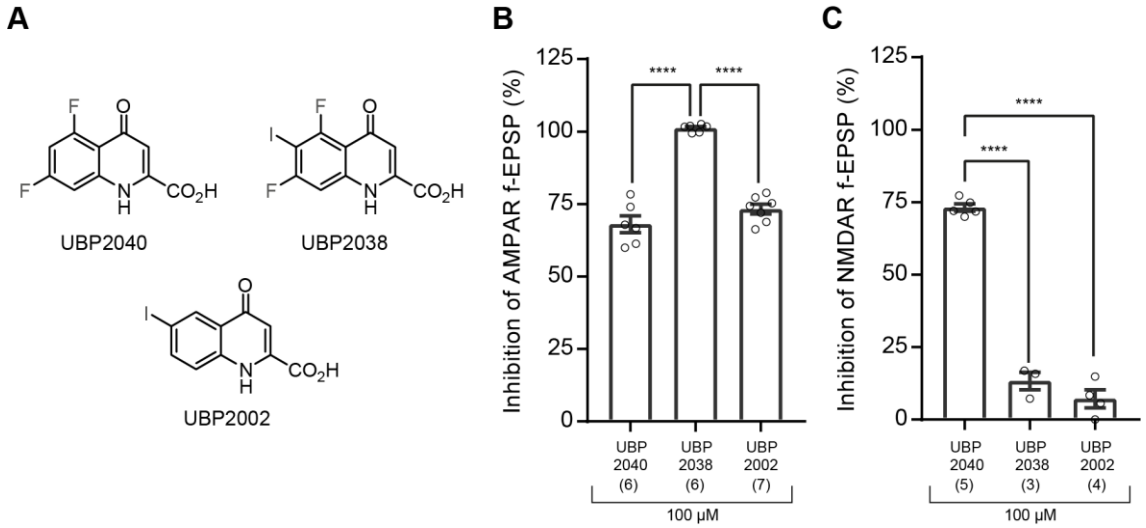

Figure 2.11. Substitution on the 6-position of phenyl ring decreases NMDAR activity of kynurenic acid derivatives. A, Structures of UBP2040, UBP2038 and UBP2002. **B**, All three compounds inhibited AMPAR-mediated f-EPSPs at 100 µM. AMPAR f-EPSPs were more significantly blocked by UBP2038 (inhibition = 101.2 ± 0.5%) compared to UBP2040 (68.1 ± 2.9%) and UBP2002 (73.3 ± 1.7%), ($p < 0.0001$ for both, ANOVA, Tukey test). Number of independent observations (n) are shown in parenthesis. Inhibition values from individual experiments are shown (clear circles), error bars represent SEM. **C**, NMDAR f-EPSPs were significantly inhibited by UBP2040 (73.2 ± 1.3%) compared to UBP2038 (13.3 ± 3.1%) and UBP2002 (7.2 ± 3.1%), ($p < 0.0001$ for both, ANOVA, Tukey test). Number of independent observations (n) are shown in parenthesis. Inhibition values from individual experiments are shown (clear circles), error bars represent SEM.

2.3.8. Characterisation of 6-substituted kynurenic acid derivatives on native AMPARs

A summary of the further characterisation of 6-substituted kynurenic acid derivatives at 100 µM on native AMPARs is shown in Figure 2.12. All 6-halogen substituted compounds inhibited AMPAR mediated f-EPSPs (Figure 2.12A) at 100 µM; UBP2038 (5,7-diF-6-I) had the highest inhibition of AMPAR f-EPSP (101 ± 0.5%, n = 6) and UBP2002 (6-I) had the lowest inhibition of AMPAR f-EPSP at 100 µM (73.3 ± 1.7%, n = 7). The rank order of inhibition of AMPAR f-EPSP for 6-halogen substituted kynurenates: UBP2038 > UBP2037 (5,7-diCl-6-I) > UBP2020 (6-Br) > UBP2002, was similar to the rank order of affinity on GluK2 and GluA1 homomeric receptors (Figure 2.6A and C, respectively): UBP2038 > UBP2037 > UBP2020 > UBP2002. The difference in activity of UBP2037

between recombinant and native systems may be explained by the more favourable solubility of UBP2037 in the buffer media used for native receptor experiments.

Polar 6-substituted kynurenic acid derivatives also inhibit AMPAR-mediated f-EPSPs (Figure 2.12B). UBP2043 (6-OMe-7-F) had the highest inhibition (91.7 ± 0.5%, n = 3) amongst polar 6-substituents tested on native receptors. UBP2049 (6-OMe), UBP2051 (6-NO_2; n = 5), and UBP2047 (5,7-diF-6-OMe; n = 3) inhibited AMPAR f-EPSPs by > 50% at 100 µM (Figure 2.12B).

Kynurenates with non-polar 6-substituents on the phenyl ring also inhibited AMPAR-mediated f-EPSPs but the non-polar substitution in UBP2054 (6-Et) had the least inhibition of native AMPARs amongst all tested compounds (inhibition at 100 µM = 7.8 ± 3%, n = 4) (Figure 2.12C). The shorter non-polar 6-substituent, UBP2034 (6-Me) inhibited AMPAR f-EPSPs by 29.2 ± 3.6% (n = 3) whereas UBP2046 (6-SMe) showed the highest inhibition of AMPAR f-EPSPs at 100 µM amongst non-polar substituents (68.2 ± 3%, n = 6) (Figure 2.12C).

The activity of UBP2054 (6-Et), UBP2038 (5,7-diF-6-I), UBP2002 (6-I) and UBP2020 (6-Br) on native AMPARs was characterised at multiple concentrations (Figure 2.13) to investigate the concentration-response relationship of these compounds on native AMPARs. UBP2054 had < 25% inhibition of AMPAR f-EPSPs at the highest concentration tested in the native system (300 µM), therefore the curve-fit was ambiguous and prediction of IC_{50} on native AMPARs included a large error (predicted IC_{50} for UBP2054 on native AMPARs > 300 µM; n = 4). The most potent kynurenic acid derivative tested, UBP2038, had an IC_{50} of 3.6 ± 0.1 µM on native AMPARs (n = 5). The potency of UBP2020 (25.6 ± 0.4 µM; n = 5) was slightly but statistically significantly higher potency compared to UBP2002 (45.2 ± 1.9 µM; n = 4) based on IC_{50} on native AMPARs ($p < 0.05$, Student's t-test). The rank order of potency on native AMPARs was similar to the rank order of affinity on homomeric GluK2 receptors (UBP2038 > UBP2020 > UBP2002 > UBP2054).

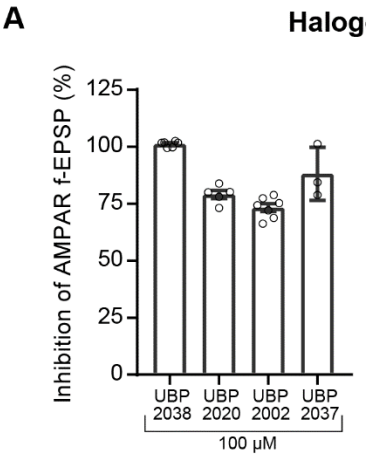

Compound	Inhibition of AMPAR f-EPSPs at 100 µM (%)
UBP2038	100.0 ± 0.5 (6)
UBP2020	79.1 ± 1.7 (5)
UBP2002	73.3 ± 1.7 (7)
UBP2037	88.2 ± 6.7 (3)

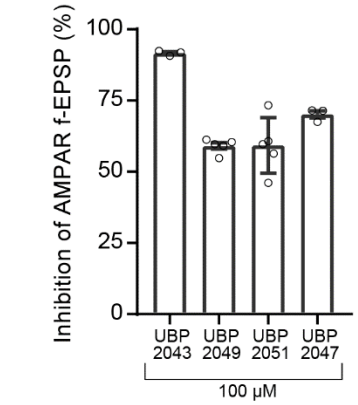

Compound	Inhibition of AMPAR f-EPSPs at 100 µM (%)
UBP2043	91.7 ± 0.5 (3)
UBP2049	59.1 ± 1.1 (5)
UBP2051	59.3 ± 4.4 (5)
UBP2047	70.2 ± 1.3 (3)

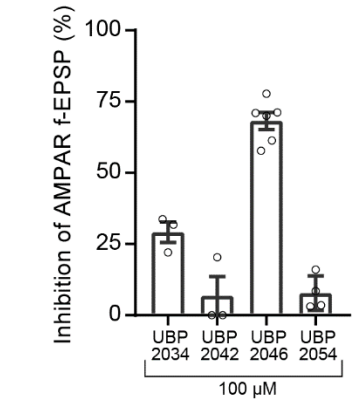

Compound	Inhibition of AMPAR f-EPSPs at 100 µM (%)
UBP2034	29.2 ± 3.6 (3)
UBP2042	5.7 ± 7.4 (3)
UBP2046	68.2 ± 3 (6)
UBP2054	7.8 ± 3 (4)

Figure 2.12. Characterisation of kynurenic acid derivatives on native AMPARs. A, Inhibition of AMPAR-mediated f-EPSPs by 6-halogen substituted kynurenic acid derivatives at 100 µM. Data from individual experiments are plotted on left (clear circles) and summary of results are shown on the right. Values in the table represent mean ± SEM %-inhibition of baseline AMPAR f-EPSPs. Compounds in the table are sorted according to activity on GluK2 homomeric receptors expressed in HEK293 cells. Number of independent observations (n) are shown in parenthesis. **B**, Similar to **A** but showing the inhibition of AMPAR f-EPSPs by kynurenates with polar 6-substituents. **C**, Similar to **A** but showing the inhibition of AMPAR f-EPSPs by kynurenates with non-polar 6-substituents.

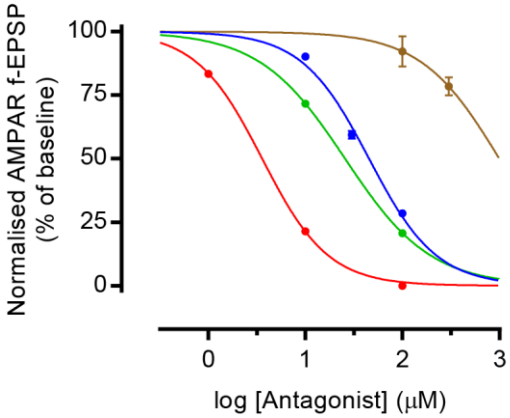

Compound	IC_{50} of AMPAR f-EPSPs (μM)
UBP2038	3.6 ± 0.1 (5)
UBP2020	25.6 ± 0.4 (5)
UBP2002	45.2 ± 1.9 (4)
UBP2054	995.5 ± 448.5 (4)

Figure 2.13. Concentration-response curves for 6-substituted kynurenates on native AMPARs in rat hippocampal slices. Concentration response curves (left) and estimated IC_{50} values (right) showing the low inhibition of AMPAR-mediated f-EPSPs by UBP2054. Key for the curves are shown next to compound names in the table. Mean ± SEM IC_{50} values for each compound were calculated from the IC_{50} values extrapolated from the respective curve. Number of experiments used to calculate the IC_{50} values are shown in parenthesis.

2.4. Discussion

In this study, various kynurenic acid derivatives were characterised using two functional assays. The first of these assays used recombinant human GluK2, GluK1 and GluA1 homomeric receptors and the second used native rat hippocampal AMPARs and NMDARs. The results from the current study have verified earlier reports (Leeson et al., 1991) that 6-substituted kynurenic acid derivatives act as non-NMDAR antagonists and have provided an understanding of their activity on individual AMPAR and KAR subunits. The current study also found that the nature of the substituent at the 6-position affects the affinities of kynurenates on KARs and AMPARs. Moreover, some 6-substituents had ~10-fold selectivity for GluK2 over GluK1 or GluA1 subunits. In summary, the results provide a better understanding of the differences between the ligand binding sites of GluK2, GluK1 and GluA1 subunits and provides information for the development of antagonists with greater subunit selectivity.

2.4.1. Correlation of results from recombinant receptors and native receptors

In the current study, both assays used to characterise the activity of compounds measured the responses mediated by receptors of interest and as such do not directly measure the affinity of compounds to KAR or AMPAR subunits. In the calcium fluorescence assay, the fluorescence increase caused by the opening of the ion channels of the homomeric receptors in response to glutamate application provided a suitable functional assay to characterise a large number of kynurenates. The IC_{50} values, slope-factors, and estimated K_i values from the assay using homomeric receptors were similar to previously published results in which homomeric GluK2 and GluK1 receptors were used to test glutamate and kynurenic acid (Alt et al., 2004). While the K_i provided an affinity constant for one receptor population corrected for the potency and concentration of the agonist, using K_i values from 2 receptor populations to calculate selectivity of the compound may be flawed, particularly between the KAR subunits and AMPAR subunits because the desensitisation blockers for KARs and AMPARs, con A and cyclothiazide, respectively, may affect binding of antagonists to the receptor. Con A has previously been shown to affect agonist pharmacology of KARs (Jones et al., 1997). However, previous results from pharmacological characterisation of GluK1 antagonists on recombinant GluK1 (using con A as desensitisation blocker) have correlated well with their inhibition of GluK1-mediated mossy-fibre synaptic potentiation

(Dolman et al., 2005; Dargan et al., 2009). Thus, due to the effect of con A on kynurenate binding being unclear, and the low affinity of compounds on on GluK1 and GluA1 cell lines, the primary use of the recombinant receptor assay was to identify GluK2 antagonists and to establish a rank order of affinities for different 6-substituted kynurenates on GluK2, GluK1 and GluA1 homomeric receptors.

The native receptor assay measured synaptic responses mediated by native AMPARs and NMDARs to characterise test compounds. The baseline SC-CA1 f-EPSPs were mediated through AMPARs in the conditions that were used in the study because application of 3 μM NBQX blocked AMPAR f-EPSPs (Figure 2.10B). NMDAR f-EPSPs were generated by changing the conditions to isolate NMDARs and the NMDAR f-EPSPs were blocked by 30 μM D-AP5. Using native receptors to characterise compounds also clearly showed that some antagonists such as UBP2054 had low native AMPAR inhibition (Figure 2.12 and Figure 2.13) and a rank-order of potencies for AMPAR inhibitory activity on native receptors was also revealed (rank order of AMPAR inhibitory potency was UBP2038 > UBP2020 > UBP2002 > UBP2054).

In addition to comparing activities between GluK2 and GluK1 or GluA1 homomeric receptors, comparison of activity in homomeric GluA1 and native AMPARs had some caveats. The native AMPARs contained a combination of GluA1 and GluA2 subunits as previously shown in the hippocampus (Lu et al., 2009). Therefore, the AMPAR inhibition of compounds in native system were likely on a mixed GluA1/GluA2 population of receptors. Although GluA2 and GluA1 subunits have > 90% sequence homology, noticeable differences in EC_{50} of glutamate on GluA1 and GluA2 subunits have been reported (Coquelle et al., 2000; Traynelis et al., 2010).

Another difference between GluA1 and GluA2 subunits is that GluA2 subunits in the hippocampus are largely in the Q/R-edited form meaning that they have lower calcium permeability (Burnashev et al., 1992b). Additionally, the concentration of glutamate in the physiological synapse is tightly regulated by glutamate re-uptake mechanisms (Bergles and Jahr, 1997). Therefore, the concentration of glutamate available in the synapse to compete with competitive antagonists is less than in the calcium fluorescence assay where the EC_{80} concentration of glutamate in the presence of 100 μM cyclothiazide could equilibrate in the

wells in the assay plate to elicit a response from GluA1 subunits. This could explain the lower activity of kynurenates at 100 μM on recombinant GluA1 homomeric receptors compared to native AMPARs (Figure 2.14). Some antagonists such as UBP2038 that may outcompete glutamate by tighter binding (due to higher affinity) to the receptor may provide similar %-inhibition in both the calcium fluorescence and synaptic AMPAR-mediated f-EPSPs at the same antagonist concentration. However, low affinity antagonists (i.e. those easily out-competed by glutamate) would produce less %-inhibition in the calcium fluorescence assay due to the much higher glutamate concentration and the equilibrium conditions in this assay compared to synaptic AMPARs where the glutamate concentration is quickly buffered by reuptake processes in astrocytes (Clark and Barbour, 1997; Bergles and Jahr, 1997).

Native KARs and AMPARs are known to be associated with auxiliary subunits such as Neto and TARP proteins, respectively (Tomita et al., 2003; Zhang et al., 2009). Auxiliary subunits affect the ion channel properties of iGluRs and therefore may affect pharmacology of the native receptor which may also explain the greater inhibition of native receptors by kynurenates at 100 μM (Figure 2.14). Another difference between recombinant- and native-AMPAR assays relate to the difference in receptor expression levels between the two assays. Expression of iGluRs in the hippocampus is cell type-specific (Kondo et al., 1997) and even specific sub-cellular regions have been shown to express AMPARs and KARs specifically (Fabian-Fine et al., 2000; Sun and Dobrunz, 2006; Schmidt-Salzmann et al., 2014). The functional implications of differences in AMPAR expression in pre-, post- and extra-synaptic compartments, on inhibition of AMPAR mediated f-EPSPs warrants further investigation. A solution to this problem may be to record the effect of compounds on post-synaptic AMPARs in the CA1 pyramidal cells by performing intracellular recordings from these neurons using techniques such as voltage-clamp.

Experimental conditions in the native and recombinant assays are different: particularly, the difference in temperature of FlexStation recordings (~25 °C) and electrophysiological recordings (~31 °C) may affect the pharmacodynamics of kynurenates by equilibrating with the slice at a higher rate than in the assay plates in FlexStation recordings. Biophysical properties of synaptic transmission in the native assay (Asztely et al., 1997) and the EC_{50}

of glutamate in the recombinant assay (by affecting receptor expression levels (Lin et al., 2015)) would also be affected.

Despite the verification of AMPAR and NMDAR mediated responses using NBQX and D-AP5, respectively, the synaptic f-EPSP response is a composite membrane potential from neurons also expressing other neuromodulatory proteins such as serotonin receptors, metabotropic glutamate receptors and GABA receptors (Vizi and Kiss, 1998; Ross et al., 2000). Whereas in the recombinant assay the Ca^{2+} influx following glutamate addition is mainly mediated through the receptor expressed on the plasma membranes of HEK293 cells and Ca^{2+} released from intracellular stores. Therefore, the effect of compounds on these "off" targets in native assays may also pose a difficulty when comparing data from recombinant and native assays. Moreover, whether the process of preparation of slices in the native assay affects AMPAR expression or function during the experiment remains unclear and therefore, experiments from in vitro slice preparations could also be complemented by comparison of activity of compounds in in vivo studies.

While the results from both functional assays provided a rank-order of potency for compounds on a receptor population, measuring the binding affinities of compounds using radioligand binding studies (with certitude of receptor population) will be necessary to obtain accurate data regarding the binding affinity of the compounds to GluK2, GluK1 and GluA1 and therefore, the selectivity of compounds for these different subunits. Furthermore, obtaining binding affinities for the 6-substituted kynurenates on recombinant GluK2, GluK1 and GluA1 homomers may also provide insights into the difference in inhibitory activities of the compounds between the recombinant and native receptors.

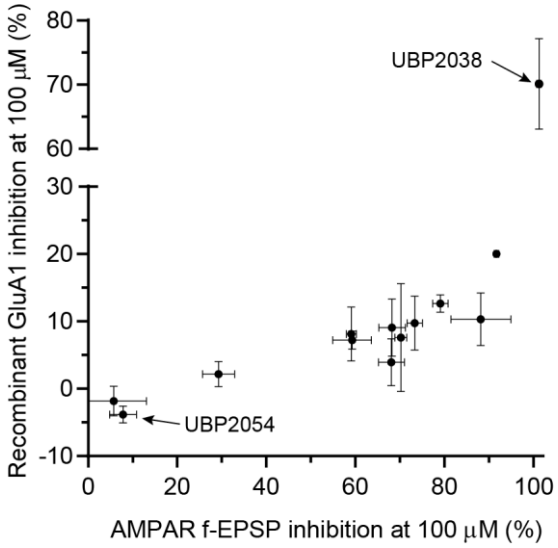

Figure 2.14. Correlation of inhibition of GluA1 recombinant receptors and native AMPARs by kynurenates. Data from single concentration screening on recombinant GluA1 subunits and native AMPAR f-EPSPs were significantly correlated ($p < 0.05$, Pearson correlation, $r = 0.6$). Data were taken from Table 2.3 and Figure 2.12.

2.4.2. Summary of results from the single concentration screening on recombinant AMPARs and KARs

Results from the single concentration screening suggest that one or more of the 1-NH, 2-carboxyl and 4-oxo groups in kynurenic acid may be involved in interactions with the binding sites of GluK2, GluK1 and GluA1 subunits. This can be concluded because the compounds in which these substitutions were removed or replaced by modifications of the heterocyclic ring, such as UBP2056, UBP2057, UBP2058, UBP2059 and UBP2063 (Figure 2.1F) had < 10% inhibition on GluK2, GluK1 or GluA1 subunits (Table 2.2). Substitution at the 8-position (UBP2052) also decreased the inhibitory activity of compounds possibly due to steric hinderance in the binding site caused by the 8-substituent. Amongst the compounds that inhibited GluK2 responses by more than 10%, those with 5,6,7- substituents (UBP2038, UBP2039) had the greatest inhibition on GluK2 homomeric receptors. This result matched the trend in previous studies that 5- and 7- substitutions on the benzene ring increased binding affinity at the glycine site of NMDARs (Leeson et al., 1991). While the single concentration screening provided a suitable overview of activity of the compounds on GluK2, GluK1 and GluA1 subunits, the activities at 100 μM could not be used as a robust measure of inhibitory activity for comparing activities on the same subunit or between different subunits because the concentration-response relationship was

unknown. Therefore, compounds which produced > 10% inhibition on GluK2 were further characterised by evaluating their concentration-response relationships to obtain IC_{50} and K_i values, and the results from concentration response curves on GluK2, GluK1 and GluA1 were used to study the effect that various substituents had on inhibitory activity of chosen compounds.

2.4.3. Inhibition of GluK2 subunits by 6-substituted kynurenates

All 6-halogen substituted compounds tested in the current study inhibited GluK2 homomeric receptors. In the earlier study by Leeson et al., 1991, addition of substituents at the 5- and 7-position on the benzene ring was shown to increase the inhibitory activity at the NMDAR glycine site. Similarly, addition of fluoro groups at 5 and 7 positions in addition to the 6-halogen substitution, UBP2038 (5,7-diF-6-I) and UBP2039 (5,7-diF-6-Br) resulted in greater inhibitory activity on the GluK2 subunit, compared to just 6-halogen alone as in UBP2002 (6-I) and UBP2020 (6-Br) (A). Moreover, the nature of the 5- and 7-substituent may also contribute to the activity because the 5,7-diCl substituted UBP2037 (5,7-diCl-6-I) and 5,6,7-trichloro substituted UBP2025 (5,6,7-triCl had lower inhibitory activity compared to the 5,7-diF substituted UBP2038 and UBP2039 on GluK2 (Figure 2.6A). In addition, the nature of the 5- and 7-halogen substituent may also affect solubility of the compound because 5,7-diCl substituted UBP2037 and UBP2025 had solubility issues at 100-2000 µM, concentrations at which 5,7-diF substituted UBP2038 and UBP2039 were water soluble.

From the polar 6-substituted kynurenates tested in the study, UBP2043 (6-OMe-7-F) had the highest affinity on GluK2, which further highlights the influence of 7-substitution for GluK2 affinity because UBP2049 (6-OMe), which had no 7-F substituent, had lower affinity on GluK2 (Figure 2.7A). UBP2047 (5-F, 6-OMe, 7-F) had lower affinity than UBP2049 on GluK2 (Figure 2.7A) and solubility issues were not observed for UBP2049 at concentrations up to 2 mM. Therefore, the nature of the substituents at the 5 and 7 positions and their electronic influence on the kynurenate molecule may affect the inhibitory activity – e.g. by affecting 4-keto/enol tautomerization and influencing the equilibrium of ionisation of the kynurenic acid molecule in an aqueous environment. Thus, the effects of different 5-,7- substituents on GluK2 affinity requires further investigation.

2.4.4. Qualitative comparison of physicochemical properties and GluK2 affinity of 6-substituted kynurenates

The GluK2 affinity of 6-substituted compounds were analysed based on the physicochemical properties of the 6-substituent such as its size (MR), hydrophobicity (π), and electronic effects (σ_m and σ_p) (Table 2.4). Lack of sufficient affinity data for a wide range of 6-substituents prevented a full quantitative structure activity relationship (QSAR) from being determined. However, the effect of one physicochemical parameter on GluK2 affinity was compared using compounds which had similar values of other physicochemical properties but varying values of the compared parameter.

The rank order of GluK2 affinity: SMe > OMe > Et, did not appear to be related to size of the 6-substituent (rank order of MR values SMe > Et > OMe) or hydrophobicity (rank order of π values: Et > SMe > OMe). However, GluK2 affinity did seem to be related to rank order of σ_m (rank order of σ_m values: SMe > OMe > Et) but not σ_p (rank order of σ_p values: SMe > Et > OMe).

Given that σ_m was related to the GluK2 affinity, it may be that more electron withdrawing 6-substituents affect the keto/enol tautomerisation of the kynurenate such that the keto-form is stabilised. In the enol form of kynurenates, the 1-NH group loses the proton and this group has been shown to be important for binding of kynurenic acid to NMDAR and therefore the keto form would have higher affinity (Furukawa and Gouaux, 2003).

An important consideration is that the electronic effects quantified by the σ_m value alone do not explain the GluK2 affinity of the 6-substituent. This is exemplified by the 6-substituent NO_2 which had the highest σ_m value but did not have the highest affinity (Table 2.4). An explanation can be reached by comparing the 6-substituents NO_2 and OMe. Both NO_2 and OMe have similar size (as judged by MR values) but OMe has higher affinity for GluK2 than NO_2. It appears that the lower hydrophobicity of NO_2 (much more negative π value than that of OMe) offsets its greater electron withdrawing ability (high σ_m value), thereby lowering affinity. The lack of activity of 6-CO_2H is likely due to the negative charge on the substituent which lowers hydrophobicity considerably.

Thus, it appears that amongst the compounds characterised in this study, electron withdrawing ability and hydrophobicity of the 6-substituent play a role in determining GluK2 affinity, while size is less important. This explains why 6-NH_2 is not tolerated, as it is electron donating (negative σ_m value) and hydrophilic (negative π value). There is likely to be an upper limit to the size of the 6-substituent. The higher GluK2 affinity of 6-Br versus 6-I, which have similar electron withdrawing and hydrophobicity parameters, suggests that the size of the iodo group (of 6-I) may be slightly detrimental to activity.

6-substituent	UBP code	GluK2 K_i (μM)	π	MR	σ_m	σ_p
H		91.8 ± 4.5	0.00	1.03	0.00	0.00
Br	2020	12.0 ± 1.5	0.86	8.88	0.39	0.23
I	2002	18.4 ± 1.5	1.12	13.94	0.35	0.18
Me (CH_3)	2034	46.5 ± 9.3	0.56	5.65	-0.07	-0.17
Et (CH_2CH_3)	2054	54.0 ± 10.4	1.02	10.30	-0.07	-0.15
OMe (OCH_3)	2049	22.0 ± 4.0	-0.02	7.87	0.12	-0.27
SMe (SCH_3)	2046	15.2 ± 3.1	0.61	13.82	0.15	0.00
CO_2H	2007	inactive	-0.32	6.93	0.37	0.45
NO_2	2051	37.7 ± 3.6	-0.28	7.36	0.71	0.78
NH_2	2022	inactive	-1.23	5.42	-0.16	-0.66

Table 2.4. Summary of GluK2 K_i and physicochemical properties of 6-substituted kynurenates. Data for GluK2 K_i was taken from Table 2.3. Data for π, MR, σ_m and σ_p were published in (Hansch et al., 1973).

2.4.5. Inhibition of GluK1 subunits by 6-substituted kynurenates

All 6-subsituted kynurenates which were further characterised after the initial screen, inhibited the GluK1 subunit (Table 2.3). UBP2054 (6-Et) had GluK1 IC_{50} > 1 mM but inhibited GluK2 receptors with K_i of ~54 μM. UBP2037 (5,6,7-triCl) also had GluK1 and GluA1 IC_{50} values > 1 mM and GluK2 K_i ~22.8 μM. As noted earlier, the solubility issues of UBP2037 prevented a consistent estimation of the concentration-response relationship (and hence the K_i). However, the high GluK1 IC_{50} of UBP2054 (6-Et) suggests that differences in the binding sites of GluK2 and GluK1 subunits may be used to improve GluK2 over GluK1 selectivity because the smaller 6-substituent in UBP2034 (6-Me)

caused greater inhibition of GluK1 compared to UBP2054 (UBP2034 GluK1 K_i ~47.8 μM; Figure 2.8B, Table 2.3).

The difference between GluK2 and GluK1 binding sites may also be due to the allowed volume available for the 6-substituent to bind because UBP2020 (6-Br) and UBP2034 (6-Me) both had higher affinity compared to their corresponding larger 6-substituted analogues UBP2002 (6-I) and UBP2054 (6-Et), respectively. Interestingly, the difference between GluK2 affinities of UBP2034 (6-Me) and the larger substituent UBP2054 (6-Et) is smaller than the difference between GluK1 affinities of UBP2034 and UBP2054 (Table 2.3), suggesting that the binding region close to the 6-substituent in GluK1 may be less tolerant of larger non-polar groups compared to the binding region in GluK2.

2.4.6. Inhibition of GluA1 subunits and native AMPARs by 6-substituted kynurenates

Data from characterisation of 6-substituted kynurenates on recombinant GluA1 homomeric receptors suggests that 6-substituted kynurenates may have lower affinity on GluA1 compared to GluK2 (Table 2.2). However, differences in AMPAR vs. KAR calcium fluorescence assay prevented the reaching of this conclusion based on activity on recombinant receptors alone as discussed above. The activity of 6-substituted kynurenates on recombinant GluA1 correlated with the activity on native AMPARs (Figure 2.14) and revealed that UBP2054 (6-Et) may have higher GluK2 over native AMPAR selectivity (Table 2.3 and Figure 2.13).

GluA1 inhibitory potency of kynurenate derivatives could not be fully characterised due to inactivity of compounds on GluA1 homomeric receptors in the recombinant assay and lack of solubility at concentrations > 1 mM. However, qualitative assessment of GluA1 K_i and inhibition of native AMPARs suggest that in GluA1, the size of the 6-substituent may be even more influential on the antagonist activity than in GluK1 and GluK2. The influence of the size of the 6-substitution is highlighted by the difference in activity between pairs of similar 6-substituted compounds with different sizes: UBP2020 (6-Br) vs. UBP2034 (6-I) and UBP2034 (6-Me) vs UBP2054 (6-Et). In both cases, inhibition of GluA1 and native AMPARs by the smaller 6-substituent is greater compared to larger 6-substituent (Table 2.3, Figure 2.12).

2.4.7. Using UBP2054 as a template for novel GluK2-selective antagonists

The first hurdle in developing GluK2-selective antagonists is to eliminate the AMPAR activity of candidate molecules. We have found that the 6-Et kynurenic acid, UBP2054, blocked GluK2 homomeric receptors with a K_i ~50 µM, while at 100 µM, minimal effect on native AMPARs was observed (Figure 2.13). As such, UBP2054 may serve as a useful pharmacological tool for investigating the physiological roles of GluK2 when used in conjunction with KAR subunit knockouts and GluK1 selective antagonists. Our results for UBP2054 in native tissue resembled results from a previous study using cortical slices which showed that UBP2054 had K_b > 100 µM on native quisqualate-activated receptors, and UBP2054 was shown to be inactive on native NMDA-activated receptors at 100 µM (Leeson et al., 1991). The results from this study have also shown that a combination of polarity and electronic effects of the 6-substituent may affect the affinity of antagonists on GluK2 homomeric receptors. The current study also confirmed that adding 5- and 7-fluoro substitutions on the benzene ring may increase affinity of the antagonist on GluK2 (Table 2.3). However, it is likely that substitutions at the 5 and 7 positions may also increase antagonist activity on GluK1 and GluA1 subunits. Therefore, further studies of 5,7-diF-6-Et substitutions on the phenyl ring may provide a better understanding of the molecular determinants of GluK2 potency and enhanced GluK2 over AMPAR selectivity. However, as already noted, the poor solubility of kynurenates might prevent the usage of kynurenates for physiological studies. Therefore, the findings of this SAR study might assist in the development of novel compounds that mimic the pharmacophore of UBP2054 while improving solubility and GluK2 affinity with the aim of producing antagonists with high selectivity for GluK2 over GluK1/AMPARs.

Chapter 3

Molecular modelling of the binding of kynurenate derivatives to ionotropic glutamate receptors

3.1. Introduction

3.1.1. Molecular docking as a tool for development of novel antagonists for GluK2

Computational molecular modelling techniques have become important tools for drug development with the advent of affordable hardware. Molecular docking has been used for virtual screening of large numbers of compounds on a well-defined target molecule such as a receptor protein (e.g. Schiavini et al., 2015; also see Kapetanovic, 2008). X-ray crystallography has been used to obtain the high resolution (< 2 Å) structures of iGluRs used for molecular docking (e.g. Møllerud et al., 2017). X-ray crystal structures of GluA2 LBD in the apo (unoccupied) form and agonist-, and antagonist-bound forms, provided early insights about the tertiary structure of the protein and the conformational changes that follow ligand binding (Armstrong et al., 1998; Armstrong and Gouaux, 2000). Particularly, the apo- and antagonist-bound forms of the LBD is a bi-lobed structure that resembles a clamshell (Armstrong et al., 1998). The amount of separation between the two lobes (or LBD opening) is lowest in the agonist-bound form and highest in the resting apo-form whereas binding of antagonists induces an intermediate separation (Armstrong and Gouaux, 2000).

Since the initial X-ray structure of GluA2, LBD X-ray structures of other iGluR subunits including the NMDAR GluN1 subunit (Furukawa and Gouaux, 2003) and KAR GluK1 and GluK2 subunits (Alushin et al., 2011; Mayer, 2005; Mayer et al., 2006; Møllerud et al., 2017) have been solved. The NMDAR and KAR LBD structures share similarities with that of the GluA2 structure, namely, agonist- and partial agonist-induced LBD closures (Furukawa and Gouaux, 2003; Mayer, 2005) and the antagonist-bound LBD in the open conformation (Furukawa and Gouaux, 2003). In subsequent years, more X-ray structures of GluK1 LBD in complex with antagonists have emerged (Naur et al., 2005; Mayer et al., 2006; Dolman et al., 2007; Dargan et al., 2009; Demmer et al., 2015). In some cases, molecular docking studies using the GluK1 X-ray structures have been helpful in developing GluK1 antagonists such as ACET (Mayer et al., 2006; Dolman et al., 2007).

Results from these and more recent studies have shown that the LBD closure in the ligand-bound GluA2 and GluK1 LBD vary significantly depending on the nature of the ligand (see Figure 3.1) and that the differences in the residues lining the ligand binding cleft could be

used to develop high-affinity GluK1 antagonists (Dolman et al., 2006; Alushin et al., 2011; Atlason et al., 2010). Particularly, mutagenesis studies have been helpful in identifying residues that are involved in binding of GluK1 antagonists based on willardiine derivatives (Atlason et al., 2010).

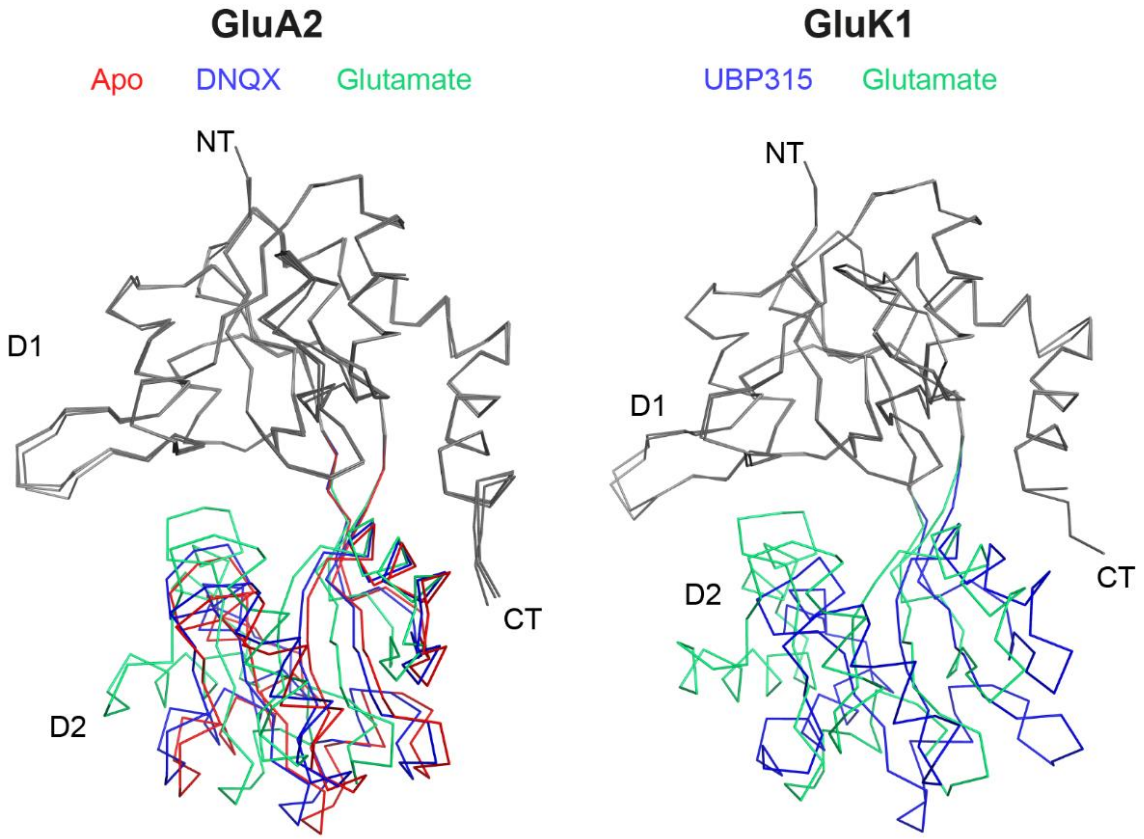

Figure 3.1. LBD closure of GluA2 and GluK1 upon agonist and antagonist binding. Alignment of D1 α-carbons (coloured grey) of the peptide chain in the GluA2 LBD in the apo form (D2 colour: red), antagonist-bound form (D2 colour: blue) or the agonist-bound form (D2 colour: green). In both the GluA2 LBD (left) and GluK1 LBD (right), antagonist binding leads to LBD opening whereas glutamate binding leads to LBD closure. Structures were obtained from Armstrong and Gouaux, 2000 and Mayer, 2005.

3.1.2. Homology modelling of GluK2 receptors

While antagonist-bound GluA2 and GluK1 X-ray crystal structures have been available (Armstrong and Gouaux, 2000; Mayer et al., 2006), X-ray structures of the antagonist-bound GluK2 LBD are lacking partly due to a lack of high affinity water-soluble antagonists (Jane et al., 2009; Mayer, 2017). Therefore, it is necessary to create models of the GluK2 LBD based on X-ray structures of homologous proteins, such as those obtained

for the GluK1 LBD in complex with antagonists (Mayer et al., 2006; Hald et al., 2007; Alushin et al., 2011). The rationale behind homology modelling is that proteins with high amino acid sequence similarity may also share the same secondary and tertiary structural features. Therefore, the unknown structure of proteins may be estimated by overlaying its amino acid sequence onto the known structure of a highly homologous protein and solving the mismatches by predicted protein folding using information from previously solved, homologous protein sequences (Greer, 1980).

3.1.3. Differences in the GluK2 LBD binding site compared to GluK1 and GluA2

The X-ray structures of glutamate bound to the GluK2 LBD reveal the residues that may form conserved interactions with all known orthosteric ligands that have been crystallised in complex with iGluR LBDs (Figure 3.2; see Møllerud et al., (2017) for a review). In the glutamate-bound state, conserved interactions formed by residues lining the GluK2 LBD D1 include: a salt-bridge between the side chain of Arg-492 and the α-carboxyl group of glutamate, hydrogen bonding (H-bond) between Ala-487 (Thr in GluK1 and GluA2) via the peptide backbone NH and the α-carboxyl oxygen of glutamate, and an H-bond between the peptide backbone carbonyl group of Pro-485 and the α-amino group of glutamate. The agonist-induced closure of the LBD clamshell allows the residues lining D2 of the LBD to form further H-bond interactions with glutamate.

The interactions of D2 residues are not conserved amongst all orthosteric ligands and depends on the domain closure and functional groups of the ligands. D2 interactions for glutamate include: H-bond interactions between the carboxyl side-chain of Glu-707 and amino group of glutamate, H-bond interactions between backbone amino group of Ala-658 (Ser in GluK1 and GluA2) and both carboxyl groups of glutamate, and H-bond interactions between the peptide backbone NH group and the side chain OH group of Thr-659 and the distal carboxyl group of glutamate.

In addition to the direct interactions provided by the LBD cleft-lining residues, glutamate also forms H-bond interactions with water molecules, which may also form indirect H-bond networks between the ligand and the residues lining the cleft, leading to further stabilisation of ligand binding and increased binding affinity. Despite the inadequate

resolution of X-ray crystallography in locating the positions of water molecules in ligand binding sites, many studies of iGluR LBDs have reported that water molecules may be critical in the binding of glutamate in the ligand binding pocket (Armstrong and Gouaux, 2000; Mayer, 2005).

Importantly, the residues lining the cleft from the D2 of GluK2, GluK1 and GluA2 are more variable compared to the cleft-lining residues from D1 (Figure 3.2). The Ala-487 residue which provides H-bond for ligand binding through its backbone oxygen is replaced by the more polar threonine residue in GluK1 and GluA2. The polar side chain of threonine residues in GluK1 and GluA2 is close enough to the α-carboxyl group of glutamate to form H-bond interactions and further stabilise the glutamate-bound state (Figure 3.2, (Armstrong and Gouaux, 2000; Mayer, 2005)). The binding pocket volumes of GluK2 and GluK1 are 16% and 40% larger, respectively, compared to GluA2 (Mayer, 2005). The intermediate volume in GluK2 compared to GluK1 and GluA2 is explained by the differences in 3 amino acids: Asn-690, Phe-704 and Thr-710 in GluK2 which are replaced by the smaller Ser-706, Leu-720 and Ser-726, respectively, in GluK1; in GluA2, these residues correspond to Thr-686, Tyr-702 and Met-708.

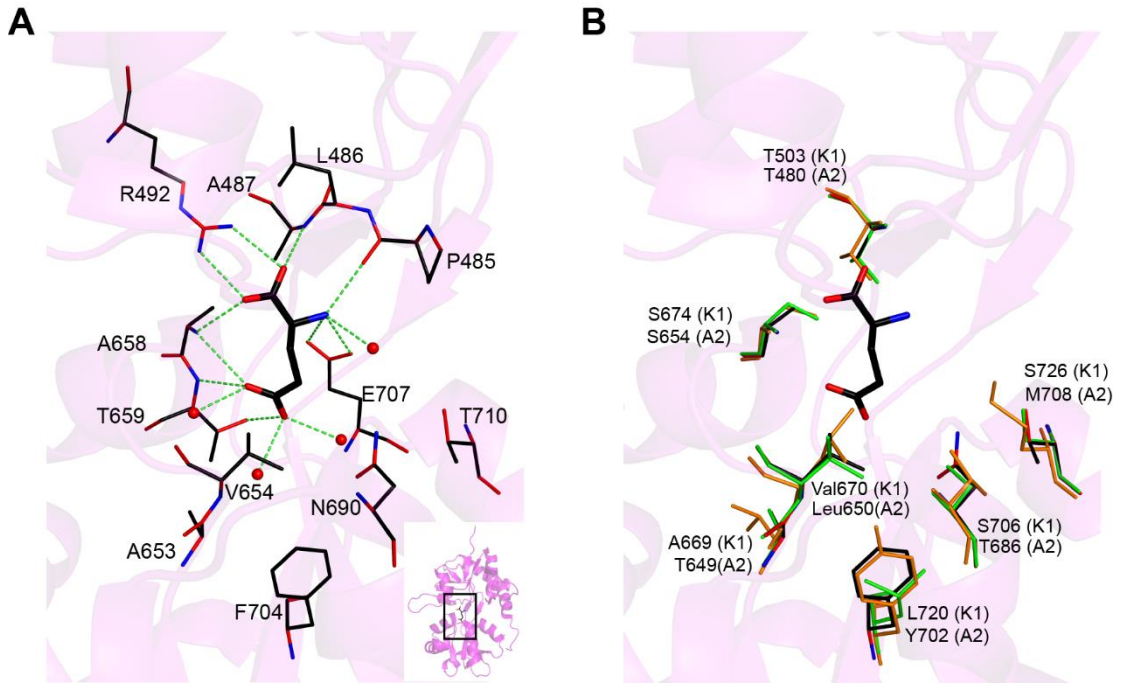

Figure 3.2. Differences in the residue composition of the orthosteric ligand GluK2 binding site compared to GluK1 and GluA2. A, D1-D2 cleft of glutamate-bound GluK2 LBD (PDB [Protein Data Bank] identifier: 1S50) and the residues that form hydrogen bonds with glutamate are shown. Also shown are residues that are different between GluK2, GluK1 and GluA2. Inset shows a cartoon representation of a single LBD and the location of the D1-D2 cleft. Glutamate and residues are shown as thick and thin sticks, respectively. Water molecules are shown as red spheres. H-bond interactions are shown as green dashed lines. **B**, Similar to **A** but different residues in GluK1 (green; PDB id: 1TXF) and GluA2 (orange; PDB id: 1FTJ; PDB id: 1S50) are also shown in addition to the corresponding GluK2 residues (black carbons) and bound agonist, glutamate, from A. Positions of GluK1 and GluA2 residues were determined by alignment of glutamate-bound LBD α-Carbons atoms in GluK2, GluK1 and GluA2.

3.1.4. Objectives

In this study of the pharmacological activity of kynurenic acid derivatives (Chapter 2), it was observed that some 5,6,7- and 6-substituted compounds have higher affinity on GluK2 compared to kynurenic acid (Table 2.3). In the present molecular docking study, predicted binding of kynurenic acid, UBP2002 (6-I) and UBP2038 (5,7-diF-6-I) was examined to identify the residues, which are necessary for interactions that improve the GluK2 affinity of kynurenic acid derivatives. It was also found that UBP2054 (6-Et) has the best GluK2 over GluK1 and GluA1 selectivity of the kynurenate derivatives that were tested (Table 2.3 and Figure 2.13). Therefore, the predicted binding of UBP2054 was compared between

GluK2, GluK1 and GluA2 in modelling studies to explain its favourable GluK2 selectivity. The GluA2 LBD was used instead of GluA1 in modelling studies, as antagonist X-ray structures are only available for GluA2 and there are no differences in ligand binding residue composition in the GluA1 and GluA2 LBDs (see methods section).

The much reduced NMDAR activity of 6-substituted kynurenates observed in the present study and in a previous study (Leeson et al., 1991) was also investigated by docking UBP2040 (5,7-diF) and UBP2002 (6-I) into the GluN1 LBD and comparing to the 5,7-diCl-GluN1 LBD X-ray structure.

The objectives of computational docking used in this chapter were to study:

1. the increased affinity of 5,6,7-trisubstituted compounds on GluK2,
2. the reduced affinity of UBP2054 on GluK1 compared to GluK2
3. the reduced affinity of UBP2054 on AMPARs compared to GluK2
4. the reduced activity of 6-substituted kynurenates on NMDARs by modelling their interaction with the glycine binding site on GluN1

3.2. Methods

3.2.1. Ionotropic glutamate receptor amino acid sequence comparison

The amino acid sequences for iGluR subunits were taken from the UniProt database (Bateman et al., 2017), and the Uniprot ID for the sequences used in this study are shown in Table 3.1. Amino acid sequence homology was calculated using the Clustal Omega webserver (Sievers et al., 2011). Most of the X-ray crystallisation studies of KARs were based on the rat version of the protein (reviewed in Møllerud et al., 2017). Therefore, the X-ray crystal structures used in this study were based on the rat version of the iGluR LBD whereas human recombinant receptors were used to pharmacologically characterise kynurenates. The amino acid sequences of rat GluK1, GluK2 and GluA2 LBD were compared to human versions and the percentage-identity of the LBD sequences are shown in Figure 3.3. The GluK2 LBD had the lowest similarity in amino acid sequence between the rat and human versions (87.6%) whereas GluA1, GluA2 and GluK1 LBDs had > 98% sequence homology (Figure 3.3). Therefore, an alignment of amino acid sequences of LBD from rat- and human-GluK2, and rat -GluK1, -GluA1, and -GluA2 was conducted to find the differences between amino acids lining the ligand binding site (Figure 3.4).

Subunit	Species	Uniprot ID
GluA1	Rat	P19490
GluA1	Human	P42261
GluA2	Rat	P19491
GluA2	Human	P42262
GluK1	Rat	P22756
GluK1	Human	P39086
GluK2	Rat	P42260
GluK2	Human	Q13002

Table 3.1. Uniprot sequences used for alignment and homology modelling.

	GluA1 (Rat)	GluA1 (Human)	GluA2 (Rat)	GluA2 (Human)	GluK1 (Rat)	GluK1 (Human)	GluK2 (Rat)	GluK2 (Human)
GluA1 (Rat)	100.0	100.0	86.6	87.0	55.1	55.6	56.2	54.9
GluA1 (Human)	100.0	100.0	86.6	87.0	55.1	55.6	56.2	54.9
GluA2 (Rat)	86.6	86.6	100.0	99.6	53.4	53.9	54.5	54.0
GluA2 (Human)	87.0	87.0	99.6	100.0	53.9	54.3	54.9	54.5
GluK1 (Rat)	55.1	55.1	53.4	53.9	100.0	98.3	85.8	86.8
GluK1 (Human)	55.6	55.6	53.9	54.3	98.3	100.0	85.4	86.3
GluK2 (Rat)	54.9	54.9	54.0	54.5	86.8	86.3	100.0	87.6
GluK2 (Human)	56.2	56.2	54.5	54.9	85.8	85.4	87.6	100.0

Figure 3.3. Percentage amino acid residue identity of rat and human versions of ligand binding domains of GluA1, GluA2, GluK1 and GluK2. Percentage identity matrix showing the %-similarity in LBD (S1 and S2 polypeptides) amino acid sequences of rat and human GluA1, GluA2, GluK1 and GluK2 subunits. Generated using Clustal Omega.

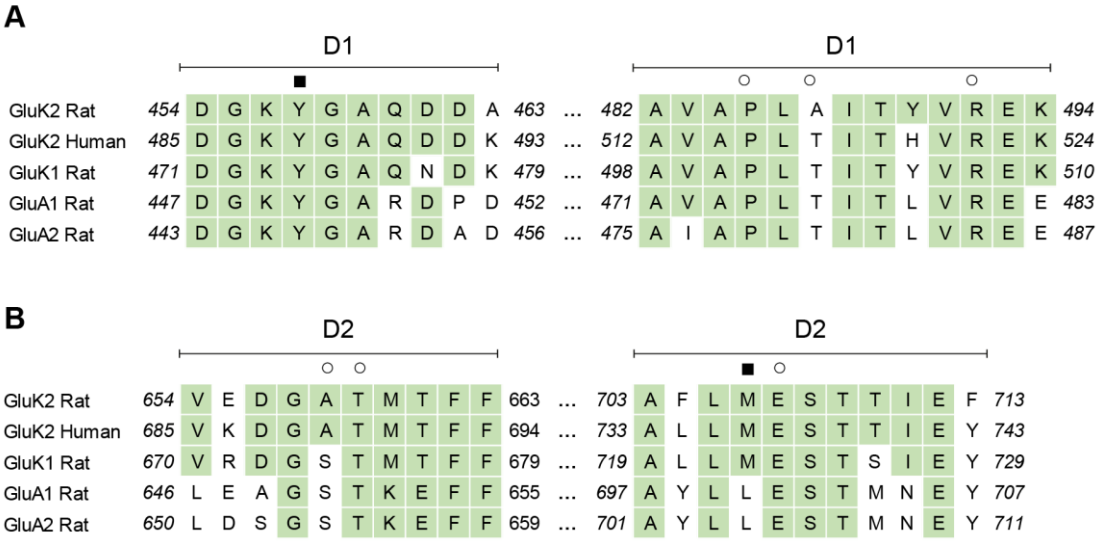

Figure 3.4. Alignment of the amino acid sequences lining the orthosteric ligand binding site. Alignment of amino acids near the glutamate binding site from D1 (**A**) and D2 (**B**) domains of the LBD. Residues which were the same as in rat GluK2 LBD are highlighted in green. Residues capable of forming hydrogen bonds and van der Waals interactions with agonists are marked with white circles and black squares, respectively.

3.2.2. Structures of ligand binding domains

X-ray crystal structures of LBDs were taken from the Research Collaboratory for Structural Bioinformatics (RCSB) protein data bank (PDB) (Berman et al., 2000). The PBD identification codes for structures used in this study are quoted in text.

3.2.3. GluK2 LBD homology model building

Homology models of the antagonist-bound GluK2 LBD were generated using the X-ray crystal structure of GluK1 in complex with antagonists. The GluK1 LBD was used because of the high amino acid sequence homology between GluK1 and GluK2 rat LBDs (~87%) (Figure 3.3). The GluK1 LBD used for obtaining the X-ray crystal structures in this study was synthesised using the S1 and S2 polypeptide segments linked by two residues: glycine and threonine (GT-linker), as S1 and S2 are not normally directly linked but are two individual polypeptide chains separated by the TMD (Armstrong and Gouaux, 2000; Alushin et al., 2011). Therefore, when building the GluK2 homology model, only the amino acid sequences of rat GluK2 S1 and S2 polypeptide chains were used.

Homology models of the GluK2 LBD from the GluK1 LBD were built using the Swiss-model server which uses the ProMod3 modelling engine (Bienert et al., 2017). The program generated homology models by initially overlaying the GluK2 S1S2 sequence onto the appropriate GluK1 LBD X-ray structure. The secondary and tertiary structures of the GluK2 LBD are predicted using information from the GluK1 structure and homologous structures in a curated database which is regularly updated using structures from the PDB (Bienert et al., 2017). Following the solving of residue conformations in the homology model, ProMod3 also performed energy minimisation on the homology model using the CHARMM27 force field to resolve any unfavourable interactions introduced by the model building (Mackerell et al., 2004).

The overall quality of the model is indicated by the Global Model Quality Estimate (GMQE) score, a value between 0 and 1, which reflects the accuracy of the model built with the alignment of the GluK1 LBD X-ray structure to the amino acid sequence of the GluK2 LBD. Therefore, the GMQE score of 0.97 obtained for the GluK2 homology model indicates a high prediction of accuracy. The QMEAN Z-score provides a measure of the total model quality based on geometrical properties of residues in the model and reports the

number of standard-deviations that the homology model differs from other structures of similar size (Benkert et al., 2008). A QMEAN Z-score value close to 0 indicates a good quality (0.33 for the GluK2 model). Another measure of the model quality is the QMEAN local quality estimate which predicts the similarity of inter-atomic distances for individual residues in the homology model compared to experimentally determined structures that have homologous amino acid sequence to the GluK2 LBD sequence (Figure 3.5). A predicted similarity less than 0.6 is typically considered a low quality and a value of 1 indicated a high quality of prediction of interatomic distances in the model.

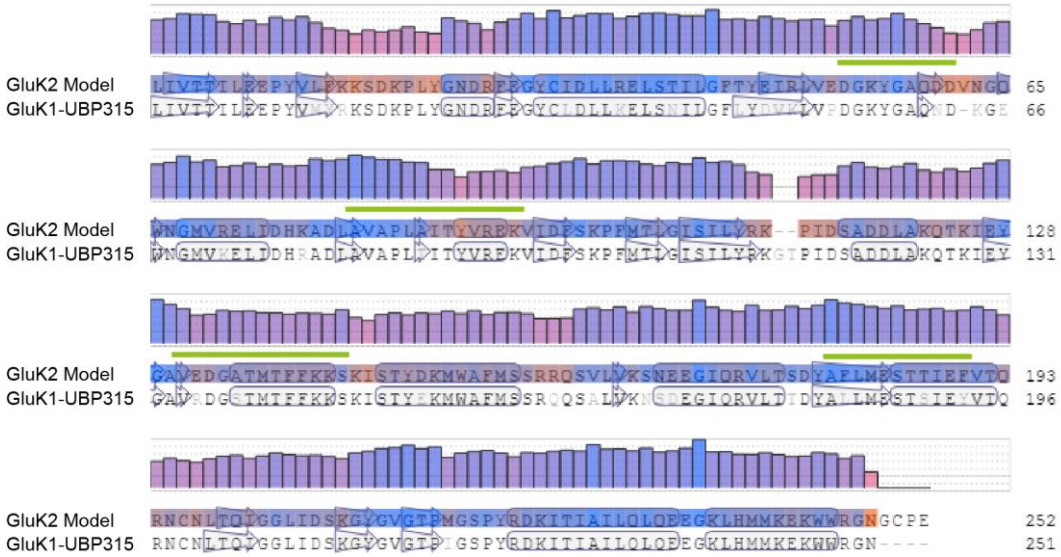

Figure 3.5. Prediction of quality of homology model using QMEAN local quality estimate for the GluK2 homology model based on GluK1-UBP315. QMEAN of individual residues in the homology model and the alignment of the model's amino acid sequence to the GluK1-UBP315 structure. The bars show local quality estimate (color scale: blue = 1, red = 0). The green lines above the alignment shows residues lining the ligand binding cleft. Adapted from Swiss-model model quality report. Majority of the residues in the model had good residue placement when compared to homologous structures (indicated by predominantly blue bars especially for the ligand binding cleft residues).

3.2.4. Preparation of protein structures for molecular docking

Protein structures obtained from PDB did not contain information regarding hydrogen atoms which are required when predicting ligand binding. In some cases, some residues were only partially resolved (usually only affects a few residues that do not take part in ligand binding) and in some cases alternative conformations of the same residue are

contained in the pdb file of the X-ray structure. Moreover, unwanted atoms such as crystallisation solvents in addition to water were sometimes present in the X-ray structure files from PDB. Water molecules and non-ligand atoms obtained from the X-ray structures were removed and hydrogen atoms were added to the X-ray crystal structures using the protein preparation routine in Schrödinger (Schrödinger LLC). Assignment of bond orders, correction of missing side chains and creation of disulphide bonds in the X-ray crystal structures were performed before energy minimisation of the protein structure using the OPLS3 force field in Schrödinger.

A further validity check for a homology model structure is to check that the backbone bond angles of the homology model structure is acceptable. A Ramachandran plot of the prepared protein structure was used to ascertain that the nitrogen-alpha carbon (Phi) and alpha carbon-carbon (Psi) bond-angles of the protein backbone fell within expected regions (Figure 3.6). The main variation from the expected distribution of angles in the structures used in the study were due to glycine residues.

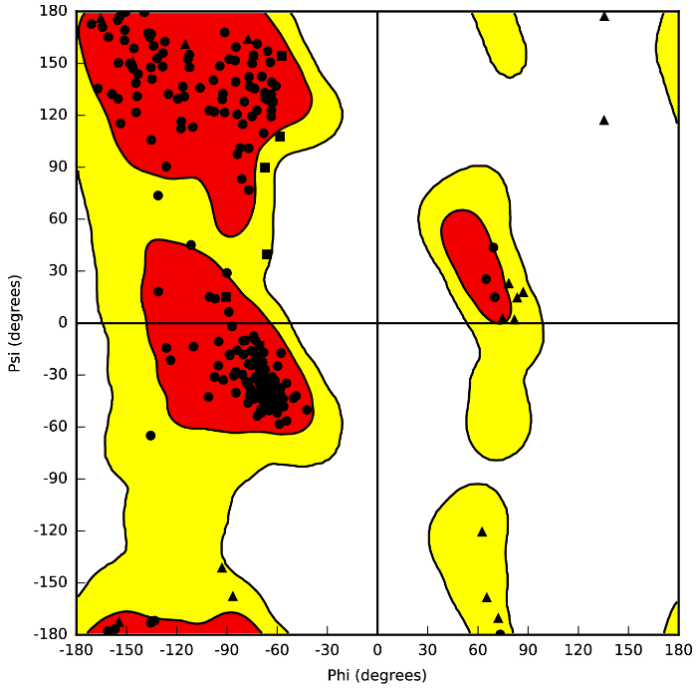

Figure 3.6. Ramachandran plot for the GluK2 homology model based on GluK1-UBP315. The phi and psi bond angles for residues in the GluK2 homology model is shown as black symbols. Triangles represent glycine, squares represent proline, and other residues are shown as circles. Preferred and acceptable regions of phi and psi angles are highlighted. Red areas show the preferred angles, yellow areas show acceptable angles and white areas show disallowed areas.

3.2.5. Building the ligand library

Ligand structures were prepared using Maestro (Schrödinger LLC) and energy minimised using the Macromodel utility in Schrödinger using the OPLS3 force field, which was shown to predict small molecule conformations with high accuracy (Harder et al., 2016). The minimum energy of the ligand structure was estimated by the gradient convergence method in which the energy minima search for the ligand structure was conducted such that the gradient was as close to 0 as possible (convergence threshold was set at 0.05). Ligand structures were further optimised using the LigPrep utility in Schrödinger: possible ionisation states within a pH range of 7.4 ± 1.0 and probable tautomers of ligands were generated using the Epik module in Schrödinger.

3.2.6. Molecular docking

The semi-automated Induced Fit Docking (IFD) workflow in Schrödinger was used to dock ligands into the LBD structures and generate ligand poses. IFD uses the Glide docking program (Friesner et al., 2004) which has been reported to have high accuracy for ranking poses for molecules in test datasets when compared with other scoring functions (Zhou et al., 2007). The first step of the IFD routine is an initial docking of ligands with reduced van der Waals radii and increased cut-off for electrostatic and other van der Waals interactions between the ligand and protein. For each pose generated from the initial docking, the Prime module in Schrödinger was used to refine the amino acid side-chains near the ligand to predict the structure of the ligand-bound binding site. Subsequently, the structures of the refined residues in complex with the ligand were energy minimised. Finally, each ligand was docked into the lowest energy binding site for the ligand determined from the Prime refinement stage using Glide extra precision (XP), which conducts extended sampling of ligand poses and scores the ligand binding using two scoring functions: Emodel and Glidescore (Friesner et al., 2004).

The areas in the receptor structure which were used by Glide to search for ligand conformations are defined as the search space for molecular docking. The search space for structures used in this study were defined by the residues around the binding cleft such that the search space encompassed the whole binding cleft. Based on GluK2 numbering, the key ligand binding residues used to define the search space were: Tyr-457, Ala-487, Arg-492, Val-654, Gly-657, Ala-658, Asn-690, Thr-709, and Thr-710. For docking of GluK1,

GluA2 and GluN1 LBDs, residues corresponding to the GluK2 residues listed above were used to mark the search space for the docking program.

3.2.7. Analysis of binding poses

When comparing docking poses, poses of docked ligands were selected based on some "conserved" interactions that have been previously observed within all iGluRs in complex with orthosteric agonists. Particularly, the Arg-492, Ala-487 and Pro-485 in GluK2 and the corresponding residues in GluK1, GluA2 and GluN1 have been shown to be involved in H-bond interactions with orthosteric ligands. Therefore, poses of ligands where one or more of these interactions were absent were excluded. Another indicator of a "poor" pose was extensive refining of some bulky hydrophobic cleft-lining residues to accommodate the ligand – suggesting that steric clashes would have occurred had the refinement been omitted.

Upon successful docking of ligands, the IFD module ranked the ligand poses based on IFD score – a composite score that accounts for the scores generated by Glide's scoring functions and the energy of the LBD with the refined residues in complex with the docked ligand (generated by the Prime module). Glide generated two scores, one of which was the Emodel score – the result of the scoring function which mainly searches for electrostatic and van der Waals ligand-receptor interactions and is used by the IFD program to choose the best pose for the prime refinement stage. The second scoring function used by Glide, Glidescore, includes terms for electrostatic and van der Waals interactions, and also includes penalties for buried polar groups and for freezing rotatable bonds (Friesner et al., 2004).

After selecting suitable poses by qualitative assessment after visual inspection, the numerical scores from the IFD workflow (IFD score, Emodel score and Glidescore) could also be considered for explaining binding affinity. However, given the exploratory nature of the current study and the similarities in the affinities of kynurenates within each type of subunits tested, the scores generated by the IFD were only used to find a rank order of ligand poses after qualitative assessment.

To analyse steric clashes between the ligand and receptor, the overlap of van der Waals volumes of the docked ligand and the LBD was calculated using the phase_volCalc utility in Schrodinger.

The choice of ligands used for the docking routine was dependent on the research question which was addressed. However, all docking studies used kynurenic acid as a reference structure to compare the effect that substitutions on the benzene ring made to the ligand interaction. Additionally, the quality of the docking program was assessed by docking the structure of the crystallised ligand (prepared using the same techniques as kynurenates) into the LBD and comparing the docked pose to the X-ray crystal pose of the ligand.

3.2.8. Presentation of poses

Images showing solvent accessible van der Waals surfaces of the LBD binding cavity and ligands were prepared using PyMol. Ligand interaction diagrams, generated in Maestro, were used to show the residues that were in 4 Å proximity to the receptor and would therefore influence ligand-receptor interactions. Images showing overlays of LBD D1 α-carbons and overlay of docked and X-ray crystal ligand poses were prepared in PyMol.

3.3. Results and Discussion of Modelling Studies

3.3.1. Choice of KAR structural models

Many high resolution (< 2 Å) X-ray structures of the GluK1 LBD in complex with antagonists are available (for a review, see Møllerud et al., 2017). The degree of LBD closure caused by different antagonists has also been shown to vary significantly (Mayer, 2005; Alushin et al., 2011; Demmer et al., 2015). Therefore, the choice of the receptor X-ray structure used for the docking study was based on a prediction of LBD closure caused by kynurenate binding to the KAR LBD. The domain closure of the LBD is an important factor for estimating an accurate binding pose for docked ligands and for interpretation of the possible ligand-receptor interactions. A domain that is closed would increase the number of good/bad ligand-receptor interactions and conversely, an open domain would decrease the number of ligand-receptor interactions assessed by the docking program when ranking the ligand poses.

The similarity of the antagonist used for X-ray crystallisation to kynurenic acid provided a good indicator of LBD opening in the kynurenate-bound structures. A ligand similar to kynurenic acid that was crystallised with GluK1 was (*S*)-2-Amino-4-(2,3-dioxo-1,2,3,4-tetrahydroquinoxalin-6-yl)butanoic acid (CNG10300) (Demmer et al., 2015). The CNG10300-bound structure showed a large variation in LBD opening compared to the glutamate bound GluK1 LBD (25 - 40°), which highlights the degree of LBD flexibility that is possible in the antagonist-bound state of the receptor (Demmer et al., 2015). The UBP series of GluK1 antagonists based on the natural product willardiine were amongst the first compounds to be crystallised with the GluK1 LBD. The UBP315-bound GluK1 LBD crystal structure has a domain opening of ~25° compared to the glutamate-bound GluK1 LBD (Alushin et al., 2011). Other UBP compounds such as UBP310 and UBP318 had higher domain opening angles (~30°) (Mayer et al., 2006; Alushin et al., 2011).

An exploratory docking routine was carried out on the UBP315 (PDB id: 2QS1), UBP318 (PDB id: 2QS2), and CNG10300 (PDB id: 4QF9) GluK1 LBD structures and the IFD routine successfully found binding poses in all three X-ray structures for the standard antagonist UBP2038 (5,7-diF-6-I). Given the similarities in the success for finding docking poses for all three X-ray structures, the UBP315-bound X-ray structure was used as the GluK1 structure for docking studies. It was also used for GluK2 homology model building because UBP315 binding led to the lowest LBD opening and therefore increases the chance of finding interactions with both D1 and D2 residues, which could then be qualitatively assessed.

3.3.2. Choice of AMPAR structural model

Currently available X-ray structures of the AMPAR subunit were based on the GluA2 subunit. Therefore, to explain the activity of kynurenate derivatives on AMPARs, the GluA2 subunit was chosen. The choice of using the GluA2 LBD X-ray crystal structure instead of a GluA1 LBD homology model based on the GluA2 structure was that the GluA1 homology model building process would reduce the accuracy of the predicted structure. Additionally, GluA2 and GluA1 are both expressed in the rat hippocampus where the kynurenates were characterised (Lu et al., 2009). Moreover, there was ~87% amino acid sequence similarity between the GluA1 and GluA2 LBD and all residues that interacted

with orthosteric agonists in the ligand binding site were conserved in rat GluA1 and GluA2 (Figure 3.4).

The degree of opening of the LBD structure to be used for docking is likely to influence the ligand-receptor interactions. In the absence of solved structures of kynurenates in complex with AMPARs, it is difficult to predict the degree of LBD closure when kynurenates are bound. The quinoxaline-2,3-dione family of AMPAR antagonists has been used to solve the structure of the antagonist-bound GluA2 LBD (Armstrong and Gouaux, 2000; Menuz et al., 2007). The number of rings in 6,7-dinitroquinoxaline-2,3-dione (DNQX) and 6-cyano-7-nitroquinoxaline-2,3-dione (CNQX) and the planarity of the molecule were similar to kynurenic acid. Moreover, both DNQX (Armstrong and Gouaux, 2000) and CNQX (Menuz et al., 2007) caused similar levels of LBD domain closure (3-7°) compared to the GluA2-apo structure. Therefore, LBD structures solved using DNQX and CNQX provided a suitable model for computationally docking kynurenic acid derivatives. In the current study, DNQX bound GluA2 (PDB id: 1FTL) was used as the structural model due to its higher resolution (1.8 Å) compared to the CNQX (2.5 Å) structure.

3.3.3. GluK2 binding site interactions of kynurenic acid

The binding mode of kynurenic acid in the GluK2 LBD revealed similarities to the glutamate-bound GluK2-LBD, such as the H-bond interactions between D1 Arg-492, Ala-487, Pro-485 and the carboxyl group of kynurenic acid (Figure 3.7). The open nature of the binding cleft of the GluK2 model based on the GluK1 LBD-UBP315 crystal structure meant that Glu-707, which was involved in H-bond interactions with glutamate was not close enough to be involved in an H-bond with the kynurenic acid carboxyl group (Figure 3.7). The Tyr-457 residue was in proximity to the ligand to allow a favourable π-π stacking interaction. The peptide chain NH group of Ala-658 in the D2 region was observed to form a H-bond with the 4-oxo group of kynurenic acid.

The structure of kynurenic acid docked into GluK2 LBD also revealed that the 5-, 7- and 6-positions may all be exposed to the solvent due to the presence of polar residues that line the phenyl ring of kynurenic acid (Figure 3.7). This could be interpreted as the reason for low affinity of GluK2 binding by kynurenic acid because the hydrophobic nature of the 5-

, 6- and 7-position of kynurenic acid would not allow favourable interactions with the nearby polar/charged residues (Figure 3.7A).

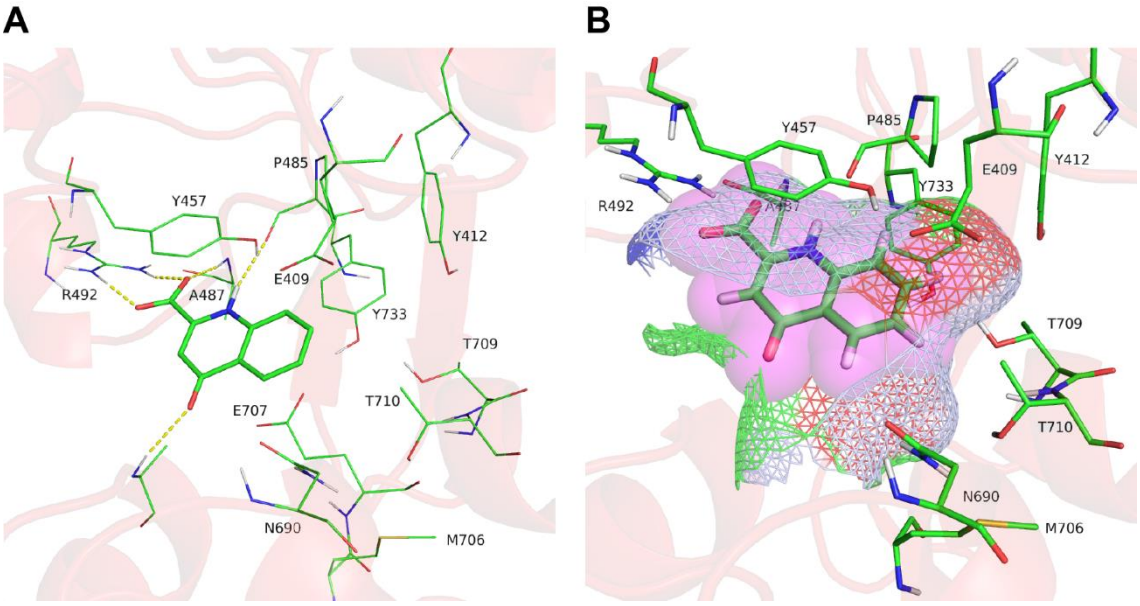

Figure 3.7. Kynurenic acid docked into GluK2 LBD homology model. A, Predicted pose of kynurenic acid docked into the GluK2 homology model based on GluK1-UBP315 (PDB id: 2QS1). Predicted H-bond interactions are shown with dashed yellow lines. Single letter amino acid code and the position of residues in the mature protein is shown in this and all 3-dimensional figures showing binding poses. **B,** Molecular surface area of the binding cavity (5 Å around kynurenic acid) in the GluK2 homology model. The cavity enclosure is shown as mesh coloured according to the electrostatic property of the cleft-lining residues (green: hydrophobic, light-blue: polar, red: negatively charged, blue: positively charged). The van der Waals volume of kynurenic acid is shown as spheres (coloured magenta). The volumes available to the 6- and 7-substituents are filled by hydrogen atoms in the kynurenic acid-docked GluK2 model.

3.3.4. Explanation for increased GluK2 affinity of UBP2038 compared to kynurenate and UBP2002

Pharmacological characterisation of kynurenates revealed an increase in GluK2 affinity of the 5,7-difluoro-6-iodo substituted UBP2038 compared to 6-iodo substituted UBP2002 and 6-H in kynurenic acid. Docking of kynurenic acid, UBP2002 and UBP2038 into the GluK2 homology model revealed the same rank order of docking scores for poses as the GluK2 affinity determined in the functional assay (Figure 3.8); rank order of IFD score for chosen poses (docking scores (unit: kcal/mol) in parenthesis, lower score indicates more

favourable pose energy): UBP2038 (-531.556) > UBP2002 (-529.871) > Kynurenic acid (-529.723). The 5-fluoro group of UBP2038 was positioned 3.1 Å and 3.7 Å from the Asn-690 and Met-706 residues, respectively, which may allow weak but favourable H-bond or van der Waals interactions. The 7-fluoro group was in proximity (3.2 Å) to Tyr-412, raising possibilities for van der Waals interactions with the tyrosine aromatic ring. The 7-fluoro substituent may also form weak electrostatic interactions with the side-chain methyl of Thr-709 (4 Å) or the hydroxyl group of Tyr-733 (3.5 Å).

In the chosen poses, the 6-I substituent of UBP2002 and UBP2038 was close to the D2 polar side-chains of Asn-690 (3.4 Å) and Thr-710 (3.3 Å) residues, which would allow electrostatic interactions and explains the increased affinity of the 6-I substitution in UBP2002 and UBP2038 compared to 6-H in kynurenic acid.

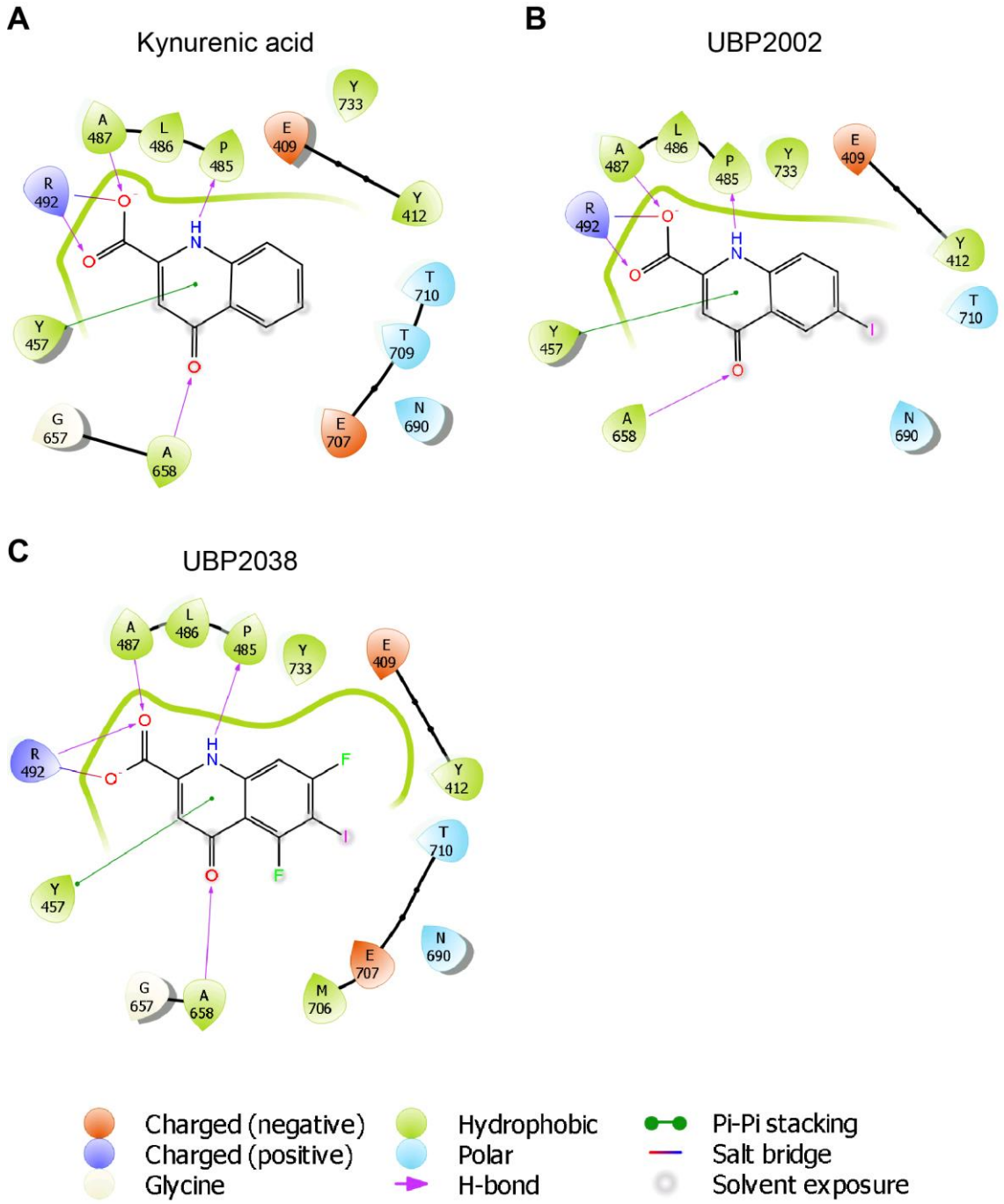

Figure 3.8. Schematic of GluK2 binding by kynurenic acid, UBP2002 and UBP2038. Ligand interaction diagrams showing the residues (single letter code) in the ligand binding cleft (4 Å from the ligand) for kynurenic acid (A), UBP2002 (B) and UBP2038 (C). Contours are coloured according to the nature of the residues lining the binding cleft (see legend for the colour scheme). Note that the 6-I substituent in UBP2002 and UBP2038 forms additional interactions with T710 and N690 compared to kynurenate. The 5,7-difluoro substituents of UBP2038 form additional interactions with M706, N690, E409, Y412 and Y733 compared to kynurenate and UBP2002.

3.3.5. Explanations for the inactivity of UBP2007 and UBP2052 on GluK2

The polar 6-substituted kynurenate, UBP2007 (6-CO_2H), had no effect on GluK2 (see Table 2.2). Compared to UBP2038, the orientation of UBP2007's quinolone ring was significantly altered such that the conserved π-π stacking interaction with Tyr-457 and the H-bond interaction with Pro-485 would be detrimentally affected (Figure 3.9A).

To accommodate UBP2007 into the binding pocket, the conformations of Asn-690, Glu-707 and Thr-710 were all refined during the induced fit procedure (Figure 3.9A). Moreover, the hydrophobic Met-706 which usually occupied the space close to the 6-position binding region of kynurenic acid was rearranged significantly to avoid clashes with the ionic 6-substituent of UBP2007 compared to the UBP2038-docked structure. These movements suggested the transformation of the binding pocket from a previously mixed hydrophobic/polar environment to a polar binding region. Such a transformation would have a high energetic penalty and may prevent UBP2007 and other charged 6-substituents from binding to GluK2.

The 6,8-dimethyl substituted kynurenic acid, UBP2052, has no activity on GluK2 homomeric receptors at concentrations up to 2 mM (see Figure 2.8). Docking revealed that the bulky 8-methyl substituent could introduce steric clashes with Pro-485 (Figure 3.9B). As a result, the quinolone ring of UBP2052 was located such that the π-π stacking interactions with Tyr-457 and the H-bond interactions with Pro-485 would be reduced. Another consequence of the relocation was the closer proximity of the non-polar 6-methyl substituent of UBP2052 to the polar Asn-690 residue in D2. Such a rearrangement would be detrimental to the binding of UBP2052 and explains the lack of activity of UBP2052 in GluK2 subunits.

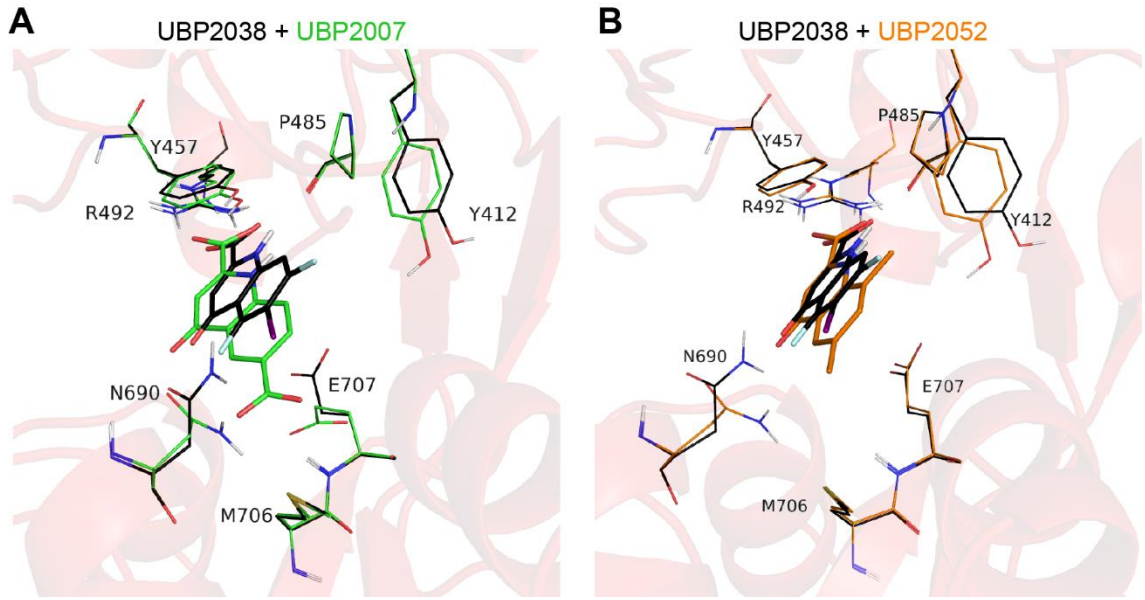

Figure 3.9. Docking of UBP2007 and UBP2052 in the GluK2 homology model reveals detrimental interactions and changes to residue conformations. A, Overlay of GluK2 docked ligand and residue structures of UBP2007 (green carbons) and UBP2038 (black carbons) showings the movement of 1-amino group in UBP2007 which may lead to weakening of the H-bond to the peptide carbonyl group of Pro-487. **B,** Similar to **A** but for UBP2052 (orange carbons). Steric clashes by the 8-methyl substituent of UBP2052 meant the 6-Me group would be in a polar environment near the Asn-690 residue.

3.3.6. Binding of kynurenates to the GluK1 LBD

Kynurenic acid docked into the GluK1-UBP315 structure (PDB id: 2QS1) (Alushin et al., 2011) highlighted the larger pocket in GluK1 compared to GluK2 in the antagonist-bound state (Figure 3.10) as previously described (Mayer, 2005). However, the larger binding pocket in GluK1 also meant that the 5-position of kynurenates would have greater exposure to solvent in GluK1 compared to GluK2 (see Figure 3.10B and Figure 3.8A). The D1 interactions of Arg-508 and Pro-501 to the 2-carboxylate and NH groups of kynurenic acid, respectively, were preserved in kynurenic acid-docked GluK1. The presence of Thr-503 in GluK1 instead of Ala-487 in GluK2 led to an extra H-bond between GluK1 D1 and kynurenic acid (Figure 3.10B). Greater exposure to solvent in GluK1 also suggests loss of weak but favourable hydrophobic interactions between the 7-substituents and residues lining the D2 domain and possibly explains lower affinity of kynurenic acid in GluK1.

The docking program also predicted a change in the positioning of kynurenates docked into the GluK1 structure – possibly due to the extra H-bond provided by the Thr-503 sidechain to the 2-carboxylate group of kynurenic acid (Figure 3.10). The change in position meant that atoms of 4-oxo group and 5- and 6-positions in kynurenic acid moved further away (1.8 Å) from D2 residues compared to the respective atoms in kynurenic acid-GluK2 docked model. This movement is likely to be detrimental to the binding of kynurenic acid as it increases the amount of ligand exposure to solvent and may also explain kynurenic acid's reduced affinity in GluK1 compared to GluK2 subunits.

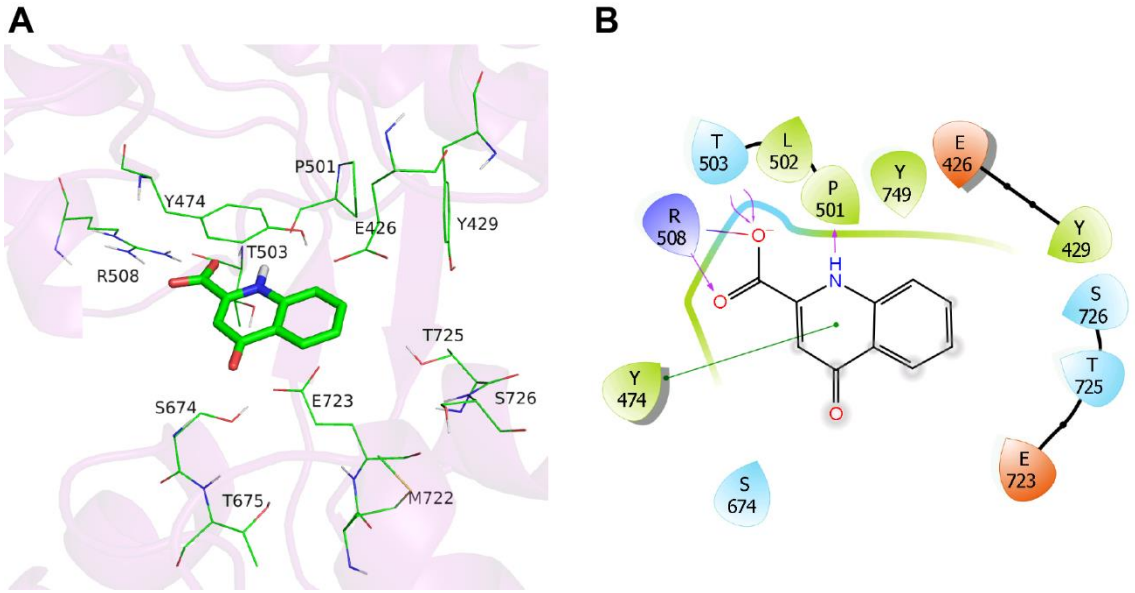

Figure 3.10. Kynurenic acid docked into GluK1 LBD. A, Kynurenic acid docked into the GluK1-UBP315 LBD (PDB id: 2QS1). **B,** Schematic showing the interactions of kynurenic acid in the GluK1-LBD. Note the grey circles denoting exposure with water in the LBD, especially around the 5- and 6-position carbon atoms.

3.3.7. Explanation for the GluK2 over GluK1 selectivity of UBP2054

In the pharmacological assay on recombinant homomeric KARs, UBP2054 (6-Et) has significant selectivity for GluK2 over GluK1 (GluK2 K_i = 54.0 ± 10.9 μM, GluK1 IC_{50} > 1 mM) (Table 2.3). To find explanations for this selectivity, the binding modes of UBP2054 in GluK1 and GluK2 LBDs were compared to that of UBP2034 (6-Me) (Figure 3.11). UBP2034 does not have the GluK2 over GluK1 selectivity of UBP2054 (UBP2034's GluK2 K_i = 46.5 ± 9.3 μM and UBP2034's GluK1 K_i = 47.8 ± 7.2 μM). Therefore, it

seemed that increasing the chain length of the hydrophobic 6-substituent may have beneficially improved GluK2 over GluK1 selectivity.

The highest ranked poses in the GluK1 LBD (Figure 3.11A) demonstrated that the orientation of UBP2054 is such that the 4-oxo group of UBP2054 is 1.5 Å above the docked 4-oxo group of UBP2038 (GluK1 K_i = 11.2 ± 1.0 μM). Such an orientation is likely to be preferred by the docking program because it avoids steric clashes and/or maximises the ligand-receptor interactions. However, whether such an orientation would be favourable in reality is unknown because it would also require the rearrangement of the Tyr-474 residue such that the hydrophobic π-π stacking interactions between the tyrosine ring and the heterocyclic ring of kynurenate are maximised.

Docking of UBP2054 and UBP2034 into the GluK2 homology model showed that the cleft-lining residues can be refined to increase ligand-receptor interactions (Figure 3.11B). The refinement of the conformation of residues to accommodate UBP2054 into GluK2 LBD is distinct such that the Met-706 residue is accommodated underneath the phenyl ring of UBP2054 and may form hydrophobic interactions with the 6-Et group. Another notable movement of a GluK2 residue in the UBP2054-docked structure is by the Asn-690 residue which may have been refined to prevent unfavourable interactions with the 6-Et substituent and/or to allow the Met-706 to be accommodated (Figure 3.11B). The UBP2034-docked GluK2 model revealed that the 6-Me substituent induces similar refinements of Asn-690 and Met-706 as kynurenic acid (Figure 3.11B) such that Met-706 could not form interactions with the 6-Me group.

The binding pocket interactions of non-polar 6-substituted compounds, UBP2034 (6-Me) and UBP2054 (6-Et), showed that the larger binding pocket of GluK1 may detrimentally expose the bulkier 6-Et to solvent (Figure 3.12A). This was reflected in the estimated affinities from pharmacological assays where UBP2054 had > 10-fold lower affinity on GluK1 compared to UBP2034: GluK1 K_i value for UBP2034 was ~48 μM whereas UBP2054 GluK1 IC_{50} was > 1 mM. However, in GluK2, increased protection from solvent exposure was provided by the larger residues (Thr-710 and Asn-690 in GluK2 instead of Ser-726 and Ser-706 in GluK1) lining the GluK2 binding cleft (Figure 3.12B).

The molecular surface of the GluK1 and GluK2 binding sites in the docked structure with UBP2054 shows that the UBP2054 van der Waals volume is well tolerated by both GluK1 and GluK2 structures (Figure 3.13). In GluK1, the 6-Et chain was closer to the polar Ser-706 residue whereas in GluK2, the positioning of Met-706 under the 6-Et chain may have protected the 6-Et chain from solvent exposure.

In summary, the molecular modelling studies suggest that UBP2054 is more selective for GluK2 compared to GluK1 due to a combination of firstly, increased hydrophobic interactions between the 6-Et of UBP2054 and Thr-710 of GluK2 and secondly, reduced exposure of 6-Et group of UBP2054 to solvent in GluK2 compared to GluK1. Moreover, the docking score for the best pose of UBP2054 (6-Et) and UBP2034 (6-Me) in GluK2 were -529.67 kcal/mol and -529.153 kcal/mol, respectively. This similarity in docking score is in accordance with the similarity in GluK2 K_i values of both UBP2054 and UBP2034 (Table 2.3). However, the docking score of the best pose of UBP2054-bound GluK1 was -536.838 kcal/mol and for UBP2034-bound GluK1 was -540.544 kcal/mol. The less favourable GluK1 docking score of UBP2054 compared to UBP2034 further highlights the GluK2 over GluK1 selectivity of UBP2054.

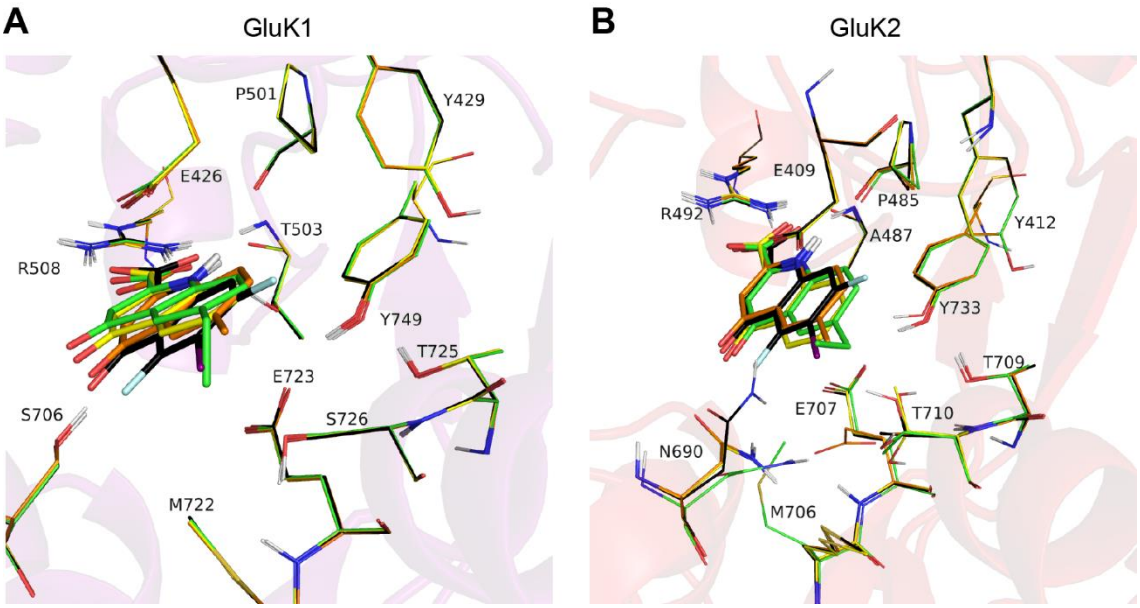

Figure 3.11. Binding of UBP2054 in GluK1 and GluK2. A, UBP2054 (green carbon atoms), UBP2034 (orange), UBP2038 (black) and kynurenic acid (yellow) were docked into GluK1-UBP315 structure (PDB id: 2QS1). There were no visible refinements of residue side chains in the binding cleft after docking of UBP2054 compared to UBP2038 or UBP2034. To accommodate the UBP2054 6-Et substituent nearer to Met-722, the ligand structure was rotated compared to the UBP2038 ligand structure such that the 4-oxo group in UBP2054 was ~1.5 Å above the 4-oxo group in UBP2038. **B,** Similar to **A** but kynurenates were docked into a GluK2 homology model based on GluK1-UBP315. Asn-690 and Met-706 conformations were refined by Prime to accommodate UBP2054.

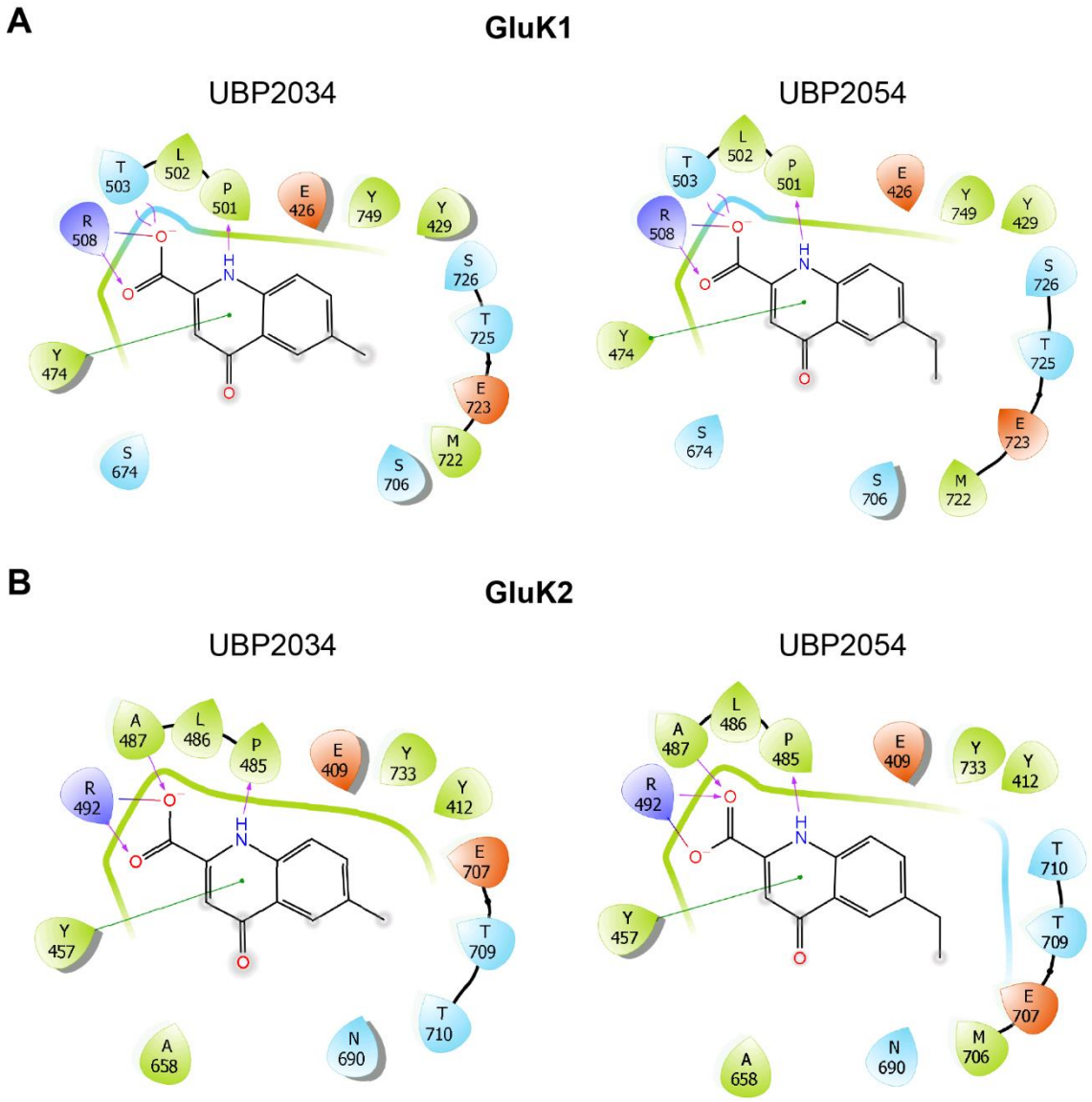

Figure 3.12. GluK1 and GluK2 LBD binding schematic for UBP2034 and UBP2054. A, In the GluK1 LBD, the 6-substituents of UBP2034 and UBP2054 are exposed to solvent in the GluK1 ligand binding pocket. Due to the larger hydrophobic 6-substituent of UBP2054, the binding of UBP2054 to GluK1 is likely to be less favourable compared to binding of UBP2034 to GluK1. **B,** In GluK2, 6-substituents of UBP2034 and UBP2054 were closer to the residues lining the binding cleft. The proximity to hydrophobic Tyr-733 and Tyr-412 of the 7-position meant that there is a greater likelihood of hydrophobic interactions in the GluK2 LBD. More importantly, the 6-ethyl in UBP2054 could form van der Waals interactions to Thr-710 and Met-706 which are absent in UBP2034 due to its smaller 6-methyl substituent.

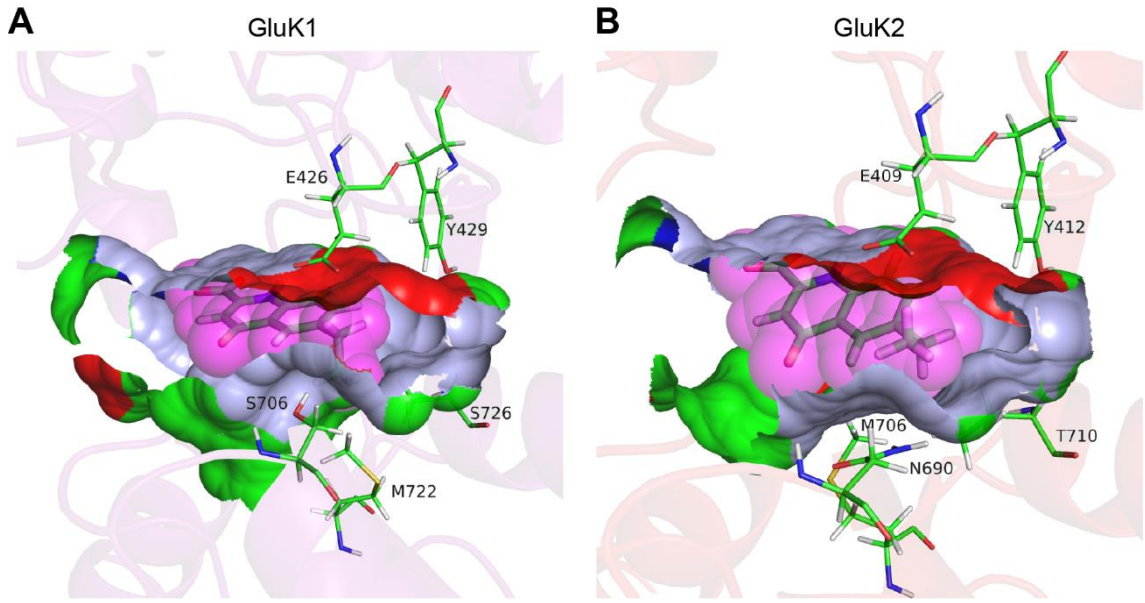

Figure 3.13. Molecular surfaces of UBP2054-bound GluK1 and GluK2 ligand clefts. A, Surface of the GluK1 binding site, coloured according to the nature of the residue side chains that form the cleft (light-blue = polar, red = negatively charged, dark-blue = positively charged, green = hydrophobic). Residues near the 5-, 6- and 7-positions of the benzene ring of the ligand are shown. UBP2054's van der Waals surface is represented as spheres (coloured magenta). **B,** Similar to **A** but showing the surfaces in GluK2 LBD. Note the interaction of the 6-ethyl group with the methyl group of Thr-710 and possibilities for van der Waals interactions between the 6-ethyl group and Met-706. These interactions explain the GluK2 over GluK1 selectivity of UBP2054.

3.3.8. GluK2 over AMPAR selectivity of UBP2054

UBP2054 (6-Et) showed > 10-fold selectivity for GluK2 (K_i value = 54.0 ± 10.9 μM) over GluA1 (IC_{50} > 2 mM) homomeric receptors, and UBP2054 also had low activity on AMPARs expressed in the hippocampus (IC_{50} > 300 μM). The GluK2 over AMPAR selectivity of UBP2054 was investigated by docking UBP2054, UBP2002 (6-I; GluA1 IC_{50} > 1mM) and the kynurenate with the highest GluA1 affinity tested in the study, UBP2038 (5,7-diF-6-I; GluA1 K_i = 22.6 ± 2.2 μM), into the GluA2-DNQX X-ray structure (PDB id: 1FTL) (Armstrong and Gouaux, 2000) (Figure 3.14).

GluA2 has a smaller binding cavity compared to GluK2 in part due to the presence of Met-708 (in the place of Thr-710 in GluK2) where the 6-position group of kynurenates is located. In GluA2, overall ligand orientation in the highest-ranking pose of UBP2054 had similarities with the UBP2054 orientations in GluK1. However, compared to the higher

affinity UBP2038, the quinolone ring in UBP2054 was oriented such that the 4-oxo group in UBP2054-GluA2 model was 2.1 Å below that of UBP2038-GluA2 (Figure 3.14A). Such an orientation would negatively influence the π-π stacking interaction provided by Tyr-450 and the conserved H-bond interactions between the ligand and Arg-485, Thr-480 and Pro-478 and therefore is an indication of a poor binding mode. The difference in orientation of UBP2054 compared to UBP2038 may have been caused by the program trying to increase the likelihood of ligand-receptor electrostatic interactions by the phenyl ring substituents of kynurenates.

The 6-Et group of UBP2054-GluA2 model was oriented in a similar manner to that found in UBP2054-GluK1 and UBP2054-GluK2, with the terminal carbon of the ethyl chain pointing towards the polar Thr-686. In the UBP2038 (5,7-diF, 6-I) docked GluA2 structure, the Met-708 residue was accommodated beneath the 6-I group and provided possibilities for hydrophobic interactions (Figure 3.14A). However, the 6-Et substituent of UBP2054 was accommodated into the GluA2 LBD by refining the conformation of Met-708 to avoid steric clashes (Figure 3.14A). The movement of Met-708 also indicated that the bulkier 6-Et substituent was less well tolerated in the GluA2 cavity compared to the 6-I substituent of UBP2002 and therefore explains the low GluA2 affinity of UBP2054. The polar side-chain of Glu-705, which was involved in H-bond interactions with glutamate, was also refined to accommodate UBP2054 whereas in the UBP2002 and UBP2038 docked structures, the corresponding Glu residues were in similar locations (Figure 3.14A).

The 6-iodo substituents of both UBP2002 and UBP2038 were found to be in locations to form favourable interactions with nearby residues Thr-686 and Met-706 in GluA2 (Figure 3.14B and Figure 3.14C). However, the hydrophobic 6-Et substituent in UBP2054 was found to be in a polar environment, which is likely to be detrimental for binding of UBP2054 (Figure 3.14D).

The overlap in the volumes of UBP2054 with the binding cavity surface was also a qualitative indicator of possibilities for steric clashes with Met-708 and Thr-686 (Figure 3.15C). In the UBP2054-bound GluA2 LBD, there was higher overlap of the ligand and receptor volumes compared to UBP2002 and UBP2038. The favourable electrostatic and van der Waals interactions involving 5- and 7-substituents of UBP2038 may explain its

lower volume overlap with the receptor because the residues lining the 5- and 7-substituents would have been conformationally refined to maximise the ligand-receptor interactions and would subsequently avoid steric clashes of those residues with the 6-iodo atom of UBP2038. An example of such refinement was seen in the Thr-686 residue which was refined to maximise interactions of the Thr-686 hydroxyl group with the 5-F atom of UBP2038 and therefore avoid steric clashes with the 6-I group of UBP2038 (Figure 3.15B). However, UBP2002- and UBP2054-docked structures did not have such refinements (Figure 3.15A and C) and therefore the Thr-686 residue contributed to the overlap in volumes of the 6-iodo group of UBP2002 and 6-ethyl group of UBP2054.

In summary, the GluK2 over GluA2 selectivity of UBP2054 can be best explained by steric clashes between the 6-ethyl substituent and the residues Thr-686 and Met-706 in the GluA2 LBD. The GluA2 binding cleft is also surrounded by the negatively charged Glu-402 and Glu-705 located above and below the quinolone ring of kynurenates, respectively. These glutamate residues are also likely to contribute to preventing the hydrophobic 6-ethyl group being located optimally in the binding cleft. Despite these detrimental interactions in the GluA2, the docking scores of best poses of GluA2 docked with UBP2002 (-499.491 kcal/mol), UBP2038 (-500.077 kcal/mol) and UBP2054 (-500.023 kcal/mol) were all similar. This shows that the docking scores alone cannot explain the affinity of the compound despite clear evidence that the unfavourable orientation of UBP2054 (Figure 3.14) and the steric clash between the 6-Et of UBP2054 and Met-708 in GluA2 (Figure 3.15) will limit the affinity of UBP2054 for GluA2 (and probably GluA1).

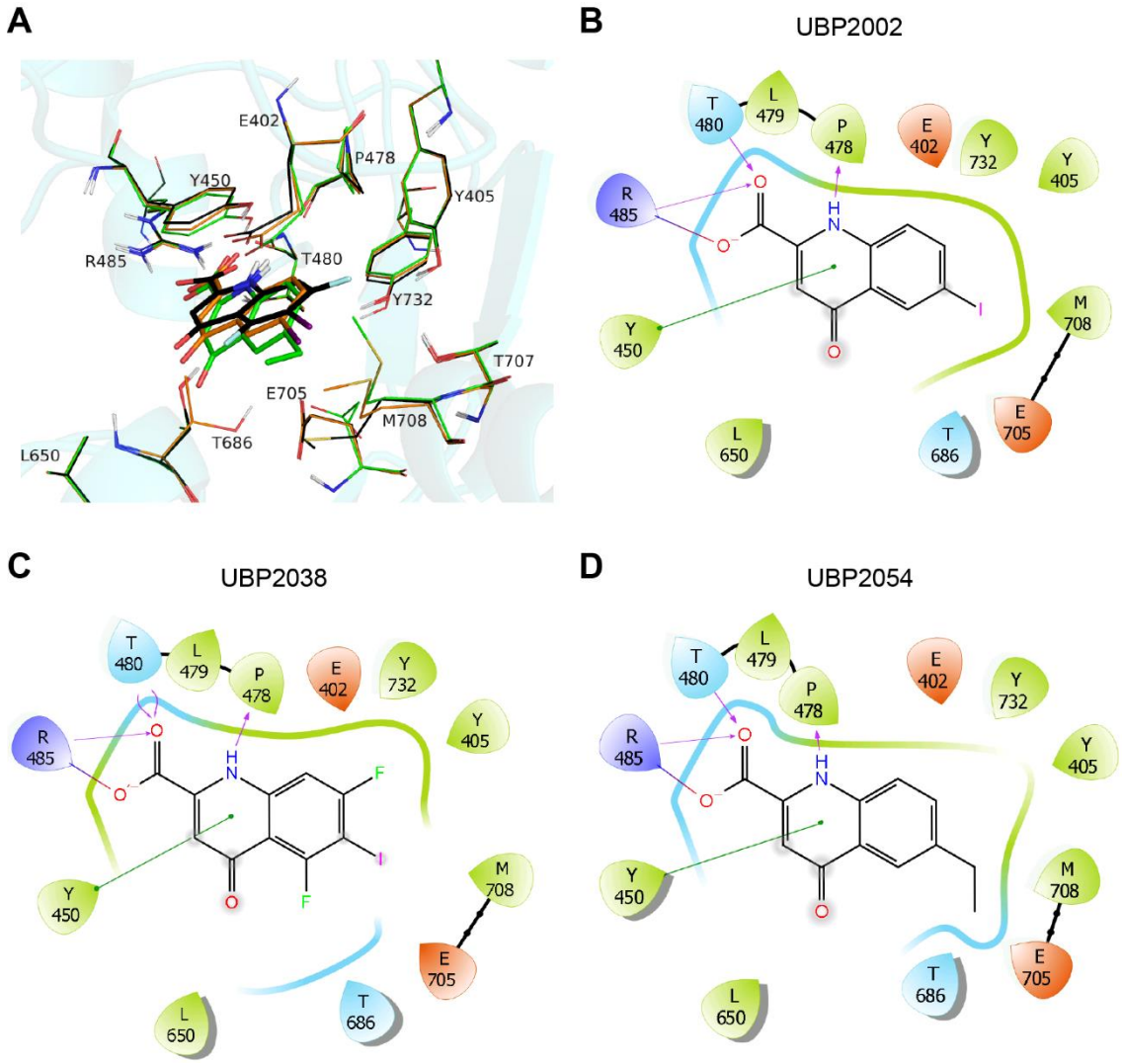

Figure 3.14. Docking of UBP2002, UBP2038 and UBP2054 into the GluA2 LBD. A, 3D overlay of binding modes and residue refinements in the GluA2 LBD docked with UBP2002 (orange carbons), UBP2038 (black carbons) and UBP2054 (green carbons). Non-polar hydrogens are hidden for clarity. **B-D,** Ligand interaction schematics for UBP2002 (B), UBP2038 (C) and UBP2054 (D) docked into the GluA2 LBD Note differences in interactions of 6-I and 6-Et substituents and possible clashes

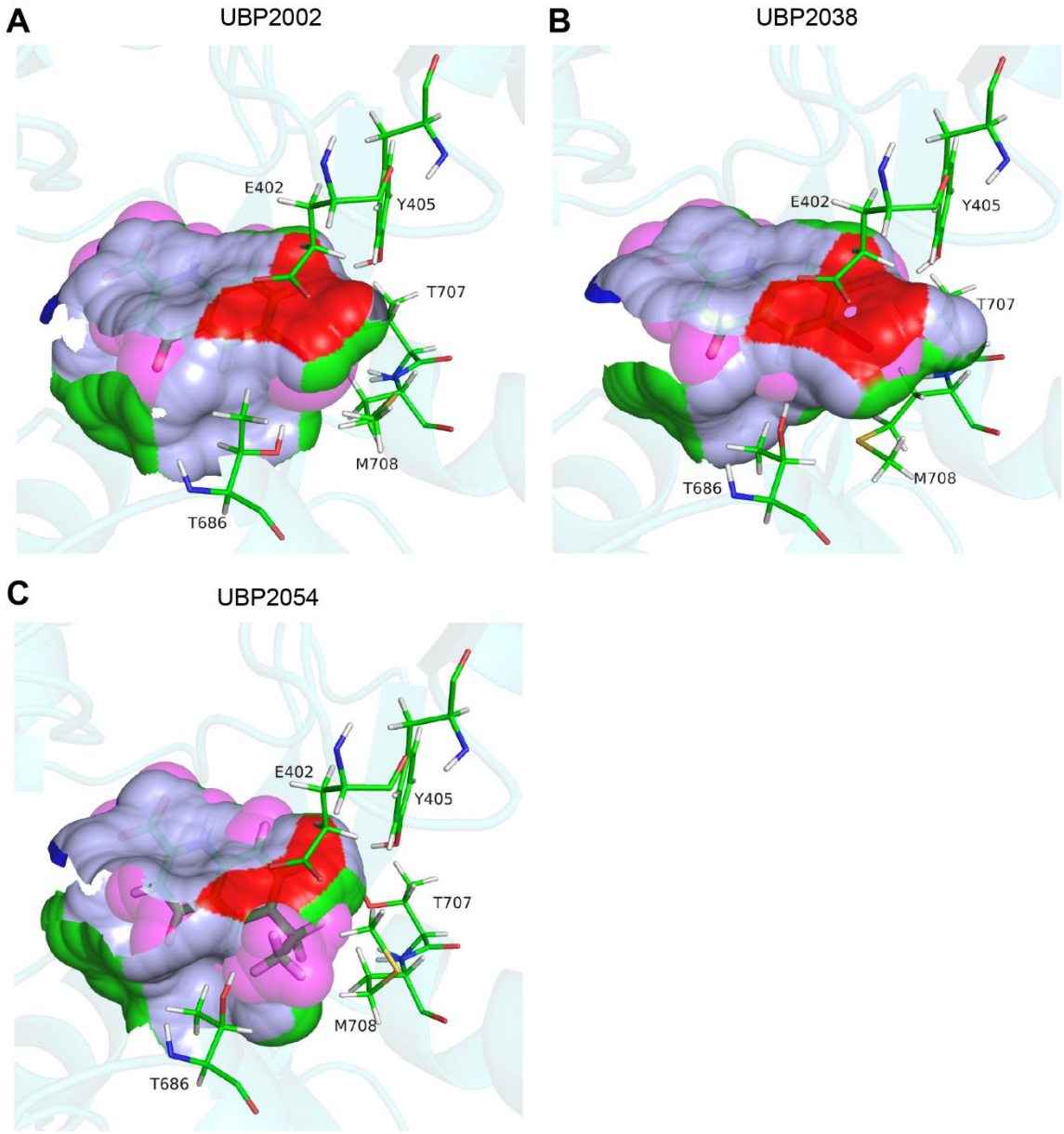

Figure 3.15. Steric clash of the 6-ethyl substituent of UBP2054 in GluA2 LBD. A-C, the molecular surfaces of the GluA2 binding cavity docked with UBP2002 (A), UBP2038 (B) and UBP2054 (C). The 6-ethyl substituent of UBP2054 occupies a disallowed space near Thr-686 and Met-708 in the GluA2 binding cavity (C). UBP2002's 6-I substituent also has steric clashes but fewer than UBP2054 (A). UBP2038's van der Waals volume is better accommodated into the GluA2 binding cavity compared to UBP2002 or UBP2054 and explains its higher affinity for GluA1. Binding cavity surface are coloured according to the nature of residues lining the cavity; light-blue = polar, red = negatively charged, dark-blue = positively charged, green = hydrophobic). Ligand van der Waals surfaces are shown as spheres (magenta and transparent).

3.3.9. Explaining the reduced NMDAR activity of 6-substituted kynurenates

Two X-ray structures of the NMDAR GluN1 LBD in complex with 5,7-diCl kynurenic acid (DCKA) are available (Furukawa and Gouaux, 2003; Jespersen et al., 2014). Given the similarities in the X-ray crystal structures, the higher resolution (1.9 compared to 2 Å) GluN1 LBD-DCKA structure was used for docking studies (PDB id: 1PBQ) (Furukawa and Gouaux, 2003). The GluN1-DCKA structure overlaid over the GluA2-apo structure suggested that LBD opening of DCKA-bound GluN1 LBD was smaller than the GluA2-apo LBD. The computationally docked DCKA had a similar pose to the X-ray crystal DCKA, which highlighted the pose predictive capability of Glide and the InducedFit protocol. The interactions of the 2-carboxyl group and 1-NH group of DCKA with the GluN1 cleft residues were similar to those predicted by computational docking of kynurenates into GluK2, GluK1 and GluA2 -LBDs. Another feature of DCKA binding to GluN1 was the π-π stacking provided by Phe-484 to the heterocyclic ring of DCKA, which is similar to the π-π stacking provided by the tyrosine aromatic ring in GluK2, GluK1 and GluA2 (Figure 3.16).

Pharmacological characterisation on native NMDARs showed that 100 μM UBP2040 (5,7-diF) inhibited native NMDARs significantly (~73%) compared to 100 μM UBP2002 (6-I) (~7%). To explain the reduced activity of 6-substituted kynurenates, UBP2002 and UBP2040 were docked into the GluN1 X-ray structure (Figure 3.16). As found with DCKA, the 5- and 7-fluoro substituents in UBP2040 form van der Waals interactions with Phe-408 and Trp-731, respectively (Figure 3.16A). Moreover, the fluoro substituents in UBP2040 are more electronegative than the chloro substituents in DCKA and therefore, may form more favourable van der waals interactions (with Phe-408 and Trp-731) compared to DCKA. However, the smaller size of fluoro substituents in UBP2040 compared to the larger 5-,7-Cl atoms in DCKA means that the van der Waals interactions are weaker between UBP2040 and GluN1 and explains the lower affinity of UBP2040 for GluN1 compared to DCKA (Leeson et al., 1991). Docking scores of UBP2040 (-597.153 kcal/mol) and DCKA (-597.672 kcal/mol) suggests that DCKA has a slightly more energetically favourable pose compared to UBP2040.

Overlay of the UBP2002-docked structure onto the DCKA-docked structure showed that the UBP2002 ligand molecule was rearranged such that the 4-oxo group moved 1 Å towards

the D2 residues compared to the DCKA ligand structure (Figure 3.16B). The bulky side-chain of Trp-731 did not relocate to accommodate UBP2002 and there was a slight conformational refinement of Val-735 (~0.8 Å movement of the side chain carbon) to accommodate UBP2002 but the movement of the Val-735 side chain was unlikely to provide enough space to accommodate the 6-iodo group of UBP2002 (Figure 3.16B).

Analysis of the molecular surfaces of the GluN1 binding cavities in the UBP2040- and UBP2002-bound structures revealed a substantial overlap of the van der Waals surfaces of the cleft lining residues and UBP2002 (Figure 3.17B). Such an overlap of volumes was not seen in the UBP2040-GluN1 model (Figure 3.17A) and suggests that steric occlusion of the 6-iodo substitution in UBP2002 may have reduced its affinity for GluN1 and therefore for NMDARs.

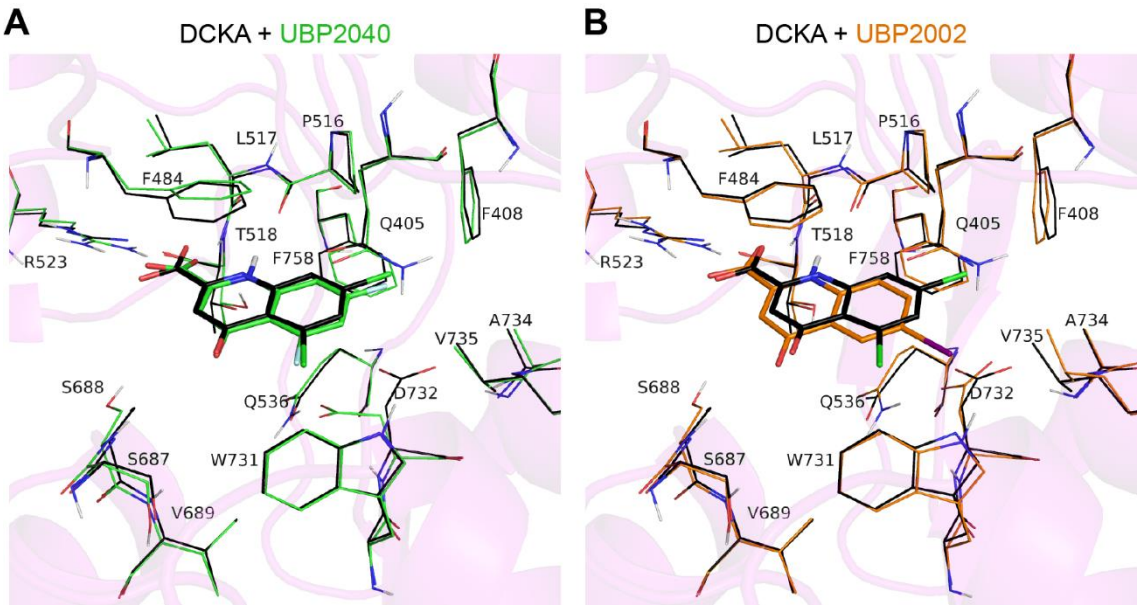

Figure 3.16. Docking of UBP2040 and UBP2002 into the GluN1 LBD showing that while DCKA and UBP2040 can be accommodated in the binding site, UBP2002 cannot. A, UBP2040 (green carbon atoms) docked into the GluN1 LBD overlaid onto the DCKA-bound GluN1 LBD structure (black carbons; PDB id: 1PBQ) for comparison of docked structure and X-ray structure. Note the 5,7-diF substituents of UBP2040 and 5,7-diCl substituents of DCKA form favourable interactions with Phe-408 and Trp-731. Only polar hydrogen atoms are shown for clarity. **B,** Overlay of docked structures of UBP2002 (orange carbons) with the DCKA-bound LBD X-ray structure (black carbons). Note the 6-iodo group of UBP2002 (purple) forms steric clashes with Val-735 and Trp-731.

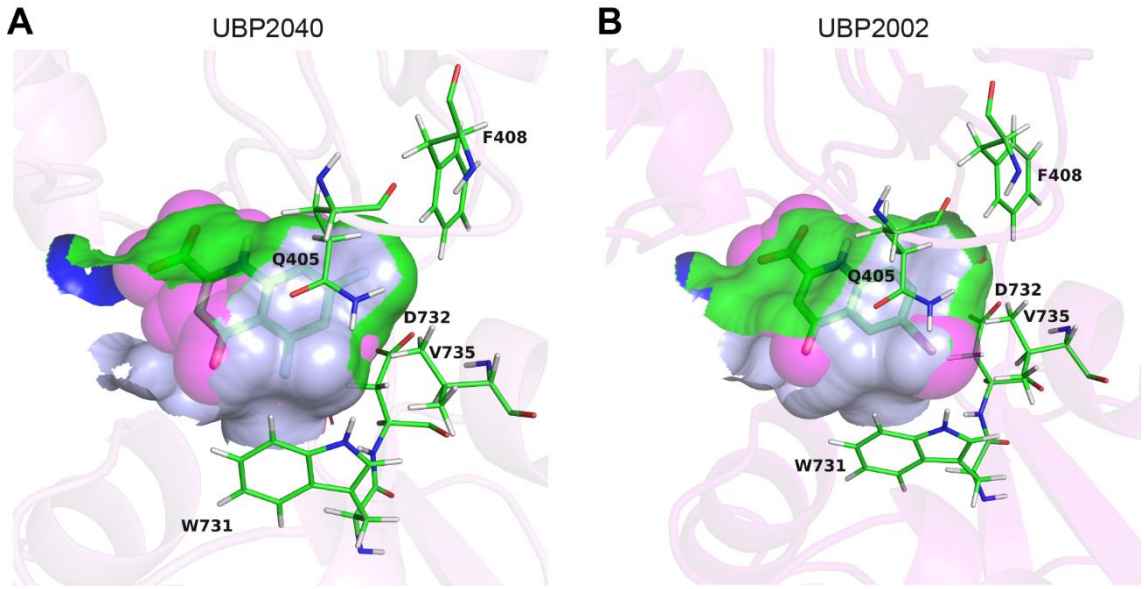

Figure 3.17. Overlap of molecular surfaces in UBP2040- and UBP2002-docked GluN1 binding cavity. Molecular surfaces of the binding cavity are shown for UBP2040 (**A**) and UBP2002 (**B**) docked into the GluN1 LBD. The binding cleft surface is coloured according to the nature of the residues lining the cleft. The van der Waals surfaces of ligands are shown as magenta spheres. Note that the 6-iodo group of UBP2002 forms steric clashes with Val-735 and Trp-731 while the 5,7-difluoro groups of UBP2040 are accommodated.

3.4. Further discussions

In this study, molecular modelling was used to explain the features of GluK2, GluK1 and GluA2 ligand binding clefts that may have determined some of the results from pharmacological characterisation experiments (Chapter 2). Using the knowledge gained from the current work, it may be possible to develop novel antagonists with greater GluK2 affinity and selectivity over AMPARs and potentially GluK1.

3.4.1. Methodological limitations

There are some caveats when using molecular modelling to predict affinity. The total binding energy of a ligand depends on the ligand-receptor interactions, the solvation-desolvation energy (the energy required for the compound to shed its solvent water molecules and displace water molecules from the ligand binding site), and the conformational energy of binding. The poor water solubility of the kynurenates suggests that the desolvation penalty of this class of antagonists may be low; therefore, the main contribution to total binding energy of the ligands may be dictated by the ligand-receptor

interactions and the conformational energy penalty during ligand binding. In this study, the Glide docking algorithm could estimate the ligand-receptor interactions using the glidescore function. While the conformational energy penalty was included in the glidescore function through a penalty for freezing rotatable bonds, the total conformational energy penalty of the ligand binding also depends on the water molecules present in the binding site. Water molecules can contribute to the total conformational energy of the binding site by decreasing the enthalpic contribution: H-bond networks provided by the binding cleft water molecules may help to increase the stability of the open LBD in the apo state of the receptor. Water molecules also contribute to the entropy of the system and removing the ordered water molecules increases entropy and therefore increases the free energy of the system – increasing the binding affinity.

Due to unavailability of X-ray crystal structures of antagonist-bound GluK2 LBD and the limitations of X-ray structures in identifying the positions of water molecules, the prediction of binding site water molecules in the GluK2 homology model was not possible. Therefore, the rank order of poses and the selection of "acceptable" poses by the docking program would likely underestimate the energy penalty that would result from releasing water molecules from the binding sites to accommodate the docked ligand. The docking program also did not estimate H-bond interactions between the ligand and the receptor that occur through water molecules. Such H-bond interactions coordinated by water molecules serve to stabilise the receptor-ligand complex and may be important for the binding of kynurenates to the LBD of iGluRs (Armstrong and Gouaux, 2000; Mayer, 2005).

Another caveat of the IFD routine was that the docking program could underestimate the conformational energy penalty which would result from moving residues that may cause unfavourable interactions with the ligand. The best example for this phenomenon is the docking of UBP2007 (6-CO_2H) to the GluK2 homology model. In the case of UBP2007, the hydrophobic sidechain of Met-706 was refined by the program to accommodate the 6-carboxy group of UBP2007 in order to gain at-least 2 H-bond interactions between the 6-carboxyl group of UBP2007 and the polar sidechains of Thr-710 and Glu-707. In reality, the movements of the residue side chains would usually require breaking of inter-residue electrostatic and van der Waals interactions and the ligand-receptor interactions must therefore overcome the energy barrier by providing more favourable interactions.

Chapter 4

Investigations into the roles of GluN2D subunits in hippocampal synaptic plasticity

4.1. Introduction

4.1.1. Biophysical features of GluN2D subunits

GluN2D subunits share the structural features of other NMDAR subunits and form functional diheteromeric receptors when assembled as a dimer of dimers with two GluN1 subunits. However, two different GluN2 subunits are also capable of forming triheteromeric receptors by assembling with two GluN1 subunits, e.g. as a GluN1/GluN2B/GluN2D or GluN1/GluN2A/GluN2D complex (Dunah et al., 1998; Cheffings and Colquhoun, 2000; Jones and Gibb, 2005). NMDARs mediate synaptic currents that have slower activation and decay kinetics than AMPARs or KARs. The gating properties of the channel and its subunit composition are responsible for dictating kinetics of NMDAR mediated macroscopic currents (Monyer et al., 1992). Particularly, GluN2D-containing diheteromeric receptors have longer agonist deactivation times compared to GluN2A-, GluN2B- and GluN2C-containing dihetermeric NMDARs, meaning that the GluN2D-containing receptor binds glutamate for longer periods compared to other NMDAR subunits (Vance et al., 2011). The physiological mechanisms that underlie NMDAR mediated synaptic plasticity are also influenced by the kinetics of Ca^{2+} influx through the NMDAR channel (Lisman, 1989; Yang et al., 1999) and therefore subunit composition of NMDARs might be responsible for regulating synaptic plasticity. Diheteromeric NMDARs containing the GluN2D subunit show slower current decay than receptors containing other GluN2 subunits, with a decay time constant in the range of 1–2 s for GluN2D diheteromeric NMDARs (compared to 22-230 ms and 110-430 ms for GluN2A and GluN2B, respectively) (Monyer et al., 1994; Vicini et al., 1998). However, when GluN2D subunits are found in triheteromeric complexes with either GluN2A or GluN2B subunits, a faster decay time is observed i.e. 2A or 2B subunits dominate over the 2D decay kinetics (Cheffings and Colquhoun, 2000; Jones and Gibb, 2005). On the basis of these findings, it has been suggested that distinct GluN2 subunits may be involved in distinct neuronal plasticity processes based on the distinct profile of Ca^{2+} charge transfer that each GluN2 subunit confers to the NMDAR (Shipton and Paulsen, 2014). GluN2A, GluN2B and GluN2D subunit containing diheteromeric and triheteromeric NMDARs may therefore act as switches that control the activity required to trigger distinct plasticity processes in the hippocampal synapse.

4.1.2. Using pharmacological tools to investigate GluN2D subunits

The GluN2D subunit, like other GluN2 subunits, has a ligand binding domain that binds glutamate as the endogenous agonist (Vance et al., 2011). Potency of glutamate for the GluN2D subunit is higher than for other GluN2 subunits; glutamate rank order of potency (represented by EC_{50} in parenthesis): GluN2D (0.5 μM) > GluN2C (1.7 μM) > GluN2B (2.9 μM) > GluN2A (3.3 μM) (Erreger et al., 2007). Another pharmacological feature of GluN2D-containing diheteromeric NMDARs is that they are less susceptible to Mg^{2+} block than GluN2A- and GluN2B-containing diheteromeric NMDARs (Monyer et al., 1994). Additionally, the prototypical NMDAR competitive antagonist D-AP5 has lower antagonist potency on GluN2D compared to other GluN2 subunits: D-AP5 rank order of antagonist activity (represented by equilibrium-dissociation constant, K_i, in parenthesis): GluN2A (0.28 μM) > GluN2B (0.46 μM) > GluN2C (1.6 μM) > GluN2D (3.7 μM) (Buller and Monaghan, 1997; Feng et al., 2005). Development of GluN2D-selective competitive antagonists in this lab has resulted in a series of antagonists with moderate selectivity for GluN2C/D over other GluN2 subunits. UBP145, which has ~10-fold selectivity for GluN2C/D over GluN2A or GluN2B subunits, is a well-characterised (using NMDARs expressed in X. laevis oocytes and HEK293 cells, see section 1.3.3) member of this family of competitive antagonists (Irvine et al., 2012; Volianskis et al., 2013a). UBP791 is a novel GluN2C/D preferring compound, which has greater selectivity for GluN2D over GluN2A (~200-fold) and GluN2B (~30-fold) (Jane and co-workers, unpublished data) than UBP145. A positive allosteric modulator selective for GluN2C and 2D subunits, CIQ, was shown to potentiate currents mediated by GluN2D diheteromeric NMDARs expressed in X. laevis oocytes and GluN2D-containing NMDARs in hippocampal slices (Mullasseril et al., 2010; Perszyk et al., 2016). Therefore, even though pharmacological studies of GluN2D subunits have lagged compared to those for GluN2A and GluN2B subunits, it has become clear that GluN2D subunits may be selectively targeted by pharmacological agents.

Physiological studies that use pharmacological agents to investigate the roles of individual GluN2 subunits in synaptic plasticity have used different antagonists which have different relative affinities for individual subunits due to a lack of antagonists with high subunit-selectivity. Particularly, GluN2A is preferably inhibited by NVP-AAM077 (NVP), a competitive antagonist with 5- to 10-fold selectivity for GluN2A over other GluN2 subunits (Feng et al., 2004; Neyton and Paoletti, 2006; Volianskis et al., 2013a). The GluN2B

subunit is selectively inhibited using the negative allosteric modulator (NAM), Ro 25-6981 (Ro), which has ~5000-fold selectivity for GluN2B over GluN2A (Fischer et al., 1997). While the effect of Ro has not been characterised in detail on native triheteromeric receptors, ifenprodil, a structurally similar allosteric modulator as Ro, inhibited GluN2A/2B triheteromeric receptors with a potency of ~6-fold that of its IC_{50} on GluN2B diheteromeric receptors (Hansen et al., 2014). Recently, the cryo-EM structure of a recombinant GluN2A/2B triheteromeric receptor in complex with Ro was solved, and Ro was found to bind recombinant GluN2A/2B triheteromer with a K_d of ~130 nM (Lü et al., 2017). Therefore, Ro can be used to detect the presence of GluN2A/GluN2B-containing triheteromeric NMDARs due to its intermediate activity on such receptors. However, Ro is also an activity dependent antagonist which blocks GluN2B currents more potently at higher agonist concentrations (Fischer et al., 1997). The activity dependence of Ro may potentially complicate interpretation of results from slice experiments where glutamate spillover and glutamate uptake mechanisms determine agonist concentration at NMDARs at different locations in relation to the release site. Such complications can be overcome whilst using different concentrations of D-AP5, NVP, Ro or UBP145 to study synaptic plasticity, which allows the relative potencies of each antagonist on the studied physiological process to be determined (Volianskis et al., 2013a; Ingram et al., 2018).

4.1.3. Expression of GluN2D subunits in the hippocampus

In the hippocampus, GluN2D subunit mRNA and protein levels are highest at birth and decreases with age (Monyer et al., 1994; Ikeda et al., 1995). GluN2A, GluN2B and GluN2C subunits are also expressed in the hippocampus (Buller et al., 1994; Monyer et al., 1994). Expression of GluN2-containing NMDARs is developmentally regulated. GluN2B subunit expression is highest after birth but decreases with age whereas GluN2A expression increases with age (Monyer et al., 1994). Immunohistochemical studies have shown that the GluN2A, GluN2B and GluN2D proteins are found in the CA1 region of the hippocampus of adult mice (Hrabetova et al., 2000; Thompson et al., 2002), and that interneurons are likely to express GluN2D subunits in the CA1 region (Engelhardt et al., 2015). GluN2D protein levels were also found at lower levels in the dendritic regions of the CA1 and GluN2D antibodies were colocalised with GluN2A and GluN2B antibodies, suggesting that GluN2D may form triheteromeric complexes with GluN2A or GluN2B subunits (Thompson et al., 2002). These findings suggest that the GluN2D subunit may be

available to participate in synaptic plasticity at hippocampal synapses involving both principal cells (pyramidal cells in the CA3 and CA1) and interneurons.

4.1.4. NMDA receptors and synaptic plasticity in the hippocampus

Long term potentiation (LTP) of synaptic transmission is believed to represent the physiological cellular processes that underlie the long-term storage of information by synapses (Bliss and Collingridge, 1993). Therefore, the hippocampal SC-CA1 synapse has been used extensively to study the properties of NMDAR subunits and the involvement of different NMDAR subunits in mediating synaptic plasticity.

Potentiation induced by moderate high-frequency stimulation (such as theta-burst stimulation (TBS) or 100 Hz tetanus for 1 s (referred to as high-frequency stimulation, HFS)) in the Schaffer collateral-CA1 pyramidal cell (SC-CA1) synapse is mediated by NMDARs (Collingridge et al., 1983; Larson et al., 1986) whereas some types of overt stimulation of the pathway activates other sources of Ca^{2+} that can also induce LTP (Jia et al., 1996; Plant et al., 2006; Park et al., 2016). NMDARs mediate induction of potentiation by allowing Ca^{2+} influx into the cell (Lynch et al., 1983; Yang et al., 1999), and by making intracellular associations with proteins such as calcium/calmodulin-dependent protein kinase II (CaMKII) (Lisman et al., 2002).

Recently, the canonical potentiation in the SC-CA1 synapse of the rat hippocampus was further divided into different phases based on the sensitivity of each phase of potentiation to GluN2A, GluN2B or GluN2D subunit-preferring antagonists (Volianskis et al., 2013a). Potentiation induced by TBS consists of the initial potentiation that decays (STP), and the stable long-lasting phase of potentiation (generally referred to as LTP). STP was found to contain two components, namely STP1 which is mediated largely by GluN2A- and GluN2B-containing NMDARs, and STP2 which is mediated by GluN2B- and GluN2D-containing NMDARs, whereas LTP was found to be mediated by GluN2A- and GluN2B-containing NMDARs (Volianskis et al., 2013a). Importantly, constructing concentration response curves for the different antagonists led to the finding that STP2 may be mediated through GluN2B- and GluN2D-containing triheteromers because STP2 had intermediate sensitivity to the GluN2B antagonist, Ro, and was sensitive to the 2D selective antagonist

UBP145 (Volianskis et al., 2013a). All of the above experiments were performed in rats and dependences of STP and LTP on NMDAR subunit activation in mice is unknown.

4.1.5. Objectives

The objectives of the current study were:

1. to verify that GluN2A- and GluN2B-containing receptors mediate LTP and the amplitude of STP in the SC-CA1 synapse of adult mice
2. to investigate the role(s) that GluN2D subunits play in LTP in the SC-CA1 synapse using a combination of genetic GluN2D knockout mice and GluN2 subunit selective antagonists
3. to characterise the effects of UBP145 and UBP791 (GluN2C/2D-preferring antagonists) on the induction of STP and LTP in the GluN2D knockout mice and in the wild type controls.

4.2. Methods

4.2.1. Animals and slice preparation

All experiments involving animals were performed according to University of Bristol regulations and the UK Scientific Procedures Act, 1986 and European Union guidelines for animal care. Adult (3-6 months old) wild type (WT) mice of the C57BL/6 strain and GluN2D KO mice generated from the WT background (Charles River, UK) were used in the study. Mice were anaesthetised with isofluorane and killed by decapitation after cervical dislocation. The hippocampus was dissected and cooled (0 – 4 °C) in artificial cerebrospinal fluid (aCSF), which contained (in mM): 124 NaCl, 3.5 KCl, 1.25 NaH_2PO_4, 26 $NaHCO_3$, 2 $CaCl_2$, 2 $MgSO_4$ and 10 glucose, saturated with 95% O_2 and 5% CO_2. Transverse slices (400 µm) of the dorsal hippocampus were cut using a McIllwain tissue chopper (The Mickle Laboratories) and incubated in aCSF (pH ~7.4) at room temperature (~20 °C) for at least 2 hours before the start of the experiments. During the experiments, slices were kept submerged and perfused with aCSF that was heated to 33 °C.

4.2.2. Chemicals

NMDAR antagonists D-AP5, Ro 25-6981 maleate, and NVP-AAM 077 were purchased from HelloBio Ltd (Bristol, UK), and L-689,560 was purchased from Tocris Bioscience (Bristol, UK). UBP145 and UBP791 were synthesized in house as described previously (Morley et al., 2005; Burnell, Fang, Irvine, Jane, unpublished data). GABA receptor antagonists, picrotoxin, (-)-bicuculline methochloride and CGP 55845 hydrochloride were purchased from HelloBio Ltd (Bristol, UK). All antagonists were prepared as stock solutions, stored as frozen and added to perfused aCSF at times indicated in Results. All other chemicals and salts were purchased from Sigma (Dorset, UK) or Fischer Scientific (Loughborough, UK).

4.2.3. Electrophysiological recordings

Field-excitatory post-synaptic potentials (f-EPSPs) were recorded from the CA1-B area of the stratum radiatum (population spikes were recorded from stratum pyramidale in some of the experiments) of the hippocampus after stimulation of the Schaffer collaterals (SCs) using a bipolar concentric platinum core electrode with a tip diameter of 12.5 µm (FHC, Inc, USA) (Figure 4.1). Recording electrodes (made of borosilicate) were filled with aCSF and had a resistance of 1.5-2 MΩ. Stimulus pulses (pulse duration of 100 µs) were generated using DS2A Mk2 (Digitimer Ltd, Hertfordshire, UK). Recorded signals were amplified and filtered at 5 kHz (AxoPatch 1D; Axon Instruments, USA), and digitised at 40 kHz (National Instruments, USA). Stimulation intensity was set to three times the threshold for evoking f-EPSPs. Signals were recorded, digitised and stored on a desktop PC using the WinLTP software (Anderson and Collingridge, 2007) for offline analysis.

Baseline and potentiated responses were evoked by stimulating once every 15 seconds and are shown in Results as averages of 4 responses. LTP was induced using either a TBS protocol which comprised of four stimuli at 100 Hz, repeated 10 times at a frequency of 5 Hz (referred to as 10-bursts herein), or a more intense stimulation protocol of 4 stimuli at 100 Hz, repeated 30 times at a frequency of 15 Hz (referred to as 30-bursts). The 30-bursts protocol was used to investigate the role of specific GluN2 subunits on the decaying phase of LTP which was shown to contribute more significantly when the number of bursts during tetanisation was increased (Volianskis and Jensen, 2003). The maximal potentiation (P_{max})

was recorded four minutes after the delivery of tetanus to prevent contamination of the P_{max} from post-tetanic potentiation (PTP).

To record baseline transmission, the input-output relationship for the Schaffer collateral-CA1 pyramidal cells (SC-CA1) synapse was obtained by recording the f-EPSP response to increasing levels of stimulation intensities (expressed as multiples of the threshold intensity required to evoke an f-EPSP) as shown in Results. Simultaneous recordings from stratum radiatum and stratum pyramidale of the CA1-B region were obtained to construct the input-output relationship for f-EPSPs and population spikes (Figure 4.1).

4.2.4. Data analysis and plotting

F-EPSP responses used for analysis of LTP experiments were measured as the rate of rise of the f-EPSPs which was obtained by dividing the amplitude of the initial deflection of f-EPSPs (following the fibre volley) by the time window of the deflection (set at 0.5 ms in this study). Responses for each experiment were normalised to the baseline responses (stable responses obtained before tetanus) and responses are shown according to the level of potentiation, baseline recordings having 0% potentiation. LTP amplitude was represented by the average potentiation at the plateau phase at the end of recordings. STP amplitude was calculated as the difference between P_{max} and LTP amplitude for each experiment. Decay of STP was calculated by fitting a mono-exponential fitting routine using non-linear regression to the decay of potentiation following tetanus delivery. The following equation was used to fit the decay of potentiation:

$$P = LTP + \left(STP \times e^{-\frac{t}{\tau}}\right) \quad (4.1)$$

Where P is the total amplitude of potentiation, LTP and STP are amplitudes of potentiation as described above, t is the time since start of decay, τ is the time constant of decay (the time required for the potentiation to decay to 1/e of P_{max}). LTP amplitude, STP amplitude, and τ were calculated for each experiment and are reported as mean ± S.E.M for experimental groups described in Results.

Baseline transmission was assessed using input-output (IO) experiments. IO experiments were carried out by measuring the following features of the response waveform in response

to various multiples of stimulus intensities required to induce the first f-EPSP: amplitude of the fibre volley (FV), the initial slope of f-EPSP recorded from the stratum radiatum, the area of the population spikes recorded from the stratum pyramidale (see also Results - Figure 4.1). The relationship between FV and stimulus intensity in IO experiments was characterised in each experiment by plotting the FV amplitude against the stimulus intensity and fitting the data using linear regression and the slope of the best-fit line was used for further comparisons. The relationship between f-EPSP slope and FV amplitude in IO experiments was characterised by fitting data from individual experiments using linear-regression where the line was constrained to pass through y = 0, x = 0, because the f-EPSP was preceded by a FV and both components were clearly visible in all experiments. The slope of the best-fit line was then used as a measure of the input-output relationship between FVs and f-EPSPs.

To characterise the excitability in slices, excitation-spike (ES) coupling relationship between f-EPSPs and population spikes were investigated. Population spike areas and f-EPSP slopes from each IO experiment were fitted using non-linear regression to a four-parameter logistic curve with the following equation:

$$Y = B + \frac{T - B}{1 + \left(\frac{X}{E_{50}}\right)^{H}} \qquad (4.2)$$

where Y is the population spike area, T is the maximum value of the curve, B is the minimum value of the curve, constrained to 0, because population spikes required f-EPSPs, X was the f-EPSP slope; E_{50} was the f-EPSP slope at half-maximal population spike area; H was the slope-factor.

Paired pulse facilitation ratio, a measure of presynaptically induced STP (see section 1.1.4.3), was measured by evoking 2 f-EPSPs using 2 stimulus pulses at an inter-pulse interval of 50 ms and dividing the rate of rise of the second f-EPSP by rate of rise of the first f-EPSP.

Analysis of data was performed offline using Platin (Morten Jensen, University of Aarhus, Denmark) and WinLTP (Anderson and Collingridge, 2007). Statistical comparisons and

plotting were performed using GraphPad Prism 7 (GraphPad Software, Inc., LaJolla, CA, USA). LTP and STP amplitudes were compared using parametric tests; analysis of variance (ANOVA) followed by Dunnett's multiple comparison test (DT) was used for multiple comparisons. Decay time constants of STP were compared using Mann-Whitney (MW) test because the pooled control decay time constant data from 10-bursts and 30-bursts experiments did not conform to samples from a normal distribution ($p < 0.01$, D'Agostino & Pearson omnibus normality test). In cases where normality of data could not be determined due to low experimental observations, paired testing of before- and after-treatment effects from the same slice was performed using Wilcoxon matched pairs signed rank (WMPSR) test. Statistical significance was set at $p < 0.05$. Significant differences in bar plots are indicated by asterisks (* $p < 0.05$, ** $p < 0.01$, *** $p < 0.001$).

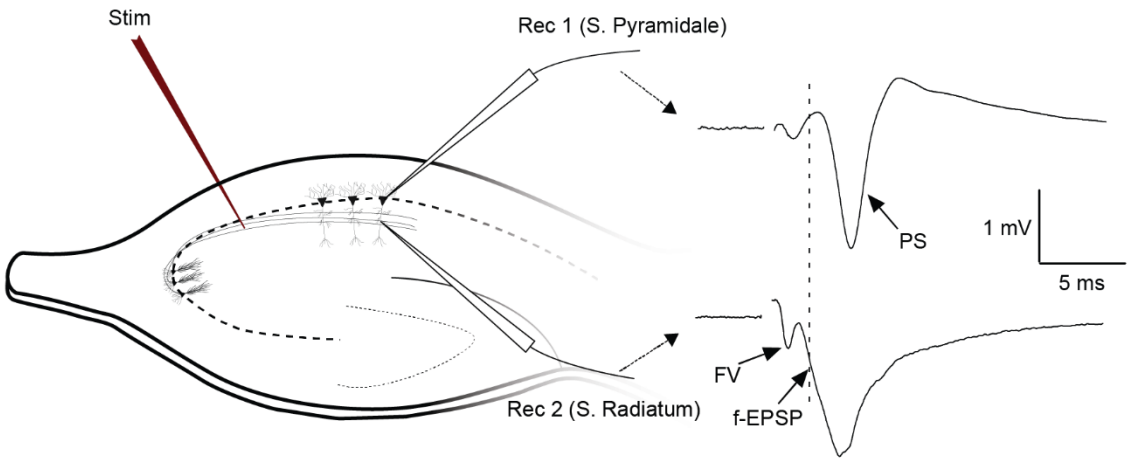

Figure 4.1. Setup for recording field potentials from the hippocampus. Schematic illustrating the positioning of stimulating and recording electrodes and showing example responses that were recorded from the stratum pyramidale and stratum radiatum in a transverse hippocampal slice. Stimulating electrode (Stim) was placed in the stratum radiatum at the border between CA1 and CA2 areas. Fibre volleys (FVs) and field excitatory post-synaptic potentials (f-EPSPs) were recorded from the stratum radiatum and population spikes (PSs) were recorded from stratum pyramidale in the CA1 area. Dashed line shows a representative time-point at which the slope of f-EPSP was measured for all experiments in this study.

4.3. Results

4.3.1. Investigation of baseline transmission in WT and GluN2D KO hippocampal slices

Baseline transmission was characterised in slices from wild type (WT) and GluN2D knockout mice (KO) (Figure 4.2). The relationship between the amplitude of fibre volley and the stimulation intensity was not significantly different between WT and GluN2D KO slices (Figure 4.2A, $p > 0.05$, Student's t-test). The input-output relationship for fibre volley and f-EPSPs suggests that slices from both genotypes generate similar f-EPSPs for the same presynaptic input (Figure 4.2B, $p > 0.05$, Student's t-test). The relationship between f-EPSP and population spike was best fit using a sigmoidal polynomial curve, which could be used to compare differences in maximal population spike (a measure of excitability in the slices) and the E_{50} (the f-EPSP slope at half-maximal population spike) between the genotypes (Figure 4.2C). Maximal population spike was larger in WT slices compared to KO slices ($p < 0.05$, Student's t-test) but the E_{50} was not significantly different between WT and KO slices ($p > 0.05$, Student's t-test). The PPF of f-EPSPs were characterised using an inter-pulse interval (IPI) of 50 ms (Figure 4.2D) and both genotypes had similar PPF ratios ($p > 0.05$, Student's t-test).

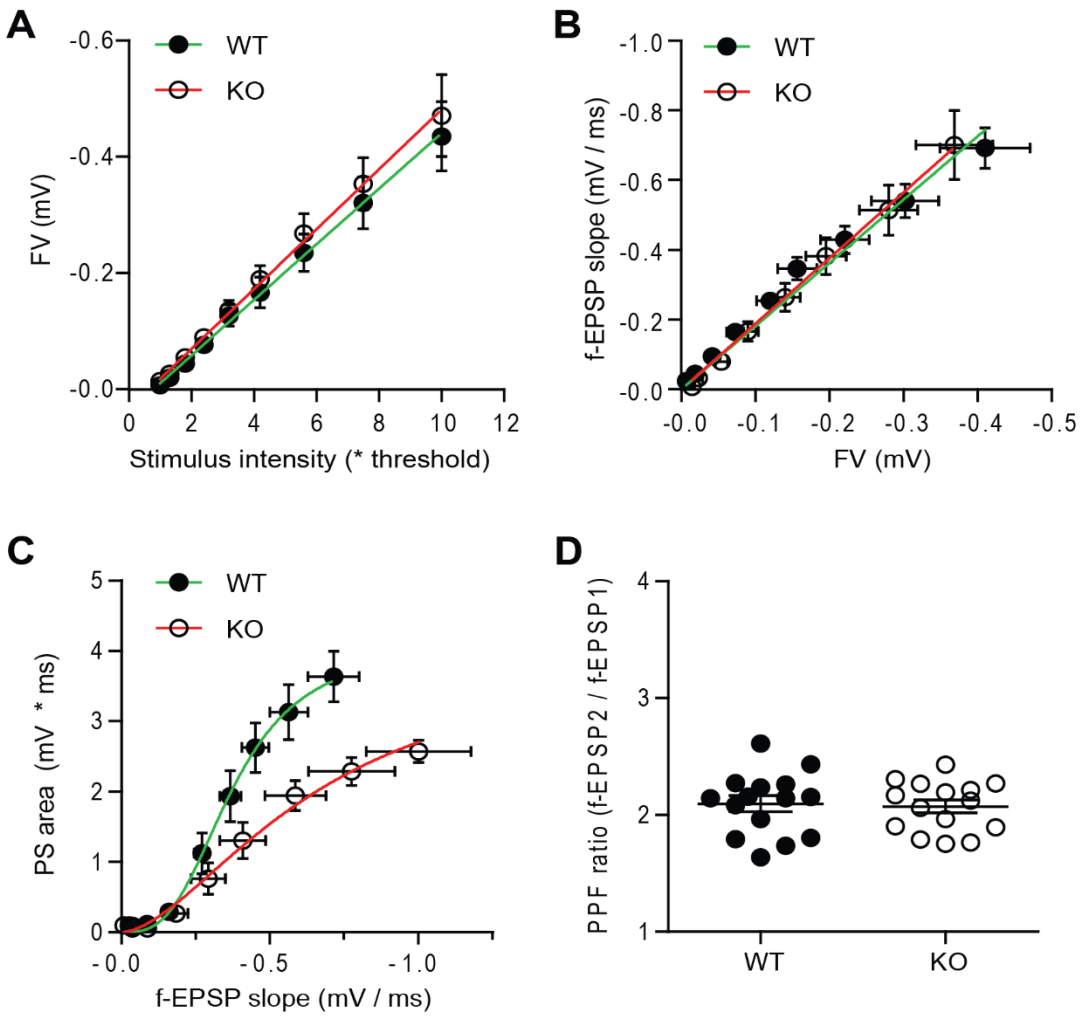

Figure 4.2. Characterisation of baseline transmission in WT and GluN2D KO hippocampal slices. A, FV was plotted against stimulus intensity and the relationship was compared between WT and GluN2D KO slices using linear regression. Slope of the WT line (-0.042 ± 0.0054 mV/stim intensity, n = 14) was not significantly different (P > 0.05, Student's t-test) from the KO line (-0.045 ± 0.0061 mV/stim intensity, n =13). **B,** f-EPSP to FV relationship was compared between the 2 genotypes. The slopes of lines for WT = 1.9 ± 0.20 ms^{-1} (n = 14) and KO = 1.91 ± 0.30 ms^{-1} (n = 13) were not significantly different (p > 0.05, Student's t-test). **C**, PS to f-EPSP input-output relationships were evaluated by fitting sigmoidal curves to WT and KO datasets. The f-EPSP slope at half maximal population spike (E_{50}) for WT slices (-0.39 ± 0.062 mV/ms) was not different from that for the KO slices (-0.44 ± 0.064 mV/ms, p > 0.05, Student's t-test). Maximal PS area for WT (4.00 ± 0.44 mV * ms, n = 8) was higher than the maximal PS area for KO (2.49 ± 0.16 mV * ms, n = 7. p < 0.05, Student's t-test). **D,** Paired pulse facilitation (PPF, 50 ms interpulse interval) ratio was not significantly different between WT (2.10 ± 0.069, n = 15) and KO (2.07 ± 0.056, n = 15, p > 0.05, Student's t-test) slices.

4.3.2. Effects of GABA receptors on baseline transmission in WT and KO slices

Maximal neuronal excitability was significantly depressed in GluN2D KO slices when compared to WT slices (Figure 4.2). Therefore, the effects that deletion of GluN2D receptors expressed on interneurons had on baseline synaptic transmission were characterised. To do this, the baseline transmission before and after inhibition of GABAergic transmission using antagonists of $GABA_A$ (50 µM picrotoxin and 20 µM bicuculline) and $GABA_B$ (2 µM CGP 55845) receptors in WT and KO slices were investigated (Figure 4.3, Figure 4.4 and Figure 4.5). In WT and KO slices, inhibition of $GABA_A$ and $GABA_B$ receptors did not affect the relationship between stimulus intensity and FV (Figure 4.3), or FV and f-EPSP (Figure 4.4), or f-EPSP and population spikes (E_{50}, Figure 4.5A3 and Figure 4.5B3) ($p > 0.05$ for all, WMPSR test). Similarly, upon inhibition of GABAergic transmission, maximum population spike was not significantly different compared to controls in WT (Figure 4.5A2) or KO (Figure 4.5B2) slices ($p > 0.05$, WMPSR test).

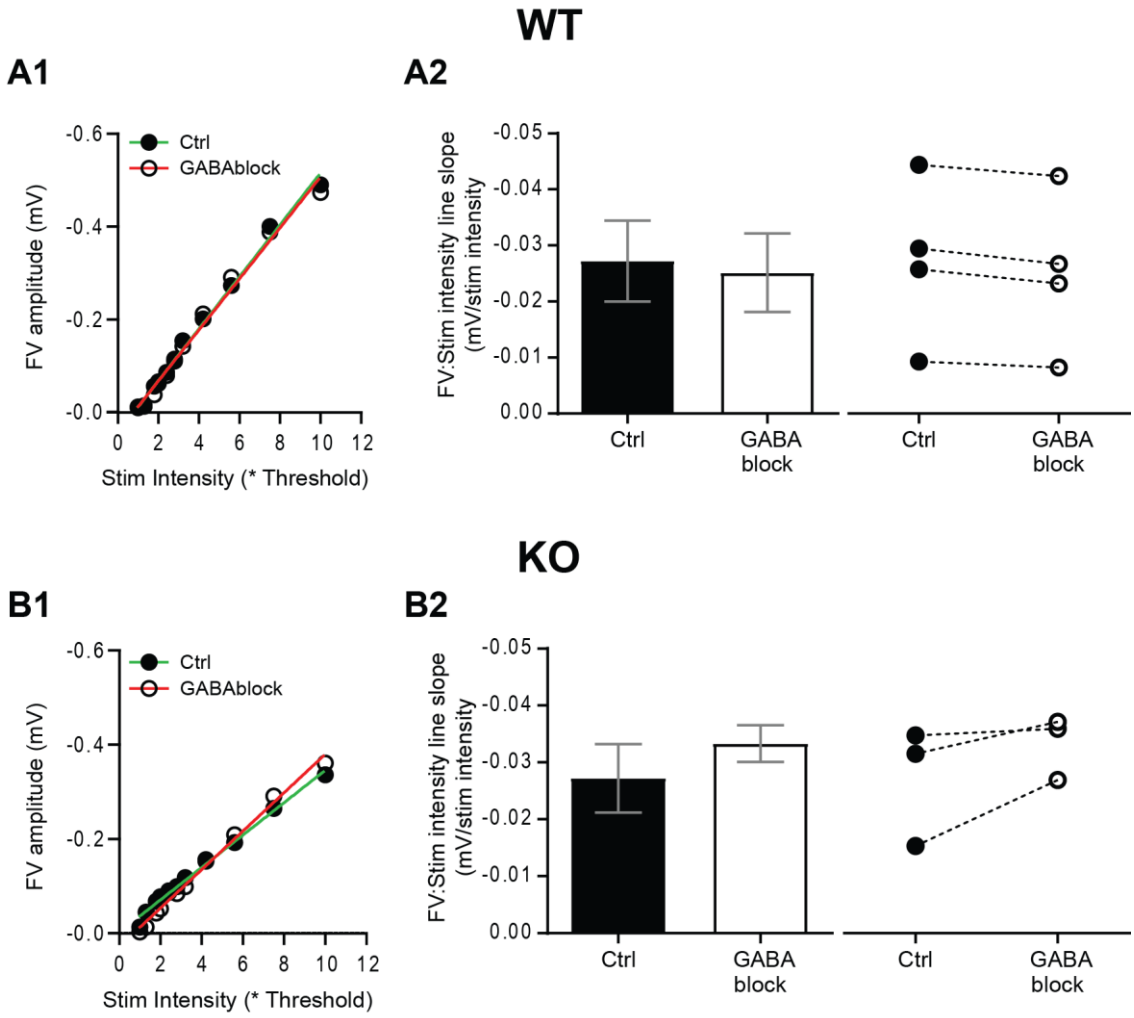

Figure 4.3. Characterisation of the effects of inhibition of GABAergic transmission on stimulus intensity to fibre volley ratio in WT and GluN2D KO slices. A1 and B1, Example experiments showing the FV to stimulus intensity relationship in WT slices (**A1**) and KO slices (**B1**) with (white circles) and without (black circles) blockage of GABAergic transmission. The data were fitted using linear regression and the best-fit lines are shown. **A2 and B2**, Pooled data (mean ± SEM, left) and data from individual experiments (right) showing the effect of inhibition of GABAergic transmission on the FV to stimulus intensity relationship in WT slices (**A2**; n = 4) and KO slices (**B2**; n = 3). In WT slices, there was no statistically significant difference in the slope of the fitted line following blockage of GABAergic transmission (-0.025 ± 0.007 mV/stim intensity) compared to controls (-0.027 ± 0.007 mV/stim intensity, $p > 0.05$, WMPSR test). In KO slices, there was no statistically significant difference in the slope of the fitted line following blockage of GABAergic transmission (-0.034 ± 0.003 mV/stim intensity) compared to controls (-0.027 ± 0.006 mV/stim intensity, $p > 0.05$, WMPSR test).

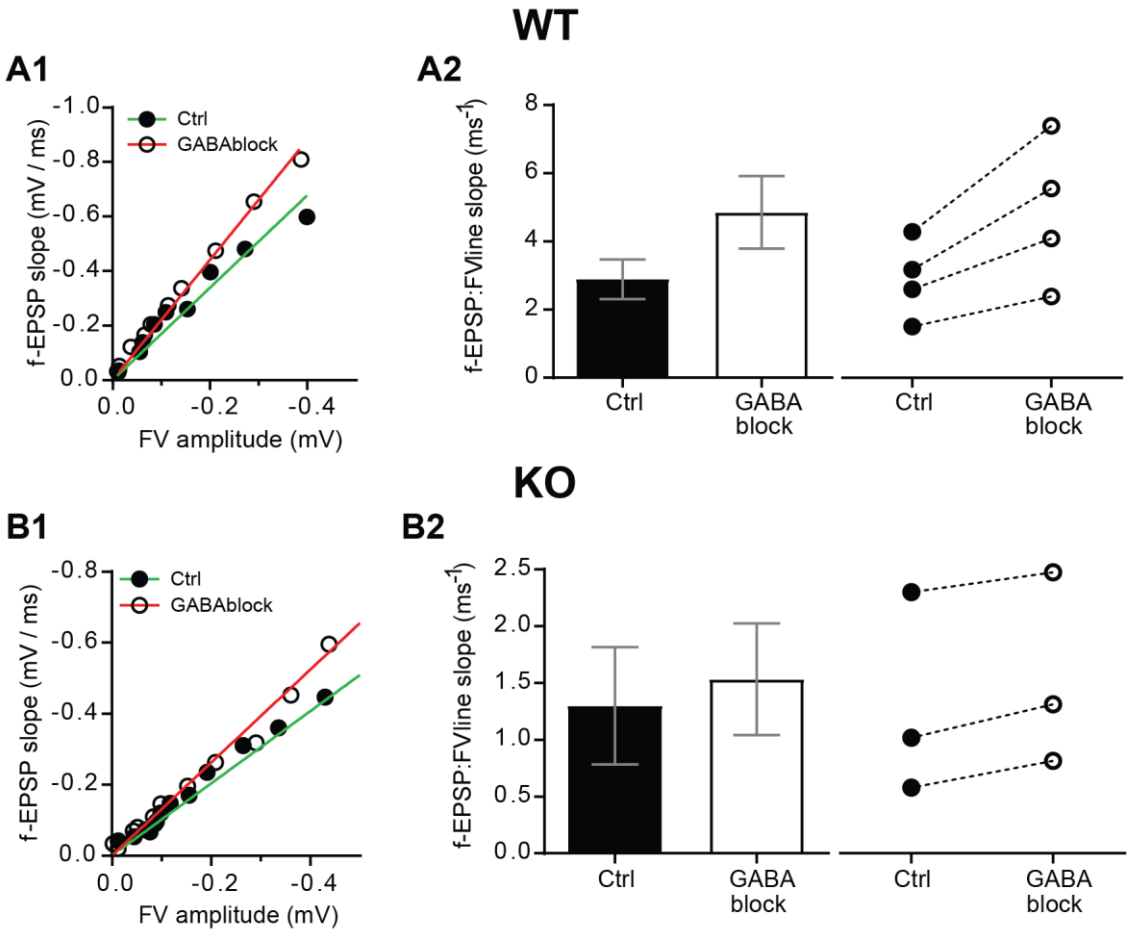

Figure 4.4. Characterisation of the effects of inhibition of GABAergic transmission on f-EPSP to stimulus intensity ratio in WT and GluN2D KO slices. A1 and B1, Example experiment showing the f-EPSP to FV relationship in WT slices (**A1**) and KO slices (**B1**) in the absence (black circles) and presence (white circles) of GABAergic transmission blockers. **A2 and B2,** Pooled data (left) and results from the individual experiments (right) showing the effect of blockage of GABAergic transmission on the f-EPSP to FV relationship in WT slices (**A2**, n = 4) and KO slices (**B2**, n = 3). In WT slices, there was no significant difference f-EPSP to FV ratio following blockage of GABAergic transmission (4.9 ± 1.1 ms^{-1}) compared to controls (2.9 ± 0.6 ms^{-1}, $p > 0.05$, WMPSR test). In KO slices, there was no significant difference after blockage of GABAergic receptors (1.5 ± 0.49 ms^{-1}) compared to controls (1.3 ± 0.52 ms^{-1}; $p > 0.05$, WMPSR test).

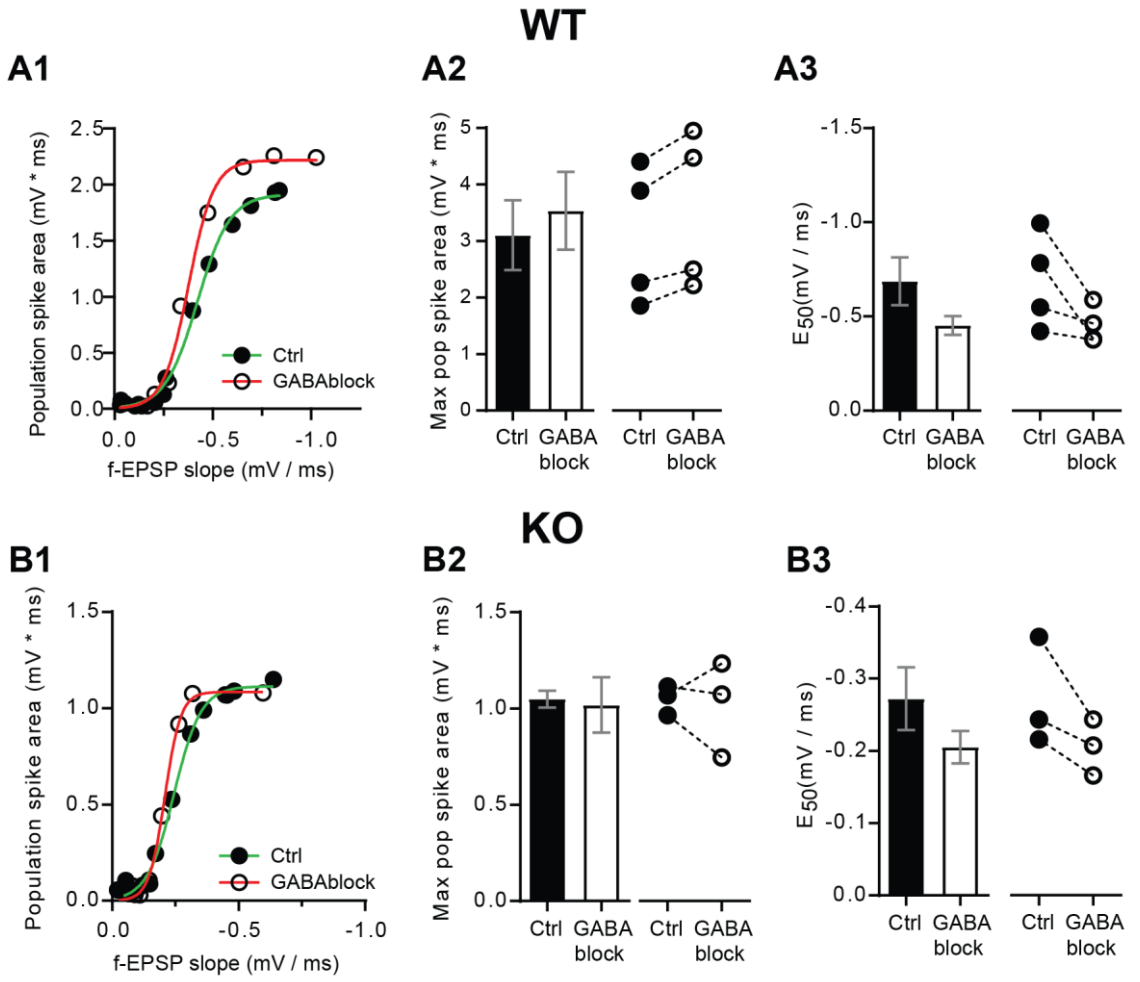

Figure 4.5. Characterisation of the effects of inhibition of GABAergic transmission on population spike in WT and GluN2D KO slices. A1 and B1, Example experiment showing the relationship between f-EPSPs and population spikes in WT slices (**A1**) and KO slices (**B1**) in the absence (black circles) and presence (white circles) of GABAergic transmission block. The data were described using a non-linear, sigmoidal fit. **A2 and B2,** In WT slices (**A2**, n = 4), maximum population spike area was not significantly different after inhibition of GABAergic transmission (3.5 ± 0.7 mV * ms) compared to the presence of GABAergic transmission (3.1 ± 0.6 mV * ms), in WT slices ($p > 0.05$, WMPSR test). In KO slices (**B2**, n = 3), maximum population spike area was similar in the presence of GABA receptor antagonists (1.0 ± 0.05 mV * ms) compared to controls (1.1 ± 0.04 mV * ms; $p > 0.05$, WMPSR test). **A3 and B3**, In WT slices (**A3**, n = 4) there was no significant difference in the E_{50} value after inhibition of GABAergic transmission (-0.45 ± 0.05 mV/ms) compared to controls (-0.69 ± 0.13 mV/ms; $p > 0.05$, WMPSR test). In KO slices (**B3**, n = 3), there was no significant difference in the E_{50} value after inhibition of GABAergic transmission E_{50} = -0.21 ± 0.02 mV/ms) compared to controls (E_{50} = -0.27 ± 0.04 mV/ms; $p > 0.05$, WMPSR test).

4.3.3. GluN2D KO hippocampal slices have higher levels of STP and LTP compared to WT hippocampal slices

Control potentiation induced by 10-bursts in WT slices had a mean amplitude of STP of 58.0 ± 5.0% that decayed to a stable LTP of 38.6 ± 4.1% with a mean decay time constant of 11.4 ± 1.5 min (Figure 4.6A). In GluN2D KO slices, potentiation induced by 10-bursts had STP of 82.8 ± 5.8% that decayed to a stable LTP of 54.29 ± 5.49% with a mean decay time constant of 11.4 ± 1.5 min (Figure 4.6A). Comparing potentiation that was induced by 10-bursts between WT and KO slices showed that STP and LTP in GluN2D KO slices were greater than in WT slices (Figure 4.6C and D, $p < 0.01$ and $p < 0.05$, respectively, Student's t-test) whereas the decay time constants of STP were similar in both WT and GluN2D KO slices ($p > 0.05$, MW test).

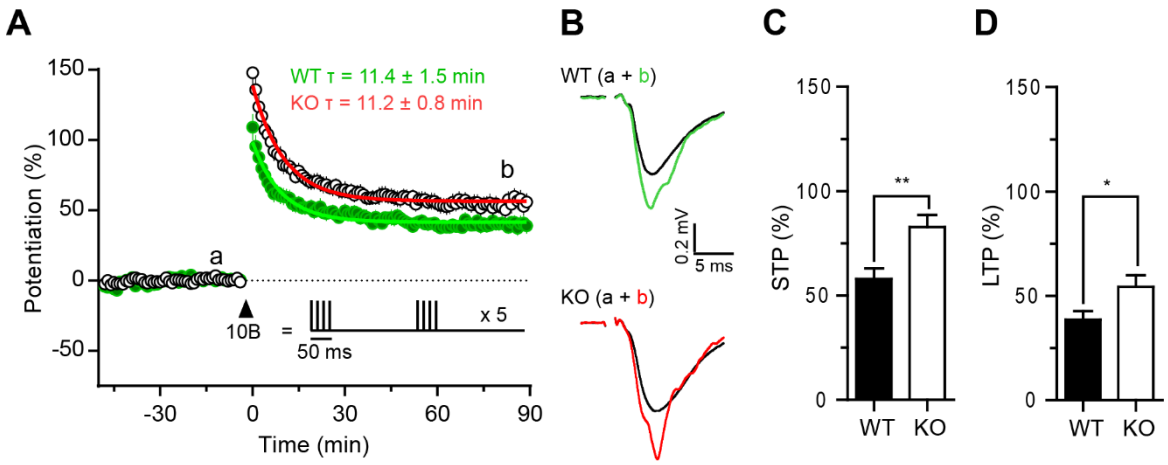

Figure 4.6. Control STP and LTP are larger in hippocampal slices from GluN2D KO mice than in the WT. A, Pooled data showing the time course of potentiation of f-EPSPs (Mean ± SEM) induced by theta burst stimulation (10-bursts (10B), 4 pulses at 100 Hz repeated 10 times at 5 Hz) in WT (green circles, n = 21) and GluN2D KO mice slices (white circles, n = 17). Arrowhead indicates the time of TBS. Decay of STP after 10-bursts was fitted using a mono-exponential decay function (green curve fits WT and red curve fits KO). Decay time constants for WT and KO (τ, indicated in figure) were not significantly different between the genotypes ($p > 0.05$, MW test). Inset shows schematic illustrating the 10-bursts protocol. **B,** Representative f-EPSPs for WT and KO at the time-points indicated in **A**. **C,** Amplitude of STP was significantly larger in GluN2D KO slices (82.8 ± 5.8%) than in WT controls (58.0 ± 5.0%, $p < 0.01$, Student's t-test). **D,** LTP was larger in GluN2D KO (54.29 ± 5.49%) when compared to LTP in WT (38.6 ± 4.1%, $p < 0.05$, Student's t-test).

4.3.4. STP and LTP amplitudes were similar in WT and GluN2D KO hippocampal slices in the presence of GABA receptor antagonists

It was previously shown that GluN2D KO slices have increased STP and LTP induced by 10-bursts compared to WT slices (Figure 4.6). A possible reason for this difference could be the expression of GluN2D receptors on GABAergic interneurons in the WT mice. GABAergic interneurons expressing GluN2D-containing NMDARs are a part of feedforward inhibition in the SC-CA1 signalling pathway (Engelhardt et al., 2015; Perszyk et al., 2016) and have been shown to be involved in induction of NMDAR-dependent potentiation (Wigström and Gustafsson, 1983). Therefore, 10-bursts LTP experiments were conducted in slices from both the WT and GluN2D KO mice after blockade of $GABA_A$ (using 50 μM picrotoxin and 20 μM bicuculline) and $GABA_B$ (using 2 μM CGP 55845) receptors (Figure 4.7A and B). STP (Figure 4.7C) and LTP (Figure 4.7D) amplitudes in WT slices and GluN2D KO slices were similar after inhibition of GABAergic transmission ($p > 0.05$, ANOVA, DT). This supports the suggestion that the greater amplitudes of STP and LTP that were observed in KO mice when compared to WT (Figure 4.6) were due to differences in GABAergic transmission. Interestingly, amplitudes of STP and LTP induced in the presence of GABA receptor antagonists were significantly higher than pooled control STP and LTP amplitudes in WT but not GluN2D KO slices (Figure 4.7C and D). While the decay of STP in WT and GluN2D KO slices was similar in the pooled control experiments ($p > 0.05$ for both, MW test), decay of STP was significantly faster in GluN2D KO slices after inhibition of GABAergic neurotransmission ($p < 0.05$, MW test).

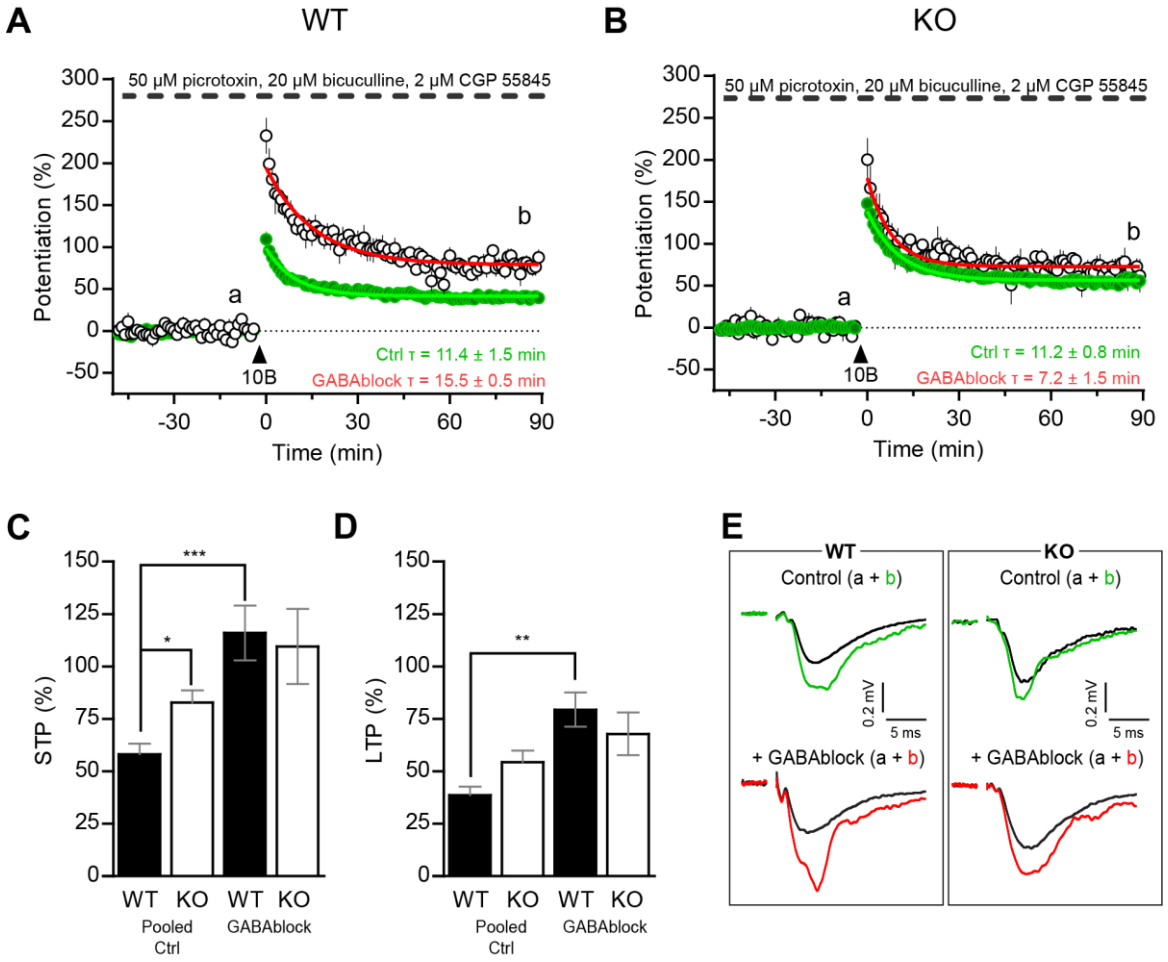

Figure 4.7. LTP and STP levels in WT and GluN2D KO slices were similar in the presence of GABA receptor antagonists. A, In WT slices, potentiation induced by 10-burst stimulation was greater after inhibition of GABA receptors (white circles, STP = 116.0 ± 13.1%, LTP = 79.4 ± 8.1%, n = 4) compared to pooled controls (green circles, STP = 58.1 ± 5%, LTP = 34.4 ± 4.6%, n = 16). In WT slices, the decay time constant of STP was not significantly different in the presence of GABA receptor antagonists compared to controls ($p > 0.05$, MW test). **B,** In KO slices, potentiation induced by 10-burst stimulation was similar when GABA receptors were blocked (white circles, STP = 109.4 ± 17.9%, LTP = 67.8 ± 10.2%, n = 5) compared to controls (green circles, STP = 82.8 ± 5.8%, LTP = 54.7 ± 5.8%, n = 16). The decay time constant of STP in experiments with GABA antagonists was significantly lower compared to control ($p < 0.05$, MW test). **C - D,** In WT slices, the amplitude of STP (**C**) and LTP (**D**) induced by 10-burst stimulation in the presence of GABA receptor antagonists was significantly greater compared to controls ($p < 0.001$ and $p < 0.01$, respectively, ANOVA, DT). Whereas in KO slices, there was no difference in amplitude of STP (**C**) or LTP (**D**) after inhibition of GABA receptors compared to controls ($p > 0.05$ for both, ANOVA, DT). **E,** Representative f-EPSPs from WT and KO slices at the time-points indicated in **A** and **B**.

4.3.5. Concentration-dependent effects of D-AP5 on STP and LTP

D-AP5, a competitive antagonist of NMDARs was used to study the inhibition of NMDAR mediated LTP in the SC-CA1 synapses of WT and GluN2D KO slices (Figure 4.8). D-AP5 blocks 2A and 2B subunits but not GluN2C or GluN2D subunits at sub-micromolar concentrations (Feng et al., 2005). Therefore, D-AP5 was tested at 100 µM, a concentration that blocks all GluN2 subunits and at 1 µM, a concentration that is selective for 2A and 2B containing receptors (Figure 4.8A, B and E). 100 µM D-AP5 blocked STP and LTP in slices from both genotypes equally (Figure 4.8C and D, $p > 0.05$ for both, Student's t-test), whereas 1 µM D-AP5 blocked more STP in GluN2D KO slices compared to WT slices (Figure 4.8C, $p < 0.05$, Student's t-test). Application of 1 µM D-AP5 led to inhibition of LTP to similar levels in both WT and GluN2D KO slices (Figure 4.8D; $p > 0.05$, Student's t-test).

A small, residual STP component was visible even in the presence of 100 µM D-AP5, this may have been a result of increased glutamate concentration during tetanus which outcompetes the competitive antagonist D-AP5 to cause potentiation. Therefore, inhibition of LTP was also verified using the NMDAR glycine site antagonist 10 µM L689,560, which blocked both STP and LTP in WT and KO slices (Figure 4.9). Application of 10 µM L689,560 caused similar levels of STP (Figure 4.9C) and LTP (Figure 4.9D) inhibition in WT and GluN2D KO slices ($p > 0.05$, Student's t-test).

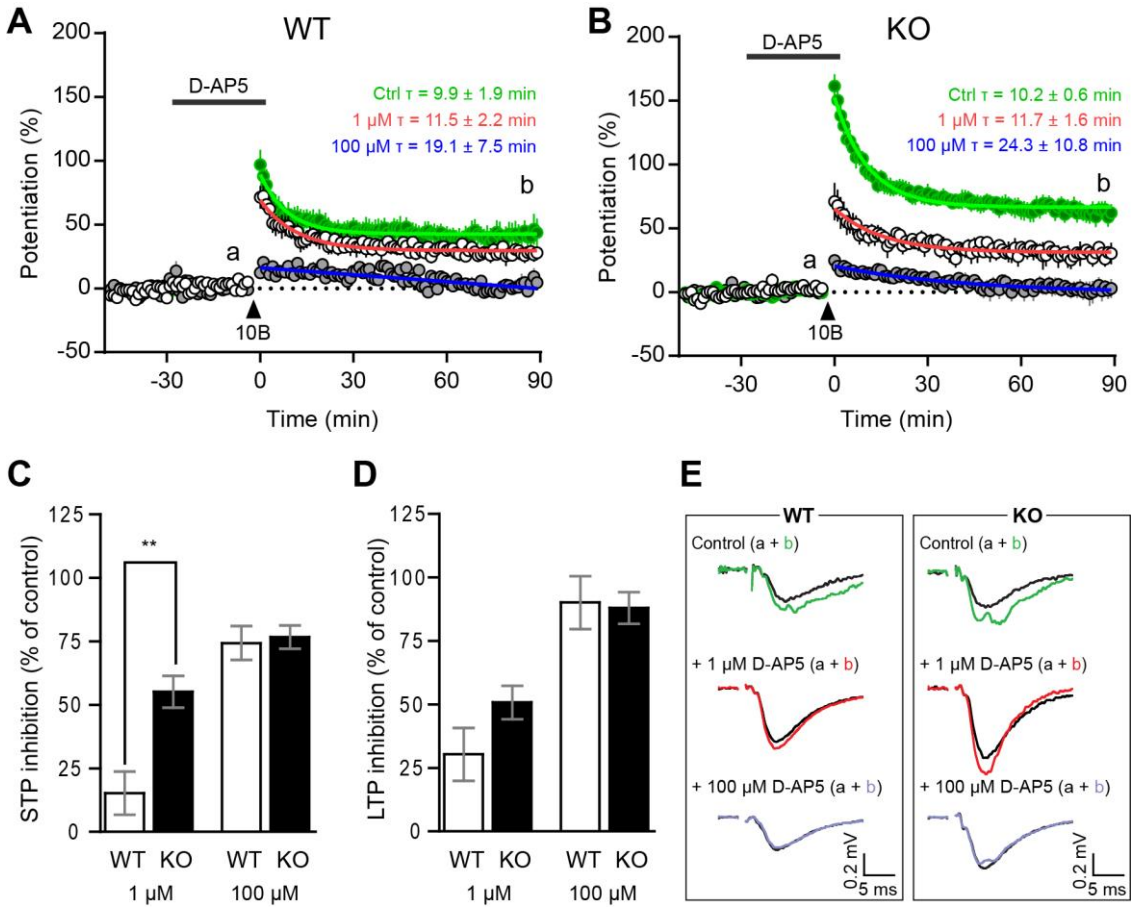

Figure 4.8. D-AP5 blocks induction of STP more potently in GluN2D KO than WT hippocampal slices. A, Pooled experiments from WT slices showing induction of STP and LTP by 10-bursts in interleaved control experiments (green circles, STP = 48.3 ± 5.0%, LTP = 38.9 ± 7.7%, n = 8), and following application of 1 µM (white circles, STP = 40.9 ± 4.1%, LTP = 27.2 ± 4.1%, n = 6) and 100 µM (grey circles, STP = 12.4 ± 3.2%, LTP = 3.8 ± 4.1%, n = 5) D-AP5. τ of STP were not significantly different following 1 µM or 100 µM D-AP5 application when compared to control ($p > 0.05$, MW test). **B,** Similar to **A** but data are from GluN2D KO slices. Interleaved controls (green circles, STP = 91 ± 7.6%, LTP = 62.1 ± 7.0%, n = 6), 1 µM D-AP5 (white circles, STP = 38.5 ± 5.4%, LTP = 30.6 ± 4.1%, n = 5), and 100 µM D-AP5 (grey circles, STP = 20 ± 4.0%, LTP = 7.5 ± 3.9%, n = 5). τ of STP for controls was not different from τ in 1 µM or 100 µM D-AP5 ($p > 0.05$, MW test). **C,** 1 µM D-AP5 inhibited the amplitude of STP in WT slices by 15.2 ± 8.6%, whereas in KO slices it was more potent (55.2 ± 6.3%, $p < 0.01$, Student's t-test). 100 µM AP5 inhibited STP to the same extent in both the WT (74.3 ± 6.7%) and KO (76.7 ± 4.6%, $p > 0.05$, Student's t-test). **D,** There was no statistical difference in LTP inhibition between the WT and GluN2D KO mice in the presence of 1 µM (30.4 ± 10.4% for WT and 50.8 ± 6.5% for KO, $p > 0.05$, Student's t-test) and 100 µM D-AP5 (90.2 ± 10.4% for WT and 88.0 ± 6.3%; for KO, $p > 0.05$, Student's t-test). **E,** Representative f-EPSPs from WT and KO slices at the time-points indicated in **A** and **B**.

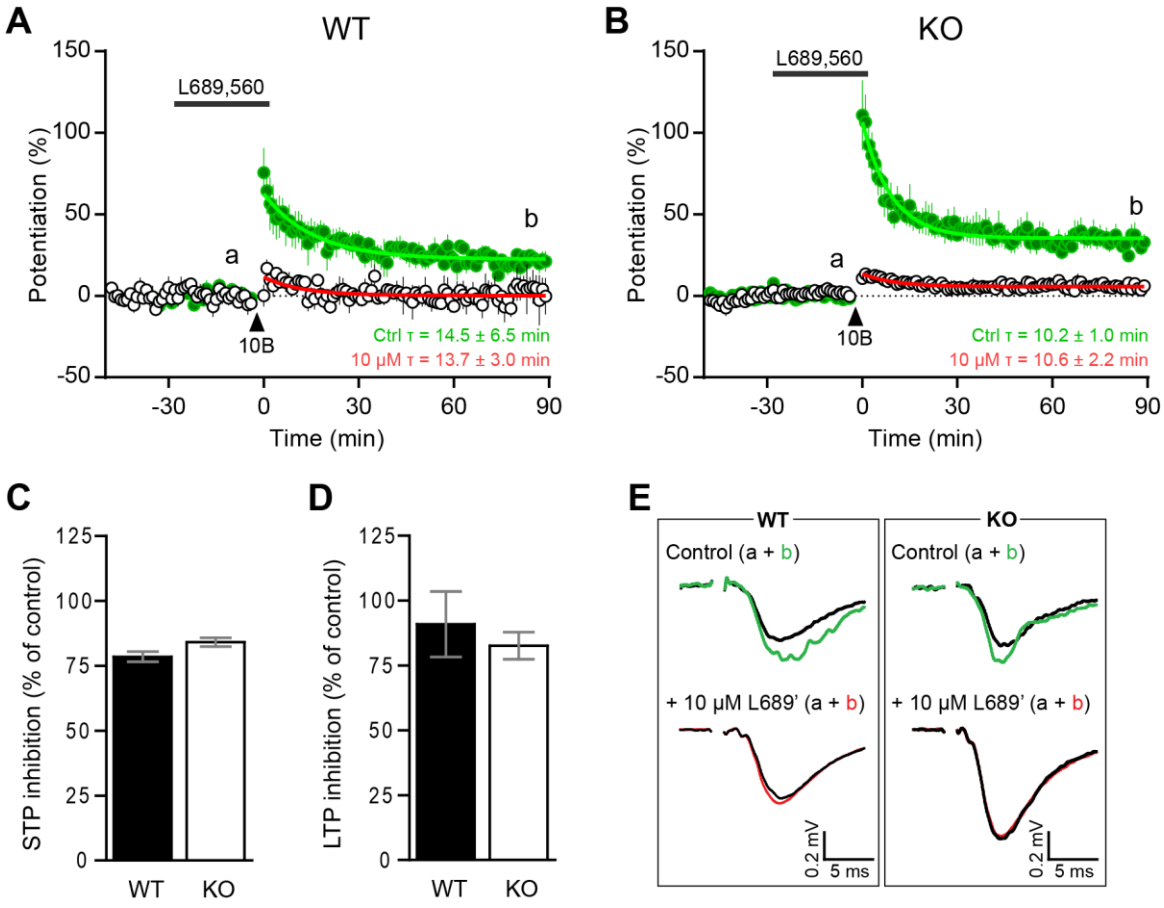

Figure 4.9. Induction of STP and LTP is blocked by glycine-site NMDAR antagonist L689,560. A, In WT slices, 10 μM L689,560 (white circles, STP = 9.6 ± 0.9%, LTP = 2.0 ± 2.8%, n = 3) blocked induction of STP and LTP compared to control (green circles, STP = 44.7 ± 8.9%, LTP = 22.4 ± 3.6%, n = 3). τ of STP were not significantly different between control and L689,560 treated groups ($p > 0.05$, MW test). **B,** Induction of LTP and STP was also blocked in GluN2D KO slices by 10 μM L689,560 (white circles, STP = 11.6 ± 1.2%, LTP = 5.6 ± 1.7%, n = 4) compared to control (green circles, STP = 73.1 ± 14.3%, LTP = 32.4 ± 5.2%, n = 4). τ of STP were not significantly different between control and L689,560 treatment groups ($p > 0.05$, MW test). **C,** 10 μM L689,560 inhibited the amplitude of STP in WT slices by 78.6 ± 2.0%, which was not different from the inhibition of STP in KO slices (84.1 ± 1.7%, $p > 0.05$, Student's t-test). **D,** LTP amplitude was inhibited by 10 μM L689,560 to similar levels in WT slices (90.9 ± 12.6%) and KO slices (82.7 ± 5.3%, $p > 0.05$, Student's t-test). **E,** Representative f-EPSPs from WT and KO slices at the time-points indicated in **A** and **B**.

4.3.6. GluN2A preferring antagonist NVP partially inhibits LTP in GluN2D KO and WT hippocampal slices

To further investigate the role of the GluN2A subunit in the induction of LTP, NVP, a competitive antagonist with modest subunit selectivity for GluN2A over 2B and 2D containing receptors was used at a concentration of 0.1 µM (Figure 4.10A and B). NVP blocked STP and LTP in GluN2D KO and WT slices by a similar extent (Figure 4.10C and D). However, there was a significant prolongation of STP decay in WT slices (Figure 4.10A, $p < 0.05$, MW test) but not GluN2D KO slices (Figure 4.10B, $p > 0.05$, MW test) by NVP. These results suggest that in SC-CA1 synapses, GluN2A-containing receptors mediate the amplitudes of STP and LTP in adult mice. These results are different from experiments in adult rat hippocampal slices where 0.1 µM NVP blocked close to 100% LTP (Volianskis et al., 2013a). Thus, LTP in SC-CA1 synapse in adult mice does not appear to be completely mediated by GluN2A-containing receptors but by a combination of GluN2A and other GluN2 subunits. Likewise, STP amplitude in SC-CA1 synapses in adult mice also appears to be mediated by GluN2A-containing receptors - a finding that was previously reported in adult rat slices (Volianskis et al., 2013a).

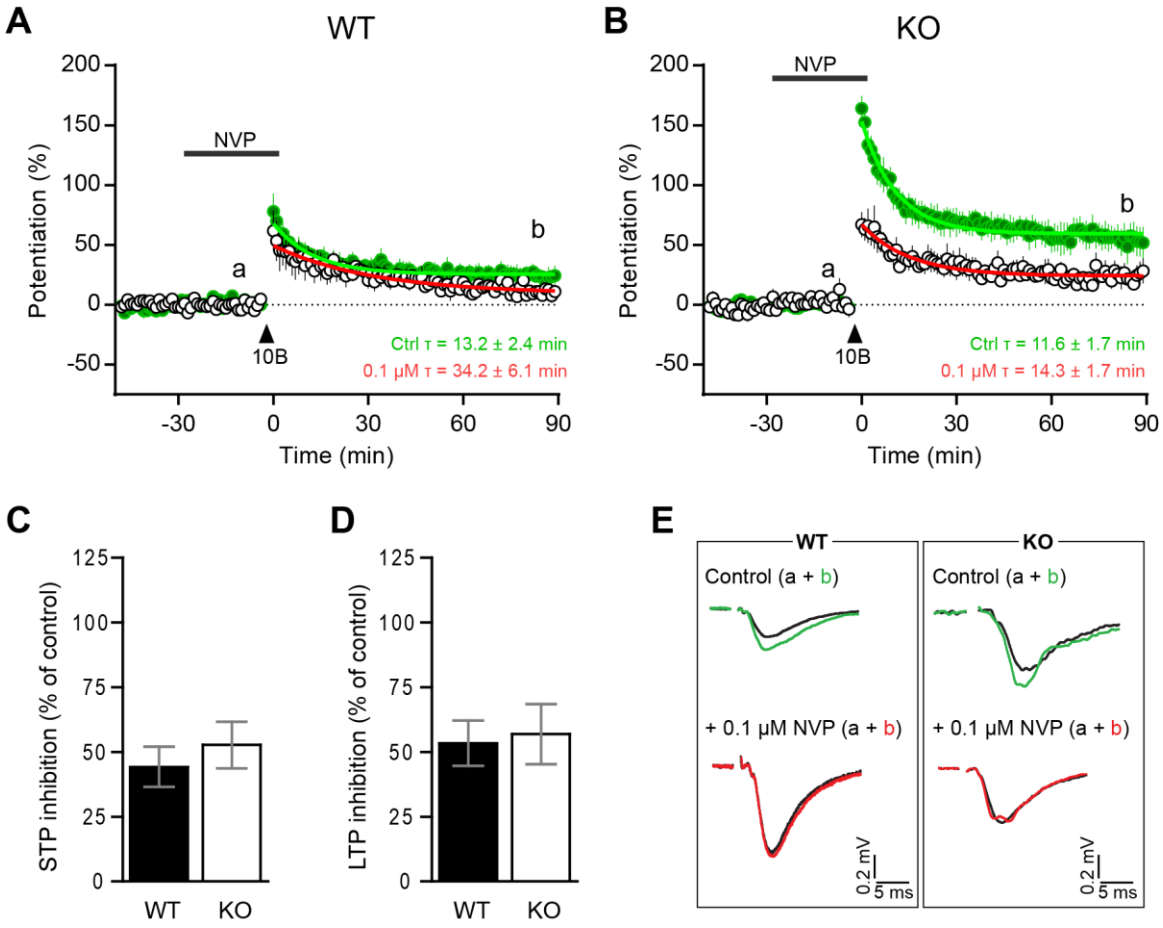

Figure 4.10. GluN2A antagonist NVP slows the decay of STP in WT but not GluN2D KO hippocampal slices. A, 0.1 μM NVP (white circles, STP = 24.4 ± 3.4%, LTP = 10.4 ± 12.2%, n = 4) partially inhibited induction of LTP compared to control (green circles, STP = 43.8 ± 7%, LTP = 22.3 ± 5.7%, n = 4) in WT slices. Application of 0.1 μM NVP also slowed the decay of STP compared to controls ($p < 0.05$, MW test). **B,** In KO slices, induction of LTP and STP was partially inhibited by 0.1 μM NVP (white circles, STP = 43.6 ± 8.3%, LTP = 23.4 ± 6.3%, n = 5) compared to control (green circles, STP = 92.3 ± 12.6%, LTP = 54.3 ± 12.3%, n = 5) however, there was no difference in decay of STP after application of 0.1 μM NVP compared to control ($p > 0.05$, MW test). **C,** The amplitude of STP was inhibited to similar levels in WT (44.2 ± 7.8%) and KO (52.7 ± 9.0%) slices by 0.1 μM NVP compared to control ($p > 0.05$, Student's t-test). **D,** 0.1 μM NVP inhibited LTP amplitude to similar levels in WT (53.4 ± 8.7%) and KO (56.9 ± 11.6%, $p > 0.05$, Student's t-test). **E,** Representative f-EPSPs from WT and KO slices at the time-points indicated in **A** and **B**.

4.3.7. Effects of GluN2B antagonist Ro (1 & 10 µM) on STP and LTP in WT and GluN2D KO hippocampal slices

The increased sensitivity of STP and LTP in KO slices to 1 µM D-AP5 concentration when compared to the WT could also be due to the inhibition of GluN2B-containing receptors (in addition to GluN2A) by sub-micromolar concentrations of D-AP5. Therefore, Ro 25-6981 (Ro), a negative allosteric modulator with 1000-fold selectivity for GluN2B over the 2A subunit (Fischer et al., 1997) was used to investigate the GluN2B component of potentiation in both genotypes (Figure 4.11). 1 µM Ro had minimal effects on both STP and LTP in WT and KO slices (Figure 4.11, $p > 0.05$, Student's t-test), whereas increasing Ro concentration to 10 µM resulted in greater block of STP and LTP in WT slices than in KO slices (Figure 4.11C, D, $p < 0.05$ for both, Student's t-test). Additionally, τ of STP after application of 10 µM Ro had a trend towards a faster decay time constant in KO slices (Figure 4.11E, $p = 0.06$, MW test).

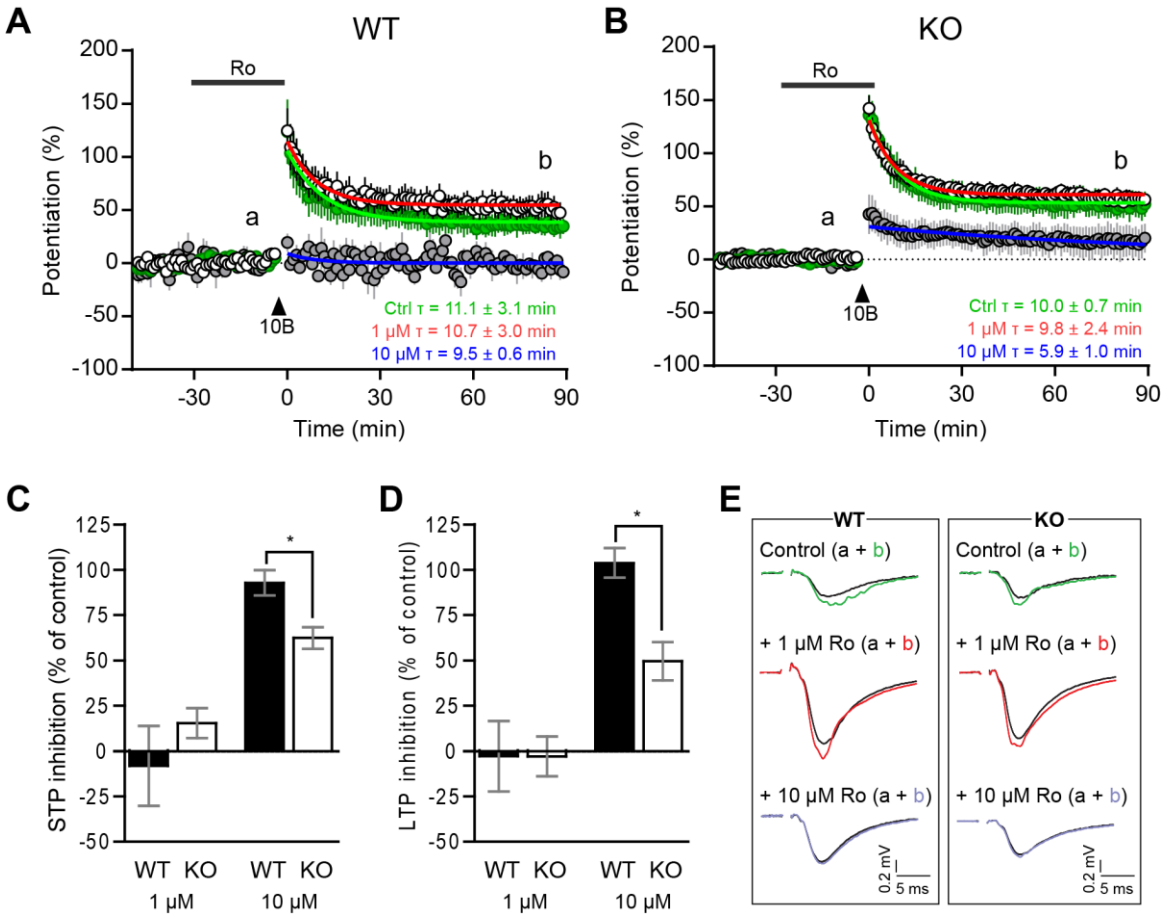

Figure 4.11. Ro 25-6981 blocks induction of STP and LTP more potently in WT than in GluN2D KO hippocampal slices. A, STP and LTP in WT slices: 1 µM Ro (white circles, STP = 63.0 ± 12.9%, LTP = 52.8 ± 10%, n = 7), 10 µM Ro (grey circles, STP = 4.2 ± 4.1%, LTP = -2.2 ± 4.7%, n = 3) and controls (green circles, STP = 58.3 ± 10.6%, LTP = 51.6 ± 2%, n = 7). Ro had no significant effects on the decay time constants of STP at 1 or 10 µM ($p > 0.05$ for both, MW test). **B,** STP and LTP in KO slices: 10 µM Ro (grey circles, STP = 31.7 ± 5.1%, LTP = 27.8 ± 5.8%, n = 5), 1 µM Ro (white circles, STP = 71.3 ± 7.0%, LTP = 56.8 ± 6.1%, n = 5), controls (green circles, STP = 84.3 ± 9.7%, LTP = 55.2 ± 3%, n = 9). The decay of STP after 10 µM Ro application had a trend towards faster decay compared to control ($p = 0.06$, MW test). Decay time constant of STP after application of 1 µM Ro was not statistically different to controls ($p > 0.05$, MW test). **C,** 10 µM Ro was more potent at inhibiting amplitude of STP in WT slices (92.8 ± 7.0%) when compared to the KO STP (62.4 ± 6.0%, $p < 0.05$, Student's t-test), but no significant differences were observed with 1 µM Ro ($p > 0.05$, Student's t-test). **D,** 10 µM Ro inhibited LTP to a greater extent in WT slices than in KO slices ($p < 0.05$, Student's t-test) whereas 1 µM Ro had no effects on LTP ($p > 0.05$, Student's t-test). **E,** Representative f-EPSPs from WT and KO slices at the time-points indicated in **A** and **B**.

4.3.8. GluN2D preferring antagonist UBP145 blocks STP and LTP in WT but not in GluN2D KO hippocampal slices

GluN2D containing receptors have been suggested to contribute to the induction of STP, especially affecting its decay time constant (Volianskis et al., 2013a; Ingram et al., 2018). To investigate the roles of GluN2D containing receptors, UBP145, a competitive antagonist with modest (~10-fold) selectivity for GluN2D over the GluN2A subunit was used in this study. 10 µM UBP145 had no significant effect on the amplitude of STP ($p > 0.05$, Student's t-test) but caused significant inhibition of LTP in WT slices (Figure 4.12A and D, $p < 0.05$, Student's t-test). Differently, STP and LTP from GluN2D KO slices were not significantly affected by 10 µM UBP145 (Figure 4.12B, $p > 0.05$, Student's t-test). These results suggest that in adult mice, GluN2D-containing NMDARs contribute to the induction of LTP and prolong the decay of STP. In contrast, in KO slices the GluN2D contribution to STP and LTP seems to be compensated by GluN2B- (Figure 4.11B) and GluN2A- (Figure 4.8 and Figure 4.10) containing receptors. Differences in decay time constants of potentiation between control and UBP145 treatment groups in WT and KO slices were not statistically significant ($p > 0.05$, MW test).

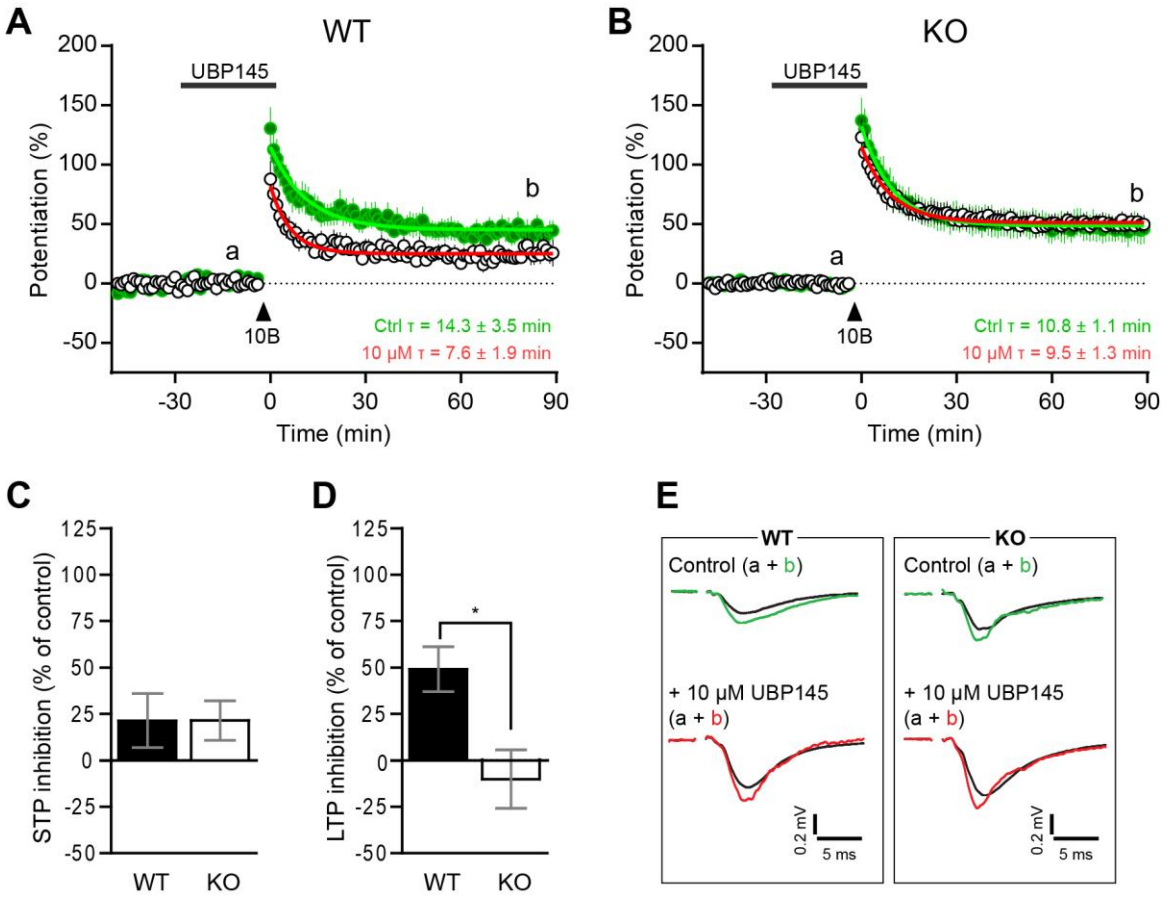

Figure 4.12. GluN2D antagonist UBP145 blocks induction of LTP in WT but not GluN2D KO hippocampal slices. A, Pooled experiments from WT slices showing that 10 μM UBP145 (white circles, STP = 55.8 ± 10.3%, LTP = 22.3 ± 5.3%, n = 7) blocked LTP compared to controls (green circles, STP = 71.0 ± 9.0%, LTP = 43.8 ± 7.4%, n = 7). UBP145 also had a moderate but non-significant effect on decay time constant of STP in WT slices ($p > 0.05$, MW test). **B,** In KO slices, UBP145 (white circles, STP = 65.3 ± 8.8%, LTP = 50.4 ± 7.2%, n = 9) had no effect on induction STP or LTP compared to controls (green circles, STP = 83.2 ± 14.0%, LTP = 45.8 ± 12.1%, n = 6). Decay time constants of STP were similar in 10 μM UBP145 and control groups in KO slices ($p > 0.05$, MW test). **C,** Inhibition of STP amplitudes were similar in WT (21.4 ± 14.5%) and KO (21.5 ± 10.6%) slices after 10 μM UBP145 application ($p > 0.05$, Student's t-test). **D,** Inhibition of LTP in WT (49.2 ± 12.1%) was greater compared to inhibition in KO slices (-10.1 ± 15.8%, $p < 0.05$). **E,** Representative f-EPSPs from WT and KO slices at the time-points indicated in **A** and **B**.

4.3.9. Increasing the number of bursts during induction of potentiation slows the decay of STP

Increasing the number of pulses during induction of potentiation has been shown to induce STP with a slower decay time constant (Volianskis and Jensen, 2003), which could suggest an increase in GluN2D and GluN2B mediated components of STP, although this has not been investigated using subunit-preferring antagonists. The contribution of GluN2B and GluN2D containing receptors to the decay phase of STP was investigated after inducing potentiation with higher number of pulses (referred to as 30-bursts in this study). In WT slices, the decay of STP was significantly slower when it was induced with 30-bursts when compared to 10-bursts (Figure 4.13A, $p < 0.05$, MW test). A noticeable slowing of STP decay was also observed in GluN2D KO slices, but the difference was non-significant ($p > 0.05$, MW test). 30-burst induction paradigm led to an increase in LTP in WT slices (Figure 4.13A and D, $p < 0.05$, Student's t-test) whereas the amplitude of STP remained the same as in the 10-bursts group (Figure 4.13A and C). In contrast, 30-burst induction did not affect the amplitudes of either STP or LTP in KO slices (Figure 4.13B, C and D). These results demonstrate that more intense stimulation can induce additional LTP in WT slices whereas LTP appears to be saturated in the KO slices (Figure 4.13D).

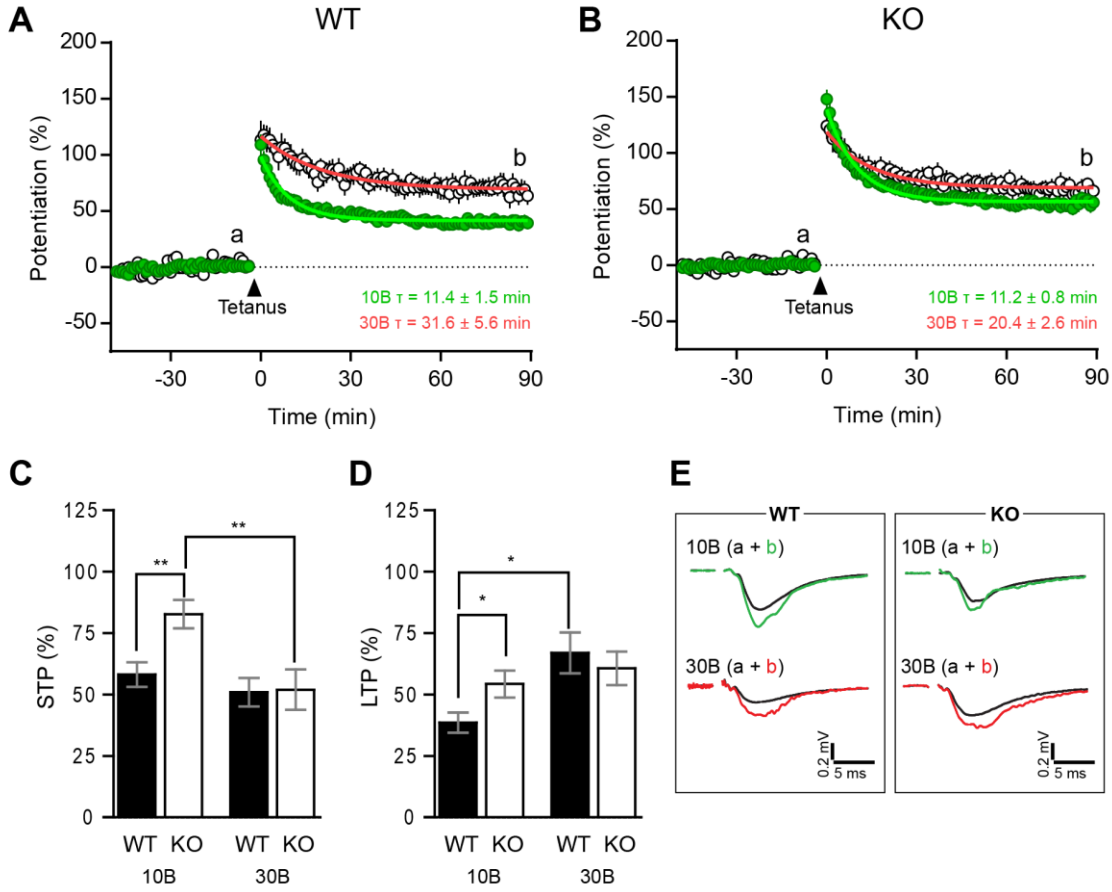

Figure 4.13. Number of bursts during LTP-induction affects the LTP and decay of STP in WT hippocampal slices. A, STP and LTP in WT slices: 10-bursts (green circles, n = 21) and 30-bursts (white circles, n = 11). Decay time constant for STP was significantly larger in the 30-bursts group compared to 10-bursts, in WT slices ($p < 0.001$, MW test). **B,** STP and LTP in KO slices: 10-bursts (green circles, n = 17) and 30-bursts (white circles, n = 16). In KO slices there was a ~2-fold increase in decay time constant of STP in 30-bursts group compared to 10-bursts group but the difference in decay time constants was not statistically significant ($p > 0.05$, MW test). **C,** STP amplitude was significantly higher in KO slices (82.8 ± 5.8%) compared to WT (58.1 ± 5.0%) in the 10-bursts group (data from Figure 4.6, $p < 0.05$, ANOVA, DT). STP amplitude were not different in the 30-bursts group between WT (51.0 ± 5.8%) and KO (52.0 ± 8.2%) slices ($p > 0.05$, ANOVA, DT). STP amplitude in KO slices was significantly lower in the 30-burst group than in the 10-burst group ($p < 0.05$, ANOVA, DT). STP amplitude was not different between 10-bursts and 30-bursts stimulation groups in WT slices ($p > 0.05$, ANOVA, DT). **D,** LTP induced by 10-bursts was significantly larger in KO slices (51.7 ± 5.7%) compared to WT slices (38.6 ± 4.5%) (data from Figure 4.6, $p < 0.05$, Student's t-test). Differently, LTP induced by 30-bursts in WT (66.9 ± 8.4%) and KO (60.7 ± 6.8%) slices were not statistically different ($p > 0.05$, Student's t-test). In WT slices, 30-bursts induced greater LTP when compared to 10-bursts ($p < 0.05$, ANOVA, DT). **E,** Representative f-EPSPs from WT and KO slices at the time-points indicated in **A** and **B**.

4.3.10. GluN2B antagonist Ro inhibits 30-bursts induced potentiation in WT and GluN2D KO slices

The amplitude and decay of STP and the amplitude of LTP, which were induced by 10-bursts in both WT and KO slices, were sensitive to 10 µM Ro but not to 1 µM Ro (Figure 4.11). These results appear to be in disagreement with the previously published observations in rat showing that decay of STP is highly sensitive to low concentrations of Ro (Volianskis et al., 2013a). Notably, STP decays noticeably slower in rat than in mice and the sensitivities of STP and LTP, which were induced by 30-bursts stimulation, to GluN2B antagonist Ro were therefore also tested (Figure 4.14). 1 µM Ro did not inhibit 30-bursts STP or LTP in WT slices but significantly blocked 30-bursts STP in GluN2D KO slices ($p < 0.01$, Student's t-test) and caused a trend towards inhibition of 30-bursts LTP ($p = 0.09$, Student's t-test) in KO slices.

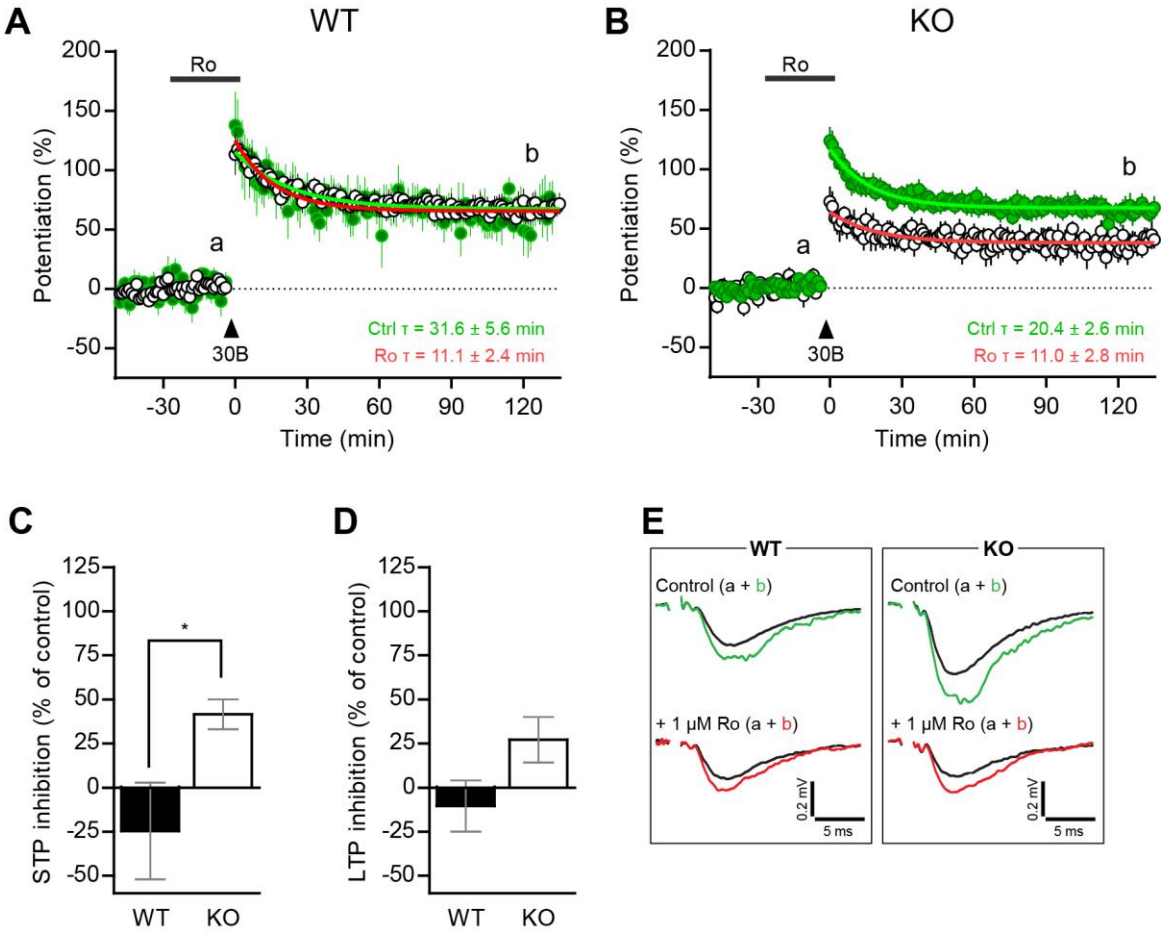

Figure 4.14. 1 µM Ro inhibits induction of STP and LTP induced by 30-bursts in GluN2D KO hippocampal slices. A, Pooled experiments from WT slices showing the effect of 1 µM Ro (white circles, STP = 63.6 ± 14.0%, LTP = 64.9 ± 8.5%, n = 4) on induction of STP and LTP compared to pooled control (green circles, STP = 51.0 ± 5.8%, LTP = 66.9 ± 8.3%, n = 11). Decay of STP was significantly faster in 1 µM Ro group compared to controls ($p < 0.05$, MW test). **B,** In KO slices, induction of STP and LTP by 30-bursts was inhibited by application of 1 µM Ro (white circles, STP = 30.4 ± 4.4%, LTP = 40.5 ± 7.2%, n = 6) compared to pooled control (green circles, STP = 52.0 ± 8.2%, LTP = 60.7 ± 6.8%, n = 16). There was a trend towards faster decay of STP by 1 µM Ro compared to control ($p = 0.07$, MW test). **C,** Inhibition of STP by 1 µM Ro was significantly higher in GluN2D KO slices (41.5 ± 8.5%) compared to WT (-24.7 ± 27.4%, $p < 0.01$, Student's t-test). **D,** Ro 1 µM produced a noticeably greater inhibition of 30-bursts induced LTP in GluN2D KO slices (27.1 ± 12.9%) compared to WT slices (-10.5 ± 14.5%); but the difference between WT and KO was not statistically significant ($p = 0.09$, Student's t-test). **E,** Representative f-EPSPs from WT and KO slices at the time-points indicated in **A** and **B**.

4.3.11. GluN2D subunits contribute to the induction of LTP by 30-bursts tetanus

In this study, GluN2D containing receptors contributed to the induction of 10-bursts LTP in WT slices, supported by the observation of a larger LTP amplitude in WT than in KO slices (Figure 4.6), and application of the GluN2D preferring antagonist UBP145 effectively reduced STP in the WT but not in the GluN2D KO (Figure 4.12). UBP145 was also tested with the 30-bursts induction paradigm (Figure 4.15). 10 μM UBP145 noticeably reduced amplitudes of STP and LTP in WT slices (Figure 4.15A, C, D) but the differences were not statistically significant compared to the effect on STP and LTP in KO slices (Figure 4.15B, C, D, $p > 0.05$ for both, Student's t-test). Interestingly, UBP145 also caused a non-significant but noticeable speeding up of the STP decay in WT (Figure 4.15A) but not KO slices (Figure 4.15B).

To further confirm the role of GluN2D in 30-bursts LTP in mice, a higher affinity antagonist with greater selectivity for GluN2D subunit, UBP791, was tested at 1 μM (Figure 4.16). UBP791 reduced 30-bursts LTP in WT slices more potently than in KO slices (Figure 4.16D, $p < 0.05$, Student's t-test) without affecting the amplitude of STP in either WT or KO slices (Figure 4.16C). However, 1 μM UBP791 caused a noticeable speeding up of decay of STP in WT (Figure 4.16A) but not GluN2D KO slices (Figure 4.16B). Taken together, these results provide further support for a role of GluN2D containing receptors in the induction of LTP in adult mice.

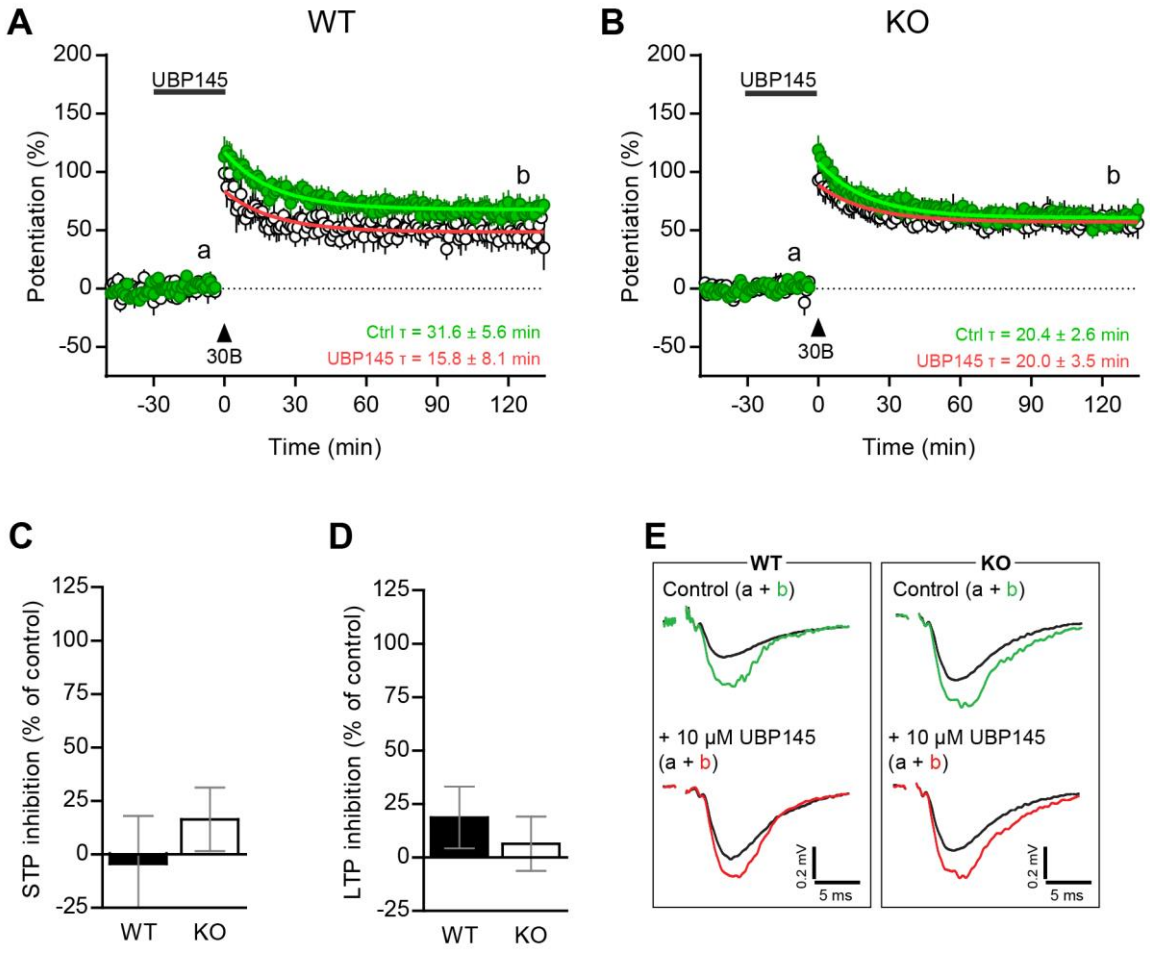

Figure 4.15. Effects of 10 µM UBP145 on 30-bursts-induced potentiation in WT slices. A, Pooled experiments from WT slices showing that 10 µM UBP145 (white circles, STP = 46.9 ± 10%, LTP = 47.8 ± 8.5%, n = 4) inhibited induction of LTP when compared to control (green circles, STP = 51.0 ± 5.8%, LTP = 66.9 ± 8.3%, n = 11). Decay time constant of STP was noticeably decreased by 10 µM UBP145 compared to controls but the difference was not statistically significant ($p > 0.05$, MW test). **B,** In KO slices, induction of STP and LTP by the 30-burst induction paradigm was not reduced by application of 10 µM UBP145 (white circles, STP = 39.9 ± 7.1%, LTP = 51.9 ± 7.1%, n = 6) compared to control (green circles, STP = 52.0 ± 8.2%, LTP = 60.7 ± 6.8%, n = 16). There was no significant difference in decay time constant of STP after application of 10 µM UBP145 compared to control ($p > 0.05$, MW test). **C,** STP induced by 30-bursts was inhibited by 10 µM UBP145 to similar levels in WT (-4.4 ± 22.3%) and KO (16.4 ± 14.9%) slices ($p > 0.05$, Student's t-test). **D,** Inhibition of 30-burst induced LTP by 10 µM UBP145 was not significantly different between WT (18.7 ± 14.4%) and GluN2D KO slices (6.4 ± 12.7%, $p > 0.05$, Student's t-test). **E,** Representative f-EPSPs from WT and KO slices at the time-points indicated in **A** and **B**.

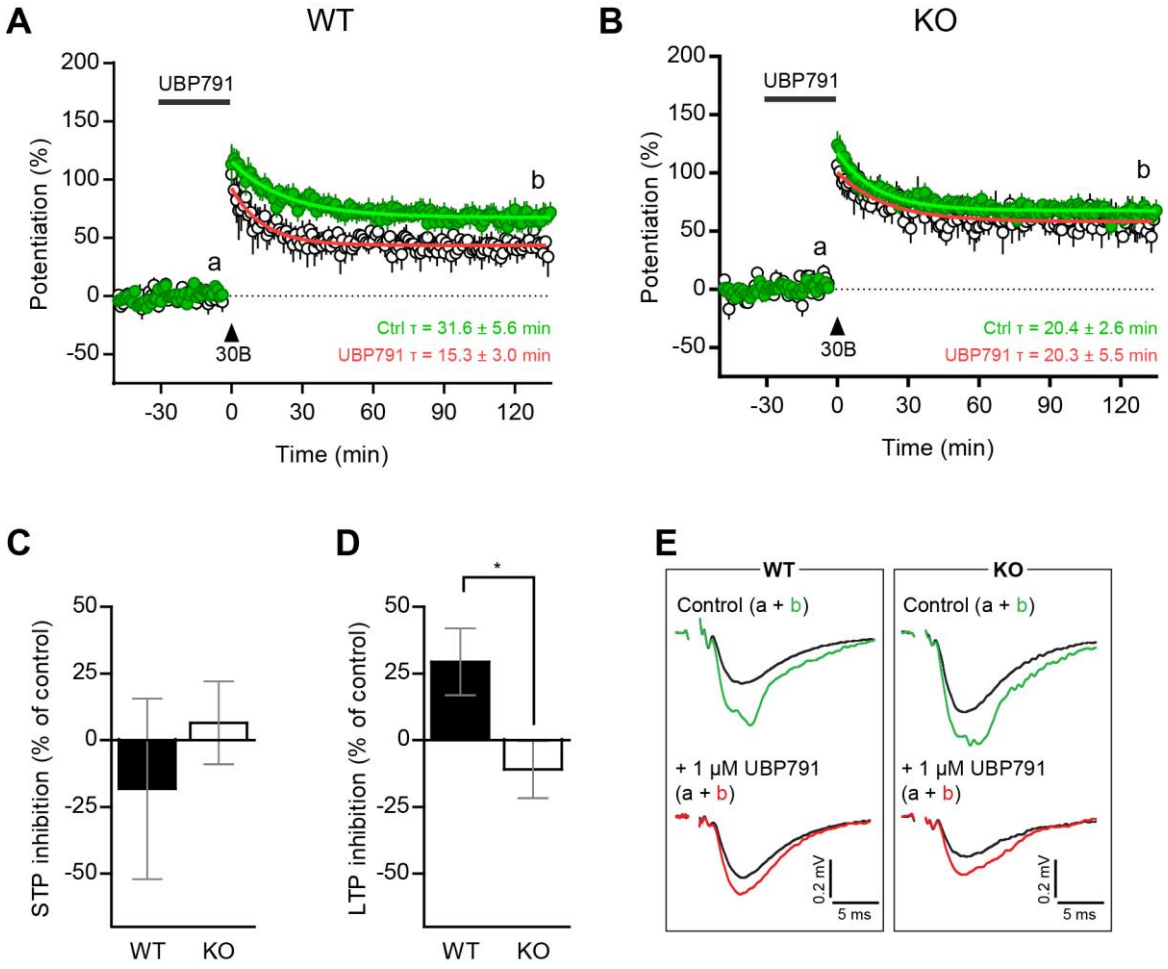

Figure 4.16. 1 µM UBP791 inhibits LTP induced by 30-bursts in WT slices. A, LTP, induced by 30-burst stimulation, was reduced by 1 µM UBP791 in WT slices (white circles, STP = 53.1 ± 15.2%, LTP = 41.5 ± 7.4%, n = 4) when compared to control (green circles, STP = 51.0 ± 5.8%, LTP = 66.9 ± 8.3%, n = 11). Decay time constant of STP was noticeably decreased in the 1 µM UBP791 group than in controls but the effect was not statistically significant ($p > 0.05$, MW test). **B,** In GluN2D KO slices, 1 µM UBP791 (white circles, STP = 44.6 ± 7.4%, LTP = 61.5 ± 6.0%, n = 4) did not inhibit induction of STP or LTP (green circles, STP = 52.0 ± 8.2%, LTP = 60.7 ± 6.8%, n = 16). There was no significant difference in the decay time constant of STP after application of 1 µM UBP791 when compared to that in the control ($p > 0.05$, MW test). **C,** The amplitude of STP induced by 30-bursts was inhibited by 1 µM UBP791 by similar levels in WT (-18.2 ± 33.8%) and in KO slices (6.6 ± 15.5%, $p > 0.05$, Student's t-test). **D,** LTP induced by 30-burst was inhibited more by 1 µM UBP791 in WT slices (29.4 ± 12.5%) compared to KO slices (-10.9 ± 10.7%, $p < 0.05$, Student's t-test). **E,** Representative f-EPSPs from WT and KO slices at the time-points indicated in **A** and **B**.

4.4. Discussion

Investigations into the contribution of GluN2D subunits to hippocampal synaptic plasticity have suffered due to a lack of GluN2D selective antagonists. In this study, a combination of global GluN2D knockout mice and GluN2A, 2B or 2D subunit antagonists with moderate-good subunit selectivity were used to dissect the roles of GluN2D receptors in synaptic plasticity in the hippocampus of adult mice.

4.4.1. Significance of GluN2D receptors for synaptic neurotransmission

WT and GluN2D KO slices had similar synaptic baseline transmission at the SC-CA1 synapse but maximum neuronal excitability in the CA1 region of the hippocampus was lower in GluN2D KO slices compared to WT slices (Figure 4.2). This change in maximum excitability may not be due to impaired interneuron function in GluN2D KO slices because blocking GABAergic transmission in GluN2D KO mice did not increase maximum population spike area (Figure 4.5). However, long-term GluN2D knockout could lead to emergence of compensating mechanisms that control maximum cell excitability independently from GABAergic transmission. Additionally, the cell excitability may also be controlled by extrasynaptic GluN2D-containing receptors in the CA1 (Lozovaya et al., 2004).

4.4.2. GluN2D receptors and STP

A GluN2A and GluN2B selective concentration of D-AP5 (1 μM) inhibited STP in WT and GluN2D KO slices (Figure 4.8). Moreover, inhibition of GluN2A subunits with 1 μM NVP reduced STP in WT and KO slices (Figure 4.10) and 10 μM (but not 1 μM) Ro reduced STP in both WT and KO slices (Figure 4.11). Collectively, these results suggest that GluN2A- and GluN2B-containing receptors (possibly as GluN2A/GluN2B triheteromeric receptors) mediate induction of STP in adult mice, as found in rats (Volianskis et al., 2013a; France et al., 2017; Ingram et al., 2018).

GluN2D KO slices had an enhanced amplitude of STP but similar decay of STP compared to WT slices (Figure 4.6). The increase in STP in KO slices may be due to the impairment of GABAergic transmission that is mediated by interneurons that express GluN2D-containing receptors (Engelhardt et al., 2015; Perszyk et al., 2016). In support of this hypothesis, inhibition of GABAergic transmission resulted in similar levels of STP in both

WT and KO slices (Figure 4.7). Another explanation for the higher levels of STP in GluN2D KO slices is that diheteromeric and/or triheteromeric formations of GluN2A and GluN2B subunits compensated for lack of GluN2D subunits in the GluN2D KO slices which may have led to higher levels of STP in KO slices. In support of this, STP in GluN2D KO slices had greater sensitivity to block by GluN2A- and GluN2B-selective concentration of D-AP5 compared to WT slices (Figure 4.8C), and 10 μM Ro inhibited STP in WT slices more potently when compared to KO slices (Figure 4.11C) whereas 1 μM Ro had no effect on STP in WT or KO slices (Figure 4.11C). Therefore, the increased STP in KO slices may be due to an increase in the contribution from GluN2A containing diheteromers and/or GluN2A/2B triheteromers to the induction of STP because 1 μM D-AP5 inhibits GluN2A and GluN2B subunits (Feng et al., 2005) and 10 μM Ro may inhibit GluN2A/2B triheteromers according to binding affinity data on the recombinant GluN2A/2B triheteromeric receptor (K_d ~130 nM) (Lü et al., 2017). Interestingly, the GluN2D-selective antagonist UBP145 had no significant effect on STP in adult WT mice (Figure 4.12C), suggesting that GluN2D-containing receptors are not directly involved in induction of STP in adult mice. This is different from previous findings that GluN2D subunits contribute to STP decay in adult rats (Volianskis et al., 2013a; Ingram et al., 2018), and this observation may be explained most simply by the difference in species. We also confirmed previous observations that GluN2B-containing diheteromeric receptors may not contribute to induction of STP in the SC-CA1 synapse of adult mice (Köhr et al., 2003; Romberg et al., 2009). This result further highlights the species difference compared to rat SC-CA1 synapse, where 1 μM Ro inhibited ~60% of STP, a large part of which contributed to the decay of STP in rat slices (Volianskis et al., 2013a). Another notable difference between mouse and rat slices is that TBS-induced STP in WT mice decayed at a faster rate ($\tau \approx 11$ min) in the current study (Figure 4.6A) compared to the study in Wistar rats ($\tau \approx 16$ min) (Volianskis et al., 2013a). Whether this difference in decay rate reflects the difference in underlying subunit population between the two species is a valid question that needs further investigation.

Increasing both the number of bursts (from 10 to 30) and the frequency of the bursts (from 5 to 15 Hz) in the train whilst keeping the total duration of the train unchanged during induction of potentiation led to a decrease in STP amplitude in GluN2D KO mice and a considerable slowing of STP decay in both WT and KO mice when compared to 10-bursts

induced STP (Figure 4.13). The simplest explanation for this increase in decay of STP in WT slices is an increase in contribution from GluN2B- and GluN2D-containing triheteromeric receptors to STP. Indirect evidence for this suggestion is provided from experiments where 1 μM Ro had no effect on 30-bursts STP amplitude or decay in WT slices but resulted in a significant inhibition of STP amplitude in GluN2D KO slices (Figure 4.9). It is possible that in GluN2D KO mice, the triheteromeric GluN2B/2D NMDARs that contribute to STP at 30-bursts in WT animals are replaced by diheteromeric GluN2B containing NMDARs. In support of this idea, UBP145 and the more GluN2D selective antagonist, UBP791, had no effect on STP amplitude or decay at concentrations that are selective for GluN2D containing diheteromeric receptors.

In summary, the 30-burst experiment results suggest that an additional population of receptors containing the GluN2B-subunit may be involved when the number of bursts during tetanus is increased to 30-bursts. Whether this receptor population also contains the GluN2D-subunit in addition to GluN2B requires further investigation. Receptors that are recruited during 30-bursts could be extrasynaptic, activated by glutamate spillover due to saturation of uptake mechanisms (Asztely et al., 1997). Whether these extrasynaptic GluN2B/2D containing receptors also contribute to neuronal excitability is a valid question that also requires further investigation.

4.4.3. GluN2D receptors and LTP

LTP in adult mice was mediated by GluN2A- (Figure 4.10), GluN2B- (Figure 4.11), and GluN2D- (Figure 4.12) containing receptors. The contribution of the GluN2B subunit to LTP in adult mice was likely as part of a triheteromeric receptor containing the GluN2A subunit. This conclusion can be reached because 1 μM Ro, which is selective for diheteromeric 2B containing receptors, had no effect on LTP (Figure 4.11D) but 10 μM Ro (Figure 4.11D) and 1 μM D-AP5 (Figure 4.8D) (both of which block GluN2A and GluN2B subunits) caused inhibition of LTP. Whether the inhibition of LTP by NVP is due to its effect on GluN2A-containing diheteromeric receptors or GluN2A/2B-containing triheteromers needs further investigation. Therefore, in adult mice as in adult and in P14 rat hippocampus (Volianskis et al., 2013a; France et al., 2017), GluN2A- and GluN2B-containing receptors are involved in the induction of LTP in the SC-CA1 synapse. However, in mouse hippocampus unlike in rat hippocampus, GluN2D-containing receptors

also contribute to the induction of LTP in the SC-CA1 synapse (Figure 4.12). This GluN2D component of LTP seems to be in addition to the GluN2A and GluN2B mediated component(s) because in WT slices, LTP is completely blocked by 10 µM Ro, a concentration of Ro that has been shown to not affect diheteromeric GluN2D-containing NMDARs expressed in HEK293 cells (Volianskis et al., 2013a).

Pooled data showed that LTP in GluN2D KO slices was enhanced compared to WT slices (Figure 4.6). One explanation for this result was that the absence of GluN2D-containing receptors in GABAergic interneurons may have caused reduced inhibitory control of LTP induction in GluN2D KO slices. Inhibition of GABAergic transmission resulted in similar levels of LTP in both WT and GluN2D KO slices (Figure 4.7). These results corroborate previous findings that postsynaptic GABAergic transmission contributes to the threshold for induction of LTP at the SC-CA1 synapse (Wigström and Gustafsson, 1983) and that GluN2D receptors may be expressed on interneurons in the CA1 (Engelhardt et al., 2015; Perszyk et al., 2016; Alsaad et al., 2019).

Another possible explanation for the enhancement of LTP induction in GluN2D KO slices is that GluN2D-containing receptors directly contribute to the induction of LTP in WT mice and that long-term deletion of the GluN2D subunit leads to compensation via increased contribution from GluN2A- and/or GluN2B-containing receptors. However, GluN2A and GluN2B selective concentrations of D-AP5 (1 µM) partially inhibited LTP induction in GluN2D KO slices and WT slices to similar amounts. LTP in WT slices was more potently inhibited by 10 µM Ro compared to KO slices (Figure 4.11D), suggesting that the contribution of GluN2A/2B triheteromeric NMDARs to LTP in WT slices is larger than in KO slices. The remaining LTP in KO slices in the presence of 10 µM Ro may have been mediated by GluN2A-containing diheteromers because this residual LTP component in GluN2D KO slices was not present when all NMDAR subunits were blocked with 100 µM D-AP5 (Figure 4.8D) or 10 µM L689,560 (Figure 4.9D).

Interestingly, when inducing LTP with 30-bursts, LTP amplitude in WT slices increased but the LTP in GluN2D KO slices remained at the same levels as after 10-burst induction (Figure 4.13D). This increase in LTP at 30-bursts in WT slices may be due to an increase in contribution from GluN2B and GluN2D containing receptors. Moreover, 10 µM

UBP145 in WT slices non-significantly reduced 30-burst LTP (Figure 4.15D) and the higher affinity GluN2D antagonist UBP791 significantly reduced LTP amplitude (Figure 4.16D), suggesting that GluN2D-containing receptors may also mediate LTP when the numbers of bursts used for induction of potentiation increase. Surprisingly, 30-burst LTP in GluN2D KO slices was sensitive to 1 μM Ro (Figure 4.14D), a concentration that produced no effect in 10-burst LTP, suggesting that in the absence of GluN2D-containing receptors, GluN2B-containing diheteromers may have had an increased contribution to induction of LTP (as in the case for STP, above) when the number of bursts is increased in KO slices. The GluN2D-containing receptors in WTs (and the compensatory GluN2Bs in KOs), which contribute to the induction of LTP in mice, may be located extrasynaptically on the CA1 pyramidal cells or presynaptically on Schaffer collateral boutons. To verify whether the CA1 pyramidal cells express GluN2D-containing receptors, the GluN2D selective antagonist UBP791 can be used to investigate the current decay of CA1 pyramidal cells when glutamate reuptake is inhibited (using TBOA, a blocker of excitatory amino acid transporters) to allow glutamate activation of the extrasynaptic GluN2D-containing receptors.

Chapter 5

General Discussion

The current study focused on enquiries into two types of studies involving the development of new pharmacological tools for GluK2-containing KARs and the functions of GluN2D-containing NMDARs. Firstly, biological characterisation and molecular modelling of chemical entities that targeted GluK2 subunits were carried out, in order to aid the development of novel high-affinity GluK2-selective antagonists. The main findings of the present study have corroborated previous observations (Culley, Mallah, Thatcher, Irvine, Wood and Jane, unpublished) and developed novel SAR hypotheses for obtaining GluK2 over GluK1/AMPAR selectivity. Using computational modelling and evidence from pharmacological characterisation of kynurenic acid derivatives, it was found that in the GluK2 LBD, the space occupied by 6-substituents of kynurenic acid derivatives, near residues Asn-690, Met-706, and Thr-710 in GluK2, may be targeted for improvement of GluK2 over AMPAR (GluA1/GluA2) and GluK1 selectivity (Chapter 3). Secondly, a physiological study of the NMDAR subunit GluN2D was conducted, which demonstrated that GluN2D subunits control neuronal excitability and contribute to potentiation of synaptic transmission in the SC-CA1 hippocampal synapse (Chapter 4). The study of GluN2D subunits also corroborated the GluN2D selectivity of UBP145 and the novel GluN2D antagonist UBP791 (Sapkota, 2016).

5.1. Conclusions from pharmacological characterisation and molecular modelling of novel GluK2-selective antagonists

5.1.1. The need for GluK2-selective antagonists

The KAR family of glutamate receptors are comprised of five subunits (GluK1-5) that are expressed throughout the CNS (Monaghan and Cotman, 1982; Wisden and Seeburg, 1993). Studies of KARs in the hippocampus have suggested that KAR subunits are expressed in a target-, region- and age-specific manner (Bahn et al., 1994; Castillo et al., 1997; Bortolotto et al., 1999; Mulle et al., 2000; Sun and Dobrunz, 2006). Therefore, studies examining the roles of distinct KAR subunits will require the ability to target specific subunits. Advances in genetic techniques mean that region- and age-specific conditional knockouts of one or more types of KAR subunits are possible (Contractor et al., 2001; Xu et al., 2017). However, structural studies, in vitro and in vivo functional studies, and therapeutic targeting of KAR subunits can be enhanced using subunit-selective pharmacological tools.

Development of KAR subunit-selective antagonists have been difficult due to the overlap in pharmacology between KARs and AMPARs, and between KAR subunits themselves. Using a combination of GluK1-selective antagonists (Dolman et al., 2005; Jones et al., 2006) (some with possible activity on GluK3 subunits (Perrais et al., 2009)), pan-KAR antagonists (Jane et al., 2009), genetic knockout mice lacking KAR subunits (Contractor et al., 2001) and AMPAR-selective antagonists (Paternain et al., 1995; Bortolotto et al., 1999) (with possible activity on GluK3 at high concentrations (Perrais et al., 2009)), KARs have been found to be involved in positive and negative regulation of synaptic transmission in the hippocampus (Carta et al., 2014). However, the identity of the specific subunits that carry out many KAR functions are still unknown due to a lack of subunit selective antagonists (Jane et al., 2009). As a result, questions regarding the contribution of GluK1 or GluK2 subunits to synaptic plasticity mechanisms have been raised (Bortolotto et al., 1999; Contractor et al., 2001; Breustedt and Schmitz, 2004), highlighting the need for GluK2 selective antagonists.

Few studies have focused on the development of GluK2-selective antagonists. The early KAR antagonist, NS-102, had ~6-fold selectivity for GluK2 over GluK1 but suffered from poor water solubility (Verdoorn et al., 1994; Wilding and Huettner, 1996). Studies in the intervening period also revealed that a class of GluK2 antagonists based on 2-aminothiopene inhibited GluK2 subunits with ~16-fold selectivity over GluK1 but these compounds were not fully characterised on other KAR subunits or AMPARs (Briel et al., 2010). Other studies too have found GluK2 antagonists with at best moderate (~10-fold) selectivity for GluK2 over GluK1 or AMPARs but suffered from lack of characterisation on GluK1, GluK3, AMPARs or NMDARs (Dildy-Mayfield et al., 1996; Schiavini et al., 2015). Therefore, a new a lead for the development of GluK2-selective antagonists was required.

5.1.2. Findings from the current study

Kynurenic acid derivatives with 5,7-substitutions have found use as potent antagonists of the glycine site of NMDARs (Baron et al., 1990). However, 6-substitutions made on kynurenic acid reduced NMDAR activity (Leeson et al., 1991). Due to the cross-activation of AMPARs and KARs by both kainate and quisqualate (the agonists first used to assay antagonists), the affinity of 6-substituted kynurenic acid derivatives on KARs and

AMPARs remained to be determined (Leeson et al., 1991). Earlier investigations by Jane and co-workers have shown that 6-substituted kynurenic acid derivatives had different activities on GluK2 subunits compared to GluK1 or GluA1 (Culley, Mallah, Thatcher, Irvine, Wood and Jane, unpublished). However, conflicting results regarding the activity of kynurenates on recombinant homomeric AMPARs warranted further characterisation of kynurenic acid derivatives. In addition to the older 6-substituted kynurenates, novel newly synthesised kynurenic acid derivatives were also characterised on two functional assays: a calcium fluorescence assay using recombinant GluK2, GluK1 and GluA1 homomeric receptors, and an electrophysiological assay in which activities of compounds were characterised on AMPAR- and NMDAR-mediated f-EPSPs from hippocampal slices.

In the current study, an SAR for the kynurenic acid derivatives was developed (Chapter 2). The results demonstrated that UBP2038 (5,7-diF-6-I) had the highest affinity on GluK2 (Table 2.3). Removal of the 5,7-diF substituents from UBP2038 leads to UBP2002 (6-I) which had noticeably lower affinity on GluK2 than UBP2038. Furthermore, presence of the 6-ethyl hydrophobic group at the 6-position led to significantly lower activity on GluK1 (IC_{50} > 1 mM) and GluA1 (IC_{50} > 2mM) but retained the GluK2 activity (K_i = 54.0 ± 10.9 μM) (Table 2.3). The activity profile of UBP2054 (6-Et) is different from that UBP2034 (6-Me) which had no GluK2 over GluK1 selectivity (ratio of GluK1 and GluK2 K_i values = 1.0, Table 2.3).

Improving the GluK2 affinity is an important factor in developing effective pharmacological agents. Based on results from the present study, a possibility for improving GluK2 affinity of kynurenates was the introduction of halo substituents on the 5,7-positions of kynurenic acid. In support of this, it was shown that the high GluK2 affinity of UBP2038 (5,7-difluoro-6-iodo) may be due to increased number of electrostatic and van der Waals interactions between the 5- and 7-substituents of UBP2038 and the Tyr-412 and Asn-690, respectively, compared to UBP2002 (6-iodo) which lacked the 5,7-substitutions (Figure 3.8). It may be possible to improve the affinity of the more GluK2 over GluK1/AMPAR selective UBP2054 (6-Et) by introducing 5,7-diF substitutions on UBP2054. Such a modification could lead to increased affinity but with no detrimental effect on selectivity because it is the 6-Et substituent's increased solvent exposure and steric clashes, which determines the GluK2 selectivity over GluK1 and AMPARs.

Validation of SAR using data from the pharmacological studies was carried out with molecular docking studies using X-ray crystal structures of GluN1, GluK1 and GluA2 LBDs (Armstrong and Gouaux, 2000; Furukawa and Gouaux, 2003; Alushin et al., 2011), and a GluK2 homology model based on the X-ray crystal structure of GluK1 bound to UBP315 (Alushin et al., 2011).

Results from the present study showed that steric clashes between the 6-substituent and Trp-731 and Val-735 residues in GluN1 LBD may explain the reduced activity of 6-substituted kynurenic acids on NMDARs (Figure 3.16). In support of this, docking revealed that the 6-substituent of UBP2002 (6-I) had steric clashes with the surface of the binding cavity near the tryptophan and valine residues, whereas UBP2040 (5,7-diF-6-H) was well accommodated into the binding cavity (Figure 3.17) with minimal van der Waals volume overlaps.

The initial hurdle for obtaining GluK2 (and other KAR subunits) selective antagonists is to ensure high selectivity of compounds for GluK2 over AMPARs. This task is made difficult by the high level of amino acid sequence similarity between the AMPARs and GluK2 at the ligand binding site (Figure 3.4). Results from the current study suggest that a combination of reduced binding site volume in AMPARs compared to GluK2, and the switch of Thr-686 and Met-708 residues in GluA2/GluA1 to Asn and Thr in GluK2 (near the kynurenic acid 6-substituent) may be exploited to obtain GluK2 over AMPAR selectivity (Figure 3.14). Using the 6-ethyl kynurenate, UBP2054, and the smaller 6-substituent in UBP2002 (6-iodo) it was shown that the bulkier 6-substituent in UBP2054 had greater steric clashes with Thr-686 and Met-708 residues in the GluA2 LBD, whereas steric clashes were reduced with UBP2002 (Figure 3.15); however, the larger 6-ethyl substituent of UBP2054 was accommodated into the binding site in the GluK2 LBD (Figure 3.13).

An additional aim of the pharmacological studies was to obtain compounds with greater GluK2 over GluK1 selectivity. This task was hampered by even greater amino acid sequence homology between the GluK2 and GluK1 subunits than between GluK2 and AMPARs (Figure 3.3). Surprisingly, we found that the UBP2054 (6-Et) had noticeably lower GluK1 activity compared to the smaller 6-substituent UBP2034 (6-Me). The

molecular modelling study provided 2 main explanations for the reduced GluK1 affinity of UBP2054: firstly, the greater volume available in the GluK1 binding site exposed larger portions of the hydrophobic 6-Et substituent of UBP2054 to solvent than the smaller 6-Me substituent in UBP2034; secondly, the smaller binding site of GluK2 meant that the hydrophobic Met-706 residue in GluK2 was in proximity to the 6-Et substituent of UBP2054 to be involved in van der Waals interactions and therefore, improve GluK2 affinity. A third explanation for the GluK2 over GluK1 affinity of UBP2054 was provided by the presence of Thr-710 in GluK2 near the 6-substituent. The non-conserved Thr-710 residue in GluK2 contains a methyl group which may be able to form hydrophobic interactions with the 6-Et substituent in UBP2054. The Thr-710 is replaced by a serine in GluK1 which lacks the methyl group that can form interactions with 6-Et group of UBP2054.

In summary, the results from the current study provide a novel basis for development of GluK2 antagonists with greater GluK2 affinity and GluK2 over GluK1 and AMPAR selectivity. In addition, UBP2054 has been identified as a GluK2 antagonist with good selectivity vs AMPARs and ~10-fold selectivity for GluK2 versus GluK1. As such it is the most selective GluK2 antagonist reported to date and will be a useful pharmacological tool in functional studies to probe the physiological roles of GluK2.

5.2. Future studies of GluK2 antagonists

5.2.1. Validating results from the current study

While pharmacological characterisation of UBP2054 has led to discovering its potential as a GluK2-selective antagonist, more work is required to validate the conclusions from SAR and modelling studies regarding the molecular basis of its GluK2 selectivity.

The hypotheses regarding GluK2 over GluK1/AMPAR selectivity of UBP2054 developed in this study can be tested by point-mutation of non-conserved GluK2 residues to those in GluK1 or GluA1 LBDs, followed by radioligand binding assays to test the affinities of UBP2054 on the receptor which containing the point-mutated version of the subunit. Similar mutagenesis studies have been used previously to explain the GluK1 selectivity of willardiine derived GluK1 antagonists such as UBP310 and ACET (Atlason et al., 2010).

The residues which were found to be responsible for GluK2 selectivity over GluK1 and GluA2 in the current modelling study were Asn-690, Met-706 and Thr-710 in GluK2, which corresponded to Ser-706, Met-722 and Ser-726 in GluK1, and Thr-686, Leu-704, Met-706 in GluA2 (residues were the same in GluA1), respectively. The GluK2 over GluK1 selectivity can be investigated by point-mutating the Asn-690 and Thr-710 residues in GluK2 to the corresponding residues found in GluK1: which expresses serine in both positions, to eliminate the hydrophobic interactions provided by the two GluK2 residues which were absent in GluK1 due to the larger binding site volume. GluK2 subunits with these point mutations should have lower binding affinity (closer to the affinity for GluK1 subunits) for UBP2054. The hypothesis for GluK2 over AMPAR selectivity can be verified by point mutating GluA2 residues (or the corresponding GluA1 residues): Thr-686 and Met-706 in GluA2 to the asparagine and threonine, respectively, found in GluK2. GluA2 or GluA1 subunits with these point-mutations should have higher affinity for binding of UBP2054 compared to the WT, non-mutated subunit.

A more time- and effort-intensive method for validation of the GluK2 binding mode of UBP2054 is to obtain the X-ray crystal structure of the isolated GluK2 LBD in complex with UBP2054. The X-ray structure of GluN1 in complex with DCKA has greatly aided the structural understanding of the GluN1 LBD in the antagonist-bound state and has helped to validate docking poses of kynurenates used in this study (Furukawa and Gouaux, 2003) (Figure 3.16). A similar advantage could be gained with solving of the GluK2 LBD structure in combination with UBP2054. The process of obtaining a GluK2 structure is made difficult by the poor affinity and water solubility of co-crystallised ligands (Jane et al., 2009; Møllerud et al., 2017). According to the current study, UBP2054 had GluK2 K_i of 54 μM (Table 2.3), which may not be sufficient to obtain X-ray crystal structures. Therefore, the higher affinity but lower GluK2-selective kynurenate, UBP2038, may be used to obtain the X-ray crystal structure, as it has greater water solubility compared to UBP2054.

Another strategy for improving GluK2 affinity of UBP2054 is to introduce substitutions on the quinolone ring at positions other than the 6-position which will lead to formation of a higher number of contacts with residues in the D2 of the GluK2 ligand binding cleft by UBP2054. GluK1 antagonists such as ACET (Dargan et al., 2009) or LY466195 (Alushin

et al., 2011) and AMPAR antagonist ATPO have all been shown to have many interactions with residues in the D2 of LBD, which likely explains their high affinities. A residue in the D2 of KARs that has been found to be important for increasing affinity of ACET is Val-654 in GluK2 and Val-670 in GluK1 which is replaced by the larger Leu-650 in GluA2. Therefore, substitutions that would interact with the valine in KARs may improve the affinity and GluK2 versus AMPAR selectivity of novel compounds.

5.2.2. Improving GluK2 affinity and selectivity of UBP2054

Improving GluK2 affinity and selectivity of UBP2054 requires additional substitutions to be made on the kynurenate's structure such that greater number of interactions with D2 residues can be made (for affinity) and specific interactions that target the non-conserved residues in GluK2 can be made (for selectivity).

However, the task of increasing ligand-receptor contacts by kynurenates is made difficult by the planarity of the kynurenate structure which reduces the number of rotatable bonds in the kynurenate structure and therefore limits the contacts it can make with non-conserved residues in the GluK2 LBD's D2 region. Kynurenates are oriented in the GluK2 ligand binding cleft to form H-bond interactions between the kynurenate's 2-carboxy group and arginine and alanine residues in the D1, and the kynurenate's 1-NH and proline residue in the D1 (Figure 3.7). Such an orientation of the kynurenate in the ligand binding site limits the number of interactions that are possible between kynurenates and D2 residues of GluK2 LBD.

One solution to improve the number of ligand-receptor interactions is to "open" the kynurenate structure by increasing the number of rotatable bonds and hence the flexibility of the ligand. However, a greater conformational penalty that is required to bind more "open" compounds means that there is a greater loss of entropy upon binding of the "open" compounds and this entropic penalty must be compensated by electrostatic or van der Waals interactions between the compound and the LBD to ensure high binding affinity. Thus, further work is needed to modify the structure of open chain compounds to increase the number of interactions with residues in the S1 and S2 domains

In addition to improving the GluK2 selectivity and affinity, the aqueous solubility of novel compounds based on UBP2054 must be adequate for use in physiological studies and therapeutics. To complement the 1-NH, 2-carboxyl, and 4-oxo groups, all of which can form H-bond interactions with water molecules, heteroatom substitutions, particularly nitrogen substitutions, can be made on the kynurenate ring structure to improve aqueous solubility. An example of improving water solubility by inducing nitrogen atoms in a structure similar to kynurenic acid was provided by the quinoxalinedione derivative, CNG-10300, which had a substituent containing a three-carbon chain terminated by electronegative oxygen and nitrogen atoms (Demmer et al., 2015). This modification improved the water solubility of CNG-10300 significantly compared to other quinoxalinediones such as DNQX which did not have this modification (Demmer et al., 2015). However, any modifications to improve water solubility in UBP2054 must not interrupt the ligand-receptor interactions that are necessary for the GluK2 affinity or selectivity.

5.2.3. Further characterisation of UBP2054

Although UBP2054 has been characterised on recombinant GluK2, GluK1, GluA1 homomeric receptors, the activity of UBP2054 and other kynurenates on heteromeric KARs is yet to be determined. The activity of potential GluK2 antagonists on heteromeric KARs is important because in native tissue, KAR subunits are found as part of a heteromeric complex containing at least two different KAR subunits – usually a high affinity subunit (GluK4 or GluK5) in combination with a low affinity subunit (GluK1-3). In the hippocampus, all five KAR subunits are expressed but GluK5 and GluK2 shows the highest level of expression (Herb et al., 1992; Wisden and Seeburg, 1993; Paternain et al., 2000). GluK1 is thought to be expressed in hippocampal CA1 interneurons due to its punctate expression throughout all layers of the hippocampus, while GluK2 is expressed in the principle cells of CA3 and CA1 (Monaghan and Cotman, 1982; Wisden and Seeburg, 1993). GluK3 expression is highest in the dentate gyrus of the hippocampus and GluK4 is highly expressed in the CA3 pyramidal cell layer (Monaghan and Cotman, 1982; Wisden and Seeburg, 1993). Functional KARs are thought to be expressed as heteromers (Mulle et al., 2000). Therefore, the characterisation of UBP2054 and other kynurenates on heteromeric GluK2/GluK5 and GluK2/GluK3 KARs requires urgent consideration. Heteromeric GluK2/GluK5 complexes of KARs that are useful for characterisation of

UBP2054 and other kynurenates may be expressed in heterologous systems such as HEK293 cells (Paternain et al., 2000; Alt et al., 2004; Perrais et al., 2009) or may be found in CA3 pyramidal cells of hippocampal slices (Herb et al., 1992).

An important validation of the usefulness of UBP2054 for physiological studies is to confirm that it inhibits native GluK2-containing KARs. Postsynaptic responses mediated by KARs have been isolated in the interneurons in CA1 (Cossart et al., 1998; Frerking et al., 1998). In the CA3 synapses made by mossy fibre axons, postsynaptic excitatory potentials mediated by GluK2-containing KARs have been observed (Castillo et al., 1997). Postsynaptic currents in the MF-CA3 synapses is mediated by GluK2, GluK4 and GluK5 subunits whereas presynaptic GluK2/GluK3-containing KARs also mediates synaptic plasticity at the MF-CA3 synapse (Castillo et al., 1997; Contractor et al., 2001, 2003). Various manifestations of synaptic plasticity including frequency facilitation of MF-CA3 postsynaptic responses, LTP, and paired pulse facilitation have all been shown to involve participation by GluK2 in the MF-CA3 pyramidal cell synapse (Mulle et al., 1998; Contractor et al., 2001). Therefore, the different forms of synaptic plasticity in the MF-CA3 synapse provides a suitable candidate for characterisation of UBP2054 on native GluK2-mediated mechanisms. Although it was shown that UBP2054 had native AMPAR IC_{50} > 300 μM in the CA1 (Figure 2.13), the slight inhibition of AMPARs in the CA3 by UBP2054 (Figure 2.12C) may complicate interpretation of physiological studies of UBP2054. Therefore AMPARs can be completely inhibited using the AMPAR-selective antagonist GYKI53655 (Paternain et al., 1995) at low concentration to avoid cross-inhibition of GluK3 subunits (or GluK2/GluK3 heteromeric KARs) (Perrais et al., 2009). Such pharmacological inhibition of AMPARs would help an isolated study of KARs and investigations into actions of KAR antagonists. In addition to AMPARs, the presence of GluK1 subunits in the MF-CA3 synapses may also complicate native inhibition of GluK2 by UBP2054 (Wisden and Seeburg, 1993). One solution is to isolate GluK2 response using GluK1 antagonists such as LY466195 or ACET (Jones et al., 2006; Dargan et al., 2009). However, the unwanted inhibition of these GluK1 antagonists on heteromeric KARs also containing the GluK2 subunit may complicate the interpretation of results because these antagonists were shown to have similar potency on GluK1 heterodimers with GluK2 or GluK5 as the potency on homodimeric receptor (Alt et al., 2004). An alternative technique is to isolate GluK2-mediated responses by using genetic knockout of GluK1 subunits

(Contractor et al., 2001). MF-CA3 synaptic responses from hippocampal slices from GluK1 knockout mice can be used to study synaptic plasticity and postsynaptic responses mediated by GluK2-containing KARs in isolation. However, long-term genetic knockouts of GluK1 may lead to compensating mechanisms that may take over the synaptic plasticity functions of GluK1. Therefore, conditional knockouts of GluK1 must be preferred for synaptic plasticity studies which investigate the roles of GluK2 using genetic knockout mice. Conditional dentate gyrus specific GluK1 knockout mice are already available (Collingridge and co-workers, Bristol) and therefore, presents a suitable model for further characterisation of UBP2054 in a native system.

KARs are also thought to be expressed with a wide range of auxiliary subunits (Lerma and Marques, 2013). One example is Neto1, which when coexpressed with GluK1 or GluK2, alters channel kinetics by decelerating the onset of desensitisation and acceleration of recovery from desensitisation (Copits et al., 2011; Fisher, 2015). Therefore, the inhibition of GluK2-containing KARs by UBP2054 must also be investigated in the presence of auxiliary subunits to better estimate the functional inhibition of GluK2-containing KARs by UBP2054. GluK2 has been expressed together with Neto1 and Neto2 auxiliary subunits in HEK293 cells (Fisher, 2015) and this provides a suitable avenue for characterising the GluK2 affinity of UBP2054 in the presence of the auxiliary subunit.

An important reason for the development of GluK2-selective antagonists was to study the roles of GluK2 in disease states such as epilepsy, pain and behavioural disorders. Following further characterisation of UBP2054 to establish its activity on native GluK2-containing KARs, it can be used to study the roles of GluK2 in disease models. The GluK2 subunit has been implicated in epilepsy because GluK2 knockout mice were found to be less susceptible to induction of seizures by kainate injections (Mulle et al., 1998). However, the contribution of the GluK2 subunit for development of seizures remains to be determined because association with the GluK2 is thought to be critical for assembly of functional KARs and therefore the lack of seizures in GluK2 knockout mice may be through the lack of KAR subunits other than GluK2, particularly the GluK1 subunit (Gryder and Rogawski, 2003). Therefore, studying the effect of UBP2054 in reducing epileptic activity in slice models of epilepsy induced through electrical stimulation, such as kindling model of epilepsy (Löscher et al., 1999), or through pharmacological induction mechanisms such as

through kainate infusions (Mulle et al., 1998) may provide an avenue to study the role of GluK2 in epilepsy.

5.3. Conclusions from the investigation of the roles of the NMDAR GluN2D subunit in synaptic plasticity in the hippocampal CA1 region

5.3.1. GluN2D subunits affect baseline excitability and mediate LTP induction in hippocampal neurons

The GluN2D subunit protein has been shown to be expressed in the CA1 region of the hippocampus (Hrabetova et al., 2000; Thompson et al., 2002) but their precise location and their roles in synaptic transmission in the CA1 region remained unclear. Although the GluN2D protein expression has been shown to decrease with age (Monyer et al., 1994), its functional role in adult hippocampus has been investigated only a few times (Harney et al., 2008; Volianskis et al., 2013a; Engelhardt et al., 2015; Ingram et al., 2018). A study by Lozovaya et al., (2004) suggested that GluN2D receptors might be expressed in extrasynaptic surfaces in CA1 of adult hippocampus based on analysis of the faster decay of NMDAR-mediated f-EPSPs induced by burst stimulation after inhibition of GluN2D using PPDA (Lozovaya et al., 2004). The speeding of the decay of f-EPSPs induced by burst stimulation may be a result of glutamate spillover due to saturation of glutamate reuptake transporter during bursts of pulses. The spillover of glutamate leads to activation of the extrasynaptic NMDARs, possibly containing GluN2D subunits (Lozovaya et al., 2004). GluN2D containing NMDARs have higher affinity for glutamate compared to other GluN2 subunits (Feng et al., 2005), which would allow them to be activated even at low glutamate concentrations in the extrasynaptic space and therefore contribute to the late phase of the synaptic response. However, PPDA's poor selectivity for GluN2D over GluN2B and GluN2A (at the concentration used in the study by Lozovaya et al: 10 μM) meant that the speeding of decay of f-EPSP in the study could also be due to inhibition of GluN2B.

Other studies, which have investigated the roles of GluN2D in the hippocampus have found that using the GluN2B NAM, ifenprodil, the GluN2D-mediated slow decay phase of the NMDAR EPSC could be uncovered in hippocampal slices from P3-12 mice (Engelhardt et al., 2015). Additionally, a possibility for the presence of GluN2B/GluN2D-containing

triheteromeric receptors was also raised based on the observation that ifenprodil reduced the amplitude but not the decay time constant of NMDAR EPSCs from interneurons of p20-25 old mice (Engelhardt et al., 2015). In another study, the GluN2D/GluN2C PAM, CIQ, potentiated NMDAR-mediated EPSCs in CA1 interneurons but not pyramidal cells (Perszyk et al., 2016).

Meanwhile, a pharmacological study that investigated the potency of GluN2A/2B or 2D antagonists with relative subunit-selectivity on LTP and STP in SC-CA1 synapses found that GluN2D and GluN2B-containing NMDARs (most likely as GluN2B/GluN2D trihetermeric receptors), which are activated during induction of potentiation, prolong the duration of STP decay (Volianskis et al., 2013a). These findings provided an exciting avenue for further investigations of the GluN2D subunit in synaptic plasticity mechanisms in the hippocampal CA1 region.

The present study utilised subunit-selective pharmacological agents for GluN2A (NVP-AAM077), GluN2B (Ro 25-6981) and GluN2D (UBP145 and UBP791) subunits, in combination with genetic knockout mice lacking the GuN2D subunit, to study the roles of GluN2D subunits in hippocampal synaptic transmission in both the knockout mouse and in the wild-type control. The lack of activity of GluN2D antagonists in the GluN2D knockout slices also provided validation for the selectivity of UBP145 (10 μM) and UBP791 (1 μM) for antagonising GluN2D-mediated components of LTP (Figure 4.15 and Figure 4.16). This further highlights the advantages of combined use of pharmacological and genetic techniques to study physiological phenomena.

A significant finding of the present study was that the amplitude of LTP of SC-CA1 synaptic transmission in WT mice hippocampal slices also involved a GluN2D component (Figure 4.12). On the contrary, the amplitude and decay time constant of STP in WT mice slices were not affected by UBP145, a GluN2D antagonist (Figure 4.12). This finding in mice was different from that in rats where inhibition of GluN2D-containing NMDARs using UBP145 decreased the decay time constant of STP but had no effect on amplitudes of STP or LTP (Volianskis et al., 2013a). These differences highlight that the roles that different GluN2 subunits play in synaptic potentiation are interchangeable between species and points to the redundancy in induction of STP and LTP by different GluN2 subunits.

Additionally, if the faster decay of STP in WT mice slices (τ of STP $\approx$ 11 min) compared to rat slices (τ of STP $\approx$ 16 min) (Volianskis et al., 2013a) is a true difference, STP in mice may be induced through NMDARs containing different subunits from those in rats.

Another key observation from the current study was that CA1 neurons in the GluN2D KO slices have lower maximal excitability compared to WT slices (Figure 4.2C). Results from the current study suggest that blocking GABAergic transmission did not increase the maximum population spike in GluN2D KO slices compared to WT slices (when comparing mean maximum population spike area values) (Figure 4.5A2 and B2). However, maximal neuron excitability after inhibition of GABAergic transmission was not significantly different from controls in GluN2D KO slices (Figure 4.5B2). Therefore, the reason(s) for the impaired neuronal excitability in GluN2D KO slices compared to controls remains to be determined.

The present study also suggests that GluN2D lacking mice may have a larger amplitude of STP and LTP due to reduced inhibitory control from GABAergic interneurons, which were shown to contain functional GluN2D-containing NMDARs (Perszyk et al., 2016), and/or due to increased expression of GluN2A or GluN2B subunits to compensate for the long-term deletion of GluN2D. In support of the GABAergic involvement, blocking $GABA_A$ and $GABA_B$ transmission prior to induction of potentiation led to similar amplitudes of STP and LTP (Figure 4.7). In support of the GluN2A/GluN2B compensation hypothesis, the GluN2B antagonist, Ro, at a concentration high enough to inhibit GluN2A/GluN2B triheteromeric NMDARs (10 μM), inhibited LTP more potently in GluN2D KO slices. Another piece of evidence for the compensation by GluN2A and GluN2B in KO slices was that D-AP5 inhibited STP more potently in GluN2D KO slices at concentrations selective for GluN2A and GluN2B (Figure 4.8).

The rate of STP decay was previously shown to depend on the number of bursts delivered during induction of potentiation (Volianskis and Jensen, 2003). Moreover, previous studies have shown that activation of GluN2B- and GluN2D-containing receptors may be responsible for prolonging STP decay (Volianskis et al., 2013a; Ingram et al., 2018). Therefore, the current study also investigated the roles of GluN2B and GluN2D subunits in STP and LTP induced by a higher number of bursts (30-bursts).

In agreement with published studies, we found that 30-bursts induced STP had slower decay in WT slices and demonstrated a trend towards slower decay in GluN2D KO slices. This slowing of decay in the WT is most simply explained by the enhanced recruitment of GluN2B/GluN2D containing triheteromeric receptors during the 30-burst tetanus. Due to the deletion of GluN2D, this extra recruited population of NMDARs may be GluN2B-containing diheteromers in GluN2D KO slices. This suggestion was supported by a significant reduction in STP amplitude and halving of decay time constant by 1 μM Ro in GluN2D KO slices, and a more potent inhibition of 30-bursts induced STP amplitude in KO slices compared to WT by 1 μM Ro (Figure 4.14).

Importantly, we also found that amplitudes of STP and LTP induced with 30-bursts were larger compared to those induced with 10-bursts in WT mice but not in GluN2D KO slices (Figure 4.13). Together, these results suggest that the presence of the GluN2D subunit limits the amount of maximal potentiation in physiological/lower frequency stimulation patterns (10-bursts, which was given as theta-burst stimulation), a characteristic that is lost upon deletion of GluN2D in the KO mice. The loss in control of maximal potentiation in GluN2D KO slices may have been due to reduced GABAergic control mediated through GluN2D-containing receptors on interneurons and/or increased contribution from GluN2A/GluN2B triheteromeric NMDARs to induction of STP and LTP after deletion of GluN2D.

The GluN2D receptors on interneurons may be involved in maintaining the excitation-inhibition balance during induction of potentiation by potentiating the interneuron (Lamsa et al., 2005) and therefore leading to lowering the threshold for generation of action potentials in the interneurons. This also explains the higher STP and LTP amplitudes in response to 10-bursts stimulation in GluN2D KO slices compared to WT slices because the excitation-inhibition balance would shift to excitation in the absence of GluN2D-mediated interneuron potentiation. The presence of GluN2A/GluN2B triheteromeric NMDARs is also in agreement with observation that 10 μM Ro more potently blocked 10-bursts induced LTP in KO compared to WT slices. In agreement with LTP induced using 10-bursts tetanus, LTP induced with 30-bursts was also dependent on GluN2D, as verified using UBP145 (~10-fold GluN2D over GluN2B selectivity) and UBP791 (~30-fold GluN2D over GluN2B selectivity).

In summary, the results from the current study show that the GluN2D subunit mediates a component of LTP in the mouse SC-CA1 synapse and GluN2D deletion affects neuronal excitability through a yet to be determined process and increases amplitudes of STP and LTP through at-least two mechanisms: 1, by reducing the influence of the GABAergic feedforward/feedback inhibition in the SC-CA1 neuronal connection and 2, by causing compensation from GluN2A- and/or GluN2B-containing receptors.

5.3.2. Physiological significance of GluN2D-induced synaptic plasticity

LTP and STP reflect synaptic plasticity mechanisms, which permit modulation of neuronal signals at the single-cell and network levels, based on the activity of afferent neurons. Previous results from long-term and whole brain GluN2B and GluN2A genetic knockout studies have suggested that there is some redundancy between different GluN2 subunits with regards to their involvement in NMDAR dependent synaptic plasticity, particularly with GluN2A subunits (Kiyama et al., 1998). However, there may also be unique contributions of individual NMDAR subunits, such as the intracellular proteins to which each subunits couple and through which they can fulfil unique roles in signal processing in the neurons. An example is the association of GluN2B subunit with CaMKII, which has been shown to be critical for activation of GluN2B-mediated protein synthesis during LTP (Li et al., 2002). Therefore, genetic models with inducible cell type and age specific, deletion or over-expression of GluN2 subunits are needed to fully understand the roles that these subunits play at specific developmental stages. GluN2D subunit knockout mice have been shown to have behavioural deficits in rearing, which may be an anxiety-like behaviour (Ikeda et al., 1995). Ketamine's anti-depressant effects have also been suggested to be due to its ability to inhibit the GluN2D mediated component of STP (Ingram et al., 2018). GluN2D containing receptors expressed on interneurons, which are important for maintaining network level synchrony in neuronal oscillations have also been implicated in schizophrenia (Sapkota et al., 2016). The roles that the GluN2D subunit plays in neuronal signalling in the human brain and how these roles are disrupted during disease are questions that require further study.

While the physiological significance of STP is yet to be determined, STP can be induced independently or in combination with LTP in in vitro and in vivo settings (Kauer et al., 1988; Buschler et al., 2012). STP may also be expressed independently or co-expressed

with LTP (Debanne et al., 1999). STP has also been shown to be activity dependent in its decay, in that stopping stimulation of the afferent neurons will "pause" the decay of potentiation for upto 6 hours, whereas restarting stimulation of afferent neurons resumes the decay of potentiation (i.e. STP) (Volianskis and Jensen, 2003). Therefore, STP has been suggested to represent short-term memory which can be stored in inactive synapses and once recalled loses relevance unless reinforced with further afferent synaptic activity (Volianskis et al., 2013a; Ingram et al., 2018). Previous studies have shown that GluN2D mediates the decay component of STP in rats (Volianskis et al., 2013a; Ingram et al., 2018).

In summary, the effect of GluN2D on LTP in mice shows the heterogeneity in the origins of synaptic plasticity between species. Our data suggests that future experiments of SC-CA1 LTP in mice must consider the role of GluN2D-containing receptors. Additionally, the results from our studies suggest that the decay time constant (τ) of STP may be lower after blockage of GluN2D receptors but these differences were not statistically significant. If the lowering of τ by GluN2D antagonists is a real effect, GluN2D-containing receptors may also play a role in SC-CA1 STP in mice. Therefore, STP and LTP may be mediated by either the same population of GluN2D-containing receptors or by two separate populations of GluN2D-containing receptors.

5.4. Future studies on the physiological roles of GluN2D subunits

5.4.1. Determining the location and composition of GluN2D-containing NMDARs in the CA1 of hippocampus

In the present study, the process(es) that contributed to the impairment of neuronal excitability in GluN2D KO slices could not be determined. Although the results suggest that inhibition of GABAergic transmission did not affect maximal excitability (Figure 4.5A2 and B2). The possibility that compensation by GluN2A- or GluN2B-containing receptors led to the impaired neuronal excitability can be tested by comparing the sizes of maximal population spikes in the presence and absence of D-AP5 in WT and GluN2D KO slices.

To investigate the possibility that extrasynaptic GluN2D-containing receptors on the CA1 pyramidal cells are responsible for the higher maximal neuronal excitability in WT slices,

the subunit composition of extrasynaptic NMDARs may be determined using the whole-cell voltage clamp recording technique. A strategy for such investigations could be to block synaptic NMDARs using a slowly dissociating channel blocker similar to MK-801 under baseline synaptic activation and study the currents mediated by the unblocked extrasynaptic NMDARs in isolation. The blocking of synaptic NMDARs with MK-801 has been successfully performed to study the contribution of extrasynaptic GluN2B subunits to synaptic plasticity in CA1 (Yang et al., 2017) and to study extrasynaptic GluN2D containing receptors in dentate gyrus principle cells (Harney et al., 2008).

Evidence from previous studies suggest that the GluN2D-containing extrasynaptic receptors in the CA1 may be triheteromeric GluN2B/GluN2D (Volianskis et al., 2013a; Engelhardt et al., 2015). But inhibition of GluN2B/GluN2D triheteromers using pharmacological tools has been rarely studied partly due to lack of information about activity of many antagonists on the GluN2B/GluN2D-containing triheteromeric receptor. Verification of the activity of UBP145 and UBP791 on GluN2B/GluN2D triheteromers is important for further physiological studies of GluN2D subunits which use these antagonists. The antagonist affinity on triheteromeric NMDARs can be determined on recombinant GluN2B/GluN2D triheteromers expressed in heterologous systems as previously characterised for the GluN2A/GluN2B triheteromer (Hansen et al., 2014), or in native CA1 hippocampal interneurons or substantia nigra pars compacta dopaminergic neurons where GluN2B/GluN2D triheteromers are believed to be expressed synaptically (Brothwell et al., 2008).

The presence of extrasynaptic diheteromeric GluN2D- or extrasynaptic triheteromeric GluN2B/GluN2D-containing receptor populations can be verified by studying the decay of extrasynaptic currents caused by glutamate spillover after the blockage of glutamate reuptake transporter using TBOA (Shimamoto et al., 1998). The deactivation time constants of currents mediated by GluN2D (2-4 s) and GluN2B (71, 538 μs) diheteromers are distinct and can be indicative of their presence at extrasynaptic sites (Monyer et al., 1992; Vicini et al., 1998).

Another possibility to reveal the subunit composition is to conduct immunohistochemistry studies using GluN2B- and GluN2D-specific antibodies. Co-staining of GluN2B and

GluN2D subunits may be able to detect the possible presence of diheteromeric or triheteromeric GluN2D-containing populations of NMDARs in the CA1 of adult mice. The biggest hurdle for such investigations is the lack of subunit-specific antibodies. But antibodies with greater specificity are emerging and may pave the way for better understanding of NMDAR subunit protein expression patterns in the brain (Swanger et al., 2015).

Another finding from the present study that GluN2D antagonists partially inhibited LTP induced by TBS and by 30-bursts in the SC-CA1 synapse provides novel evidence for a GluN2D diheteromeric component in LTP in these synapses. In many experiments in the present study, the inhibition of STP and LTP by one antagonist was partial. However, high concentrations of D-AP5 (100 μM) or L689,560 (10 μM) inhibited both STP and LTP completely (Figure 4.8 and Figure 4.9). Therefore, further experiments using a combination of 10 μM UBP145 (or 1 μM UBP791) and 1 μM Ro may help to isolate the GluN2A component of potentiation. In a similar manner, combinations of 10 μM UBP145 (or 1 μM UBP791) and 0.1 μM NVP may help to isolate the GluN2B component of potentiation. However, the lack of GluN2A over GluN2B selectivity of NVP (5- to 10-fold) may limit its use and would require another novel antagonist with higher GluN2A selectivity. Moreover, the block of GABA receptors before induction of potentiation using 30-bursts may give clues as to the contribution of interneurons to maximal potentiation.

In addition to the activities of UBP145 and UBP791 on triheteromeric GluN2D-containing NMDARs, activity of Ro on GluN2B/GluN2D triheteromeric NMDAR remains to be determined. A recent structural study of a recombinant GluN2A/GluN2B triheteromer revealed that affinity (K_b) for Ro was ~130 nM (Lü et al., 2017). This affinity is closer to Ro's affinity on GluN2B diheteromer than to its affinity on GluN2A diheteromer (Fischer et al., 1997). Therefore, whether Ro's affinity on GluN2B/GluN2D triheteromer is in a range that would selectively inhibit the GluN2B/GluN2D triheteromer without inhibiting GluN2A diheteromeric receptors requires further study using triheteromers expressed in heterologous or native systems. Once the activities of both UBP145 and Ro on GluN2B/GluN2D triheteromers are determined, a suitable next step would be to inhibit GluN2B/GluN2D-containing triheteromeric receptors without affecting GluN2A-containing receptors to show that STP is completely blocked in WT slices. This could be

done by development of novel antagonists that binds to GluN2B/GluN2D selectively – one approach is to improve the selectivity of UBP791 such that it binds to GluN2B with similar affinity as GluN2D but without affinity on GluN2A. Another approach is to develop allosteric antagonists that bind selectively to the interface between GluN2B/GluN2D subunits, thus being a triheteromeric GluN2B/GluN2D selective antagonist.

References

Abe, T., Sugihara, H., Nawa, H., Shigemoto, R., Mizuno, N., and Nakanishi, S. (1992). Molecular characterization of a novel metabotropic glutamate receptor mGluR5 coupled to inositol phosphate/Ca2+ signal transduction. J. Biol. Chem. *267*, 13361–13368.

Abraham, W.C., Gustafsson, B., and Wigström, H. (1986). Single high strength afferent volleys can produce long-term potentiation in the hippocampus in vitro. Neurosci. Lett. *70*, 217–222.

Agrawal, S.G., and Evans, R.H. (1986). The primary afferent depolarizing action of kainate in the rat. Br. J. Pharmacol. *87*, 345–355.

Ahmadi, S., Muth-Selbach, U., Lauterbach, A., Lipfert, P., Neuhuber, W.L., and Zeilhofer, H.U. (2003). Facilitation of spinal NMDA receptor currents by spillover of synaptically released glycine. Science *300*, 2094–2097.

Akashi, K., Kakizaki, T., Kamiya, H., Fukaya, M., Yamasaki, M., Abe, M., Natsume, R., Watanabe, M., and Sakimura, K. (2009). NMDA receptor GluN2B (GluRε2/NR2B) subunit is crucial for channel function, postsynaptic macromolecular organization, and actin cytoskeleton at hippocampal CA3 synapses. J. Neurosci. *29*, 10869–10882.

Alford, S., Frenguelli, B.G., Schofield, J.G., and Collingridge, G.L. (1993). Characterization of Ca2+ signals induced in hippocampal CA1 neurones by the synaptic activation of NMDA receptors. J. Physiol. *469*, 693–716.

Alger, B.E., and Nicoll, R.A. (1982). Feed-forward dendritic inhibition in rat hippocampal pyramidal cells studied in vitro. J. Physiol. *328*, 105–123.

Alsaad, H.A., DeKorver, N.W., Mao, Z., Dravid, S.M., Arikkath, J., and Monaghan, D.T. (2019). In the telencephalon, GluN2C NMDA receptor subunit mRNA is predominately expressed in glial cells and GluN2D mRNA in interneurons. Neurochem. Res. *44*, 61–77.

Alt, A., Weiss, B., Ogden, A.M., Knauss, J.L., Oler, J., Ho, K., Large, T.H., and Bleakman, D. (2004). Pharmacological characterization of glutamatergic agonists and antagonists at recombinant human homomeric and heteromeric kainate receptors in vitro. Neuropharmacology *46*, 793–806.

Alushin, G.M., Jane, D., and Mayer, M.L. (2011). Binding site and ligand flexibility revealed by high resolution crystal structures of GluK1 competitive antagonists. Neuropharmacology *60*, 126–134.

Andersen, P., Eccles, J.C., and Lyning, Y. (1964a). Location of postsynaptic inhibitory synapses on hippocampal pyramids. J. Neurophysiol. *27*, 592–607.

Andersen, P., Eccles, J.C., and Lyning, Y. (1964b). Pathway of postsynaptic inhibition in the hippocampus. J. Neurophysiol. *27*, 608–619.

Andersen, P., Bliss, T.V., and Skrede, K.K. (1971). Unit analysis of hippocampal polulation spikes. Exp. Brain Res. *13*, 208–221.

Andersen, P., Sundberg, S.H., Sveen, O., and Wigström, H. (1977). Specific long-lasting potentiation of synaptic transmission in hippocampal slices. Nature *266*, 736–737.

Anderson, W., and Collingridge, G. (2007). Capabilities of the WinLTP data acquisition program extending beyond basic LTP experimental functions. J. Neurosci. Methods *162*, 346–356.

Anis, N.A., Berry, S.C., Burton, N.R., and Lodge, D. (1983). The dissociative anaesthetics, ketamine and phencyclidine, selectively reduce excitation of central mammalian neurones by N-methyl-aspartate. Br. J. Pharmacol. *79*, 565–575.

Anwyl, R., Lee, W.L., and Rowan, M. (1988). The role of calcium in short-term potentiation in the rat hippocampal slice. Brain Res. *459*, 192–195.

Aramori, I., and Nakanishi, S. (1992). Signal transduction and pharmacological characteristics of a metabotropic glutamate receptor, mGluR1, in transfected CHO cells. Neuron *8*, 757–765.

Armstrong, N., and Gouaux, E. (2000). Mechanisms for activation and antagonism of an AMPA-sensitive glutamate receptor: crystal structures of the GluR2 ligand binding core. Neuron *28*, 165–181.

Armstrong, N., Sun, Y., Chen, G.-Q., and Gouaux, E. (1998). Structure of a glutamate-receptor ligand-binding core in complex with kainate. Nature *395*, 913–917.

Artinian, J., Peret, A., Marti, G., Epsztein, J., and Crépel, V. (2011). Synaptic kainate receptors in interplay with INaP shift the sparse firing of dentate granule cells to a sustained rhythmic mode in temporal lobe epilepsy. J. Neurosci. Off. J. Soc. Neurosci. *31*, 10811–10818.

Artinian, J., Peret, A., Mircheva, Y., Marti, G., and Crépel, V. (2015). Impaired neuronal operation through aberrant intrinsic plasticity in epilepsy. Ann. Neurol. *77*, 592–606.

Artola, A., and Singer, W. (1987). Long-term potentiation and NMDA receptors in rat visual cortex. Nature *330*, 649–652.

Ascher, P., and Nowak, L. (1988). The role of divalent cations in the N-methyl-D-aspartate responses of mouse central neurones in culture. J. Physiol. *399*, 247–266.

Asztely, F., Erdemli, G., and Kullmann, D.M. (1997). Extrasynaptic glutamate spillover in the hippocampus: dependence on temperature and the role of active glutamate uptake. Neuron *18*, 281–293.

Atlason, P.T., Scholefield, C.L., Eaves, R.J., Mayo-Martin, M.B., Jane, D.E., and Molnar, E. (2010). Mapping the ligand binding sites of kainate receptors: molecular determinants of subunit-selective binding of the antagonist [3H]UBP310. Mol. Pharmacol. *78*, 1036–1045.

Auberson, Y.P., Allgeier, H., Bischoff, S., Lingenhoehl, K., Moretti, R., and Schmutz, M. (2002). 5-Phosphonomethylquinoxalinediones as competitive NMDA receptor antagonists with a preference for the human 1A/2A, rather than 1A/2B receptor composition. Bioorg. Med. Chem. Lett. *12*, 1099–1102.

Ault, B., and Hildebrand, L.M. (1993). Activation of nociceptive reflexes by peripheral

kainate receptors. J. Pharmacol. Exp. Ther. *265*, 927–932.

Ayalon, G., Segev, E., Elgavish, S., and Stern-Bach, Y. (2005). Two regions in the N-terminal domain of ionotropic glutamate receptor 3 form the subunit oligomerization interfaces that control subtype-specific receptor assembly. J. Biol. Chem. *280*, 15053–15060.

Bagal, A.A., Kao, J.P.Y., Tang, C.-M., and Thompson, S.M. (2005). Long-term potentiation of exogenous glutamate responses at single dendritic spines. Proc. Natl. Acad. Sci. *102*, 14434–14439.

Bahn, S., Volk, B., and Wisden, W. (1994). Kainate receptor gene expression in the developing rat brain. J. Neurosci. *14*, 5525–5547.

Baker, S.R., Bleakman, D., Ezquerra, J., Ballyk, B.A., Deverill, M., Ho, K., Kamboj, R.K., Collado, I., Domínguez, C., Escribano, A., et al. (2000). 4-Alkylidenyl glutamic acids, potent and selective GluR5 agonists. Bioorg. Med. Chem. Lett. *10*, 1807–1810.

Barker, G.R.I., Warburton, E.C., Koder, T., Dolman, N.P., More, J.C.A., Aggleton, J.P., Bashir, Z.I., Auberson, Y.P., Jane, D.E., and Brown, M.W. (2006). The different effects on recognition memory of perirhinal kainate and NMDA glutamate receptor antagonism: implications for underlying plasticity mechanisms. J. Neurosci. *26*, 3561–3566.

Baron, B.M., Harrison, B.L., Miller, F.P., McDonald, I.A., Salituro, F.G., Schmidt, C.J., Sorensen, S.M., White, H.S., and Palfreyman, M.G. (1990). Activity of 5,7-dichlorokynurenic acid, a potent antagonist at the N-methyl-D-aspartate receptor-associated glycine binding site. Mol. Pharmacol. *38*, 554–561.

Barria, A., Derkach, V., and Soderling, T. (1997). Identification of the Ca2+/calmodulin-dependent protein kinase II regulatory phosphorylation site in the alpha-amino-3-hydroxyl-5-methyl-4-isoxazole-propionate-type glutamate receptor. J. Biol. Chem. *272*, 32727–32730.

Bartlett, T.E., Bannister, N.J., Collett, V.J., Dargan, S.L., Massey, P.V., Bortolotto, Z.A., Fitzjohn, S.M., Bashir, Z.I., Collingridge, G.L., and Lodge, D. (2007). Differential roles of NR2A and NR2B-containing NMDA receptors in LTP and LTD in the CA1 region of two-week old rat hippocampus. Neuropharmacology *52*, 60–70.

Basbaum, A.I., Bautista, D.M., Scherrer, G., and Julius, D. (2009). Cellular and molecular mechanisms of pain. Cell *139*, 267–284.

Bashir, Z.I., Tam, B., and Collingridge, G.L. (1990). Activation of the glycine site in the NMDA receptor is necessary for the induction of LTP. Neurosci. Lett. *108*, 261–266.

Bashir, Z.I., Bortolotto, Z.A., Davies, C.H., Berretta, N., Irving, A.J., Seal, A.J., Henley, J.M., Jane, D.E., Watkins, J.C., and Collingridge, G.L. (1993). Induction of LTP in the hippocampus needs synaptic activation of glutamate metabotropic receptors. Nature *363*, 347–350.

Bateman, A., Martin, M.J., O'Donovan, C., Magrane, M., Alpi, E., Antunes, R., Bely, B., Bingley, M., Bonilla, C., Britto, R., et al. (2017). UniProt: the universal protein

knowledgebase. Nucleic Acids Res. *45*, D158–D169.

Ben-Ari, Y. (1985). Limbic seizure and brain damage produced by kainic acid: mechanisms and relevance to human temporal lobe epilepsy. Neuroscience *14*, 375–403.

Ben-Ari, Y., and Cossart, R. (2000). Kainate, a double agent that generates seizures: two decades of progress. Trends Neurosci. *23*, 580–587.

Ben-Ari, Y., Lagowska, J., Tremblay, E., and Le Gal La Salle, G. (1979). A new model of focal status epilepticus: intra-amygdaloid application of kainic acid elicits repetitive secondarily generalized convulsive seizures. Brain Res. *163*, 176–179.

Ben-Ari, Y., Crepel, V., and Represa, A. (2008). Seizures beget seizures in temporal lobe epilepsies: the boomerang effects of newly formed aberrant kainatergic synapses. Epilepsy Curr. *8*, 68–72.

Benkert, P., Tosatto, S.C.E., and Schomburg, D. (2008). QMEAN: A comprehensive scoring function for model quality assessment. Proteins Struct. Funct. Bioinforma. *71*, 261–277.

Bennett, M.V.L., and Zukin, R.S. (2004). Electrical coupling and neuronal synchronization in the Mammalian brain. Neuron *41*, 495–511.

Benveniste, H. (1989). Brain microdialysis. J. Neurochem. *52*, 1667–1679.

Berger, A.J., Dieudonné, S., and Ascher, P. (1998). Glycine uptake governs glycine site occupancy at NMDA receptors of excitatory synapses. J. Neurophysiol. *80*, 3336–3340.

Bergeron, R., Meyer, T.M., Coyle, J.T., and Greene, R.W. (1998). Modulation of N-methyl-D-aspartate receptor function by glycine transport. Proc. Natl. Acad. Sci. U. S. A. *95*, 15730–15734.

Bergles, D.E., and Jahr, C.E. (1997). Synaptic activation of glutamate transporters in hippocampal astrocytes. Neuron *19*, 1297–1308.

Berman, H.M., Westbrook, J., Feng, Z., Gilliland, G., Bhat, T.N., Weissig, H., Shindyalov, I.N., and Bourne, P.E. (2000). The protein data bank. Nucleic Acids Res. *28*, 235–242.

Berretta, N., and Jones, R.S. (1996). Tonic facilitation of glutamate release by presynaptic N-methyl-D-aspartate autoreceptors in the entorhinal cortex. Neuroscience *75*, 339–344.

Bettler, B., and Mulle, C. (1995). Review: neurotransmitter receptors. II. AMPA and kainate receptors. Neuropharmacology *34*, 123–139.

Bettler, B., Boulter, J., Hermans-Borgmeyer, I., O'Shea-Greenfield, A., Deneris, E.S., Moll, C., Borgmeyer, U., Hollmann, M., and Heinemann, S. (1990). Cloning of a novel glutamate receptor subunit, GluR5: Expression in the nervous system during development. Neuron *5*, 583–595.

Betz, W.J. (1970). Depression of transmitter release at the neuromuscular junction of the frog. J. Physiol. *206*, 629–644.

Bi, G., and Poo, M. (1998). Synaptic modifications in cultured hippocampal neurons: dependence on spike timing, synaptic strength, and postsynaptic cell type. J. Neurosci. *18*, 10464–10472.

Bienert, S., Waterhouse, A., de Beer, T.A.P., Tauriello, G., Studer, G., Bordoli, L., and Schwede, T. (2017). The SWISS-MODEL Repository—new features and functionality. Nucleic Acids Res. *45*, D313–D319.

Billups, D., and Attwell, D. (2003). Active release of glycine or D-serine saturates the glycine site of NMDA receptors at the cerebellar mossy fibre to granule cell synapse. Eur. J. Neurosci. *18*, 2975–2980.

Birch, P.J., Grossman, C.J., and Hayes, A.G. (1988). Kynurenic acid antagonises responses to NMDA via an action at the strychnine-insensitive glycine receptor. Eur. J. Pharmacol. *154*, 85–87.

Biscoe, T.J., and Duchen, M.R. (1985). An intracellular study of dentate, CA1 and CA3 neurones in the mouse hippocampal slice. Q. J. Exp. Physiol. Camb. Engl. *70*, 189–202.

Biscoe, T.J., and Straughan, D.W. (1966). Micro-electrophoretic studies of neurones in the cat hippocampus. J. Physiol. *183*, 341–359.

Biscoe, T.J., Evans, R.H., Headley, P.M., Martin, M., and Watkins, J.C. (1975). Domoic and quisqualic acids as potent amino acid excitants of frog and rat spinal neurones. Nature *255*, 166–167.

Bland, B.H., Andersen, P., Ganes, T., and Sveen, O. (1980). Automated analysis of rhythmicity of physiologically identified hippocampal formation neurons. Exp. Brain Res. *38*, 205–219.

Blanpied, T.A., Boeckman, F.A., Aizenman, E., and Johnson, J.W. (1997). Trapping channel block of NMDA-activated responses by amantadine and memantine. J. Neurophysiol. *77*, 309–323.

Blaustein, M.P. (1988). Calcium transport and buffering in neurons. Trends Neurosci. *11*, 438–443.

Bleakman, D., Ballyk, B.A., Schoepp, D.D., Palmer, A.J., Bath, C.P., Sharpe, E.F., Woolley, M.L., Bufton, H.R., Kamboj, R.K., Tarnawa, I., et al. (1996). Activity of 2,3-benzodiazepines at native rat and recombinant human glutamate receptors in vitro: stereospecificity and selectivity profiles. Neuropharmacology *35*, 1689–1702.

Bleisch, T.J., Ornstein, P.L., Allen, N.K., Wright, R.A., Lodge, D., and Schoepp, D.D. (1997). Structure-activity studies of aryl-spaced decahydroisoquinoline-3-carboxylic acid ampa receptor antagonists. Bioorg. Med. Chem. Lett. *7*, 1161–1166.

Bliss, T.V., and Collingridge, G.L. (2013). Expression of NMDA receptor-dependent LTP in the hippocampus: bridging the divide. Mol. Brain *6*, 5.

Bliss, T.V., and Gardner-Medwin, A.R. (1973). Long-lasting potentiation of synaptic transmission in the dentate area of the unanaestetized rabbit following stimulation of the

perforant path. J. Physiol. *232*, 357–374.

Bliss, T.V., and Lømo, T. (1970). Plasticity in a monosynaptic cortical pathway. J. Physiol. *207*, 61P.

Bliss, T.V.P., and Collingridge, G.L. (1993). A synaptic model of memory: long-term potentiation in the hippocampus. Nature *361*, 31–39.

Bliss, T.V.P., and Lømo, T. (1973). Long-lasting potentiation of synaptic transmission in the dentate area of the anaesthetized rabbit following stimulation of the perforant path. J. Physiol. *232*, 331–356.

Blundon, J.A., and Zakharenko, S.S. (2008). Dissecting the components of long-term potentiation. Neurosci. Rev. J. Bringing Neurobiol. Neurol. Psychiatry *14*, 598–608.

Boeckers, T.M. (2006). The postsynaptic density. Cell Tissue Res. *326*, 409–422.

Boehm, J., Kang, M.-G., Johnson, R.C., Esteban, J., Huganir, R.L., and Malinow, R. (2006). Synaptic incorporation of AMPA receptors during LTP is controlled by a PKC phosphorylation site on GluR1. Neuron *51*, 213–225.

Böhme, G.A., Bon, C., Stutzmann, J.M., Doble, A., and Blanchard, J.C. (1991). Possible involvement of nitric oxide in long-term potentiation. Eur. J. Pharmacol. *199*, 379–381.

Bortolotto, Z.A., and Collingridge, G.L. (1993). Characterisation of LTP induced by the activation of glutamate metabotropic receptors in area CA1 of the hippocampus. Neuropharmacology *32*, 1–9.

Bortolotto, Z.A., Clarke, V.R.J., Delany, C.M., Parry, M.C., Smolders, I., Vignes, M., Ho, K.H., Miu, P., Brinton, B.T., Fantaske, R., et al. (1999). Kainate receptors are involved in synaptic plasticity. Nature *402*, 297–301.

Boulter, J., Hollmann, M., O'Shea-Greenfield, A., Hartley, M., Deneris, E., Maron, C., and Heinemann, S. (1990). Molecular cloning and functional expression of glutamate receptor subunit genes. Science *249*, 1033–1037.

Bowie, D., and Mayer, M.L. (1995). Inward rectification of both AMPA and kainate subtype glutamate receptors generated by polyamine-mediated ion channel block. Neuron *15*, 453–462.

Brackley, P.T., Bell, D.R., Choi, S.K., Nakanishi, K., and Usherwood, P.N. (1993). Selective antagonism of native and cloned kainate and NMDA receptors by polyamine-containing toxins. J. Pharmacol. Exp. Ther. *266*, 1573–1580.

Brenowitz, S., and Trussell, L.O. (2001). Minimizing synaptic depression by control of release probability. J. Neurosci. Off. J. Soc. Neurosci. *21*, 1857–1867.

Bresink, I., Benke, T.A., Collett, V.J., Seal, A.J., Parsons, C.G., Henley, J.M., and Collingridge, G.L. (1996). Effects of memantine on recombinant rat NMDA receptors expressed in HEK 293 cells. Br. J. Pharmacol. *119*, 195–204.

Breustedt, J., and Schmitz, D. (2004). Assessing the role of GLUK5 and GLUK6 at hippocampal mossy fiber synapses. J. Neurosci. *24*, 10093–10098.

Brickley, S.G., Misra, C., Mok, M.S., Mishina, M., and Cull-Candy, S.G. (2003). NR2B and NR2D subunits coassemble in cerebellar Golgi cells to form a distinct NMDA receptor subtype restricted to extrasynaptic sites. J. Neurosci. *23*, 4958–4966.

Briel, D., Rybak, A., Kronbach, C., and Unverferth, K. (2010). Substituted 2-Aminothiopen-derivatives: A potential new class of GluR6-Antagonists. Eur. J. Med. Chem. *45*, 69–77.

Brigman, J.L., Wright, T., Talani, G., Prasad-Mulcare, S., Jinde, S., Seabold, G.K., Mathur, P., Davis, M.I., Bock, R., Gustin, R.M., et al. (2010). Loss of GluN2B-containing NMDA receptors in CA1 hippocampus and cortex impairs long-term depression, reduces dendritic spine density, and disrupts learning. J. Neurosci. Off. J. Soc. Neurosci. *30*, 4590–4600.

Brothwell, S.L.C., Barber, J.L., Monaghan, D.T., Jane, D.E., Gibb, A.J., and Jones, S. (2008). NR2B- and NR2D-containing synaptic NMDA receptors in developing rat substantia nigra pars compacta dopaminergic neurones. J. Physiol. *586*, 739–750.

Bufler, J., Cordes, A., Heineke, W., Dengler, R., and Krampfl, K. (2001). Pentobarbital and brilliant green modulate the current response of recombinant rat kainate-type GluR6 receptor channels differentially. Neurosci. Lett. *312*, 91–94.

Buller, A.L., and Monaghan, D.T. (1997). Pharmacological heterogeneity of NMDA receptors: characterization of NR1a/NR2D heteromers expressed in Xenopus oocytes. Eur. J. Pharmacol. *320*, 87–94.

Buller, A.L., Larson, H.C., Schneider, B.E., Beaton, J.A., Morrisett, R.A., and Monaghan, D.T. (1994). The molecular basis of NMDA receptor subtypes: native receptor diversity is predicted by subunit composition. J. Neurosci. *14*, 5471–5484.

Bureau, I., Bischoff, S., Heinemann, S.F., and Mulle, C. (1999). Kainate receptor-mediated responses in the CA1 Field of wild-type and GluR6-deficient mice. J. Neurosci. *19*, 653–663.

Burnashev, N., Schoepfer, R., Monyer, H., Ruppersberg, J.P., Günther, W., Seeburg, P.H., and Sakmann, B. (1992a). Control by asparagine residues of calcium permeability and magnesium blockade in the NMDA receptor. Science *257*, 1415–1419.

Burnashev, N., Monyer, H., Seeburg, P.H., and Sakmann, B. (1992b). Divalent ion permeability of AMPA receptor channels is dominated by the edited form of a single subunit. Neuron *8*, 189–198.

Burnashev, N., Zhou, Z., Neher, E., and Sakmann, B. (1995). Fractional calcium currents through recombinant GluR channels of the NMDA, AMPA and kainate receptor subtypes. J. Physiol. *485 (Pt 2)*, 403–418.

Burnashev, N., Villarroel, A., and Sakmann, B. (1996). Dimensions and ion selectivity of recombinant AMPA and kainate receptor channels and their dependence on Q/R site

residues. J. Physiol. *496*, 165.

Buschler, A., Goh, J.J., and Manahan-Vaughan, D. (2012). Frequency dependency of NMDA receptor-dependent synaptic plasticity in the hippocampal CA1 region of freely behaving mice. Hippocampus *22*, 2238–2248.

Carbone, A.L., and Plested, A.J.R. (2016). Superactivation of AMPA receptors by auxiliary proteins. Nat. Commun. *7*, 10178.

Carlton, S.M., and Coggeshall, R.E. (1999). Inflammation-induced changes in peripheral glutamate receptor populations. Brain Res. *820*, 63–70.

Carta, M., Fièvre, S., Gorlewicz, A., and Mulle, C. (2014). Kainate receptors in the hippocampus. Eur. J. Neurosci. *39*, 1835–1844.

Castillo, P.E., Malenka, R.C., and Nicoll, R.A. (1997). Kainate receptors mediate a slow postsynaptic current in hippocampal CA3 neurons. Nature *388*, 182–186.

Chapman, P.F., Kairiss, E.W., Keenan, C.L., and Brown, T.H. (1990). Long-term synaptic potentiation in the amygdala. Synap. N. Y. N *6*, 271–278.

Chatterton, J.E., Awobuluyi, M., Premkumar, L.S., Takahashi, H., Talantova, M., Shin, Y., Cui, J., Tu, S., Sevarino, K.A., Nakanishi, N., et al. (2002). Excitatory glycine receptors containing the NR3 family of NMDA receptor subunits. Nature *415*, 793–798.

Cheffings, C.M., and Colquhoun, D. (2000). Single channel analysis of a novel NMDA channel from Xenopus oocytes expressing recombinant NR1a, NR2A and NR2D subunits. J. Physiol. *526 Pt 3*, 481–491.

Chen, H.-S.V., and Lipton, S.A. (2005). Pharmacological implications of two distinct mechanisms of interaction of memantine with N-methyl-D-aspartate-gated channels. J. Pharmacol. Exp. Ther. *314*, 961–971.

Chen, L., Chetkovich, D.M., Petralia, R.S., Sweeney, N.T., Kawasaki, Y., Wenthold, R.J., Bredt, D.S., and Nicoll, R.A. (2000). Stargazin regulates synaptic targeting of AMPA receptors by two distinct mechanisms. Nature *408*, 936–943.

Chen, L., El-Husseini, A., Tomita, S., Bredt, D.S., and Nicoll, R.A. (2003). Stargazin differentially controls the trafficking of alpha-amino-3-hydroxyl-5-methyl-4-isoxazolepropionate and kainate receptors. Mol. Pharmacol. *64*, 703–706.

Chen, N., Moshaver, A., and Raymond, L.A. (1997). Differential sensitivity of recombinant N-methyl-D-aspartate receptor subtypes to zinc inhibition. Mol. Pharmacol. *51*, 1015–1023.

Chen, P.E., Geballe, M.T., Katz, E., Erreger, K., Livesey, M.R., O'Toole, K.K., Le, P., Lee, C.J., Snyder, J.P., Traynelis, S.F., et al. (2008). Modulation of glycine potency in rat recombinant NMDA receptors containing chimeric NR2A/2D subunits expressed in Xenopus laevis oocytes. J. Physiol. *586*, 227–245.

Chenard, B.L., Bordner, J., Butler, T.W., Chambers, L.K., Collins, M.A., De Costa, D.L.,

Ducat, M.F., Dumont, M.L., Fox, C.B., and Mena, E.E. (1995). (1S,2S)-1-(4-hydroxyphenyl)-2-(4-hydroxy-4-phenylpiperidino)-1-propanol: a potent new neuroprotectant which blocks N-methyl-D-aspartate responses. J. Med. Chem. *38*, 3138–3145.

Cheng, Y., and Prusoff, W.H. (1973). Relationship between the inhibition constant (K1) and the concentration of inhibitor which causes 50 per cent inhibition (I50) of an enzymatic reaction. Biochem. Pharmacol. *22*, 3099–3108.

Chittajallu, R., Vignes, M., Dev, K.K., Barnes, J.M., Collingridge, G.L., and Henley, J.M. (1996). Regulation of glutamate release by presynaptic kainate receptors in the hippocampus. Nature *379*, 78–81.

Chittajallu, R., Braithwaite, S.P., Clarke, V.R.J., and Henley, J.M. (1999). Kainate receptors: subunits, synaptic localization and function. Trends Pharmacol. Sci. *20*, 26–35.

Cho, C.-H., St-Gelais, F., Zhang, W., Tomita, S., and Howe, J.R. (2007). Two families of TARP isoforms that have distinct effects on the kinetic properties of AMPA receptors and synaptic currents. Neuron *55*, 890–904.

Cho, S.W., Yoon, H.Y., Ahn, J.Y., Lee, E.Y., and Lee, J. (2001). Cassette mutagenesis of lysine 130 of human glutamate dehydrogenase. An essential residue in catalysis. Eur. J. Biochem. *268*, 3205–3213.

Christensen, B.N., and Hida, E. (1990). Protonation of histidine groups inhibits gating of the quisqualate/kainate channel protein in isolated catfish cone horizontal cells. Neuron *5*, 471–478.

Christensen, J.K., Varming, T., Ahring, P.K., Jørgensen, T.D., and Nielsen, E.Ø. (2004a). In vitro characterization of 5-carboxyl-2,4-di-benzamidobenzoic acid (NS3763), a noncompetitive antagonist of GLUK5 receptors. J. Pharmacol. Exp. Ther. *309*, 1003–1010.

Christensen, J.K., Paternain, A.V., Selak, S., Ahring, P.K., and Lerma, J. (2004b). A mosaic of functional kainate receptors in hippocampal interneurons. J. Neurosci. *24*, 8986–8993.

Christie, J.M., and Jahr, C.E. (2006). Multivesicular release at Schaffer collateral–CA1 hippocampal synapses. J. Neurosci. Off. J. Soc. Neurosci. *26*, 210–216.

Christine, C.W., and Choi, D.W. (1990). Effect of zinc on NMDA receptor-mediated channel currents in cortical neurons. J. Neurosci. Off. J. Soc. Neurosci. *10*, 108–116.

Clark, B.A., and Barbour, B. (1997). Currents evoked in Bergmann glial cells by parallel fibre stimulation in rat cerebellar slices. J. Physiol. *502 (Pt 2)*, 335–350.

Clarke, V.R.J., Ballyk, B.A., Hoo, K.H., Mandelzys, A., Pellizzari, A., Bath, C.P., Thomas, J., Sharpe, E.F., Davies, C.H., Ornstein, P.L., et al. (1997). A hippocampal GluR5 kainate receptor regulating inhibitory synaptic transmission. Nature *389*, 599–603.

Clausen, R.P., Christensen, C., Hansen, K.B., Greenwood, J.R., Jørgensen, L., Micale, N.,

Madsen, J.C., Nielsen, B., Egebjerg, J., Bräuner-Osborne, H., et al. (2008). N-Hydroxypyrazolyl glycine derivatives as selective N-methyl-D-aspartic acid receptor ligands. J. Med. Chem. *51*, 4179–4187.

Coan, E.J., Saywood, W., and Collingridge, G.L. (1987). MK-801 blocks NMDA receptor-mediated synaptic transmission and long term potentiation in rat hippocampal slices. Neurosci. Lett. *80*, 111–114.

Colbert, C.M., and Johnston, D. (1996). Axonal action-potential initiation and Na+ channel densities in the soma and axon initial segment of subicular pyramidal neurons. J. Neurosci. Off. J. Soc. Neurosci. *16*, 6676–6686.

Collingridge, G.L. (1985). Long term potentiation in the hippocampus: mechanisms of initiation and modulation by neurotransmitters. Trends Pharmacol. Sci. *6*, 407–411.

Collingridge, G.L., Kehl, S.J., and McLennan, H. (1983). Excitatory amino acids in synaptic transmission in the Schaffer collateral-commissural pathway of the rat hippocampus. J. Physiol. *334*, 33–46.

Collingridge, G.L., Olsen, R.W., Peters, J., and Spedding, M. (2009). A nomenclature for ligand-gated ion channels. Neuropharmacology *56*, 2–5.

Connors, B.W., and Long, M.A. (2004). Electrical synapses in the mammalian brain. Annu. Rev. Neurosci. *27*, 393–418.

Contractor, A., Swanson, G.T., Sailer, A., O'Gorman, S., and Heinemann, S.F. (2000). Identification of the kainate receptor subunits underlying modulation of excitatory synaptic transmission in the CA3 region of the hippocampus. J. Neurosci. *20*, 8269–8278.

Contractor, A., Swanson, G., and Heinemann, S.F. (2001). Kainate receptors are involved in short- and long-term plasticity at mossy fiber synapses in the hippocampus. Neuron *29*, 209–216.

Contractor, A., Sailer, A.W., Darstein, M., Maron, C., Xu, J., Swanson, G.T., and Heinemann, S.F. (2003). Loss of kainate receptor-mediated heterosynaptic facilitation of mossy-fiber synapses in KA2−/− mice. J. Neurosci. *23*, 422–429.

Contractor, A., Mulle, C., and Swanson, G.T. (2011). Kainate receptors coming of age: milestones of two decades of research. Trends Neurosci. *34*, 154–163.

Copits, B.A., Robbins, J.S., Frausto, S., and Swanson, G.T. (2011). Synaptic targeting and functional modulation of GluK1 kainate receptors by the auxiliary neuropilin and tolloid-like (NETO) proteins. J. Neurosci. Off. J. Soc. Neurosci. *31*, 7334–7340.

Coquelle, T., Christensen, J.K., Banke, T.G., Madsen, U., Schousboe, A., and Pickering, D.S. (2000). Agonist discrimination between AMPA receptor subtypes: NeuroReport *11*, 2643–2648.

Cormier, R.J., and Kelly, P.T. (1996). Glutamate-induced long-term potentiation enhances spontaneous EPSC amplitude but not frequency. J. Neurophysiol. *75*, 1909–1918.

Cossart, R., Esclapez, M., Hirsch, J.C., Bernard, C., and Ben-Ari, Y. (1998). GluR5 kainate receptor activation in interneurons increases tonic inhibition of pyramidal cells. Nat. Neurosci. *1*, 470–478.

Costa, B.M., Feng, B., Tsintsadze, T.S., Morley, R.M., Irvine, M.W., Tsintsadze, V., Lozovaya, N.A., Jane, D.E., and Monaghan, D.T. (2009). N-Methyl-d-aspartate (NMDA) receptor NR2 subunit selectivity of a series of novel piperazine-2,3-dicarboxylate derivatives: Preferential blockade of extrasynaptic NMDA receptors in the rat hippocampal CA3-CA1 synapse. J. Pharmacol. Exp. Ther. *331*, 618–626.

Costigan, M., Scholz, J., and Woolf, C.J. (2009). Neuropathic pain: a maladaptive response of the nervous system to damage. Annu. Rev. Neurosci. *32*, 1–32.

Cousins, S.L., Innocent, N., and Stephenson, F.A. (2013). Neto1 associates with the NMDA receptor/amyloid precursor protein complex. J. Neurochem. *126*, 554–564.

Cull-Candy, S., Brickley, S., and Farrant, M. (2001). NMDA receptor subunits: diversity, development and disease. Curr. Opin. Neurobiol. *11*, 327–335.

Curtis, D.R., and Johnston, G.A. (1974). Amino acid transmitters in the mammalian central nervous system. Ergeb. Physiol. *69*, 97–188.

Curtis, D.R., and Watkins, J.C. (1960). The excitation and depression of spinal neurones by structurally related amino acids. J. Neurochem. *6*, 117–141.

Curtis, D.R., and Watkins, J.C. (1963). Acidic amino acids with strong excitatory actions on mammalian neurones. J. Physiol. *166*, 1–14.

Dale, N., and Roberts, A. (1985). Dual-component amino-acid-mediated synaptic potentials: excitatory drive for swimming in Xenopus embryos. J. Physiol. *363*, 35–59.

Danbolt, N.C. (2001). Glutamate uptake. Prog. Neurobiol. *65*, 1–105.

Dargan, S.L., Clarke, V.R.J., Alushin, G.M., Sherwood, J.L., Nisticò, R., Bortolotto, Z.A., Ogden, A.M., Bleakman, D., Doherty, A.J., Lodge, D., et al. (2009). ACET is a highly potent and specific kainate receptor antagonist: Characterisation and effects on hippocampal mossy fibre function. Neuropharmacology *56*, 121–130.

Darstein, M., Petralia, R.S., Swanson, G.T., Wenthold, R.J., and Heinemann, S.F. (2003). Distribution of kainate receptor subunits at hippocampal mossy fiber synapses. J. Neurosci. *23*, 8013–8019.

Das, S., Sasaki, Y.F., Rothe, T., Premkumar, L.S., Takasu, M., Crandall, J.E., Dikkes, P., Conner, D.A., Rayudu, P.V., Cheung, W., et al. (1998). Increased NMDA current and spine density in mice lacking the NMDA receptor subunit NR3A. Nature *393*, 377–381.

Davies, J., and Watkins, J.C. (1979). Selective antagonism of amino acid-induced and synaptic excitation in the cat spinal cord. J. Physiol. *297*, 621–635.

Davies, J., and Watkins, J.C. (1981). Differentiation of kainate and quisqualate receptors in the cat spinal cord by selective antagonism with gamma-D(and L)-glutamylglycine.

Brain Res. *206*, 172–177.

Davies, J., and Watkins, J.C. (1985). Depressant actions of γ-d-glutamylaminomethyl sulfonate (GAMS) on amino acid-induced and synaptic excitation in the cat spinal cord. Brain Res. *327*, 113–120.

Davies, S.N., and Collingridge, G. (1989). Role of excitatory amino acid receptors in synaptic transmission in area CA1 of rat hippocampus. Proc. R. Soc. Lond. B Biol. Sci. *236*, 373–384.

Davies, C.H., Davies, S.N., and Collingridge, G.L. (1990). Paired-pulse depression of monosynaptic GABA-mediated inhibitory postsynaptic responses in rat hippocampus. J. Physiol. *424*, 513–531.

Davies, C.H., Starkey, S.J., Pozza, M.F., and Collingridge, G.L. (1991). GABA autoreceptors regulate the induction of LTP. Nature *349*, 609–611.

Davies, J., Evans, R.H., Francis, A.A., Jones, A.W., and Watkins, J.C. (1981a). Antagonism of excitatory amino acid-induced and synaptic excitation of spinal neurones by cis-2,3-piperidine dicarboxylate. J. Neurochem. *36*, 1305–1307.

Davies, J., Francis, A.A., Jones, A.W., and Watkins, J.C. (1981b). 2-Amino-5-phosphonovalerate (2APV), a potent and selective antagonist of amino acid-induced and synaptic excitation. Neurosci. Lett. *21*, 77–81.

Davies, J., Jones, A.W., Sheardown, M.J., Smith, D.A., and Watkins, J.C. (1984). Phosphono dipeptides and piperazine derivatives as antagonists of amino acid-induced and synaptic excitation in mammalian and amphibian spinal cord. Neurosci. Lett. *52*, 79–84.

Davies, J., Evans, R.H., Herrling, P.L., Jones, A.W., Olverman, H.J., Pook, P., and Watkins, J.C. (1986). CPP, a new potent and selective NMDA antagonist. Depression of central neuron responses, affinity for [3H]D-AP5 binding sites on brain membranes and anticonvulsant activity. Brain Res. *382*, 169–173.

Debanne, D., Gähwiler, B.H., and Thompson, S.M. (1999). Heterogeneity of synaptic plasticity at unitary CA3–CA1 and CA3–CA3 connections in rat hippocampal slice cultures. J. Neurosci. *19*, 10664–10671.

Deming, D., Cheng, Q., and Jayaraman, V. (2003). Is the isolated ligand binding domain a good model of the domain in the native receptor? J. Biol. Chem. *278*, 17589–17592.

Demmer, C.S., Møller, C., Brown, P.M.G.E., Han, L., Pickering, D.S., Nielsen, B., Bowie, D., Frydenvang, K., Kastrup, J.S., and Bunch, L. (2015). Binding mode of an α-amino acid-linked quinoxaline-2,3-dione analogue at glutamate receptor subtype GluK1. ACS Chem. Neurosci. *6*, 845–854.

Derkach, V., Barria, A., and Soderling, T.R. (1999). Ca2+/calmodulin-kinase II enhances channel conductance of alpha-amino-3-hydroxy-5-methyl-4-isoxazolepropionate type glutamate receptors. Proc. Natl. Acad. Sci. U. S. A. *96*, 3269–3274.

Dildy-Mayfield, J.E., Eger, E.I., and Harris, R.A. (1996). Anesthetics produce subunit-selective actions on glutamate receptors. J. Pharmacol. Exp. Ther. *276*, 1058–1065.

Dingledine, R., Hynes, M.A., and King, G.L. (1986). Involvement of N-methyl-D-aspartate receptors in epileptiform bursting in the rat hippocampal slice. J. Physiol. *380*, 175–189.

Dittman, J.S., and Regehr, W.G. (1998). Calcium dependence and recovery kinetics of presynaptic depression at the climbing fiber to purkinje cell synapse. J. Neurosci. *18*, 6147–6162.

Do, K.Q., Herrling, P.L., Streit, P., Turski, W.A., and Cuenod, M. (1986). In vitro release and electrophysiological effects in situ of homocysteic acid, an endogenous N-methyl-(D)-aspartic acid agonist, in the mammalian striatum. J. Neurosci. Off. J. Soc. Neurosci. *6*, 2226–2234.

Do, K.Q., Herrling, P.L., Streit, P., and Cuénod, M. (1988). Release of neuroactive substances: homocysteic acid as an endogenous agonist of the NMDA receptor. J. Neural Transm. *72*, 185–190.

Dolman, N.P., Troop, H.M., More, J.C.A., Alt, A., Knauss, J.L., Nistico, R., Jack, S., Morley, R.M., Bortolotto, Z.A., Roberts, P.J., et al. (2005). Synthesis and pharmacology of willardiine derivatives acting as antagonists of kainate receptors. J. Med. Chem. *48*, 7867–7881.

Dolman, N.P., More, J.C.A., Alt, A., Knauss, J.L., Troop, H.M., Bleakman, D., Collingridge, G.L., and Jane, D.E. (2006). Structure−activity relationship studies on N3-substituted willardiine derivatives acting as AMPA or kainate receptor antagonists. J. Med. Chem. *49*, 2579–2592.

Dolman, N.P., More, J.C.A., Alt, A., Knauss, J.L., Pentikäinen, O.T., Glasser, C.R., Bleakman, D., Mayer, M.L., Collingridge, G.L., and Jane, D.E. (2007). Synthesis and pharmacological characterization of N3-substituted willardiine derivatives: role of the substituent at the 5-position of the uracil ring in the development of highly potent and selective GLUK5 kainate receptor antagonists. J. Med. Chem. *50*, 1558–1570.

Dolphin, A.C., Errington, M.L., and Bliss, T.V.P. (1982). Long-term potentiation of the perforant path in vivo is associated with increased glutamate release. Nature *297*, 496.

Dominguez, E., Iyengar, S., Shannon, H.E., Bleakman, D., Alt, A., Arnold, B.M., Bell, M.G., Bleisch, T.J., Buckmaster, J.L., Castano, A.M., et al. (2005). Two prodrugs of potent and selective GluR5 kainate receptor antagonists actives in three animal models of pain. J. Med. Chem. *48*, 4200–4203.

Donevan, S.D., and Rogawski, M.A. (1995). Intracellular polyamines mediate inward rectification of Ca(2+)-permeable alpha-amino-3-hydroxy-5-methyl-4-isoxazolepropionic acid receptors. Proc. Natl. Acad. Sci. U. S. A. *92*, 9298–9302.

Donevan, S.D., Beg, A., Gunther, J.M., and Twyman, R.E. (1998). The methylglutamate, SYM 2081, is a potent and highly selective agonist at kainate receptors. J. Pharmacol. Exp. Ther. *285*, 539–545.

Dravid, S.M., Erreger, K., Yuan, H., Nicholson, K., Le, P., Lyuboslavsky, P., Almonte, A., Murray, E., Mosely, C., Barber, J., et al. (2007). Subunit-specific mechanisms and proton sensitivity of NMDA receptor channel block. J. Physiol. *581*, 107–128.

Dravid, S.M., Burger, P.B., Prakash, A., Geballe, M.T., Yadav, R., Le, P., Vellano, K., Snyder, J.P., and Traynelis, S.F. (2010). Structural determinants of D-cycloserine efficacy at the NR1/NR2C NMDA receptors. J. Neurosci. Off. J. Soc. Neurosci. *30*, 2741–2754.

Du, J., Zhou, S., and Carlton, S.M. (2006). Kainate-induced excitation and sensitization of nociceptors in normal and inflamed rat glabrous skin. Neuroscience *137*, 999–1013.

Duggan, A.W. (1974). The differential sensitivity to L-glutamate and L-aspartate of spinal interneurones and Renshaw cells. Exp. Brain Res. *19*, 522–528.

Duggan, A.W., and Johnston, G.A. (1970). Glutamate and related amino acids in cat spinal roots, dorsal root ganglia and peripheral nerves. J. Neurochem. *17*, 1205–1208.

Dumuis, A., Sebben, M., Haynes, L., Pin, J.P., and Bockaert, J. (1988). NMDA receptors activate the arachidonic acid cascade system in striatal neurons. Nature *336*, 68–70.

Dunah, A.W., Luo, J., Wang, Y.-H., Yasuda, R.P., and Wolfe, B.B. (1998). Subunit composition of N-Methyl-D-aspartate receptors in the central nervous system that contain the NR2D subunit. Mol. Pharmacol. *53*, 429–437.

Dunwiddie, T., and Lynch, G. (1978). Long-term potentiation and depression of synaptic responses in the rat hippocampus: localization and frequency dependency. J. Physiol. *276*, 353–367.

Eccles, J.C., Katz, B., and Kuffler, S.W. (1941). Nature of the “endplate potential” in curarized muscle. J. Neurophysiol. *4*, 362–387.

Edman, S., McKay, S., Macdonald, L.J., Samadi, M., Livesey, M.R., Hardingham, G.E., and Wyllie, D.J.A. (2012). TCN 201 selectively blocks GluN2A-containing NMDARs in a GluN1 co-agonist dependent but non-competitive manner. Neuropharmacology *63*, 441–449.

Edmonds, B., Gibb, A.J., and Colquhoun, D. (1995). Mechanisms of activation of glutamate receptors and the time course of excitatory synaptic currents. Annu. Rev. Physiol. *57*, 495–519.

Egebjerg, J., Bettler, B., Hermans-Borgmeyer, I., and Heinemann, S. (1991). Cloning of a cDNA for a glutamate receptor subunit activated by kainate but not AMPA. Nature *351*, 745.

Ehlers, M.D., Fung, E.T., O’Brien, R.J., and Huganir, R.L. (1998). Splice variant-specific interaction of the NMDA receptor subunit NR1 with neuronal intermediate filaments. J. Neurosci. Off. J. Soc. Neurosci. *18*, 720–730.

Engelhardt, J. von, Doganci, B., Jensen, V., Hvalby, Ø., Göngrich, C., Taylor, A., Barkus, C., Sanderson, D.J., Rawlins, J.N.P., Seeburg, P.H., et al. (2008). Contribution of hippocampal and extra-hippocampal NR2B-containing NMDA receptors to performance

on spatial learning tasks. Neuron *60*, 846–860.

Engelhardt, J. von, Bocklisch, C., Tönges, L., Herb, A., Mishina, M., and Monyer, H. (2015). GluN2D-containing NMDA receptors-mediate synaptic currents in hippocampal interneurons and pyramidal cells in juvenile mice. Front. Cell. Neurosci. *9*.

Engert, F., and Bonhoeffer, T. (1997). Synapse specificity of long-term potentiation breaks down at short distances. Nature *388*, 279–284.

Epsztein, J., Represa, A., Jorquera, I., Ben-Ari, Y., and Crépel, V. (2005). Recurrent mossy fibers establish aberrant kainate receptor-operated synapses on granule cells from epileptic rats. J. Neurosci. Off. J. Soc. Neurosci. *25*, 8229–8239.

Erreger, K., Chen, P.E., Wyllie, D.J.A., and Traynelis, S.F. (2004). Glutamate receptor gating. Crit. Rev. Neurobiol. *16*, 187–224.

Erreger, K., Dravid, S.M., Banke, T.G., Wyllie, D.J.A., and Traynelis, S.F. (2005). Subunit-specific gating controls rat NR1/NR2A and NR1/NR2B NMDA channel kinetics and synaptic signalling profiles. J. Physiol. *563*, 345–358.

Erreger, K., Geballe, M.T., Kristensen, A., Chen, P.E., Hansen, K.B., Lee, C.J., Yuan, H., Le, P., Lyuboslavsky, P.N., Micale, N., et al. (2007). Subunit-specific agonist activity at NR2A-, NR2B-, NR2C-, and NR2D-containing N-Methyl-d-aspartate glutamate receptors. Mol. Pharmacol. *72*, 907–920.

Evans, R.H., Francis, A.A., Jones, A.W., Smith, D.A., and Watkins, J.C. (1982). The effects of a series of omega-phosphonic alpha-carboxylic amino acids on electrically evoked and excitant amino acid-induced responses in isolated spinal cord preparations. Br. J. Pharmacol. *75*, 65–75.

Evans, R.H., Evans, S.J., Pook, P.C., and Sunter, D.C. (1987). A comparison of excitatory amino acid antagonists acting at primary afferent C fibres and motoneurones of the isolated spinal cord of the rat. Br. J. Pharmacol. *91*, 531–537.

Fabian-Fine, R., Volknandt, W., Fine, A., and Stewart, M.G. (2000). Age-dependent pre- and postsynaptic distribution of AMPA receptors at synapses in CA3 stratum radiatum of hippocampal slice cultures compared with intact brain. Eur. J. Neurosci. *12*, 3687–3700.

Fang, L., Wu, J., Lin, Q., and Willis, W.D. (2002). Calcium-calmodulin-dependent protein kinase II contributes to spinal cord central sensitization. J. Neurosci. Off. J. Soc. Neurosci. *22*, 4196–4204.

Feng, B., Tse, H.W., Skifter, D.A., Morley, R., Jane, D.E., and Monaghan, D.T. (2004). Structure-activity analysis of a novel NR2C/NR2D-preferring NMDA receptor antagonist: 1-(phenanthrene-2-carbonyl) piperazine-2,3-dicarboxylic acid. Br. J. Pharmacol. *141*, 508–516.

Feng, B., Morley, R., Jane, D., and Monaghan, D. (2005). The effect of competitive antagonist chain length on NMDA receptor subunit selectivity. Neuropharmacology *48*, 354–359.

Fernandes, H.B., Catches, J.S., Petralia, R.S., Copits, B.A., Xu, J., Russell, T.A., Swanson, G.T., and Contractor, A. (2009). High-affinity kainate receptor subunits are necessary for ionotropic but not metabotropic signaling. Neuron *63*, 818–829.

Fernández-Chacón, R., Königstorfer, A., Gerber, S.H., García, J., Matos, M.F., Stevens, C.F., Brose, N., Rizo, J., Rosenmund, C., and Südhof, T.C. (2001). Synaptotagmin I functions as a calcium regulator of release probability. Nature *410*, 41–49.

Fisahn, A., Contractor, A., Traub, R.D., Buhl, E.H., Heinemann, S.F., and McBain, C.J. (2004). Distinct roles for the kainate receptor subunits GluR5 and GluR6 in kainate-induced hippocampal gamma oscillations. J. Neurosci. *24*, 9658–9668.

Fischer, G., Mutel, V., Trube, G., Malherbe, P., Kew, J.N.C., Mohacsi, E., Heitz, M.P., and Kemp, J.A. (1997). Ro 25–6981, a highly potent and selective blocker of N-Methyl-D-aspartate receptors containing the NR2B subunit. Characterization in vitro. J. Pharmacol. Exp. Ther. *283*, 1285–1292.

Fisher, J.L. (2015). The auxiliary subunits Neto1 and Neto2 have distinct, subunit-dependent effects at recombinant GluK1- and GluK2-containing kainate receptors. Neuropharmacology *99*, 471–480.

Fleck, M.W., Henze, D.A., Barrionuevo, G., and Palmer, A.M. (1993). Aspartate and glutamate mediate excitatory synaptic transmission in area CA1 of the hippocampus. J. Neurosci. Off. J. Soc. Neurosci. *13*, 3944–3955.

Fletcher, E.J., Martin, D., Aram, J.A., Lodge, D., and Honoré, T. (1988). Quinoxalinediones selectively block quisqualate and kainate receptors and synaptic events in rat neocortex and hippocampus and frog spinal cord in vitro. Br. J. Pharmacol. *95*, 585–597.

Foster, M. (Michael), and Sherrington, C.S. (1897). A textbook of physiology, part three (London : Macmillan).

France, G., Fernández-Fernández, D., Burnell, E.S., Irvine, M.W., Monaghan, D.T., Jane, D.E., Bortolotto, Z.A., Collingridge, G.L., and Volianskis, A. (2017). Multiple roles of GluN2B-containing NMDA receptors in synaptic plasticity in juvenile hippocampus. Neuropharmacology *112*, 76–83.

Frederickson, C.J. (1989). Neurobiology of zinc and zinc-containing neurons. Int. Rev. Neurobiol. *31*, 145–238.

Frerking, M., and Ohliger-Frerking, P. (2002). AMPA receptors and kainate receptors encode different features of afferent activity. J. Neurosci. Off. J. Soc. Neurosci. *22*, 7434–7443.

Frerking, M., Malenka, R.C., and Nicoll, R.A. (1998). Synaptic activation of kainate receptors on hippocampal interneurons. Nat. Neurosci. *1*, 479–486.

Frerking, M., Schmitz, D., Zhou, Q., Johansen, J., and Nicoll, R.A. (2001). Kainate receptors depress excitatory synaptic transmission at CA3→CA1 synapses in the hippocampus via a direct presynaptic action. J. Neurosci. *21*, 2958–2966.

Frey, U., Krug, M., Reymann, K.G., and Matthies, H. (1988). Anisomycin, an inhibitor of protein synthesis, blocks late phases of LTP phenomena in the hippocampal CA1 region in vitro. Brain Res. *452*, 57–65.

Friesner, R.A., Banks, J.L., Murphy, R.B., Halgren, T.A., Klicic, J.J., Mainz, D.T., Repasky, M.P., Knoll, E.H., Shelley, M., Perry, J.K., et al. (2004). Glide: a new approach for rapid, accurate docking and scoring. 1. Method and assessment of docking accuracy. J. Med. Chem. *47*, 1739–1749.

Fritsch, B., Reis, J., Gasior, M., Kaminski, R.M., and Rogawski, M.A. (2014). Role of GluK1 kainate receptors in seizures, epileptic discharges, and epileptogenesis. J. Neurosci. Off. J. Soc. Neurosci. *34*, 5765–5775.

Frizelle, P.A., Chen, P.E., and Wyllie, D.J.A. (2006). Equilibrium constants for (R)-[(S)-1-(4-bromo-phenyl)-ethylamino]-(2,3-dioxo-1,2,3,4-tetrahydroquinoxalin-5-yl)-methyl]-phosphonic acid (NVP-AAM077) acting at recombinant NR1/NR2A and NR1/NR2B N-methyl-D-aspartate receptors: Implications for studies of synaptic transmission. Mol. Pharmacol. *70*, 1022–1032.

Fujisawa, H., Dawson, D., Browne, S.E., MacKay, K.B., Bullock, R., and McCulloch, J. (1993). Pharmacological modification of glutamate neurotoxicity in vivo. Brain Res. *629*, 73–78.

Fukata, Y., Tzingounis, A.V., Trinidad, J.C., Fukata, M., Burlingame, A.L., Nicoll, R.A., and Bredt, D.S. (2005). Molecular constituents of neuronal AMPA receptors. J. Cell Biol. *169*, 399–404.

Furukawa, H., and Gouaux, E. (2003). Mechanisms of activation, inhibition and specificity: crystal structures of the NMDA receptor NR1 ligand-binding core. EMBO J. *22*, 2873–2885.

Furukawa, H., Singh, S.K., Mancusso, R., and Gouaux, E. (2005). Subunit arrangement and function in NMDA receptors. Nature *438*, 185–192.

Gallyas, F., Ball, S.M., and Molnar, E. (2003). Assembly and cell surface expression of KA-2 subunit-containing kainate receptors. J. Neurochem. *86*, 1414–1427.

Ganong, A.H., Lanthorn, T.H., and Cotman, C.W. (1983). Kynurenic acid inhibits synaptic and acidic amino acid-induced responses in the rat hippocampus and spinal cord. Brain Res. *273*, 170–174.

Ganong, A.H., Jones, A.W., Watkins, J.C., and Cotman, C.W. (1986). Parallel antagonism of synaptic transmission and kainate/quisqualate responses in the hippocampus by piperazine-2,3-dicarboxylic acid analogs. J. Neurosci. Off. J. Soc. Neurosci. *6*, 930–937.

Garcia, E.P., Mehta, S., Blair, L.A.C., Wells, D.G., Shang, J., Fukushima, T., Fallon, J.R., Garner, C.C., and Marshall, J. (1998). SAP90 binds and clusters kainate receptors causing incomplete desensitization. Neuron *21*, 727–739.

Gardoni, F., Caputi, A., Cimino, M., Pastorino, L., Cattabeni, F., and Di Luca, M. (1998). Calcium/calmodulin-dependent protein kinase II is associated with NR2A/B subunits of

NMDA receptor in postsynaptic densities. J. Neurochem. *71*, 1733–1741.

Geiger, J.R., Lübke, J., Roth, A., Frotscher, M., and Jonas, P. (1997). Submillisecond AMPA receptor-mediated signaling at a principal neuron-interneuron synapse. Neuron *18*, 1009–1023.

Gielen, M., Retchless, B.S., Mony, L., Johnson, J.W., and Paoletti, P. (2009). Mechanism of differential control of NMDA receptor activity by NR2 subunits. Nature *459*, 703–707.

Giffard, R.G., Monyer, H., Christine, C.W., and Choi, D.W. (1990). Acidosis reduces NMDA receptor activation, glutamate neurotoxicity, and oxygen-glucose deprivation neuronal injury in cortical cultures. Brain Res. *506*, 339–342.

Gilron, I., Max, M.B., Lee, G., Booher, S.L., Sang, C.N., Chappell, A.S., and Dionne, R.A. (2000). Effects of the 2-amino-3-hydroxy-5-methyl-4-isoxazole-proprionic acid/kainate antagonist LY293558 on spontaneous and evoked postoperative pain. Clin. Pharmacol. Ther. *68*, 320–327.

Glickstein, M. (2006). Golgi and Cajal: The neuron doctrine and the 100th anniversary of the 1906 Nobel Prize. Curr. Biol. CB *16*, R147-151.

Goldenberg, M.M. (2010). Overview of drugs used for epilepsy and seizures. Pharm. Ther. *35*, 392–415.

Graham, L.T., Shank, R.P., Werman, R., and Aprison, M.H. (1967). Distribution of some synaptic transmitter suspects in cat spinal cord: glutamic acid, aspartic acid, gamma-aminobutyric acid, glycine and glutamine. J. Neurochem. *14*, 465–472.

Greer, J. (1980). Model for haptoglobin heavy chain based upon structural homology. Proc. Natl. Acad. Sci. U. S. A. *77*, 3393–3397.

Grover, L.M., and Teyler, T.J. (1990). Two components of long-term potentiation induced by different patterns of afferent activation. Nature *347*, 477–479.

Gryder, D.S., and Rogawski, M.A. (2003). Selective antagonism of GluR5 kainate-receptor-mediated synaptic currents by topiramate in rat basolateral amygdala neurons. J. Neurosci. Off. J. Soc. Neurosci. *23*, 7069–7074.

Gustafsson, B., and Wigström, H. (1990). Long-term potentiation in the hippocampal CA1 region: its induction and early temporal development. Prog. Brain Res. *83*, 223–232.

Gustafsson, B., Galvan, M., Grafe, P., and Wigström, H. (1982). A transient outward current in a mammalian central neurone blocked by 4-aminopyridine. Nature *299*, 252–254.

Gustafsson, B., Wigström, H., Abraham, W.C., and Huang, Y.Y. (1987). Long-term potentiation in the hippocampus using depolarizing current pulses as the conditioning stimulus to single volley synaptic potentials. J. Neurosci. Off. J. Soc. Neurosci. *7*, 774–780.

Ha, G.E., and Cheong, E. (2017). Spike frequency adaptation in neurons of the central

nervous system. Exp. Neurobiol. *26*, 179–185.

Hald, H., Naur, P., Pickering, D.S., Sprogøe, D., Madsen, U., Timmermann, D.B., Ahring, P.K., Liljefors, T., Schousboe, A., Egebjerg, J., et al. (2007). Partial agonism and antagonism of the ionotropic glutamate receptor iGLuR5: structures of the ligand-binding core in complex with domoic acid and 2-amino-3-[5-tert-butyl-3-(phosphonomethoxy)-4-isoxazolyl]propionic acid. J. Biol. Chem. *282*, 25726–25736.

Hansch, C., Leo, A., Unger, S.H., Kim, K.H., Nikaitani, D., and Lien, E.J. (1973). Aromatic substituent constants for structure-activity correlations. J. Med. Chem. *16*, 1207–1216.

Hansen, K.B., and Traynelis, S.F. (2011). Structural and mechanistic determinants of a novel site for non-competitive inhibition of GluN2D-containing NMDA receptors. J. Neurosci. Off. J. Soc. Neurosci. *31*, 3650–3661.

Hansen, K.B., Yuan, H., and Traynelis, S.F. (2007). Structural aspects of AMPA receptor activation, desensitization and deactivation. Curr. Opin. Neurobiol. *17*, 281–288.

Hansen, K.B., Ogden, K.K., and Traynelis, S.F. (2012). Subunit-selective allosteric inhibition of glycine binding to NMDA receptors. J. Neurosci. *32*, 6197–6208.

Hansen, K.B., Ogden, K.K., Yuan, H., and Traynelis, S.F. (2014). Distinct functional and pharmacological properties of triheteromeric GluN1/GluN2A/GluN2B NMDA receptors. Neuron *81*, 1084–1096.

Hansen, K.B., Yi, F., Perszyk, R.E., Furukawa, H., Wollmuth, L.P., Gibb, A.J., and Traynelis, S.F. (2018). Structure, function, and allosteric modulation of NMDA receptors. J. Gen. Physiol. *150*, 1081–1105.

Harder, E., Damm, W., Maple, J., Wu, C., Reboul, M., Xiang, J.Y., Wang, L., Lupyan, D., Dahlgren, M.K., Knight, J.L., et al. (2016). OPLS3: A force field providing broad coverage of drug-like small molecules and proteins. J. Chem. Theory Comput. *12*, 281–296.

Harney, S.C., Jane, D.E., and Anwyl, R. (2008). Extrasynaptic NR2D-containing NMDARs are recruited to the synapse during LTP of NMDAR-EPSCs. J. Neurosci. *28*, 11685–11694.

Harris, E.W., and Cotman, C.W. (1986). Long-term potentiation of guinea pig mossy fiber responses is not blocked by N-methyl D-aspartate antagonists. Neurosci. Lett. *70*, 132–137.

Harris, K.M., and Sultan, P. (1995). Variation in the number, location and size of synaptic vesicles provides an anatomical basis for the nonuniform probability of release at hippocampal CA1 synapses. Neuropharmacology *34*, 1387–1395.

Harris, E.W., Ganong, A.H., and Cotman, C.W. (1984). Long-term potentiation in the hippocampus involves activation of N-methyl-D-aspartate receptors. Brain Res. *323*, 132–137.

Harvey, J., and Collingridge, G.L. (1992). Thapsigargin blocks the induction of long-term potentiation in rat hippocampal slices. Neurosci. Lett. *139*, 197–200.

Hashimoto, K., Fukaya, M., Qiao, X., Sakimura, K., Watanabe, M., and Kano, M. (1999). Impairment of AMPA receptor function in cerebellar granule cells of ataxic mutant mouse stargazer. J. Neurosci. Off. J. Soc. Neurosci. *19*, 6027–6036.

Hatton, C.J., and Paoletti, P. (2005). Modulation of triheteromeric NMDA receptors by N-terminal domain ligands. Neuron *46*, 261–274.

Hayashi, T. (1954). Effects of sodium glutamate on the nervous system. Keio J Med *3*, 192–193.

Hebb, D.O. (1949). The organization of behavior: A neuropsychological theory (Wiley).

von Heijne, G. (1986). A new method for predicting signal sequence cleavage sites. Nucleic Acids Res. *14*, 4683–4690.

van der Hel, W.S., Verlinde, S.A.M.W., Meijer, D.H.M., de Wit, M., Rensen, M.G., van Gassen, K.L.I., van Rijen, P.C., van Veelen, C.W.M., and de Graan, P.N.E. (2009). Hippocampal distribution of vesicular glutamate transporter 1 in patients with temporal lobe epilepsy. Epilepsia *50*, 1717–1728.

Hellier, J.L., Patrylo, P.R., Buckmaster, P.S., and Dudek, F.E. (1998). Recurrent spontaneous motor seizures after repeated low-dose systemic treatment with kainate: assessment of a rat model of temporal lobe epilepsy. Epilepsy Res. *31*, 73–84.

Herb, A., Burnashev, N., Werner, P., Sakmann, B., Wisden, W., and Seeburg, P.H. (1992). The KA-2 subunit of excitatory amino acid receptors shows widespread expression in brain and forms ion channels with distantly related subunits. Neuron *8*, 775–785.

Herron, C.E., Williamson, R., and Collingridge, G.L. (1985). A selective N-methyl-D-aspartate antagonist depresses epileptiform activity in rat hippocampal slices. Neurosci. Lett. *61*, 255–260.

Hess, S.D., Daggett, L.P., Crona, J., Deal, C., Lu, C.C., Urrutia, A., Chavez-Noriega, L., Ellis, S.B., Johnson, E.C., and Veliçelebi, G. (1996). Cloning and functional characterization of human heteromeric N-methyl-D-aspartate receptors. J. Pharmacol. Exp. Ther. *278*, 808–816.

Hess, S.D., Daggett, L.P., Deal, C., Lu, C.C., Johnson, E.C., and Veliçelebi, G. (1998). Functional characterization of human N-methyl-D-aspartate subtype 1A/2D receptors. J. Neurochem. *70*, 1269–1279.

Heuser, J.E., and Reese, T.S. (1973). Evidence for recycling of synaptic vesicle membrane during transmitter release at the frog neuromuscular junction. J. Cell Biol. *57*, 315–344.

Hille, B. (1992). Ionic channels of excitable membranes (Sunderland, Mass: Sinauer Associates).

Hirbec, H., Francis, J.C., Lauri, S.E., Braithwaite, S.P., Coussen, F., Mulle, C., Dev, K.K., Couthino, V., Meyer, G., Isaac, J.T.R., et al. (2003). Rapid and differential regulation of AMPA and kainate receptors at hippocampal mossy fibre synapses by PICK1 and GRIP. Neuron *37*, 625–638.

Hirose, K., and Chan, P.H. (1993). Blockade of glutamate excitotoxicity and its clinical applications. Neurochem. Res. *18*, 479–483.

Hodgkin, A.L., and Huxley, A.F. (1952). A quantitative description of membrane current and its application to conduction and excitation in nerve. J. Physiol. *117*, 500–544.

Hodgkin, A.L., Huxley, A.F., and Katz, B. (1952). Measurement of current-voltage relations in the membrane of the giant axon of Loligo. J. Physiol. *116*, 424–448.

Hollmann, M., and Heinemann, S. (1994). Cloned glutamate receptors. Annu. Rev. Neurosci. *17*, 31–108.

Hollmann, M., O'Shea-Greenfield, A., Rogers, S.W., and Heinemann, S. (1989). Cloning by functional expression of a member of the glutamate receptor family. Nature *342*, 643–648.

Holm, M.M., Lunn, M.-L., Traynelis, S.F., Kastrup, J.S., and Egebjerg, J. (2005). Structural determinants of agonist-specific kinetics at the ionotropic glutamate receptor 2. Proc. Natl. Acad. Sci. U. S. A. *102*, 12053–12058.

Honoré, T., Davies, S.N., Drejer, J., Fletcher, E.J., Jacobsen, P., Lodge, D., and Nielsen, F.E. (1988). Quinoxalinediones: potent competitive non-NMDA glutamate receptor antagonists. Science *241*, 701–703.

Hoo, K.H., Nutt, S.L., Fletcher, E.J., Elliott, C.E., Korczak, B., Deverill, R.M., Rampersad, V., Fantaske, R.P., and Kamboj, R.K. (1994). Functional expression and pharmacological characterization of the human EAA4 (GluR6) glutamate receptor: a kainate selective channel subunit. Receptors Channels *2*, 327–337.

Hood, W.F., Compton, R.P., and Monahan, J.B. (1989). D-cycloserine: a ligand for the N-methyl-D-aspartate coupled glycine receptor has partial agonist characteristics. Neurosci. Lett. *98*, 91–95.

Hrabetova, S., Serrano, P., Blace, N., Tse, H.W., Skifter, D.A., Jane, D.E., Monaghan, D.T., and Sacktor, T.C. (2000). Distinct NMDA receptor subpopulations contribute to long-term potentiation and long-term depression induction. J. Neurosci. *20*, RC81.

Hu, W., Zhang, C., Wu, R., Sun, Y., Levine, A., and Feng, Z. (2010). Glutaminase 2, a novel p53 target gene regulating energy metabolism and antioxidant function. Proc. Natl. Acad. Sci. U. S. A. *107*, 7455–7460.

Huang, Y.Y., and Kandel, E.R. (1994). Recruitment of long-lasting and protein kinase A-dependent long-term potentiation in the CA1 region of hippocampus requires repeated tetanization. Learn. Mem. Cold Spring Harb. N *1*, 74–82.

Huang, Y.-S., Jung, M.-Y., Sarkissian, M., and Richter, J.D. (2002). N-methyl-D-aspartate

receptor signaling results in Aurora kinase-catalyzed CPEB phosphorylation and alpha CaMKII mRNA polyadenylation at synapses. EMBO J. *21*, 2139–2148.

Huang, Y.Y., Colino, A., Selig, D.K., and Malenka, R.C. (1992). The influence of prior synaptic activity on the induction of long-term potentiation. Science *255*, 730–733.

Huber, K.M., Kayser, M.S., and Bear, M.F. (2000). Role for rapid dendritic protein synthesis in hippocampal mGluR-dependent long-term depression. Science *288*, 1254–1257.

Huettner, J.E. (1990). Glutamate receptor channels in rat DRG neurons: activation by kainate and quisqualate and blockade of desensitization by Con A. Neuron *5*, 255–266.

Huettner, J.E., and Bean, B.P. (1988). Block of N-methyl-D-aspartate-activated current by the anticonvulsant MK-801: selective binding to open channels. Proc. Natl. Acad. Sci. U. S. A. *85*, 1307–1311.

Hume, R.I., Dingledine, R., and Heinemann, S.F. (1991). Identification of a site in glutamate receptor subunits that controls calcium permeability. Science *253*, 1028–1031.

Hunter, J.C., and Singh, L. (1994). Role of excitatory amino acid receptors in the mediation of the nociceptive response to formalin in the rat. Neurosci. Lett. *174*, 217–221.

Huttner, W.B., Schiebler, W., Greengard, P., and De Camilli, P. (1983). Synapsin I (protein I), a nerve terminal-specific phosphoprotein. III. Its association with synaptic vesicles studied in a highly purified synaptic vesicle preparation. J. Cell Biol. *96*, 1374–1388.

Huxter, J.R., Zinyuk, L.E., Roloff, E. v L., Clarke, V.R.J., Dolman, N.P., More, J.C.A., Jane, D.E., Collingridge, G.L., and Muller, R.U. (2007). Inhibition of kainate receptors reduces the frequency of hippocampal theta oscillations. J. Neurosci. *27*, 2212–2223.

Ikeda, K., Araki, K., Takayama, C., Inoue, Y., Yagi, T., Aizawa, S., and Mishina, M. (1995). Reduced spontaneous activity of mice defective in the ε4 subunit of the NMDA receptor channel. Mol. Brain Res. *33*, 61–71.

Ingram, R., Kang, H., Lightman, S., Jane, D.E., Bortolotto, Z.A., Collingridge, G.L., Lodge, D., and Volianskis, A. (2018). Some distorted thoughts about ketamine as a psychedelic and a novel hypothesis based on NMDA receptor-mediated synaptic plasticity. Neuropharmacology *142*, 30–40.

Irvine, M.W., Costa, B.M., Dlaboga, D., Culley, G.R., Hulse, R., Scholefield, C.L., Atlason, P., Fang, G., Eaves, R., Morley, R., et al. (2012). Piperazine-2,3-dicarboxylic acid derivatives as dual antagonists of NMDA and GluK1-containing kainate receptors. J. Med. Chem. *55*, 327–341.

Isaac, J.T., Nicoll, R.A., and Malenka, R.C. (1995). Evidence for silent synapses: implications for the expression of LTP. Neuron *15*, 427–434.

Ito, I., Hidaka, H., and Sugiyama, H. (1991). Effects of KN-62, a specific inhibitor of

calcium/calmodulin-dependent protein kinase II, on long-term potentiation in the rat hippocampus. Neurosci. Lett. *121*, 119–121.

Ivakine, E.A., Acton, B.A., Mahadevan, V., Ormond, J., Tang, M., Pressey, J.C., Huang, M.Y., Ng, D., Delpire, E., Salter, M.W., et al. (2013). Neto2 is a KCC2 interacting protein required for neuronal Cl− regulation in hippocampal neurons. Proc. Natl. Acad. Sci. *110*, 3561–3566.

Jackson, D.L., Graff, C.B., Richardson, J.D., and Hargreaves, K.M. (1995). Glutamate participates in the peripheral modulation of thermal hyperalgesia in rats. Eur. J. Pharmacol. *284*, 321–325.

Jane, D.E., Hoo, K., Kamboj, R., Deverill, M., Bleakman, D., and Mandelzys, A. (1997). Synthesis of willardiine and 6-azawillardiine analogs: pharmacological characterization on cloned homomeric human AMPA and kainate receptor subtypes. J. Med. Chem. *40*, 3645–3650.

Jane, D.E., Lodge, D., and Collingridge, G.L. (2009). Kainate receptors: Pharmacology, function and therapeutic potential. Neuropharmacology *56*, 90–113.

Jatzke, C., Watanabe, J., and Wollmuth, L.P. (2002). Voltage and concentration dependence of Ca(2+) permeability in recombinant glutamate receptor subtypes. J. Physiol. *538*, 25–39.

Jeong, S.M., Hahm, K.D., Shin, J.W., Leem, J.G., Lee, C., and Han, S.M. (2006). Changes in magnesium concentration in the serum and cerebrospinal fluid of neuropathic rats. Acta Anaesthesiol. Scand. *50*, 211–216.

Jespersen, A., Tajima, N., Fernandez-Cuervo, G., Garnier-Amblard, E.C., and Furukawa, H. (2014). Structural insights into competitive antagonism in NMDA receptors. Neuron *81*, 366–378.

Jessen, M., Frederiksen, K., Yi, F., Clausen, R.P., Hansen, K.B., Bräuner-Osborne, H., Kilburn, P., and Damholt, A. (2017). Identification of AICP as a GluN2C-selective N-methyl-D-aspartate receptor superagonist at the GluN1 glycine site. Mol. Pharmacol. *92*, 151–161.

Jia, Z., Agopyan, N., Miu, P., Xiong, Z., Henderson, J., Gerlai, R., Taverna, F.A., Velumian, A., MacDonald, J., Carlen, P., et al. (1996). Enhanced LTP in mice deficient in the AMPA receptor GluR2. Neuron *17*, 945–956.

Jiang, L., Xu, J., Nedergaard, M., and Kang, J. (2001). A kainate receptor increases the efficacy of GABAergic synapses. Neuron *30*, 503–513.

Jin, R., Clark, S., Weeks, A.M., Dudman, J.T., Gouaux, E., and Partin, K.M. (2005). Mechanism of positive allosteric modulators acting on AMPA receptors. J. Neurosci. Off. J. Soc. Neurosci. *25*, 9027–9036.

Johansen, T.H., Chaudhary, A., and Verdoorn, T.A. (1995). Interactions among GYKI-52466, cyclothiazide, and aniracetam at recombinant AMPA and kainate receptors. Mol. Pharmacol. *48*, 946–955.

Johnson, J.W., and Ascher, P. (1987). Glycine potentiates the NMDA response in cultured mouse brain neurons. Nature *325*, 529–531.

Johnston, G.A. (1968). The intraspinal distribution of some depressant amino acids. J. Neurochem. *15*, 1013–1017.

Jones, S., and Gibb, A.J. (2005). Functional NR2B- and NR2D-containing NMDA receptor channels in rat substantia nigra dopaminergic neurones. J. Physiol. *569*, 209–221.

Jones, C.K., Alt, A., Ogden, A.M., Bleakman, D., Simmons, R.M.A., Iyengar, S., Dominguez, E., Ornstein, P.L., and Shannon, H.E. (2006). Antiallodynic and antihyperalgesic effects of selective competitive GLUK5 (GluR5) ionotropic glutamate receptor antagonists in the capsaicin and carrageenan models in rats. J. Pharmacol. Exp. Ther. *319*, 396–404.

Jones, K.A., Wilding, T.J., Huettner, J.E., and Costa, A.M. (1997). Desensitization of kainate receptors by kainate, glutamate and diastereomers of 4-methylglutamate. Neuropharmacology *36*, 853–863.

Kamboj, S.K., Swanson, G.T., and Cull-Candy, S.G. (1995). Intracellular spermine confers rectification on rat calcium-permeable AMPA and kainate receptors. J. Physiol. *486 (Pt 2)*, 297–303.

Kamiya, H., and Ozawa, S. (1998). Kainate receptor-mediated inhibition of presynaptic Ca2+ influx and EPSP in area CA1 of the rat hippocampus. J. Physiol. *509*, 833–845.

Kang, H., and Schuman, E.M. (1996). A requirement for local protein synthesis in neurotrophin-induced hippocampal synaptic plasticity. Science *273*, 1402–1406.

Kapetanovic, I.M. (2008). Computer-aided drug discovery and development (CADDD): In silico-chemico-biological approach. Chem. Biol. Interact. *171*, 165–176.

Karakas, E., and Furukawa, H. (2014). Crystal structure of a heterotetrameric NMDA receptor ion channel. Science *344*, 992–997.

Karakas, E., Simorowski, N., and Furukawa, H. (2009). Structure of the zinc-bound amino-terminal domain of the NMDA receptor NR2B subunit. EMBO J. *28*, 3910–3920.

Kato, A.S., Siuda, E.R., Nisenbaum, E.S., and Bredt, D.S. (2008). AMPA receptor subunit-specific regulation by a distinct family of type II TARPs. Neuron *59*, 986–996.

Kauer, J.A., Malenka, R.C., and Nicoll, R.A. (1988). NMDA application potentiates synaptic transmission in the hippocampus. Nature *334*, 250–252.

Kavalali, E.T., Zhuo, M., Bito, H., and Tsien, R.W. (1997). Dendritic Ca2+ channels characterized by recordings from isolated hippocampal dendritic segments. Neuron *18*, 651–663.

Kelso, S.R., Ganong, A.H., and Brown, T.H. (1986). Hebbian synapses in hippocampus. Proc. Natl. Acad. Sci. *83*, 5326–5330.

Kemp, J.A., Foster, A.C., Leeson, P.D., Priestley, T., Tridgett, R., Iversen, L.L., and Woodruff, G.N. (1988). 7-Chlorokynurenic acid is a selective antagonist at the glycine modulatory site of the N-methyl-D-aspartate receptor complex. Proc. Natl. Acad. Sci. U. S. A. *85*, 6547–6550.

Kemp, N., McQueen, J., Faulkes, S., and Bashir, Z.I. (2000). Different forms of LTD in the CA1 region of the hippocampus: role of age and stimulus protocol. Eur. J. Neurosci. *12*, 360–366.

Kerchner, G.A., Wilding, T.J., Li, P., Zhuo, M., and Huettner, J.E. (2001). Presynaptic kainate receptors regulate spinal sensory transmission. J. Neurosci. *21*, 59–66.

Kerchner, G.A., Wilding, T.J., Huettner, J.E., and Zhuo, M. (2002). Kainate receptor subunits underlying presynaptic regulation of transmitter release in the dorsal horn. J. Neurosci. *22*, 8010–8017.

Khalilov, I., Hirsch, J., Cossart, R., and Ben-Ari, Y. (2002). Paradoxical anti-epileptic effects of a GluR5 agonist of kainate receptors. J. Neurophysiol. *88*, 523–527.

Khatri, A., Burger, P.B., Swanger, S.A., Hansen, K.B., Zimmerman, S., Karakas, E., Liotta, D.C., Furukawa, H., Snyder, J.P., and Traynelis, S.F. (2014). Structural determinants and mechanism of action of a GluN2C-selective NMDA receptor positive allosteric modulator. Mol. Pharmacol. *86*, 548–560.

Kidd, F.L., and Isaac, J.T. (1999). Developmental and activity-dependent regulation of kainate receptors at thalamocortical synapses. Nature *400*, 569–573.

Kidd, F.L., and Isaac, J.T.R. (2001). Kinetics and activation of postsynaptic kainate receptors at thalamocortical synapses: Role of glutamate clearance. J. Neurophysiol. *86*, 1139–1148.

Kiskin, N.I., Krishtal, O.A., and Tsyndrenko, A.Ya. (1986). Excitatory amino acid receptors in hippocampal neurons: kainate fails to desensitize them. Neurosci. Lett. *63*, 225–230.

Kiyama, Y., Manabe, T., Sakimura, K., Kawakami, F., Mori, H., and Mishina, M. (1998). Increased thresholds for long-term potentiation and contextual learning in mice lacking the NMDA-type glutamate receptor ε1 subunit. J. Neurosci. *18*, 6704–6712.

Klausberger, T., and Somogyi, P. (2008). Neuronal diversity and temporal dynamics: the unity of hippocampal circuit operations. Science *321*, 53–57.

Kleckner, N.W., and Dingledine, R. (1988). Requirement for glycine in activation of NMDA-receptors expressed in Xenopus oocytes. Science *241*, 835–837.

Ko, S., Zhao, M.-G., Toyoda, H., Qiu, C.-S., and Zhuo, M. (2005). Altered behavioral responses to noxious stimuli and fear in glutamate receptor 5 (GluR5)- or GluR6-deficient mice. J. Neurosci. Off. J. Soc. Neurosci. *25*, 977–984.

Koester, H.J., and Sakmann, B. (2000). Calcium dynamics associated with action potentials in single nerve terminals of pyramidal cells in layer 2/3 of the young rat

neocortex. J. Physiol. *529 Pt 3*, 625–646.

Köhr, G., and Seeburg, P.H. (1996). Subtype-specific regulation of recombinant NMDA receptor-channels by protein tyrosine kinases of the src family. J. Physiol. *492 (Pt 2)*, 445–452.

Köhr, G., Jensen, V., Koester, H.J., Mihaljevic, A.L.A., Utvik, J.K., Kvello, A., Ottersen, O.P., Seeburg, P.H., Sprengel, R., and Hvalby, Ø. (2003). Intracellular domains of NMDA receptor subtypes are determinants for long-term potentiation induction. J. Neurosci. *23*, 10791–10799.

Kondo, M., Sumino, R., and Okado, H. (1997). Combinations of AMPA receptor subunit expression in individual cortical neurons correlate with expression of specific calcium-binding proteins. J. Neurosci. *17*, 1570–1581.

Konorski, J. (1948). Conditioned reflexes and neuron organization (New York, NY, US: Cambridge University Press).

Korczak, B., Nutt, S.L., Fletcher, E.J., Hoo, K.H., Elliott, C.E., Rampersad, V., McWhinnie, E.A., and Kamboj, R.K. (1995). cDNA cloning and functional properties of human glutamate receptor EAA3 (GluR5) in homomeric and heteromeric configuration. Receptors Channels *3*, 41–49.

Kotermanski, S.E., and Johnson, J.W. (2009). Mg2+ imparts NMDA receptor subtype selectivity to the Alzheimer's drug memantine. J. Neurosci. Off. J. Soc. Neurosci. *29*, 2774–2779.

Kott, S., Werner, M., Körber, C., and Hollmann, M. (2007). Electrophysiological properties of AMPA receptors are differentially modulated depending on the associated member of the TARP family. J. Neurosci. *27*, 3780–3789.

Krug, M., Lössner, B., and Ott, T. (1984). Anisomycin blocks the late phase of long-term potentiation in the dentate gyrus of freely moving rats. Brain Res. Bull. *13*, 39–42.

Kumar, J., Schuck, P., Jin, R., and Mayer, M.L. (2009). The N-terminal domain of GluR6-subtype glutamate receptor ion channels. Nat. Struct. Mol. Biol. *16*, 631–638.

Kumar, J., Schuck, P., and Mayer, M.L. (2011). Structure and assembly mechanism for heteromeric kainate receptors. Neuron *71*, 319–331.

Kuner, T., Seeburg, P.H., and Guy, H.R. (2003). A common architecture for K+ channels and ionotropic glutamate receptors? Trends Neurosci. *26*, 27–32.

Kutsuwada, T., Kashiwabuchi, N., Mori, H., Sakimura, K., Kushiya, E., Araki, K., Meguro, H., Masaki, H., Kumanishi, T., and Arakawa, M. (1992). Molecular diversity of the NMDA receptor channel. Nature *358*, 36–41.

Kutsuwada, T., Sakimura, K., Manabe, T., Takayama, C., Katakura, N., Kushiya, E., Natsume, R., Watanabe, M., Inoue, Y., Yagi, T., et al. (1996). Impairment of suckling response, trigeminal neuronal pattern formation, and hippocampal LTD in NMDA receptor epsilon 2 subunit mutant mice. Neuron *16*, 333–344.

Kuusinen, A., Arvola, M., and Keinänen, K. (1995). Molecular dissection of the agonist binding site of an AMPA receptor. EMBO J. *14*, 6327–6332.

Kuusinen, A., Abele, R., Madden, D.R., and Keinänen, K. (1999). Oligomerization and ligand-binding properties of the ectodomain of the α-Amino-3-hydroxy-5-methyl-4-isoxazole propionic acid receptor subunit GluRD. J. Biol. Chem. *274*, 28937–28943.

Laake, J.H., Slyngstad, T.A., Haug, F.M., and Ottersen, O.P. (1995). Glutamine from glial cells is essential for the maintenance of the nerve terminal pool of glutamate: immunogold evidence from hippocampal slice cultures. J. Neurochem. *65*, 871–881.

Laezza, F., Wilding, T.J., Sequeira, S., Coussen, F., Zhang, X.Z., Hill-Robinson, R., Mulle, C., Huettner, J.E., and Craig, A.M. (2007). KRIP6: a novel BTB/kelch protein regulating function of kainate receptors. Mol. Cell. Neurosci. *34*, 539–550.

Lamsa, K., Heeroma, J.H., and Kullmann, D.M. (2005). Hebbian LTP in feed-forward inhibitory interneurons and the temporal fidelity of input discrimination. Nat. Neurosci. *8*, 916.

Larsen, A.P., Fièvre, S., Frydenvang, K., Francotte, P., Pirotte, B., Kastrup, J.S., and Mulle, C. (2017). Identification and structure-function study of positive allosteric modulators of kainate receptors. Mol. Pharmacol. *91*, 576–585.

Larson, J., Wong, D., and Lynch, G. (1986). Patterned stimulation at the theta frequency is optimal for the induction of hippocampal long-term potentiation. Brain Res. *368*, 347–350.

Lash, L.L., Sanders, J.M., Akiyama, N., Shoji, M., Postila, P., Pentikäinen, O.T., Sasaki, M., Sakai, R., and Swanson, G.T. (2008). Novel analogs and stereoisomers of the marine toxin neodysiherbaine with specificity for kainate receptors. J. Pharmacol. Exp. Ther. *324*, 484–496.

Lauri, S.E., Bortolotto, Z.A., Bleakman, D., Ornstein, P.L., Lodge, D., Isaac, J.T.R., and Collingridge, G.L. (2001). A critical role of a facilitatory presynaptic kainate receptor in mossy fiber LTP. Neuron *32*, 697–709.

Lauri, S.E., Bortolotto, Z.A., Nistico, R., Bleakman, D., Ornstein, P.L., Lodge, D., Isaac, J.T.R., and Collingridge, G.L. (2003). A role for Ca2+ stores in kainate receptor-dependent synaptic facilitation and LTP at mossy fiber synapses in the hippocampus. Neuron *39*, 327–341.

Lee, C.J., Bardoni, R., Tong, C.-K., Engelman, H.S., Joseph, D.J., Magherini, P.C., and MacDermott, A.B. (2002). Functional expression of AMPA receptors on central terminals of rat dorsal root ganglion neurons and presynaptic inhibition of glutamate release. Neuron *35*, 135–146.

Lee, H.-J., Pogatzki-Zahn, E.M., and Brennan, T.J. (2006). The effect of the AMPA/kainate receptor antagonist LY293558 in a rat model of postoperative pain. J. Pain Off. J. Am. Pain Soc. *7*, 768–777.

Lee, H.K., Barbarosie, M., Kameyama, K., Bear, M.F., and Huganir, R.L. (2000).

Regulation of distinct AMPA receptor phosphorylation sites during bidirectional synaptic plasticity. Nature *405*, 955–959.

Leeson, P.D., Baker, R., Carling, R.W., Curtis, N.R., Moore, K.W., Williams, B.J., Foster, A.C., Donald, A.E., Kemp, J.A., and Marshall, G.R. (1991). Kynurenic acid derivatives. Structure-activity relationships for excitatory amino acid antagonism and identification of potent and selective antagonists at the glycine site on the N-methyl-D-aspartate receptor. J. Med. Chem. *34*, 1243–1252.

Legendre, P., and Westbrook, G.L. (1990). The inhibition of single N-methyl-D-aspartate-activated channels by zinc ions on cultured rat neurones. J. Physiol. *429*, 429–449.

Lei, N., Mellem, J.E., Brockie, P.J., Madsen, D.M., and Maricq, A.V. (2017). NRAP-1 is a presynaptically released NMDA receptor auxiliary protein that modifies synaptic strength. Neuron *96*, 1303-1316.e6.

Leite, J.P., Bortolotto, Z.A., and Cavalheiro, E.A. (1990). Spontaneous recurrent seizures in rats: an experimental model of partial epilepsy. Neurosci. Biobehav. Rev. *14*, 511–517.

Lerma, J., and Marques, J.M. (2013). Kainate receptors in health and disease. Neuron *80*, 292–311.

Lester, R.A.J., Clements, J.D., Westbrook, G.L., and Jahr, C.E. (1990). Channel kinetics determine the time course of NMDA receptor-mediated synaptic currents. Nature *346*, 565.

Letts, V.A., Felix, R., Biddlecome, G.H., Arikkath, J., Mahaffey, C.L., Valenzuela, A., Bartlett, F.S., Mori, Y., Campbell, K.P., and Frankel, W.N. (1998). The mouse stargazer gene encodes a neuronal Ca2+-channel gamma subunit. Nat. Genet. *19*, 340–347.

Leuschner, W.D., and Hoch, W. (1999). Subtype-specific assembly of alpha-amino-3-hydroxy-5-methyl-4-isoxazole propionic acid receptor subunits is mediated by their n-terminal domains. J. Biol. Chem. *274*, 16907–16916.

Levy, W.B., and Steward, O. (1979). Synapses as associative memory elements in the hippocampal formation. Brain Res. *175*, 233–245.

Li, J.-M., Zeng, Y.-J., Peng, F., Li, L., Yang, T.-H., Hong, Z., Lei, D., Chen, Z., and Zhou, D. (2010). Aberrant glutamate receptor 5 expression in temporal lobe epilepsy lesions. Brain Res. *1311*, 166–174.

Liao, D., Hessler, N.A., and Malinow, R. (1995). Activation of postsynaptically silent synapses during pairing-induced LTP in CA1 region of hippocampal slice. Nature *375*, 400–404.

Lin, C.-Y., Huang, Z., Wen, W., Wu, A., Wang, C., and Niu, L. (2015). Enhancing protein expression in HEK-293 cells by lowering culture temperature. PLOS ONE *10*, e0123562.

Ling, D.S.F., Benardo, L.S., Serrano, P.A., Blace, N., Kelly, M.T., Crary, J.F., and Sacktor, T.C. (2002). Protein kinase Mzeta is necessary and sufficient for LTP maintenance. Nat. Neurosci. *5*, 295–296.

Lisman, J. (1989). A mechanism for the Hebb and the anti-Hebb processes underlying learning and memory. Proc. Natl. Acad. Sci. U. S. A. *86*, 9574–9578.

Lisman, J., Schulman, H., and Cline, H. (2002). The molecular basis of CaMKII function in synaptic and behavioural memory. Nat. Rev. Neurosci. *3*, 175–190.

Liu, L., Wong, T.P., Pozza, M.F., Lingenhoehl, K., Wang, Y., Sheng, M., Auberson, Y.P., and Wang, Y.T. (2004). Role of NMDA receptor subtypes in governing the direction of hippocampal synaptic plasticity. Science *304*, 1021–1024.

Lodge, D. (2009). The history of the pharmacology and cloning of ionotropic glutamate receptors and the development of idiosyncratic nomenclature. Neuropharmacology *56*, 6–21.

Lomeli, H., Sprengel, R., Laurie, D.J., Köhr, G., Herb, A., Seeburg, P.H., and Wisden, W. (1993). The rat delta-1 and delta-2 subunits extend the excitatory amino acid receptor family. FEBS Lett. *315*, 318–322.

Löscher, W., Lehmann, H., Behl, B., Seemann, D., Teschendorf, H.J., Hofmann, H.P., Lubisch, W., Höger, T., Lemaire, H.G., and Gross, G. (1999). A new pyrrolyl-quinoxalinedione series of non-NMDA glutamate receptor antagonists: pharmacological characterization and comparison with NBQX and valproate in the kindling model of epilepsy. Eur. J. Neurosci. *11*, 250–262.

Lothman, E.W., Bertram, E.H., and Stringer, J.L. (1991). Functional anatomy of hippocampal seizures. Prog. Neurobiol. *37*, 1–82.

Low, C.-M., Lyuboslavsky, P., French, A., Le, P., Wyatte, K., Thiel, W.H., Marchan, E.M., Igarashi, K., Kashiwagi, K., Gernert, K., et al. (2003). Molecular determinants of proton-sensitive N-methyl-D-aspartate receptor gating. Mol. Pharmacol. *63*, 1212–1222.

Lowry, E.R., Kruyer, A., Norris, E.H., Cederroth, C.R., and Strickland, S. (2013). The GluK4 kainate receptor subunit regulates memory, mood, and excitotoxic neurodegeneration. Neuroscience *235*, 215–225.

Lozovaya, N.A., Grebenyuk, S.E., Tsintsadze, T.Sh., Feng, B., Monaghan, D.T., and Krishtal, O.A. (2004). Extrasynaptic NR2B and NR2D subunits of NMDA receptors shape 'superslow' afterburst EPSC in rat hippocampus. J. Physiol. *558*, 451–463.

Lu, C.-R., Willcockson, H.H., Phend, K.D., Lucifora, S., Darstein, M., Valtschanoff, J.G., and Rustioni, A. (2005). Ionotropic glutamate receptors are expressed in GABAergic terminals in the rat superficial dorsal horn. J. Comp. Neurol. *486*, 169–178.

Lu, W., Shi, Y., Jackson, A.C., Bjorgan, K., During, M.J., Sprengel, R., Seeburg, P.H., and Nicoll, R.A. (2009). Subunit composition of synaptic AMPA receptors revealed by a single-cell genetic approach. Neuron *62*, 254–268.

Lü, W., Du, J., Goehring, A., and Gouaux, E. (2017). Cryo-EM structures of the triheteromeric NMDA receptor and its allosteric modulation. Science *355*, eaal3729.

Lucas, D.R., and Newhouse, J.P. (1957). The toxic effect of sodium L-glutamate on the

inner layers of the retina. AMA Arch. Ophthalmol. *58*, 193–201.

Lucifora, S., Willcockson, H.H., Lu, C.-R., Darstein, M., Phend, K.D., Valtschanoff, J.G., and Rustioni, A. (2006). Presynaptic low- and high-affinity kainate receptors in nociceptive spinal afferents. Pain *120*, 97–105.

Lv, Q., Liu, Y., Han, D., Xu, J., Zong, Y.-Y., Wang, Y., and Zhang, G.-Y. (2012). Neuroprotection of GluK1 kainate receptor agonist ATPA against ischemic neuronal injury through inhibiting GluK2 kainate receptor-JNK3 pathway via GABA(A) receptors. Brain Res. *1456*, 1–13.

Lynch, G., Larson, J., Kelso, S., Barrionuevo, G., and Schottler, F. (1983). Intracellular injections of EGTA block induction of hippocampal long-term potentiation. Nature *305*, 719–721.

Lynch, G.S., Dunwiddie, T., and Gribkoff, V. (1977). Heterosynaptic depression: a postsynaptic correlate of long-term potentiation. Nature *266*, 737–739.

MacDermott, A.B., Mayer, M.L., Westbrook, G.L., Smith, S.J., and Barker, J.L. (1986). NMDA-receptor activation increases cytoplasmic calcium concentration in cultured spinal cord neurones. Nature *321*, 519–522.

MacDougall, M.J., and Fine, A. (2013). The expression of long-term potentiation: reconciling the preists and the postivists. Philos. Trans. R. Soc. B Biol. Sci. *369*, 20130135–20130135.

Mackerell, A.D., Feig, M., and Brooks, C.L. (2004). Extending the treatment of backbone energetics in protein force fields: limitations of gas-phase quantum mechanics in reproducing protein conformational distributions in molecular dynamics simulations. J. Comput. Chem. *25*, 1400–1415.

Malenka, R.C. (1991). Postsynaptic factors control the duration of synaptic enhancement in area CA1 of the hippocampus. Neuron *6*, 53–60.

Malenka, R.C., Madison, D.V., and Nicoll, R.A. (1986). Potentiation of synaptic transmission in the hippocampus by phorbol esters. Nature *321*, 175–177.

Malenka, R.C., Kauer, J.A., Zucker, R.S., and Nicoll, R.A. (1988). Postsynaptic calcium is sufficient for potentiation of hippocampal synaptic transmission. Science *242*, 81–84.

Malenka, R.C., Lancaster, B., and Zucker, R.S. (1992). Temporal limits on the rise in postsynaptic calcium required for the induction of long-term potentiation. Neuron *9*, 121–128.

Malinow, R., and Malenka, R.C. (2002). AMPA receptor trafficking and synaptic plasticity. Annu. Rev. Neurosci. *25*, 103–126.

Malinow, R., and Miller, J.P. (1986). Postsynaptic hyperpolarization during conditioning reversibly blocks induction of long-term potentiation. Nature *320*, 529–530.

Malinow, R., Schulman, H., and Tsien, R.W. (1989). Inhibition of postsynaptic PKC or

CaMKII blocks induction but not expression of LTP. Science *245*, 862–866.

Marcaggi, P., and Attwell, D. (2004). Role of glial amino acid transporters in synaptic transmission and brain energetics. Glia *47*, 217–225.

Martin, D., and Lodge, D. (1985). Ketamine acts as a non-competitive N-methyl-D-aspartate antagonist on frog spinal cord in vitro. Neuropharmacology *24*, 999–1003.

Martinez-Hernandez, A., Bell, K.P., and Norenberg, M.D. (1977). Glutamine synthetase: glial localization in brain. Science *195*, 1356–1358.

Matsuzaki, M., Honkura, N., Ellis-Davies, G.C.R., and Kasai, H. (2004). Structural basis of long-term potentiation in single dendritic spines. Nature *429*, 761–766.

Mayer, M.L. (2005). Crystal structures of the GluR5 and GluR6 ligand binding cores: molecular mechanisms underlying kainate receptor selectivity. Neuron *45*, 539–552.

Mayer, M.L. (2017). The structure and function of glutamate receptors: Mg2+ Block to X-ray diffraction. Neuropharmacology *112*, 4–10.

Mayer, M.L., and Westbrook, G.L. (1987). Permeation and block of N-methyl-D-aspartic acid receptor channels by divalent cations in mouse cultured central neurones. J. Physiol. *394*, 501–527.

Mayer, A., Wickner, W., and Haas, A. (1996). Sec18p (NSF)-driven release of Sec17p (alpha-SNAP) can precede docking and fusion of yeast vacuoles. Cell *85*, 83–94.

Mayer, M.L., Westbrook, G.L., and Guthrie, P.B. (1984). Voltage-dependent block by Mg2+ of NMDA responses in spinal cord neurones. Nature *309*, 261–263.

Mayer, M.L., Westbrook, G.L., and Vyklický, L. (1988). Sites of antagonist action on N-methyl-D-aspartic acid receptors studied using fluctuation analysis and a rapid perfusion technique. J. Neurophysiol. *60*, 645–663.

Mayer, M.L., Ghosal, A., Dolman, N.P., and Jane, D.E. (2006). Crystal structures of the kainate receptor GluR5 ligand binding core dimer with novel GluR5-selective antagonists. J. Neurosci. *26*, 2852–2861.

McBain, C.J., Kleckner, N.W., Wyrick, S., and Dingledine, R. (1989). Structural requirements for activation of the glycine coagonist site of N-methyl-D-aspartate receptors expressed in Xenopus oocytes. Mol. Pharmacol. *36*, 556–565.

McGuinness, L., Taylor, C., Taylor, R.D.T., Yau, C., Langenhan, T., Hart, M.L., Christian, H., Tynan, P.W., Donnelly, P., and Emptage, N.J. (2010). Presynaptic NMDARs in the hippocampus facilitate transmitter release at theta frequency. Neuron *68*, 1109–1127.

Mclennan, H., Huffman, R.D., and Marshall, K.C. (1968). Patterns of excitation of thalamic neurones by amino-acids and by acetylcholine. Nature *219*, 387.

McNaughton, B.L. (1980). Evidence for two physiologically distinct perforant pathways to the fascia dentata. Brain Res. *199*, 1–19.

McNaughton, B.L. (1982). Long-term synaptic enhancement and short-term potentiation in rat fascia dentata act through different mechanisms. J. Physiol. *324*, 249–262.

McNaughton, B.L., Douglas, R.M., and Goddard, G.V. (1978). Synaptic enhancement in fascia dentata: cooperativity among coactive afferents. Brain Res. *157*, 277–293.

Melyan, Z., Wheal, H.V., and Lancaster, B. (2002). Metabotropic-mediated kainate receptor regulation of IsAHP and excitability in pyramidal cells. Neuron *34*, 107–114.

Melyan, Z., Lancaster, B., and Wheal, H.V. (2004). Metabotropic regulation of intrinsic excitability by synaptic activation of kainate receptors. J. Neurosci. Off. J. Soc. Neurosci. *24*, 4530–4534.

Menuz, K., Stroud, R.M., Nicoll, R.A., and Hays, F.A. (2007). TARP auxiliary subunits switch AMPA receptor antagonists into partial agonists. Science *318*, 815–817.

Meunier, C., Wang, N., Yi, C., Dallerac, G., Ezan, P., Koulakoff, A., Leybaert, L., and Giaume, C. (2017). Contribution of astroglial Cx43 hemichannels to the modulation of glutamatergic currents by D-Serine in the mouse prefrontal cortex. J. Neurosci. Off. J. Soc. Neurosci. *37*, 9064–9075.

Meyerson, J.R., Kumar, J., Chittori, S., Rao, P., Pierson, J., Bartesaghi, A., Mayer, M.L., and Subramaniam, S. (2014). Structural mechanism of glutamate receptor activation and desensitization. Nature *514*, 328–334.

Miyamoto, Y., Yamada, K., Noda, Y., Mori, H., Mishina, M., and Nabeshima, T. (2002). Lower sensitivity to stress and altered monoaminergic neuronal function in mice lacking the NMDA receptor ε4 subunit. J. Neurosci. *22*, 2335–2342.

Møllerud, S., Frydenvang, K., Pickering, D.S., and Kastrup, J.S. (2017). Lessons from crystal structures of kainate receptors. Neuropharmacology *112*, 16–28.

Monaghan, D.T., and Cotman, C.W. (1982). The distribution of [3H]kainic acid binding sites in rat CNS as determined by autoradiography. Brain Res. *252*, 91–100.

Monaghan, D.T., Bridges, R.J., and Cotman, C.W. (1989). The excitatory amino acid receptors: their classes, pharmacology, and distinct properties in the function of the central nervous system. Annu. Rev. Pharmacol. Toxicol. *29*, 365–402.

Monyer, H., Sprengel, R., Schoepfer, R., Herb, A., Higuchi, M., Lomeli, H., Burnashev, N., Sakmann, B., and Seeburg, P.H. (1992). Heteromeric NMDA receptors: molecular and functional distinction of subtypes. Science *256*, 1217–1221.

Monyer, H., Burnashev, N., Laurie, D.J., Sakmann, B., and Seeburg, P.H. (1994). Developmental and regional expression in the rat brain and functional properties of four NMDA receptors. Neuron *12*, 529–540.

More, J.C.A., Nistico, R., Dolman, N.P., Clarke, V.R.J., Alt, A.J., Ogden, A.M., Buelens, F.P., Troop, H.M., Kelland, E.E., Pilato, F., et al. (2004). Characterisation of UBP296: a novel, potent and selective kainate receptor antagonist. Neuropharmacology *47*, 46–64.

Mori, H., Masaki, H., Yamakura, T., and Mishina, M. (1992). Identification by mutagenesis of a Mg(2+)-block site of the NMDA receptor channel. Nature *358*, 673–675.

Moriyoshi, K., Masu, M., Ishii, T., Shigemoto, R., Mizuno, N., and Nakanishi, S. (1991). Molecular cloning and characterization of the rat NMDA receptor. Nature *354*, 31–37.

Morley, R.M., Tse, H.-W., Feng, B., Miller, J.C., Monaghan, D.T., and Jane, D.E. (2005). Synthesis and pharmacology of N1-substituted piperazine-2,3-dicarboxylic acid derivatives acting as NMDA receptor antagonists. J. Med. Chem. *48*, 2627–2637.

Morris, R.G., Davis, S., and Butcher, S.P. (1990). Hippocampal synaptic plasticity and NMDA receptors: a role in information storage? Philos. Trans. R. Soc. Lond. B. Biol. Sci. *329*, 187–204.

Mosbacher, J., Schoepfer, R., Monyer, H., Burnashev, N., Seeburg, P.H., and Ruppersberg, J.P. (1994). A molecular determinant for submillisecond desensitization in glutamate receptors. Science *266*, 1059–1062.

Moser, E., Moser, M.B., and Andersen, P. (1993). Synaptic potentiation in the rat dentate gyrus during exploratory learning. Neuroreport *5*, 317–320.

Moser, E.I., Moser, M.B., and Andersen, P. (1994). Potentiation of dentate synapses initiated by exploratory learning in rats: dissociation from brain temperature, motor activity, and arousal. Learn. Mem. *1*, 55–73.

Mosley, C.A., Acker, T.M., Hansen, K.B., Mullasseril, P., Andersen, K.T., Le, P., Vellano, K.M., Bräuner-Osborne, H., Liotta, D.C., and Traynelis, S.F. (2010). Quinazolin-4-one derivatives: A novel class of non-competitive NR2C/D subunit-selective N-methyl-D-aspartate receptor antagonists. J. Med. Chem. *53*, 5476–5490.

Mothet, J.-P., Le Bail, M., and Billard, J.-M. (2015). Time and space profiling of NMDA receptor co-agonist functions. J. Neurochem. *135*, 210–225.

Mott, D.D., Doherty, J.J., Zhang, S., Washburn, M.S., Fendley, M.J., Lyuboslavsky, P., Traynelis, S.F., and Dingledine, R. (1998). Phenylethanolamines inhibit NMDA receptors by enhancing proton inhibition. Nat. Neurosci. *1*, 659–667.

Mullasseril, P., Hansen, K.B., Vance, K.M., Ogden, K.K., Yuan, H., Kurtkaya, N.L., Santangelo, R., Orr, A.G., Le, P., Vellano, K.M., et al. (2010). A subunit-selective potentiator of NR2C- and NR2D-containing NMDA receptors. Nat. Commun. *1*, 1–8.

Mulle, C., Sailer, A., Pérez-Otaño, I., Dickinson-Anson, H., Castillo, P.E., Bureau, I., Maron, C., Gage, F.H., Mann, J.R., Bettler, B., et al. (1998). Altered synaptic physiology and reduced susceptibility to kainate-induced seizures in GluR6-deficient mice. Nature *392*, 601–605.

Mulle, C., Sailer, A., Swanson, G.T., Brana, C., O'Gorman, S., Bettler, B., and Heinemann, S.F. (2000). Subunit composition of kainate receptors in hippocampal interneurons. Neuron *28*, 475–484.

Müller, W., and Connor, J.A. (1991). Dendritic spines as individual neuronal compartments for synaptic Ca2+ responses. Nature *354*, 73–76.

Murphy, M., Mellberg, S., Kurtz, N., and Graham, E. (2008). AMPA/Kainate receptor antagonist tezampanel is effective in treating acute migraine. Headache *48*.

Nadler, J.V. (1981). Minireview. Kainic acid as a tool for the study of temporal lobe epilepsy. Life Sci. *29*, 2031–2042.

Nadler, J.V., Perry, B.W., and Cotman, C.W. (1978). Intraventricular kainic acid preferentially destroys hippocampal pyramidal cells. Nature *271*, 676–677.

Naito, S., and Ueda, T. (1983). Adenosine triphosphate-dependent uptake of glutamate into protein I-associated synaptic vesicles. J. Biol. Chem. *258*, 696–699.

Nakagawa, T., Cheng, Y., Ramm, E., Sheng, M., and Walz, T. (2005). Structure and different conformational states of native AMPA receptor complexes. Nature *433*, 545–549.

Nakanishi, S. (1992). Molecular diversity of glutamate receptors and implications for brain function. Science *258*, 597–603.

Nakanishi, N., Shneider, N.A., and Axel, R. (1990). A family of glutamate receptor genes: evidence for the formation of heteromultimeric receptors with distinct channel properties. Neuron *5*, 569–581.

Nakashiba, T., Young, J.Z., McHugh, T.J., Buhl, D.L., and Tonegawa, S. (2008). Transgenic inhibition of synaptic transmission reveals role of CA3 output in hippocampal learning. Science *319*, 1260–1264.

Naur, P., Vestergaard, B., Skov, L.K., Egebjerg, J., Gajhede, M., and Kastrup, J.S. (2005). Crystal structure of the kainate receptor GluR5 ligand-binding core in complex with (S)-glutamate. FEBS Lett. *579*, 1154–1160.

Nayeem, N., Mayans, O., and Green, T. (2011). Conformational flexibility of the ligand-binding domain dimer in kainate receptor gating and desensitization. J. Neurosci. *31*, 2916–2924.

Nayeem, N., Mayans, O., and Green, T. (2013). Correlating efficacy and desensitization with GluK2 ligand-binding domain movements. Open Biol. *3*, 130051–130051.

Neely, A., and Lingle, C.J. (1986). Trapping of an open-channel blocker at the frog neuromuscular acetylcholine channel. Biophys. J. *50*, 981–986.

Neher, E., and Sakmann, B. (1976). Single-channel currents recorded from membrane of denervated frog muscle fibres. Nature *260*, 799–802.

Newberry, N.R., and Nicoll, R.A. (1985). Comparison of the action of baclofen with gamma-aminobutyric acid on rat hippocampal pyramidal cells in vitro. J. Physiol. *360*, 161–185.

Neyton, J., and Paoletti, P. (2006). Relating NMDA receptor function to receptor subunit composition: Limitations of the pharmacological approach. J. Neurosci. *26*, 1331–1333.

Ng, D., Pitcher, G.M., Szilard, R.K., Sertié, A., Kanisek, M., Clapcote, S.J., Lipina, T., Kalia, L.V., Joo, D., McKerlie, C., et al. (2009). Neto1 Is a novel CUB-domain NMDA receptor–interacting protein required for synaptic plasticity and learning. PLoS Biol. *7*, e1000041.

Nicholls, D.G. (1989). Release of glutamate, aspartate, and gamma-aminobutyric acid from isolated nerve terminals. J. Neurochem. *52*, 331–341.

Nisticò, R., Dargan, S.L., Amici, M., Collingridge, G.L., and Bortolotto, Z.A. (2011). Synergistic interactions between kainate and mGlu receptors regulate bouton Ca2+ signalling and mossy fibre LTP. Sci. Rep. *1*.

Niswender, C.M., and Conn, P.J. (2010). Metabotropic glutamate receptors: Physiology, pharmacology, and disease. Annu. Rev. Pharmacol. Toxicol. *50*, 295–322.

Nitta, I., Watase, H., and Tomiie, Y. (1958). Structure of kainic acid and its isomer, allokainic acid. Nature *181*, 761.

Nowak, L., Bregestovski, P., Ascher, P., Herbet, A., and Prochiantz, A. (1984). Magnesium gates glutamate-activated channels in mouse central neurones. Nature *307*, 462.

Obenaus, A., Mody, I., and Baimbridge, K.G. (1989). Dantrolene-Na (Dantrium) blocks induction of long-term potentiation in hippocampal slices. Neurosci. Lett. *98*, 172–178.

O'Keefe, J., and Dostrovsky, J. (1971). The hippocampus as a spatial map. Preliminary evidence from unit activity in the freely-moving rat. Brain Res. *34*, 171–175.

O'Keefe, J., and Nadel, L. (1978). The hippocampus as a cognitive map (Clarendon Press).

Olney, J.W. (1969). Brain lesions, obesity, and other disturbances in mice treated with monosodium glutamate. Science *164*, 719–721.

Olney, J.W. (1971). Glutamate-induced neuronal necrosis in the infant mouse hypothalamus. An electron microscopic study. J. Neuropathol. Exp. Neurol. *30*, 75–90.

Olney, J.W., Price, M.T., Salles, K.S., Labruyere, J., Ryerson, R., Mahan, K., Frierdich, G., and Samson, L. (1987). L-homocysteic acid: an endogenous excitotoxic ligand of the NMDA receptor. Brain Res. Bull. *19*, 597–602.

Ottersen, O.P., Storm-Mathisen, J., Bramham, C., Torp, R., Laake, J., and Gundersen, V. (1990). A quantitative electron microscopic immunocytochemical study of the distribution and synaptic handling of glutamate in rat hippocampus. Prog. Brain Res. *83*, 99–114.

Ottersen, O.P., Zhang, N., and Walberg, F. (1992). Metabolic compartmentation of glutamate and glutamine: morphological evidence obtained by quantitative immunocytochemistry in rat cerebellum. Neuroscience *46*, 519–534.

Ozkan, E.D., and Ueda, T. (1998). Glutamate transport and storage in synaptic vesicles. Jpn. J. Pharmacol. *77*, 1–10.

Padamsey, Z., and Emptage, N. (2013). Two sides to long-term potentiation: a view towards reconciliation. Philos. Trans. R. Soc. B Biol. Sci. *369*, 20130154–20130154.

Palay, S.L., and Palade, G.E. (1955). The fine structure of neurons. J. Biophys. Biochem. Cytol. *1*, 69–88.

Pananceau, M., Chen, H., and Gustafsson, B. (1998). Short-term facilitation evoked during brief afferent tetani is not altered by long-term potentiation in the guinea-pig hippocampal CA1 region. J. Physiol. *508 (Pt 2)*, 503–514.

Panatier, A., Theodosis, D.T., Mothet, J.-P., Touquet, B., Pollegioni, L., Poulain, D.A., and Oliet, S.H.R. (2006). Glia-derived D-serine controls NMDA receptor activity and synaptic memory. Cell *125*, 775–784.

Paoletti, P., Perin-Dureau, F., Fayyazuddin, A., Le Goff, A., Callebaut, I., and Neyton, J. (2000). Molecular organization of a zinc binding n-terminal modulatory domain in a NMDA receptor subunit. Neuron *28*, 911–925.

Paoletti, P., Vergnano, A.M., Barbour, B., and Casado, M. (2009). Zinc at glutamatergic synapses. Neuroscience *158*, 126–136.

Paoletti, P., Bellone, C., and Zhou, Q. (2013). NMDA receptor subunit diversity: impact on receptor properties, synaptic plasticity and disease. Nat. Rev. Neurosci. *14*, 383–400.

Papouin, T., Ladépêche, L., Ruel, J., Sacchi, S., Labasque, M., Hanini, M., Groc, L., Pollegioni, L., Mothet, J.-P., and Oliet, S.H.R. (2012). Synaptic and extrasynaptic NMDA receptors are gated by different endogenous coagonists. Cell *150*, 633–646.

Park, P., Sanderson, T.M., Amici, M., Choi, S.-L., Bortolotto, Z.A., Zhuo, M., Kaang, B.-K., and Collingridge, G.L. (2016). Calcium-permeable AMPA receptors mediate the induction of the protein kinase A-dependent component of long-term potentiation in the hippocampus. J. Neurosci. *36*, 622–631.

Parsons, C.G., Quack, G., Bresink, I., Baran, L., Przegalinski, E., Kostowski, W., Krzascik, P., Hartmann, S., and Danysz, W. (1995). Comparison of the potency, kinetics and voltage-dependency of a series of uncompetitive NMDA receptor antagonists in vitro with anticonvulsive and motor impairment activity in vivo. Neuropharmacology *34*, 1239–1258.

Partin, K.M., Patneau, D.K., Winters, C.A., Mayer, M.L., and Buonanno, A. (1993). Selective modulation of desensitization at AMPA versus kainate receptors by cyclothiazide and concanavalin A. Neuron *11*, 1069–1082.

Partin, K.M., Patneau, D.K., and Mayer, M.L. (1994). Cyclothiazide differentially modulates desensitization of alpha-amino-3-hydroxy-5-methyl-4-isoxazolepropionic acid receptor splice variants. Mol. Pharmacol. *46*, 129–138.

Partin, K.M., Bowie, D., and Mayer, M.L. (1995). Structural determinants of allosteric

regulation in alternatively spliced AMPA receptors. Neuron *14*, 833–843.

Partin, K.M., Fleck, M.W., and Mayer, M.L. (1996). AMPA receptor flip/flop mutants affecting deactivation, desensitization, and modulation by cyclothiazide, aniracetam, and thiocyanate. J. Neurosci. *16*, 6634–6647.

Paternain, A.V., Morales, M., and Lerma, J. (1995). Selective antagonism of AMPA receptors unmasks kainate receptor-mediated responses in hippocampal neurons. Neuron *14*, 185–189.

Paternain, A.V., Rodríguez-Moreno, A., Villarroel, A., and Lerma, J. (1998). Activation and desensitization properties of native and recombinant kainate receptors. Neuropharmacology *37*, 1249–1259.

Paternain, A.V., Herrera, M.T., Nieto, M.A., and Lerma, J. (2000). GluR5 and GluR6 kainate receptor subunits coexist in hippocampal neurons and coassemble to form functional receptors. J. Neurosci. *20*, 196–205.

Peret, A., Christie, L.A., Ouedraogo, D.W., Gorlewicz, A., Epsztein, J., Mulle, C., and Crépel, V. (2014). Contribution of aberrant GluK2-containing kainate receptors to chronic seizures in temporal lobe epilepsy. Cell Rep. *8*, 347–354.

Pérez-Clausell, J., and Danscher, G. (1985). Intravesicular localization of zinc in rat telencephalic boutons. A histochemical study. Brain Res. *337*, 91–98.

Perez-Otano, I., Schulteis, C.T., Contractor, A., Lipton, S.A., Trimmer, J.S., Sucher, N.J., and Heinemann, S.F. (2001). Assembly with the NR1 subunit is required for surface expression of NR3A-containing NMDA receptors. J. Neurosci. Off. J. Soc. Neurosci. *21*, 1228–1237.

Perin-Dureau, F., Rachline, J., Neyton, J., and Paoletti, P. (2002). Mapping the binding site of the neuroprotectant ifenprodil on NMDA receptors. J. Neurosci. *22*, 5955–5965.

Perrais, D., Pinheiro, P.S., Jane, D.E., and Mulle, C. (2009). Antagonism of recombinant and native GluK3-containing kainate receptors. Neuropharmacology *56*, 131–140.

Perszyk, R.E., DiRaddo, J.O., Strong, K.L., Low, C.-M., Ogden, K.K., Khatri, A., Vargish, G.A., Pelkey, K.A., Tricoire, L., Liotta, D.C., et al. (2016). GluN2D-containing N-methyl-D-aspartate receptors mediate synaptic transmission in hippocampal interneurons and regulate interneuron activity. Mol. Pharmacol. *90*, 689–702.

Perucca, E., and Meador, K.J. (2005). Adverse effects of antiepileptic drugs. Acta Neurol. Scand. Suppl. *181*, 30–35.

Peters, S., Koh, J., and Choi, D.W. (1987). Zinc selectively blocks the action of N-methyl-D-aspartate on cortical neurons. Science *236*, 589–593.

Petrovic, M.M., Viana da Silva, S., Clement, J.P., Vyklicky, L., Mulle, C., González-González, I.M., and Henley, J.M. (2017). Metabotropic action of postsynaptic kainate receptors triggers hippocampal long-term potentiation. Nat. Neurosci. *20*, 529–539.

Pfau, D.B., Klein, T., Putzer, D., Pogatzki-Zahn, E.M., Treede, R.-D., and Magerl, W. (2011). Analysis of hyperalgesia time courses in humans after painful electrical high-frequency stimulation identifies a possible transition from early to late LTP-like pain plasticity. Pain *152*, 1532–1539.

Philipson, K.D., Nicoll, D.A., Ottolia, M., Quednau, B.D., Reuter, H., John, S., and Qiu, Z. (2002). The Na+/Ca2+ exchange molecule: an overview. Ann. N. Y. Acad. Sci. *976*, 1–10.

Pinheiro, P., and Mulle, C. (2006). Kainate receptors. Cell Tissue Res. *326*, 457–482.

Pinheiro, P.S., Perrais, D., Coussen, F., Barhanin, J., Bettler, B., Mann, J.R., Malva, J.O., Heinemann, S.F., and Mulle, C. (2007). GluR7 is an essential subunit of presynaptic kainate autoreceptors at hippocampal mossy fiber synapses. Proc. Natl. Acad. Sci. U. S. A. *104*, 12181–12186.

Pinheiro, P.S., Lanore, F., Veran, J., Artinian, J., Blanchet, C., Crépel, V., Perrais, D., and Mulle, C. (2013). Selective block of postsynaptic kainate receptors reveals their function at hippocampal mossy fiber synapses. Cereb. Cortex *23*, 323–331.

Plant, K., Pelkey, K.A., Bortolotto, Z.A., Morita, D., Terashima, A., McBain, C.J., Collingridge, G.L., and Isaac, J.T.R. (2006). Transient incorporation of native GluR2-lacking AMPA receptors during hippocampal long-term potentiation. Nat. Neurosci. *9*, 602–604.

Pullan, L.M., Olney, J.W., Price, M.T., Compton, R.P., Hood, W.F., Michel, J., and Monahan, J.B. (1987). Excitatory amino acid receptor potency and subclass specificity of sulfur-containing amino acids. J. Neurochem. *49*, 1301–1307.

Qiu, C.-S., Lash-Van Wyhe, L., Sasaki, M., Sakai, R., Swanson, G.T., and Gereau, R.W. (2011). Antinociceptive effects of MSVIII-19, a functional antagonist of the GluK1 kainate receptor. Pain *152*, 1052–1060.

Rachline, J., Perin-Dureau, F., Le Goff, A., Neyton, J., and Paoletti, P. (2005). The micromolar zinc-binding domain on the NMDA receptor subunit NR2B. J. Neurosci. Off. J. Soc. Neurosci. *25*, 308–317.

Rang, H.P., and Ritchie, J.M. (1968). On the electrogenic sodium pump in mammalian non-myelinated nerve fibres and its activation by various external cations. J. Physiol. *196*, 183–221.

Regehr, W.G., and Tank, D.W. (1990). Postsynaptic NMDA receptor-mediated calcium accumulation in hippocampal CA1 pyramidal cell dendrites. Nature *345*, 807–810.

Represa, A., Tremblay, E., and Ben-Ari, Y. (1987). Kainate binding sites in the hippocampal mossy fibers: localization and plasticity. Neuroscience *20*, 739–748.

Represa, A., Robain, O., Tremblay, E., and Ben-Ari, Y. (1989). Hippocampal plasticity in childhood epilepsy. Neurosci. Lett. *99*, 351–355.

Rivera, R., Rozas, J.L., and Lerma, J. (2007). PKC-dependent autoregulation of

membrane kainate receptors. EMBO J. *26*, 4359–4367.

Rodríguez-Moreno, A., and Lerma, J. (1998). Kainate receptor modulation of GABA release involves a metabotropic function. Neuron *20*, 1211–1218.

Rodríguez-Moreno, A., Herreras, O., and Lerma, J. (1997). Kainate receptors presynaptically downregulate GABAergic inhibition in the rat hippocampus. Neuron *19*, 893–901.

Rodríguez-Moreno, A., López-García, J.C., and Lerma, J. (2000). Two populations of kainate receptors with separate signaling mechanisms in hippocampal interneurons. Proc. Natl. Acad. Sci. U. S. A. *97*, 1293–1298.

Rogawski, M.A., Gryder, D., Castaneda, D., Yonekawa, W., Banks, M.K., and Lia, H. (2003). GluR5 kainate receptors, seizures, and the amygdala. Ann. N. Y. Acad. Sci. *985*, 150–162.

Romberg, C., Raffel, J., Martin, L., Sprengel, R., Seeburg, P.H., Rawlins, J.N.P., Bannerman, D.M., and Paulsen, O. (2009). Induction and expression of GluA1 (GluR-A)-independent LTP in the hippocampus. Eur. J. Neurosci. *29*, 1141–1152.

Ross, F.M., Cassidy, J., Wilson, M., and Davies, S.N. (2000). Developmental regulation of hippocampal excitatory synaptic transmission by metabotropic glutamate receptors. Br. J. Pharmacol. *131*, 453–464.

Rothman, S.M. (1983). Synaptic activity mediates death of hypoxic neurons. Science *220*, 536–537.

Rouach, N., Byrd, K., Petralia, R.S., Elias, G.M., Adesnik, H., Tomita, S., Karimzadegan, S., Kealey, C., Bredt, D.S., and Nicoll, R.A. (2005). TARP γ-8 controls hippocampal AMPA receptor number, distribution and synaptic plasticity. Nat. Neurosci. *8*, 1525–1533.

Rowley, M., Leeson, P.D., Stevenson, G.I., Moseley, A.M., Stansfield, I., Sanderson, I., Robinson, L., Baker, R., and Kemp, J.A. (1993). 3-Acyl-4-hydroxyquinolin-2(1H)-ones. Systemically active anticonvulsants acting by antagonism at the glycine site of the N-methyl-D-aspartate receptor complex. J. Med. Chem. *36*, 3386–3396.

Rozas, J.L., Paternain, A.V., and Lerma, J. (2003). Noncanonical signaling by ionotropic kainate receptors. Neuron *39*, 543–553.

Rozov, A., and Burnashev, N. (1999). Polyamine-dependent facilitation of postsynaptic AMPA receptors counteracts paired-pulse depression. Nature *401*, 594–598.

Ruiz, A., Sachidhanandam, S., Utvik, J.K., Coussen, F., and Mulle, C. (2005). Distinct subunits in heteromeric kainate receptors mediate ionotropic and metabotropic function at hippocampal mossy fiber synapses. J. Neurosci. *25*, 11710–11718.

Rusakov, D.A., Saitow, F., Lehre, K.P., and Konishi, S. (2005). Modulation of presynaptic Ca2+ entry by AMPA receptors at individual GABAergic synapses in the cerebellum. J. Neurosci. *25*, 4930–4940.

Sachidhanandam, S., Blanchet, C., Jeantet, Y., Cho, Y.H., and Mulle, C. (2009). Kainate receptors act as conditional amplifiers of spike transmission at hippocampal mossy fiber synapses. J. Neurosci. *29*, 5000–5008.

Sakai, R., Kamiya, H., Murata, M., and Shimamoto, K. (1997). Dysiherbaine: A new neurotoxic amino acid from the micronesian marine sponge dysidea herbacea. J. Am. Chem. Soc. *119*, 4112–4116.

Sakamoto, T., Porter, L.L., and Asanuma, H. (1987). Long-lasting potentiation of synaptic potentials in the motor cortex produced by stimulation of the sensory cortex in the cat: a basis of motor learning. Brain Res. *413*, 360–364.

Sakimura, K., Kutsuwada, T., Ito, I., Manabe, T., Takayama, C., Kushiya, E., Yagi, T., Aizawa, S., Inoue, Y., and Sugiyama, H. (1995). Reduced hippocampal LTP and spatial learning in mice lacking NMDA receptor epsilon 1 subunit. Nature *373*, 151–155.

Sander, T., Hildmann, T., Kretz, R., Fürst, R., Sailer, U., Bauer, G., Schmitz, B., Beck-Mannagetta, G., Wienker, T.F., and Janz, D. (1997). Allelic association of juvenile absence epilepsy with a GluR5 kainate receptor gene (GRIK1) polymorphism. Am. J. Med. Genet. *74*, 416–421.

Sang, C.N., Hostetter, M.P., Gracely, R.H., Chappell, A.S., Schoepp, D.D., Lee, G., Whitcup, S., Caruso, R., and Max, M.B. (1998). AMPA/kainate antagonist LY293558 reduces capsaicin-evoked hyperalgesia but not pain in normal skin in humans. Anesthesiology *89*, 1060–1067.

Sapkota, K. (2016). Target validation and pharmacological characterization of novel NMDAR modulators. University of Nebraska Medical Center.

Sapkota, K., Mao, Z., Synowicki, P., Lieber, D., Liu, M., Ikezu, T., Gautam, V., and Monaghan, D.T. (2016). GluN2D N-Methyl-D-aspartate receptor subunit contribution to the stimulation of brain activity and gamma oscillations by ketamine: Implications for schizophrenia. J. Pharmacol. Exp. Ther. *356*, 702–711.

Sasaki, Y.F., Rothe, T., Premkumar, L.S., Das, S., Cui, J., Talantova, M.V., Wong, H.-K., Gong, X., Chan, S.F., Zhang, D., et al. (2002). Characterization and comparison of the NR3A subunit of the NMDA receptor in recombinant systems and primary cortical neurons. J. Neurophysiol. *87*, 2052–2063.

Scheetz, A.J., Nairn, A.C., and Constantine-Paton, M. (2000). NMDA receptor-mediated control of protein synthesis at developing synapses. Nat. Neurosci. *3*, 211–216.

Schiavini, P., Dawe, G.B., Bowie, D., and Moitessier, N. (2015). Discovery of novel small-molecule antagonists for GluK2. Bioorg. Med. Chem. Lett. *25*, 2416–2420.

Schiffer, H.H., Swanson, G.T., and Heinemann, S.F. (1997). Rat GluR7 and a carboxy-terminal splice variant, GluR7b, are functional kainate receptor subunits with a low sensitivity to glutamate. Neuron *19*, 1141–1146.

Schmidt-Salzmann, C., Li, L., and Bischofberger, J. (2014). Functional properties of extrasynaptic AMPA and NMDA receptors during postnatal hippocampal neurogenesis. J.

Physiol. *592*, 125–140.

Schneggenburger, R. (1996). Simultaneous measurement of Ca2+ influx and reversal potentials in recombinant N-methyl-D-aspartate receptor channels. Biophys. J. *70*, 2165–2174.

Schoepp, D.D., Smith, C.L., Lodge, D., Millar, J.D., Leander, J.D., Sacaan, A.I., and Lunn, W.H. (1991). D,L-(tetrazol-5-yl) glycine: a novel and highly potent NMDA receptor agonist. Eur. J. Pharmacol. *203*, 237–243.

Schorge, S., and Colquhoun, D. (2003). Studies of NMDA receptor function and stoichiometry with truncated and tandem subunits. J. Neurosci. Off. J. Soc. Neurosci. *23*, 1151–1158.

Schulz, P.E., and Fitzgibbons, J.C. (1997). Differing mechanisms of expression for short- and long-term potentiation. J. Neurophysiol. *78*, 321–334.

Scott, R., and Rusakov, D.A. (2006). Main determinants of presynaptic Ca2+ dynamics at individual mossy fiber-CA3 pyramidal cell synapses. J. Neurosci. Off. J. Soc. Neurosci. *26*, 7071–7081.

Seal, R.P., Wang, X., Guan, Y., Raja, S.N., Woodbury, C.J., Basbaum, A.I., and Edwards, R.H. (2009). Injury-induced mechanical hypersensitivity requires C-low threshold mechanoreceptors. Nature *462*, 651–655.

Seeburg, P.H., Higuchi, M., and Sprengel, R. (1998). RNA editing of brain glutamate receptor channels: mechanism and physiology. Brain Res. Brain Res. Rev. *26*, 217–229.

Seifert, G., Zhou, M., Dietrich, D., Schumacher, T.B., Dybek, A., Weiser, T., Wienrich, M., Wilhelm, D., and Steinhäuser, C. (2000). Developmental regulation of AMPA-receptor properties in CA1 pyramidal neurons of rat hippocampus. Neuropharmacology *39*, 931–942.

Selig, D.K., Nicoll, R.A., and Malenka, R.C. (1999). Hippocampal long-term potentiation preserves the fidelity of postsynaptic responses to presynaptic bursts. J. Neurosci. Off. J. Soc. Neurosci. *19*, 1236–1246.

Serrano, P., Yao, Y., and Sacktor, T.C. (2005). Persistent phosphorylation by protein kinase Mzeta maintains late-phase long-term potentiation. J. Neurosci. Off. J. Soc. Neurosci. *25*, 1979–1984.

Sheardown, M.J., Nielsen, E.O., Hansen, A.J., Jacobsen, P., and Honoré, T. (1990). 2,3-Dihydroxy-6-nitro-7-sulfamoyl-benzo(F)quinoxaline: a neuroprotectant for cerebral ischemia. Science *247*, 571–574.

Sheinin, A., Shavit, S., and Benveniste, M. (2001). Subunit specificity and mechanism of action of NMDA partial agonist D-cycloserine. Neuropharmacology *41*, 151–158.

Sherwood, J.L., Amici, M., Dargan, S.L., Culley, G.R., Fitzjohn, S.M., Jane, D.E., Collingridge, G.L., Lodge, D., and Bortolotto, Z.A. (2012). Differences in kainate receptor involvement in hippocampal mossy fibre long-term potentiation depending on

slice orientation. Neurochem. Int. *61*, 482–489.

Shigemoto, R., Nakanishi, S., and Mizuno, N. (1992). Distribution of the mRNA for a metabotropic glutamate receptor (mGluR1) in the central nervous system: an in situ hybridization study in adult and developing rat. J. Comp. Neurol. *322*, 121–135.

Shimamoto, K., Lebrun, B., Yasuda-Kamatani, Y., Sakaitani, M., Shigeri, Y., Yumoto, N., and Nakajima, T. (1998). DL-threo-beta-benzyloxyaspartate, a potent blocker of excitatory amino acid transporters. Mol. Pharmacol. *53*, 195–201.

Shinozaki, H., and Konishi, S. (1970). Actions of several anthelmintics and insecticides on rat cortical neurones. Brain Res. *24*, 368–371.

Shinozaki, H., Ishida, M., Shimamoto, K., and Ohfune, Y. (1989). A conformationally restricted analogue of L-glutamate, the (2S,3R,4S) isomer of L-alpha-(carboxycyclopropyl)glycine, activates the NMDA-type receptor more markedly than NMDA in the isolated rat spinal cord. Brain Res. *480*, 355–359.

Shipton, O.A., and Paulsen, O. (2014). GluN2A and GluN2B subunit-containing NMDA receptors in hippocampal plasticity. Philos. Trans. R. Soc. B Biol. Sci. *369*, 20130163.

Sievers, F., Wilm, A., Dineen, D., Gibson, T.J., Karplus, K., Li, W., Lopez, R., McWilliam, H., Remmert, M., Söding, J., et al. (2011). Fast, scalable generation of high-quality protein multiple sequence alignments using Clustal Omega. Mol. Syst. Biol. *7*, 539.

Silva, A.J., Stevens, C.F., Tonegawa, S., and Wang, Y. (1992). Deficient hippocampal long-term potentiation in alpha-calcium-calmodulin kinase II mutant mice. Science *257*, 201–206.

Simmons, R.M., Li, D.L., Hoo, K.H., Deverill, M., Ornstein, P.L., and Iyengar, S. (1998). Kainate GluR5 receptor subtype mediates the nociceptive response to formalin in the rat. Neuropharmacology *37*, 25–36.

Skrede, K.K., and Westgaard, R.H. (1971). The transverse hippocampal slice: a well-defined cortical structure maintained in vitro. Brain Res. *35*, 589–593.

Small, B., Thomas, J., Kemp, M., Hoo, K., Ballyk, B., Deverill, M., Ogden, A.M., Rubio, A., Pedregal, C., and Bleakman, D. (1998). LY339434, a GluR5 kainate receptor agonist. Neuropharmacology *37*, 1261–1267.

Smolders, I., Bortolotto, Z.A., Clarke, V.R.J., Warre, R., Khan, G.M., O'Neill, M.J., Ornstein, P.L., Bleakman, D., Ogden, A., Weiss, B., et al. (2002). Antagonists of GLU(K5)-containing kainate receptors prevent pilocarpine-induced limbic seizures. Nat. Neurosci. *5*, 796–804.

Sobczyk, A., Scheuss, V., and Svoboda, K. (2005). NMDA receptor subunit-dependent [Ca2+] signaling in individual hippocampal dendritic spines. J. Neurosci. Off. J. Soc. Neurosci. *25*, 6037–6046.

Sobolevsky, A.I., Rosconi, M.P., and Gouaux, E. (2009). X-ray structure, symmetry and

mechanism of an AMPA-subtype glutamate receptor. Nature *462*, 745–756.

Söllner, T., Whiteheart, S.W., Brunner, M., Erdjument-Bromage, H., Geromanos, S., Tempst, P., and Rothman, J.E. (1993a). SNAP receptors implicated in vesicle targeting and fusion. Nature *362*, 318–324.

Söllner, T., Bennett, M.K., Whiteheart, S.W., Scheller, R.H., and Rothman, J.E. (1993b). A protein assembly-disassembly pathway in vitro that may correspond to sequential steps of synaptic vesicle docking, activation, and fusion. Cell *75*, 409–418.

Sommer, B., Keinänen, K., Verdoorn, T.A., Wisden, W., Burnashev, N., Herb, A., Köhler, M., Takagi, T., Sakmann, B., and Seeburg, P.H. (1990). Flip and flop: a cell-specific functional switch in glutamate-operated channels of the CNS. Science *249*, 1580–1585.

Sommer, B., Köhler, M., Sprengel, R., and Seeburg, P.H. (1991). RNA editing in brain controls a determinant of ion flow in glutamate-gated channels. Cell *67*, 11–19.

Son, H., Hawkins, R.D., Martin, K., Kiebler, M., Huang, P.L., Fishman, M.C., and Kandel, E.R. (1996). Long-term potentiation is reduced in mice that are doubly mutant in endothelial and neuronal nitric oxide synthase. Cell *87*, 1015–1023.

Soto, D., Coombs, I.D., Kelly, L., Farrant, M., and Cull-Candy, S.G. (2007). Stargazin attenuates intracellular polyamine block of calcium-permeable AMPA receptors. Nat. Neurosci. *10*, 1260–1267.

Soto, D., Coombs, I.D., Renzi, M., Zonouzi, M., Farrant, M., and Cull-Candy, S.G. (2009). Selective regulation of long-form calcium-permeable AMPA receptors by an atypical TARP, gamma-5. Nat. Neurosci. *12*, 277–285.

Sprengel, R., Suchanek, B., Amico, C., Brusa, R., Burnashev, N., Rozov, A., Hvalby, Ø., Jensen, V., Paulsen, O., Andersen, P., et al. (1998). Importance of the intracellular domain of NR2 subunits for NMDA receptor function in vivo. Cell *92*, 279–289.

Squire, L.R. (1992). Memory and the hippocampus: a synthesis from findings with rats, monkeys, and humans. Psychol. Rev. *99*, 195–231.

Stafstrom, C.E., and Carmant, L. (2015). Seizures and epilepsy: An overview for neuroscientists. Cold Spring Harb. Perspect. Med. *5*.

Stanfa, L.C., and Dickenson, A.H. (1999). The role of non-N-methyl-D-aspartate ionotropic glutamate receptors in the spinal transmission of nociception in normal animals and animals with carrageenan inflammation. Neuroscience *93*, 1391–1398.

Stevens, C.F., and Tsujimoto, T. (1995). Estimates for the pool size of releasable quanta at a single central synapse and for the time required to refill the pool. Proc. Natl. Acad. Sci. U. S. A. *92*, 846–849.

Storm, J.F. (1990). Potassium currents in hippocampal pyramidal cells. Prog. Brain Res. *83*, 161–187.

Storm-Mathisen, J., and Iversen, L.L. (1979). Uptake of [3H]Glutamic acid in excitatory

nerve endings: light and electronmicroscopic observations in the hippocampal formation of the rat. Neuroscience *4*, 1237–1253.

Strack, S., and Colbran, R.J. (1998). Autophosphorylation-dependent targeting of calcium/ calmodulin-dependent protein kinase II by the NR2B subunit of the N-methyl-D-aspartate receptor. J. Biol. Chem. *273*, 20689–20692.

Straub, C., Hunt, D.L., Yamasaki, M., Kim, K.S., Watanabe, M., Castillo, P.E., and Tomita, S. (2011). Distinct functions of kainate receptors in the brain are determined by the auxiliary subunit Neto1. Nat. Neurosci. *14*, 866–873.

Stricker, C., Cowan, A.I., Field, A., and Redman, S.J. (1999). Analysis of NMDA-independent long-term potentiation induced at CA3—CA1 synapses in rat hippocampus in vitro. J. Physiol. *520*, 513–525.

Stuart, G., and Sakmann, B. (1995). Amplification of EPSPs by axosomatic sodium channels in neocortical pyramidal neurons. Neuron *15*, 1065–1076.

Südhof, T.C. (2012). The presynaptic active zone. Neuron *75*, 11–25.

Südhof, T.C. (2013). Neurotransmitter release: The last millisecond in the life of a synaptic vesicle. Neuron *80*, 675–690.

Sun, H.Y., and Dobrunz, L.E. (2006). Presynaptic kainate receptor activation is a novel mechanism for target cell-specific short-term facilitation at Schaffer collateral synapses. J. Neurosci. *26*, 10796–10807.

Sun, Y., Olson, R., Horning, M., Armstrong, N., Mayer, M., and Gouaux, E. (2002). Mechanism of glutamate receptor desensitization. Nature *417*, 245–253.

Sutton, J.L., Maccecchini, M.L., and Kajander, K.C. (1999). The kainate receptor antagonist 2S,4R-4-methylglutamate attenuates mechanical allodynia and thermal hyperalgesia in a rat model of nerve injury. Neuroscience *91*, 283–292.

Sutula, T.P., and Dudek, F.E. (2007). Unmasking recurrent excitation generated by mossy fiber sprouting in the epileptic dentate gyrus: an emergent property of a complex system. Prog. Brain Res. *163*, 541–563.

Swanger, S.A., Vance, K.M., Pare, J.-F., Sotty, F., Fog, K., Smith, Y., and Traynelis, S.F. (2015). NMDA receptors containing the GluN2D subunit control neuronal function in the subthalamic nucleus. J. Neurosci. *35*, 15971–15983.

Swanson, G.T. (2009). Targeting AMPA and kainate receptors in neurological disease: therapies on the horizon? Neuropsychopharmacol. Off. Publ. Am. Coll. Neuropsychopharmacol. *34*, 249–250.

Swanson, G.T., and Heinemann, S.F. (1998). Heterogeneity of homomeric GluR5 kainate receptor desensitization expressed in HEK293 cells. J. Physiol. *513 (Pt 3)*, 639–646.

Swanson, G.T., Gereau, R.W., Green, T., and Heinemann, S.F. (1997). Identification of amino acid residues that control functional behavior in GluR5 and GluR6 kainate

receptors. Neuron *19*, 913–926.

Sylwestrak, E.L., and Ghosh, A. (2012). Elfn1 regulates target-specific release probability at CA1-interneuron synapses. Science *338*, 536–540.

Ta, L.E., Dionne, R.A., Fricton, J.R., Hodges, J.S., and Kajander, K.C. (2000). SYM-2081 a kainate receptor antagonist reduces allodynia and hyperalgesia in a freeze injury model of neuropathic pain. Brain Res. *858*, 106–120.

Tajima, N., Karakas, E., Grant, T., Simorowski, N., Diaz-Avalos, R., Grigorieff, N., and Furukawa, H. (2016). Activation of NMDA receptors and the mechanism of inhibition by ifenprodil. Nature *534*, 63–68.

Takeuchi, A., and Takeuchi, N. (1963). Glutamate-induced depolarization in crustacean muscle. Nature *198*, 490.

Tang, M., Pelkey, K.A., Ng, D., Ivakine, E., McBain, C.J., Salter, M.W., and McInnes, R.R. (2011). Neto1 is an auxiliary subunit of native synaptic kainate receptors. J. Neurosci. Off. J. Soc. Neurosci. *31*, 10009–10018.

Tauck, D.L., and Nadler, J.V. (1985). Evidence of functional mossy fiber sprouting in hippocampal formation of kainic acid-treated rats. J. Neurosci. Off. J. Soc. Neurosci. *5*, 1016–1022.

Thompson, C.L., Drewery, D.L., Atkins, H.D., Stephenson, F.A., and Chazot, P.L. (2002). Immunohistochemical localization of N-methyl-d-aspartate receptor subunits in the adult murine hippocampal formation: evidence for a unique role of the NR2D subunit. Mol. Brain Res. *102*, 55–61.

Tingley, W.G., Ehlers, M.D., Kameyama, K., Doherty, C., Ptak, J.B., Riley, C.T., and Huganir, R.L. (1997). Characterization of protein kinase A and protein kinase C phosphorylation of the N-methyl-D-aspartate receptor NR1 subunit using phosphorylation site-specific antibodies. J. Biol. Chem. *272*, 5157–5166.

Tomita, S. (2010). Regulation of ionotropic glutamate receptors by their auxiliary subunits. Physiology *25*, 41–49.

Tomita, S., and Castillo, P.E. (2012). Neto1 and Neto2: auxiliary subunits that determine key properties of native kainate receptors. J. Physiol. *590*, 2217–2223.

Tomita, S., Chen, L., Kawasaki, Y., Petralia, R.S., Wenthold, R.J., Nicoll, R.A., and Bredt, D.S. (2003). Functional studies and distribution define a family of transmembrane AMPA receptor regulatory proteins. J. Cell Biol. *161*, 805–816.

Tomita, S., Fukata, M., Nicoll, R.A., and Bredt, D.S. (2004). Dynamic interaction of stargazin-like TARPs with cycling AMPA receptors at synapses. Science *303*, 1508–1511.

Tomita, S., Adesnik, H., Sekiguchi, M., Zhang, W., Wada, K., Howe, J.R., Nicoll, R.A., and Bredt, D.S. (2005). Stargazin modulates AMPA receptor gating and trafficking by distinct domains. Nature *435*, 1052–1058.

Traynelis, S.F., and Cull-Candy, S.G. (1990). Proton inhibition of N-methyl-D-aspartate receptors in cerebellar neurons. Nature *345*, 347–350.

Traynelis, S.F., Hartley, M., and Heinemann, S.F. (1995). Control of proton sensitivity of the NMDA receptor by RNA splicing and polyamines. Science *268*, 873–876.

Traynelis, S.F., Burgess, M.F., Zheng, F., Lyuboslavsky, P., and Powers, J.L. (1998). Control of voltage-independent zinc inhibition of NMDA receptors by the NR1 subunit. J. Neurosci. Off. J. Soc. Neurosci. *18*, 6163–6175.

Traynelis, S.F., Wollmuth, L.P., McBain, C.J., Menniti, F.S., Vance, K.M., Ogden, K.K., Hansen, K.B., Yuan, H., Myers, S.J., and Dingledine, R. (2010). Glutamate receptor ion channels: Structure, regulation, and function. Pharmacol. Rev. *62*, 405–496.

Turner, M.S., Hamamoto, D.T., Hodges, J.S., Maccecchini, M.L., and Simone, D.A. (2003). SYM 2081, an agonist that desensitizes kainate receptors, attenuates capsaicin and inflammatory hyperalgesia. Brain Res. *973*, 252–264.

Ulbrich, M.H., and Isacoff, E.Y. (2007). Subunit counting in membrane-bound proteins. Nat. Methods *4*, 319–321.

Ulbrich, M.H., and Isacoff, E.Y. (2008). Rules of engagement for NMDA receptor subunits. Proc. Natl. Acad. Sci. U. S. A. *105*, 14163–14168.

Valgeirsson, J., Nielsen, E.Ø., Peters, D., Varming, T., Mathiesen, C., Kristensen, A.S., and Madsen, U. (2003). 2-Arylureidobenzoic acids: Selective noncompetitive antagonists for the homomeric kainate receptor subtype GluR5. J. Med. Chem. *46*, 5834–5843.

Valgeirsson, J., Nielsen, E.Ø., Peters, D., Mathiesen, C., Kristensen, A.S., and Madsen, U. (2004). Bioisosteric modifications of 2-arylureidobenzoic acids: Selective noncompetitive antagonists for the homomeric kainate receptor subtype GluR5. J. Med. Chem. *47*, 6948–6957.

Vance, K.M., Simorowski, N., Traynelis, S.F., and Furukawa, H. (2011). Ligand-specific deactivation time course of GluN1/GluN2D NMDA receptors. Nat. Commun. *2*, 294.

Vandenberghe, W., Nicoll, R.A., and Bredt, D.S. (2005). Interaction with the unfolded protein response reveals a role for stargazin in biosynthetic AMPA receptor transport. J. Neurosci. *25*, 1095–1102.

VanElzakker, M., Fevurly, R.D., Breindel, T., and Spencer, R.L. (2008). Environmental novelty is associated with a selective increase in Fos expression in the output elements of the hippocampal formation and the perirhinal cortex. Learn. Mem. Cold Spring Harb. N *15*, 899–908.

Verdoorn, T.A., Johansen, T.H., Drejer, J., and Nielsen, E.Ø. (1994). Selective block of recombinant glur6 receptors by NS-102, a novel non-NMDA receptor antagonist. Eur. J. Pharmacol. Mol. Pharmacol. *269*, 43–49.

Vicini, S., Wang, J.F., Li, J.H., Zhu, W.J., Wang, Y.H., Luo, J.H., Wolfe, B.B., and Grayson, D.R. (1998). Functional and pharmacological differences between recombinant

N-methyl-D-aspartate receptors. J. Neurophysiol. *79*, 555–566.

Vignes, M., and Collingridge, G.L. (1997). The synaptic activation of kainate receptors. Nature *388*, 179–182.

Vignes, M., Bleakman, D., Lodge, D., and Collingridge, G.L. (1997). The synaptic activation of the GluR5 subtype of kainate receptor in area CA3 of the rat hippocampus. Neuropharmacology *36*, 1477–1481.

Vizi, E.S., and Kiss, J.P. (1998). Neurochemistry and pharmacology of the major hippocampal transmitter systems: synaptic and nonsynaptic interactions. Hippocampus *8*, 566–607.

Volianskis, A., and Jensen, M.S. (2003). Transient and sustained types of long-term potentiation in the CA1 area of the rat hippocampus. J. Physiol. *550*, 459–492.

Volianskis, A., Bannister, N., Collett, V.J., Irvine, M.W., Monaghan, D.T., Fitzjohn, S.M., Jensen, M.S., Jane, D.E., and Collingridge, G.L. (2013a). Different NMDA receptor subtypes mediate induction of long-term potentiation and two forms of short-term potentiation at CA1 synapses in rat hippocampus *in vitro*: NMDAR subtypes in STP and LTP. J. Physiol. *591*, 955–972.

Volianskis, A., Collingridge, G.L., and Jensen, M.S. (2013b). The roles of STP and LTP in synaptic encoding. PeerJ *1*, e3.

Walker, M.C., Galley, P.T., Errington, M.L., Shorvon, S.D., and Jefferys, J.G. (1995). Ascorbate and glutamate release in the rat hippocampus after perforant path stimulation: a “dialysis electrode” study. J. Neurochem. *65*, 725–731.

Wallace, M.S., Lam, V., and Schettler, J. (2012). NGX426, an oral AMPA-kainate antagonist, is effective in human capsaicin-induced pain and hyperalgesia. Pain Med. Malden Mass *13*, 1601–1610.

Wallis, J.L., Irvine, M.W., Jane, D.E., Lodge, D., Collingridge, G.L., and Bortolotto, Z.A. (2015). An interchangeable role for kainate and metabotropic glutamate receptors in the induction of rat hippocampal mossy fiber long-term potentiation in vivo. Hippocampus *25*, 1407–1417.

Watanabe, J., Beck, C., Kuner, T., Premkumar, L.S., and Wollmuth, L.P. (2002). DRPEER: a motif in the extracellular vestibule conferring high Ca2+ flux rates in NMDA receptor channels. J. Neurosci. Off. J. Soc. Neurosci. *22*, 10209–10216.

Watanabe-Iida, I., Konno, K., Akashi, K., Abe, M., Natsume, R., Watanabe, M., and Sakimura, K. (2016). Determination of kainate receptor subunit ratios in mouse brain using novel chimeric protein standards. J. Neurochem. *136*, 295–305.

Watkins, J.C., and Jane, D.E. (2006). The glutamate story. Br. J. Pharmacol. *147 Suppl 1*, S100-108.

Weiss, B., Alt, A., Ogden, A.M., Gates, M., Dieckman, D.K., Clemens-Smith, A., Ho, K.H., Jarvie, K., Rizkalla, G., Wright, R.A., et al. (2006). Pharmacological

characterization of the competitive GLUK5 receptor antagonist decahydroisoquinoline LY466195 in vitro and in vivo. J. Pharmacol. Exp. Ther. *318*, 772–781.

Werner, P., Voigt, M., Keinänen, K., Wisden, W., and Seeburg, P.H. (1991). Cloning of a putative high-affinity kainate receptor expressed predominantly in hippocampal CA3 cells. Nature *351*, 742–744.

Westbrook, G.L., and Mayer, M.L. (1987). Micromolar concentrations of Zn2+ antagonize NMDA and GABA responses of hippocampal neurons. Nature *328*, 640–643.

Wickelgren, W.O., Leonard, J.P., Grimes, M.J., and Clark, R.D. (1985). Ultrastructural correlates of transmitter release in presynaptic areas of lamprey reticulospinal axons. J. Neurosci. *5*, 1188–1201.

Wigström, H., and Gustafsson, B. (1983). Facilitated induction of hippocampal long-lasting potentiation during blockade of inhibition. Nature *301*, 603–604.

Wigström, H., and Gustafsson, B. (1985). On long-lasting potentiation in the hippocampus: a proposed mechanism for its dependence on coincident pre- and postsynaptic activity. Acta Physiol. Scand. *123*, 519–522.

Wilding, T.J., and Huettner, J.E. (1996). Antagonist pharmacology of kainate- and alpha-amino-3-hydroxy-5-methyl-4-isoxazolepropionic acid-preferring receptors. Mol. Pharmacol. *49*, 540–546.

Wilding, T.J., and Huettner, J.E. (1997). Activation and desensitization of hippocampal kainate receptors. J. Neurosci. Off. J. Soc. Neurosci. *17*, 2713–2721.

Wilding, T.J., and Huettner, J.E. (2001). Functional diversity and developmental changes in rat neuronal kainate receptors. J. Physiol. *532*, 411–421.

Williams, K. (1993). Ifenprodil discriminates subtypes of the N-methyl-D-aspartate receptor: selectivity and mechanisms at recombinant heteromeric receptors. Mol. Pharmacol. *44*, 851–859.

Williams, K. (1996). Separating dual effects of zinc at recombinant N-methyl-D-aspartate receptors. Neurosci. Lett. *215*, 9–12.

Williams, J.H., and Bliss, T.V. (1988). Induction but not maintenance of calcium-induced long-term potentiation in dentate gyrus and area CA1 of the hippocampal slice is blocked by nordihydroguaiaretic acid. Neurosci. Lett. *88*, 81–85.

Williams, P.A., White, A.M., Clark, S., Ferraro, D.J., Swiercz, W., Staley, K.J., and Dudek, F.E. (2009). Development of spontaneous recurrent seizures after kainate-induced status epilepticus. J. Neurosci. Off. J. Soc. Neurosci. *29*, 2103–2112.

Wisden, W., and Seeburg, P.H. (1993). A complex mosaic of high-affinity kainate receptors in rat brain. J. Neurosci. Off. J. Soc. Neurosci. *13*, 3582–3598.

Witschi, R., Punnakkal, P., Paul, J., Walczak, J.-S., Cervero, F., Fritschy, J.-M., Kuner, R., Keist, R., Rudolph, U., and Zeilhofer, H.U. (2011). Presynaptic alpha2-GABAA receptors

in primary afferent depolarization and spinal pain control. J. Neurosci. Off. J. Soc. Neurosci. *31*, 8134–8142.

Wo, Z.G., and Oswald, R.E. (1995). Unraveling the modular design of glutamate-gated ion channels. Trends Neurosci. *18*, 161–168.

Wondolowski, J., and Frerking, M. (2009). Subunit-dependent postsynaptic expression of kainate receptors on hippocampal interneurons in area CA1. J. Neurosci. Off. J. Soc. Neurosci. *29*, 563–574.

Wong, E.H., Kemp, J.A., Priestley, T., Knight, A.R., Woodruff, G.N., and Iversen, L.L. (1986). The anticonvulsant MK-801 is a potent N-methyl-D-aspartate antagonist. Proc. Natl. Acad. Sci. U. S. A. *83*, 7104–7108.

Wong, L.A., Mayer, M.L., Jane, D.E., and Watkins, J.C. (1994). Willardiines differentiate agonist binding sites for kainate- versus AMPA-preferring glutamate receptors in DRG and hippocampal neurons. J. Neurosci. *14*, 3881–3897.

Woolf, C.J. (2011). Central sensitization: implications for the diagnosis and treatment of pain. Pain *152*, S2-15.

Wu, L.G., and Saggau, P. (1994). Adenosine inhibits evoked synaptic transmission primarily by reducing presynaptic calcium influx in area CA1 of hippocampus. Neuron *12*, 1139–1148.

Wu, L.-J., Ko, S.W., and Zhuo, M. (2007). Kainate receptors and pain: from dorsal root ganglion to the anterior cingulate cortex. Curr. Pharm. Des. *13*, 1597–1605.

Wyeth, M.S., Pelkey, K.A., Petralia, R.S., Salter, M.W., McInnes, R.R., and McBain, C.J. (2014). Neto auxiliary protein interactions regulate kainate and NMDA receptor subunit localization at mossy fiber-CA3 pyramidal cell synapses. J. Neurosci. Off. J. Soc. Neurosci. *34*, 622–628.

Wyllie, D.J., Béhé, P., and Colquhoun, D. (1998). Single-channel activations and concentration jumps: comparison of recombinant NR1a/NR2A and NR1a/NR2D NMDA receptors. J. Physiol. *510 (Pt 1)*, 1–18.

Xu, J., Marshall, J.J., Fernandes, H.B., Nomura, T., Copits, B.A., Procissi, D., Mori, S., Wang, L., Zhu, Y., Swanson, G.T., et al. (2017). Complete disruption of the kainate receptor gene family results in corticostriatal dysfunction in mice. Cell Rep. *18*, 1848–1857.

Yamakura, T., Mori, H., Masaki, H., Shimoji, K., and Mishina, M. (1993). Different sensitivities of NMDA receptor channel subtypes to non-competitive antagonists. Neuroreport *4*, 687–690.

Yang, Q., Zhu, G., Liu, D., Ju, J.-G., Liao, Z.-H., Xiao, Y.-X., Zhang, Y., Chao, N., Wang, J., Li, W., et al. (2017). Extrasynaptic NMDA receptor dependent long-term potentiation of hippocampal CA1 pyramidal neurons. Sci. Rep. *7*, 3045.

Yang, S.N., Tang, Y.G., and Zucker, R.S. (1999). Selective induction of LTP and LTD by

postsynaptic [Ca2+]i elevation. J. Neurophysiol. *81*, 781–787.

Yao, Y., and Mayer, M.L. (2006). Characterization of a soluble ligand binding domain of the NMDA receptor regulatory subunit NR3A. J. Neurosci. Off. J. Soc. Neurosci. *26*, 4559–4566.

Yao, Y., Harrison, C.B., Freddolino, P.L., Schulten, K., and Mayer, M.L. (2008). Molecular mechanism of ligand recognition by NR3 subtype glutamate receptors. EMBO J. *27*, 2158–2170.

Yelshanskaya, M.V., Singh, A.K., Sampson, J.M., Narangoda, C., Kurnikova, M., and Sobolevsky, A.I. (2016). Structural bases of noncompetitive inhibition of AMPA-subtype ionotropic glutamate receptors by antiepileptic drugs. Neuron *91*, 1305–1315.

Yi, F., Mou, T.-C., Dorsett, K.N., Volkmann, R.A., Menniti, F.S., Sprang, S.R., and Hansen, K.B. (2016). Structural basis for negative allosteric modulation of GluN2A-containing NMDA receptors. Neuron *91*, 1316–1329.

Youn, D.-H., and Randic, M. (2004). Modulation of excitatory synaptic transmission in the spinal substantia gelatinosa of mice deficient in the kainate receptor GluR5 and/or GluR6 subunit. J. Physiol. *555*, 683–698.

Yu, L.M.Y., Polygalov, D., Wintzer, M.E., Chiang, M.-C., and McHugh, T.J. (2016). CA3 synaptic silencing attenuates kainic acid-induced seizures and hippocampal network oscillations. ENeuro *3*.

Yuan, H., Hansen, K.B., Vance, K.M., Ogden, K.K., and Traynelis, S.F. (2009a). Control of NMDA receptor function by the NR2 subunit amino-terminal domain. J. Neurosci. *29*, 12045–12058.

Yuan, H., Vance, K.M., Junge, C.E., Geballe, M.T., Snyder, J.P., Hepler, J.R., Yepes, M., Low, C.-M., and Traynelis, S.F. (2009b). The serine protease plasmin cleaves the amino-terminal domain of the NR2A subunit to relieve zinc inhibition of the N-methyl-D-aspartate receptors. J. Biol. Chem. *284*, 12862–12873.

Zerangue, N., and Kavanaugh, M.P. (1996). Flux coupling in a neuronal glutamate transporter. Nature *383*, 634–637.

Zhang, W., St-Gelais, F., Grabner, C.P., Trinidad, J.C., Sumioka, A., Morimoto-Tomita, M., Kim, K.S., Straub, C., Burlingame, A.L., Howe, J.R., et al. (2009). A transmembrane accessory subunit that modulates kainate-type glutamate receptors. Neuron *61*, 385–396.

Zhou, L.M., Gu, Z.Q., Costa, A.M., Yamada, K.A., Mansson, P.E., Giordano, T., Skolnick, P., and Jones, K.A. (1997). (2S,4R)-4-methylglutamic acid (SYM 2081): a selective, high-affinity ligand for kainate receptors. J. Pharmacol. Exp. Ther. *280*, 422–427.

Zhou, N., Hammerland, L.G., and Parks, T.N. (1993). Gamma-D-glutamylaminomethyl sulfonic acid (GAMS) distinguishes kainic acid- from AMPA-induced responses in Xenopus oocytes expressing chick brain glutamate receptors. Neuropharmacology *32*, 767–775.

Zhou, Z., Felts, A.K., Friesner, R.A., and Levy, R.M. (2007). Comparative performance of several flexible docking programs and scoring functions: enrichment studies for a diverse set of pharmaceutically relevant targets. J. Chem. Inf. Model. *47*, 1599–1608.

Zucker, R.S., and Regehr, W.G. (2002). Short-term synaptic plasticity. Annu. Rev. Physiol. *64*, 355–405.

Zucker, R.S., Kullmann, D.M., and Kaeser, P.S. (2014). Chapter 15 - Release of neurotransmitters. In From Molecules to Networks (Third Edition), J.H. Byrne, R. Heidelberger, and M.N. Waxham, eds. (Boston: Academic Press), pp. 443–488.